

UNIVERSITY OF BELGRADE
FACULTY OF CIVIL ENGINEERING

Saša D. Kovačević

**STABILITY AND ULTIMATE CAPACITY OF
THIN-WALLED STEEL PLATE GIRDERS
SUBJECTED TO PATCH LOADING**

Doctoral Dissertation

Belgrade, 2021

УНИВЕРЗИТЕТ У БЕОГРАДУ
ГРАЂЕВИНСКИ ФАКУЛТЕТ

Саша Д. Ковачевић

**СТАБИЛНОСТ И ГРАНИЧНА НОСИВОСТ
ТАНКОВИДНИХ ЧЕЛИЧНИХ НОСАЧА
ПОД УТИЦАЈЕМ ДЕЛИМИЧНОГ
ОПТЕРЕЂЕЊА**

докторска дисертација

Београд, 2021

Advisor:

Dr. Dragoslav M. Šumarac

Professor

University of Belgrade, Faculty of Civil Engineering

Committee members:

Dr. Dragoslav M. Šumarac

Professor

University of Belgrade, Faculty of Civil Engineering

Dr. Ratko M. Salatić

Professor

University of Belgrade, Faculty of Civil Engineering

Dr. Duško Lučić

Professor

University of Montenegro, Faculty of Civil Engineering

Dr. Stanko B. Ćorić

Assistant Professor

University of Belgrade, Faculty of Civil Engineering

Dr. Milan J. Spremić

Assistant Professor

University of Belgrade, Faculty of Civil Engineering

Defense date: _____

Ментор:

др Драгослав М. Шумарац
редовни професор
Универзитет у Београду, Грађевински факултет

Чланови комисије:

др Драгослав М. Шумарац
редовни професор
Универзитет у Београду, Грађевински факултет

др Ратко М. Салатић
редовни професор
Универзитет у Београду, Грађевински факултет

др Душко Лучић
редовни професор
Универзитет Црне Горе, Грађевински факултет

др Станко Б. Ћорић
доцент
Универзитет у Београду, Грађевински факултет

др Милан Ј. Спремић
доцент
Универзитет у Београду, Грађевински факултет

Датум одбране: _____

To my parents

Acknowledgements

I wish to thank my advisor Dr. Dragoslav Sumarac for his collaboration and professional guidance. I want to express my deepest gratitude to Dr. Nenad Markovic for his support, guidance, encouragement, and careful review of reports, papers, and this dissertation. Your perpetual energy and enthusiasm in research and education have motivated me and traced my further life directions. Thank you for being such a good Professor. It was a pleasure and honor working with and learning from you. Thanks for all these years.

My gratitude also goes to my committee members, Dr. Ratko Salatic, Dr. Dusko Lucic, Dr. Stanko Coric, and Dr. Milan Spremic for their valuable comments.

I want to acknowledge the Faculty of Civil Engineering, University of Montenegro, for support and the technical staff who assisted in conducting the experimental research in a highly professional way.

Special thanks to all my dear colleagues and friends for giving me support in many different ways. I want to thank deceased Prof. Gligor Radenkovic for discussions during my studies and collaborations on projects. Special appreciation are addressed to my friends Aleksandar Borkovic and Konstantinos Lazaridis for valuable discussions during last years.

Last but not least, special thanks to my family for their continuous support and endless love. Thanks to my mother, father, and sisters for support during my education. Of course, a heartfelt thanks to Anči for her support, love, and patience for all these years. I would not finish this dissertation if I did not have you all. I hope this dissertation will incentive my nieces to pursue academic careers. I love you all!

Abstract

STABILITY AND ULTIMATE CAPACITY OF THIN-WALLED STEEL PLATE GIRDERS SUBJECTED TO PATCH LOADING

Patch loading or partially distributed load is a special load case in which plate and box girders are subjected to localized compressive edge loads in the plane of the web. This load case is present in many applications, including beam-beam and beam-column connections as well as deep crane runway beams loaded by crane wheels. The most realistic load case is during the incremental launching of multi-span steel and composite bridges over temporary or permanent supports. In all these applications, plate girders are frequently supported at cross-sections where no vertical web stiffener exists, and the load is transferred into the web panel through the loaded flange. By using longitudinal stiffeners for flexural and shear strength, the patch loading resistance can be increased as well. However, scarce work has been found in the literature for the influence of patch load length on the ultimate strength of longitudinally stiffened steel plate girders.

The present research experimentally and numerically investigates the behavior and ultimate capacity of longitudinally unstiffened and stiffened I-steel plate girders reinforced by a single longitudinal stiffener subjected exclusively to patch loading. The main objective of the experimental study is to elucidate and systematically analyze the influence of patch load length on the patch loading resistance. The experiments are described in detail, and the main conclusions are presented. The experimentally obtained patch loading resistances are juxtaposed with ultimate loads available in the literature and determined by the design standard EN 1993-1-5. The ultimate strengths of longitudinally unstiffened and stiffened steel plate girders determined by the design standard are smaller than the experimentally obtained ones, especially for longitudinally stiffened girders and longer patch load lengths. This experimental investigation shows that the patch load length and girder width significantly influence the ultimate strength of steel plate girders. The patch loading resistance increases as the patch load length is increased. After a specific patch load length, the carrying capacity of longitudinally stiffened steel plate girders increases much faster with increasing patch load length. By using longer patch load lengths and longitudinal stiffeners, the ultimate strength can be significantly increased. Increasing the web panel aspect ratio leads to smaller ultimate loads.

Numerical modeling is based on current and previous experimental studies. The finite

element model incorporates the experimentally measured geometric imperfections and material properties based on the laboratory tests. Geometrically and materially nonlinear finite element analysis is performed to assess the patch loading resistance. The numerical model is verified by comparing numerically and experimentally obtained results for the ultimate capacity and elastoplastic behavior of steel plate girders. Experimental and numerical results are in good agreement, which enabled a fruitful basis for parametric analysis.

Experimental studies have shown that the current EN 1993-1-5 patch loading resistance model underestimates the ultimate strength of steel plate girders in certain cases. In addition to this resistance model, the design standard allows the use of finite element analysis for the ultimate limit state. The existing design recommendations for an adequate ultimate limit state design are found insufficient. The essential data for an adequate ultimate limit state design comprises information on unavoidable geometric and structural imperfections. However, the design standard lacks information on these imperfections. Therefore, imperfection sensitivity analysis of steel plate girders subjected to patch loading is performed in the current numerical research. The finite element parametric study is designed to determine the influence of a variety of geometric imperfections, in combination with various patch load lengths, on the patch loading resistance of longitudinally unstiffened and stiffened steel plate girders. Experimentally measured, buckling mode-affine, and hand-defined sinusoidal geometric imperfections are varied in the study in combination with varying patch load lengths and relative stiffnesses of the longitudinal stiffener.

The ultimate strength of longitudinally unstiffened and stiffened steel plate girders increases as the patch load length is increased for all the geometric imperfections considered. For relatively small patch load lengths, the relative stiffness of the longitudinal stiffener has no significant influence on the ultimate load regardless of the geometric imperfection. For longer patch load lengths, the ultimate strength is highly dependent on geometric imperfections. The influence of the web panel aspect ratio is shown to be negligible for smaller patch load lengths regardless of the geometric imperfection, while for longer applied loads, the impact of this ratio is dependent on the geometric imperfection.

It is concluded from the imperfection sensitivity analysis that the ultimate strength of patch-loaded steel plate girders is more sensitive to local than global geometric imperfections. Local geometric imperfections defined in the upper web sub-panel yield lower ultimate strengths than global geometric imperfections (defined over the whole web depth). Unfavorable geometric imperfections in steel plate girders subjected to patch loading are governed by the patch load length and the relative stiffness of the longitudinal stiffener. Different unfavorable geometric imperfections were found for different patch load lengths and relative stiffnesses. The lowest patch loading resistances were returned for geometric imperfections that resembled the deformation at collapse (collapse-affine geometric imperfections). Although the concept of collapse-affine geometric imperfections seems impractical for design purposes (a geometrically and materially nonlinear analysis must be conducted before collapse-affine geometric imperfec-

tion shapes are determined), the use of these imperfection shapes is recommended.

Keywords: Patch loading; Ultimate capacity; Steel plate girder; Longitudinal stiffeners; Experimental investigation; Finite element analysis; Parametric study, Unfavorable geometric imperfections

Scientific field: Civil Engineering

Scientific subfield: Engineering Mechanics and Theory of Structures, and Metal Structures

UDC number:

Резиме

СТАБИЛНОСТ И ГРАНИЧНА НОСИВОСТ ТАНКОЗИДНИХ ЧЕЛИЧНИХ НОСАЧА ПОД УТИЦАЈЕМ ДЕЛИМИЧНОГ ОПТЕРЕЋЕЊА

Делимично оптерећење или парцијално распоређено оптерећење је специјалан случај оптерећења при којем су лимени и кутијасте носачи оптерећени локализованим ивичним силама притиска у равни ребра. Овај случај оптерећења је присутан у многим ситуацијама, укључујући греда-греда и греда-стуб везе као и код кранских стаза оптерећених кранским точковима. Најреалнији случај оптерећења је за време инкременталног лансирања вишераспонских челичних и спрегнутих мостова преко привремених и сталних ослонаца. У свим овим ситуацијама, лимени носачи су обично ослоњени на пресецима у којима нема вертикалних укрућења, и оптерећење се преноси у ребро преко оптерећене ножице. Употребом подужних укрућења за носивост на извијање и смицање, гранична носивост на делимично оптерећење се такође може повећати. Ипак, оскудно истраживање је пронађено у литератури за утицај дужине оптерећења на граничну носивост подужно укрућених лимених челичних носача.

Ово истраживање експериментално и нумерички испитује понашање и граничну носивост подужно неукрућених и укрућених лимених челичних носача I-пресека ојачаних са једним подужним укрућењем оптерећених искључиво са делимичним оптерећењем. Главни циљ експерименталног испитивања је да расветли и систематично анализира утицај дужине оптерећења на граничну носивост при делимичном оптерећењу. Експерименти су детаљно описани, и главни закључци су дати. Експериментално добијене граничне силе су упоређене са граничним оптерећењем доступним у литератури и одређеним користећи стандард за пројектовање EN 1993-1-5. Граничне носивости подужно неукрућених и укрућених лимених челичних носача срачунате помоћу стандарда за пројектовање су мање него експериментално добијене вредности, посебно за подужно укрућене носаче и дужа делимична оптерећења. Ово експериментално испитивање показује да дужина оптерећења и распон носача знатно утичу на граничну носивост лимених челичних носача. Гранична носивост при делимичном оптерећењу се повећава са повећањем дужине оптерећења. После одређене дужине оптерећења, гранична носивост подужно укрућених лимених челичних носача се много брже повећава са повећањем дужине оптерећења. Употребом већих дужина оптерећења и подужних укрућења, гранична носивост се може знатно повећати. Повећање распона носача доводи до смањења граничне носивости.

Нумеричко моделирање је базирано на тренутном и претходном експерименталном истраживању. Модел са коначним елементима укључује експериментално мерене имперфекције и материјалне карактеристике добијене експерименталним тестовима. Геометријски и материјално нелинеарна анализа коначним елементима је изведена да би се одредила гранична носивост при делимичном оптерећењу. Нумерички модел је верификован поређењем нумеричко и експериментално добијених вредности граничних носивости и еластопластичног понашања лимених челичних носача. Експерименталне и нумеричке вредности се добро поклапају, што је обезбедило добру основу за разноврсну параметарску анализу.

Експериментална испитивања су показала да важећи EN 1993-1-5 модел за граничну носивост при делимичном оптерећењу у појединим случајевима потцењује граничне носивости лимених челичних носача. Поред овог модела за граничну носивост, стандард за пројектовање допушта употребу анализа коначним елементима за гранична стања. Постојеће препоруке за пројектовање нису довољне за адекватну анализу коначним елементима. Неопходни подаци за адекватну анализу граничних стања коначним елементима укључују информације о неизбежним геометријским и структуралним имперфекцијама. Ипак, у стандарду за пројектовање недостају информације о овим имперфекцијама. Стога, анализа осетљивости на имперфекције танкозидних челичних носача оптерећених делимичним оптерећењем је дата у нумеричком делу истраживања. Параметарска анализа коначним елементима је планирана са циљем да одреди утицај разних геометријских имперфекција, у комбинацији са различитим дужинама оптерећења, на граничну носивост подужно неукрућених и укрућених лимених челичних носача под делимичним оптерећењем. Експериментално мерене, тоновима осциловања сличне, и ручно задане синусоидне геометријске имперфекције су мењане у параметарској анализи у комбинацији са варирањем дужине оптерећења и релативне крутости подужног оптерећења.

Гранична носивост подужно неукрућених и укрућених танкозидних челичних носача се повећава са повећањем дужине оптерећења за све размотрене имперфекције. За релативно мале дужине делимичног оптерећења, релативна крутост подужног оптерећења нема значајан утицај на граничну носивост без обзира на геометријску имперфекцију. За веће дужине оптерећења, гранична носивост је веома зависна од геометријских имперфекција. Утицај односа дужине и висине ребра се показао занемарљив за мале дужине оптерећења независно од геометријске имперфекције, док за дужа оптерећења, утицај овог односа зависи од геометријске имперфекције.

Закључено је из анализе осетљивости на имперфекције да је гранична носивост лимених челичних носача оптерећених делимичним оптерећењем више осетљива на локалне него на глобалне геометријске имперфекције. Локалне геометријске имперфекције дефинисане у горњем делу ребра дају ниже граничне носивости него глобалне геометријске имперфекције (дефинисане целом висином ребра). Неповољне геометријске имперфекције лимених челичних носача оптерећених делимичним оптерећењем су вођене дужином

оптерећења и релативном крутости подужног оптерећења. Различите неповољне геометријске имперфекције су добијене за различите дужине оптерећења и релативне крутости. Најниже граничне носивости при делимичном оптерећењу су добијене за геометријске имперфекције које подсећају на деформацију при лому (лomu сличне геометријске имперфекције). Иако се концепт лому сличних геометријских имперфекција чини непрактичан за сврхе пројектовања (геометријски и материјално нелинеарна анализа се мора спровести пре него се лому сличне геометријске имперфекције одреде), препоручена је употреба ових облика имперфекција.

Кључне речи: Делимично оптерећење, Гранична носивост, Челични носачи, Подужна укрућења, Експериментална анализа, Анализа коначним елементима, Параметарска студија, Неповољне геометријске имперфекције

Научна област: Грађевинско инжењерство

Ужа научна област: Техничка механика и теорија конструкција и Металне конструкције

УДК број:

Contents

Acknowledgements	iv
Abstract	iii
Резиме	vii
Contents	xi
List of Figures	xv
List of Tables	xxv
Nomenclature	xxvii
Chapter 1 Introduction	1
1.1 Motivation	1
1.2 Goals	3
1.3 Objectives	3
1.4 Methodology	4
1.5 Thesis layout	4
1.6 Selected publications	6
Chapter 2 Literature review	7
2.1 Experimental study	7
2.2 Numerical study	11
2.3 European design standard EN 1993-1-5	12
2.4 Summary	13
Chapter 3 Experimental work	15
3.1 Experimental testing	16
3.1.1 Test specimens	16
3.1.2 Testing setup and disposition	17
3.1.3 Initial geometric imperfections	20
3.1.4 Testing process	20
3.2 Test results and discussion	23
3.2.1 Ultimate strength	23

3.2.2	Web deformation	27
3.2.3	Flange deformation	31
3.2.4	Elastoplastic behavior	31
3.3	Summary	34
Chapter 4	Numerical Model	41
4.1	Introduction	41
4.2	Finite element model	42
4.2.1	Geometry	42
4.2.2	Geometry	43
4.2.3	Boundary and loading conditions	44
4.2.4	Material properties	46
4.2.5	Initial imperfections	47
4.3	Model validation	49
4.3.1	Patch loading resistance	50
4.3.2	Elastoplastic behavior	50
4.4	Summary	53
Chapter 5	Parametric Study	57
5.1	Parameters	57
5.2	Geometric imperfection shapes	59
5.3	Results and discussion	61
5.3.1	Experimentally measured geometric imperfections	62
5.3.2	Buckling mode-affine geometric imperfections	68
5.3.3	Hand-defined sinusoidal geometric imperfections	74
5.4	Influence of the web panel aspect ratio	81
5.5	Influence of relative stiffness γ_s	83
5.6	Contribution of the web panel yield stress	85
5.7	Summary	87
Chapter 6	Unfavorable geometric imperfections	89
6.1	Introduction	89
6.2	Unfavorable geometric imperfections	90
6.3	Summary	96
Chapter 7	Conclusions and future work	99
References	103
Appendix A	Steel material properties	113
Appendix B	Web panel deformation for girders of Series A	119

Appendix C Web panel deformation for girders of Series B	125
Biography	131
Биографија	133

List of Figures

Figure. 1.1	Thin-walled plate girder subjected to localized compressive edge load and typical failure mode.	2
Figure. 3.1	Longitudinally stiffened plate girder under transverse concentrated loading, general notation.	17
Figure. 3.2	Test configurations for all the test plate girders. Longitudinally unstiffened (top row) and longitudinally stiffened steel plate girders (bottom row).	18
Figure. 3.3	Schematic drawing of the laboratory and equipment: 1) test girder, 2) steel closed frame, 3) frame slider for guiding a transducer for web deformations, 4) frame slider for holding a transducer for the upper flange deformation, 5) press, 6) load cell, 7) rigid steel block for load introduction, 8) electrical transducers, 9) pipes for oil supply for hydraulic pump, 10) electrical cables for connecting the load cell and measuring devices.	19
Figure. 3.4	Different load blocks (clockwise from top left): $s_s = 0, 25, 250,$ and 100 mm.	19
Figure. 3.5	Measuring initial geometric web panel imperfections using a rectangular grid size of 21×11 points.	20
Figure. 3.6	Measuring out-of-plane deflection at a characteristic point near the loaded flange (top row) and deflection of the loaded flange (bottom row) during the testing process.	21
Figure. 3.7	Arrangement of strain gauges for the web panel and the loaded flange.	22
Figure. 3.8	Failure modes.	22
Figure. 3.9	Experimentally obtained ultimate strength for all the tested girders and corresponding values according to EN 1993-1-5.	25
Figure. 3.10	Vertical web profiles for different levels of the ultimate load for unstiffened and stiffened steel plate girder: (a) $s_s = 0$ mm: B16 <i>vs.</i> B13. (b) $s_s = 50$ mm: B1 <i>vs.</i> B3.	28
Figure. 3.11	Vertical web profiles for different levels of the ultimate load for unstiffened and stiffened steel plate girder: (a) $s_s = 100$ mm: B15 <i>vs.</i> B5. (b) $s_s = 150$ mm: B2 <i>vs.</i> B7.	28

Figure. 3.12	Vertical web profiles for different levels of the ultimate load for unstiffened and stiffened steel plate girder: (a) $s_s = 200$ mm: B12 <i>vs.</i> B4. (b) $s_s = 250$ mm: B11 <i>vs.</i> B6.	29
Figure. 3.13	Vertical web profiles for different levels of the ultimate load for unstiffened steel plate girder B14 $s_s = 25$ mm (left) and stiffened steel plate girder B17 $s_s = 150$ mm (right).	29
Figure. 3.14	Increase in deformation (obtained as the difference between the residual and initial deformation) for unstiffened (left column) and stiffened (right column) steel plate girders (in mm). The dashed line represents the longitudinal stiffener.	31
Figure. 3.15	Web and flange deformation for applied forces near the ultimate strength for girders (clockwise from top left) B16, B14, B11, and B15.	32
Figure. 3.16	Position of strain gauges (in mm) for girders: (a) B15 (unstiffened); (b) B5 (stiffened). Positions of vertical strains given in this section are marked in red.	33
Figure. 3.17	Vertical strain in the web plate on both sides (front-rear) for unstiffened girder B15 ($s_s = 100$ mm) at points placed 10 mm from the loaded flange and horizontally displaced from the vertical symmetry line for: (a) 12.5 mm; (b) 62.50 mm.	34
Figure. 3.18	Vertical strain in the web plate on both sides (front-rear) for unstiffened girder B15 ($s_s = 100$ mm) at points placed 37.50 mm from the loaded flange and horizontally displaced from the vertical symmetry line for: (a) 12.5 mm; (b) 62.50 mm.	35
Figure. 3.19	Vertical strain in the web plate on both sides (front-rear) for unstiffened girder B15 ($s_s = 100$ mm) at points placed 62.50 mm from the loaded flange and horizontally displaced from the vertical symmetry line for: (a) 12.5 mm; (b) 62.50 mm.	36
Figure. 3.20	Vertical strain in the web plate on both sides (front-rear) for stiffened girder B5 ($s_s = 100$ mm) at points placed 10 mm from the loaded flange and horizontally displaced from the vertical symmetry line for: (a) 25 mm; (b) 50 mm.	37
Figure. 3.21	Vertical strain in the web plate on both sides (front-rear) for stiffened girder B5 ($s_s = 100$ mm) at points placed 37.50 mm from the loaded flange and horizontally displaced from the vertical symmetry line for: (a) 25 mm; (b) 50 mm.	38
Figure. 3.22	Vertical strain in the web plate on both sides (front-rear) for stiffened girder B5 ($s_s = 100$ mm) at points placed 62.50 mm from the loaded flange and horizontally displaced from the vertical symmetry line for: (a) 25 mm; (b) 50 mm.	38

Figure. 3.23	Vertical strain in the web plate on both sides (front-rear) for stiffened girder B5 ($s_s = 100$ mm) at points placed 112.50 mm from the loaded flange and horizontally displaced from the vertical symmetry line for: (a) 25 mm; (b) 50 mm.	39
Figure. 4.1	Finite element mesh for three representative models. Rigid blocks for $0 < s_s \leq 150$ mm (top-left), 4 independent rigid blocks for $s_s = 150$ mm (top-middle) and half-round bar for $s_s = 0$ mm (top-right). For the setup configuration of these loading blocks in the experiment, see Fig. 4 in Refs. [25] and Fig. 3.4 in Chapter 3. . . .	43
Figure. 4.2	Convergence plot for the ultimate strength for longitudinally unstiffened (a) and stiffened (b) steel plate girders.	44
Figure. 4.3	Engineering stress-strain curves obtained by tensile test vs. curves used in the simulations for (a) web plate, and (b) flanges, transverse and longitudinal stiffeners for all the girders of Series A.	47
Figure. 4.4	Engineering stress-strain curves obtained by tensile test vs. curves used in the simulations for (a) web plate, and (b) flanges, transverse and longitudinal stiffeners for girders B1 and B6.	47
Figure. 4.5	Engineering stress-strain curves obtained by tensile test vs. curves used in the simulations for (a) web plate, and (b) flanges, transverse and longitudinal stiffeners for girder B2.	48
Figure. 4.6	Engineering stress-strain curves obtained by tensile test vs. curves used in the simulations for (a) web plate, and (b) flanges, transverse and longitudinal stiffeners for girders B3, B4, B5, and B7.	48
Figure. 4.7	Modeling technique for measured initial geometric imperfections.	49
Figure. 4.8	Comparison between the experimentally and numerically obtained ultimate strengths for the girders of Series A.	50
Figure. 4.9	Comparison between the experimentally and numerically obtained ultimate strengths for the girders of Series B.	51
Figure. 4.10	von Mises stress contour plots [MPa] for unstiffened steel plate girder A1 ($s_s = 50$ mm) at different levels of the ultimate load. The contour plots at the top represent stresses in the shell surface facing the reader while the bottom plots represent the other surface.	53
Figure. 4.11	von Mises stress contour plots [MPa] for stiffened girder A3 ($s_s = 50$ mm) at different levels of the ultimate load. The contour plots at the top represent stresses in the shell surface facing the reader (longitudinal stiffener's side) while the bottom plots represent the other surface.	53

Figure. 4.12	von Mises stress contour plots [MPa] for unstiffened girder A2 ($s_s = 150$ mm) at different levels of the ultimate load. The contour plots at the top represent stresses in the shell surface facing the reader while the bottom plots represent the other surface.	54
Figure. 4.13	von Mises stress contour plots [MPa] for stiffened girder A7 ($s_s = 150$ mm) at different levels of the ultimate load. The contour plots at the top represent stresses in the shell surface facing the reader (longitudinal stiffener's side) while the bottom plots represent the other surface.	54
Figure. 4.14	Load-displacement response for unstiffened and stiffened steel plate girder under the patch load length of: (a) $s_s = 0$ mm; (b) $s_s = 25$ mm.	55
Figure. 4.15	Load-displacement response for unstiffened and stiffened steel plate girder under the patch load length of: (a) $s_s = 50$ mm; (b) $s_s = 100$ mm.	55
Figure. 4.16	Load-displacement response for unstiffened and stiffened steel plate girder under the patch load length of: (a) $s_s = 150$ mm; (b) $s_s = 150$ mm (distribution block).	55
Figure. 5.1	Experimentally measured geometric imperfections for girder A1 (left) and girder B1 (right). Refer to Appendix B and Appendix C for the other experimentally measured imperfection shapes for the girders of Series A and B, respectively. Units are in mm.	59
Figure. 5.2	First buckling mode of longitudinally unstiffened and stiffened steel plate girders for all patch load lengths considered ($s_s/h_w \leq 0.50$) for girders of Series A.	59
Figure. 5.3	Second buckling mode of longitudinally unstiffened and stiffened steel plate girders for all patch load lengths considered ($s_s/h_w \leq 0.50$) for girders of Series A.	60
Figure. 5.4	Third buckling mode of longitudinally unstiffened and stiffened steel plate girders (valid for $s_s/h_w \leq 0.40$) of Series A.	60
Figure. 5.5	Third buckling mode of longitudinally unstiffened and stiffened steel plate girders (valid for $s_s/h_w = 0.50$) of Series A.	61
Figure. 5.6	First buckling mode of longitudinally unstiffened and stiffened steel plate girders for all patch load lengths considered ($s_s/h_w \leq 0.50$) for girders of Series B.	61
Figure. 5.7	Second buckling mode of longitudinally unstiffened and stiffened steel plate girders for all patch load lengths considered ($s_s/h_w \leq 0.50$) for girders of Series B.	62

Figure. 5.8	Third buckling mode of longitudinally unstiffened (valid for $s_s/h_w \leq 0.50$) and stiffened steel plate girders (valid for $s_s/h_w \leq 0.25$ for $\gamma_s = 21.67$ and for $s_s/h_w \leq 0.10$ for $\gamma_s = 103.46$) of Series B.	62
Figure. 5.9	Third buckling mode of longitudinally stiffened steel plate girders (valid for $s_s/h_w \geq 0.30$ for $\gamma_s = 21.67$ and $s_s/h_w \geq 0.15$ for $\gamma_s = 103.46$) of Series B.	63
Figure. 5.10	Sine (left) and cosine (right) hand-defined geometric imperfections for both series of girders A and B.	63
Figure. 5.11	Ultimate strength of longitudinally unstiffened and stiffened steel plate girders using experimentally measured geometric imperfections from (a) girder A1 and (b) girder A2.	69
Figure. 5.12	Ultimate strength of longitudinally unstiffened and stiffened steel plate girders using experimentally measured geometric imperfections from (a) girder A11 and (b) girder A12.	69
Figure. 5.13	Ultimate strength of longitudinally unstiffened and stiffened steel plate girders using experimentally measured geometric imperfections from (a) girder A13 and (b) girder A15.	70
Figure. 5.14	Ultimate strength of longitudinally unstiffened and stiffened steel plate girders using experimentally measured geometric imperfections from (a) girder A3 and (b) girder A4.	70
Figure. 5.15	Ultimate strength of longitudinally unstiffened and stiffened steel plate girders using experimentally measured geometric imperfections from (a) girder A5 and (b) girder A6.	71
Figure. 5.16	Ultimate strength of longitudinally unstiffened and stiffened steel plate girders using experimentally measured geometric imperfections from (a) girder A7 and (b) girder A14.	71
Figure. 5.17	Ultimate strength of longitudinally unstiffened and stiffened steel plate girders using experimentally measured geometric imperfections from (a) girder A16 and (b) girder A17.	72
Figure. 5.18	Strengthening effect employing the experimentally measured geometric imperfections from initially (a) unstiffened and (b) stiffened steel plate girders.	72
Figure. 5.19	Ultimate strength of: (a) longitudinally unstiffened steel plate girders using geometric imperfections from the experimentally unstiffened girders; (b) longitudinally stiffened steel plate girders using geometric imperfections from the experimentally stiffened girders.	73
Figure. 5.20	Ultimate strength of longitudinally unstiffened and stiffened steel plate girders using experimentally measured geometric imperfections from (a) girder B1 and girder B2.	73

Figure. 5.21	Ultimate strength of longitudinally unstiffened and stiffened steel plate girders using experimentally measured geometric imperfections from (a) girder B3 and (b) girder B4.	74
Figure. 5.22	Ultimate strength of longitudinally unstiffened and stiffened steel plate girders using experimentally measured geometric imperfections from (a) girder B5 and (b) girder B6.	74
Figure. 5.23	Ultimate strength of longitudinally unstiffened and stiffened steel plate girders using experimentally measured geometric imperfections from (a) girder B7 and (b) girder B11.	75
Figure. 5.24	Ultimate strength of longitudinally unstiffened and stiffened steel plate girders using experimentally measured geometric imperfections from (a) girder B12 and (b) girder B13.	75
Figure. 5.25	Ultimate strength of longitudinally unstiffened and stiffened steel plate girders using experimentally measured geometric imperfections from (a) girder B14 and (b) girder B15.	76
Figure. 5.26	Ultimate strength of longitudinally unstiffened and stiffened steel plate girders using experimentally measured geometric imperfections from (a) girder B16 and (b) girder B17.	76
Figure. 5.27	Ultimate strength of longitudinally unstiffened steel plate girders using experimentally measured imperfections from the originally unstiffened girders.	77
Figure. 5.28	Ultimate strength of longitudinally stiffened steel plate girders using experimentally measured imperfections from the originally stiffened girders employing (a) relatively weak ($\gamma_s = 21.67$) and (b) strong longitudinal stiffener ($\gamma_s = 103.46$).	77
Figure. 5.29	Ultimate strength of longitudinally unstiffened and stiffened steel plate girders using geometric imperfections from buckling mode: (a) 1 st mode; (b) 2 nd mode.	78
Figure. 5.30	Ultimate strength of longitudinally unstiffened and stiffened steel plate girders using geometric imperfections from buckling mode: (a) 3 rd mode; (b) combination of modes (1 st + 2 nd + 3 rd).	78
Figure. 5.31	Strengthening effect employing the buckling modes as initial geometric imperfections for girders of Series A.	79
Figure. 5.32	Ultimate strength of longitudinally unstiffened and stiffened steel plate girders using the first (a) and second buckling mode shape (b) as initial geometric imperfections.	79
Figure. 5.33	Ultimate strength of longitudinally unstiffened and stiffened steel plate girders using the third (a) and combination (b) of buckling mode shapes (1 st + 2 nd + 3 rd) as initial geometric imperfections.	80

Figure. 5.34	Ultimate strength of longitudinally unstiffened and stiffened steel plate girders using sine (a) and cosine (b) hand-defined geometric imperfections. Web panel aspect ratio $\alpha = 1$	80
Figure. 5.35	Ultimate strength of longitudinally unstiffened and stiffened steel plate girders using sine (a) and cosine (b) hand-defined geometric imperfections. Web panel aspect ratio $\alpha = 2$	81
Figure. 5.36	Strengthening effect employing initial geometric imperfections by sine and cosine functions for (a) girders of Series A and (b) girders of Series B ($\gamma_s = 21.67$).	81
Figure. 5.37	Ultimate strength of longitudinally (a) unstiffened and (b) stiffened steel plate girders using various geometric imperfections. Web panel aspect ratio $\alpha = 1$	82
Figure. 5.38	Ultimate strength of longitudinally unstiffened steel plate girders using various geometric imperfections. Web panel aspect ratio $\alpha = 2$	83
Figure. 5.39	Ultimate strength of longitudinally stiffened steel plate girders using various geometric imperfections employing (a) relatively weak ($\gamma_s = 21.67$) and (b) strong longitudinal stiffener ($\gamma_s = 103.46$). Web panel aspect ratio $\alpha = 2$	84
Figure. 6.1	(a) Contour plot of experimentally measured geometric imperfection B1. (b) Center line cross-section of the first buckling mode-affine (unstiffened girders), cosine hand-defined, and experimentally measured geometric imperfection B1.	91
Figure. 6.2	Center line cross-section of the first three buckling mode-affine geometric imperfections (magnified 50 times) and corresponding failure modes at collapse (magnified 5 times) for longitudinally unstiffened and stiffened steel plate girders for $s_s/h_w = 0.10$	93
Figure. 6.3	Center line cross section of the first three buckling mode-affine geometric imperfections (magnified 50 times) and corresponding failure modes at collapse (magnified 5 times) for longitudinally unstiffened and stiffened steel plate girders for $s_s/h_w = 0.30$	94
Figure. 6.4	Out-of-plane displacement (units are in mm) and failure mechanism for longitudinally unstiffened and stiffened steel plate girders at ultimate load level for $s_s/h_w = 0.10$. The first buckling mode-affine geometric imperfections are employed. Deformation is magnified ten times.	95
Figure. 6.5	Out-of-plane displacement (units are in mm) and failure mechanism for longitudinally unstiffened and stiffened steel plate girders at ultimate load level for $s_s/h_w = 0.30$. The first buckling mode-affine geometric imperfections are employed. Deformation is magnified ten times.	95

Figure. 6.6	Deformed shape at collapse for girder A5 [21] (left) and third buckling mode (right). Units are in mm.	96
Figure. A.1	Universal Testing Machine Shimadzu AG-Xplus and extensometer with an initial length of 50 mm.	113
Figure. A.2	Typical coupon specimen failure.	114
Figure. A.3	Engineering stress-strain diagram for different coupon tests for web panel – B1.	115
Figure. A.4	Engineering stress-strain diagram for different coupon tests for web panel – B2.	115
Figure. A.5	Engineering stress-strain diagram for different coupon tests for web panel – B3.	116
Figure. A.6	Engineering stress-strain diagram for different coupon tests for web panel – B4.	116
Figure. A.7	Engineering stress-strain diagram for different coupon tests for web panel – B5.	117
Figure. A.8	Engineering stress-strain diagram for different coupon tests for web panel – B6.	117
Figure. A.9	Engineering stress-strain diagram for different coupon tests for web panel – B7.	118
Figure. B.1	Girder A14 with stiffening $s_s = 0$ mm: initial deformation (top left), residual deformation (top right), and increase in deformation (bottom) [mm].	119
Figure. B.2	Girder A15 without stiffening $s_s = 0$ mm: initial deformation (top left), residual deformation (top right), and increase in deformation (bottom) [mm].	120
Figure. B.3	Girder A4 with stiffening $s_s = 25$ mm: initial deformation (top left), residual deformation (top right), and increase in deformation (bottom) [mm].	120
Figure. B.4	Girder A12 without stiffening $s_s = 25$ mm: initial deformation (top left), residual deformation (top right), and increase in deformation (bottom) [mm].	120
Figure. B.5	Girder A3 with stiffening $s_s = 50$ mm: initial deformation (top left), residual deformation (top right), and increase in deformation (bottom) [mm].	121
Figure. B.6	Girder A1 without stiffening $s_s = 50$ mm: initial deformation (top left), residual deformation (top right), and increase in deformation (bottom) [mm].	121

Figure. B.7	Girder A17 with stiffening $s_s = 75$ mm: initial deformation (top left), residual deformation (top right), and increase in deformation (bottom) [mm].	121
Figure. B.8	Girder A5 with stiffening $s_s = 100$ mm: initial deformation (top left), residual deformation (top right), and increase in deformation (bottom) [mm].	122
Figure. B.9	Girder A11 without stiffening $s_s = 100$ mm: initial deformation (top left), residual deformation (top right), and increase in deformation (bottom) [mm].	122
Figure. B.10	Girder A6 with stiffening $s_s = 125$ mm: initial deformation (top left), residual deformation (top right), and increase in deformation (bottom) [mm].	122
Figure. B.11	Girder A7 with stiffening $s_s = 150$ mm: initial deformation (top left), residual deformation (top right), and increase in deformation (bottom) [mm].	123
Figure. B.12	Girder A16 with stiffening $s_s = 150$ mm: initial deformation (top left), residual deformation (top right), and increase in deformation (bottom) [mm].	123
Figure. B.13	Girder A2 without stiffening $s_s = 150$ mm: initial deformation (top left), residual deformation (top right), and increase in deformation (bottom) [mm].	123
Figure. B.14	Girder A13 without stiffening $s_s = 150$ mm: initial deformation (top left), residual deformation (top right), and increase in deformation (bottom) [mm].	124
Figure. C.1	Girder B13 with stiffening $s_s = 0$ mm: initial deformation (top left), residual deformation (top right), and increase in deformation (bottom) [mm]. The dashed lines represent the longitudinal stiffener.	125
Figure. C.2	Girder B16 without stiffening $s_s = 0$ mm: initial deformation (top left), residual deformation (top right), and increase in deformation (bottom) [mm]. The dashed line represents the longitudinal stiffener.	126
Figure. C.3	Girder B14 without stiffening $s_s = 25$ mm: initial deformation (top left), residual deformation (top right), and increase in deformation (bottom) [mm]. The dashed line represents the longitudinal stiffener.	126
Figure. C.4	Girder B3 with stiffening $s_s = 50$ mm: initial deformation (top left), residual deformation (top right), and increase in deformation (bottom) [mm]. The dashed line represents the longitudinal stiffener.	126
Figure. C.5	Girder B1 without stiffening $s_s = 50$ mm: initial deformation (top left), residual deformation (top right), and increase in deformation (bottom) [mm].	127

Figure. C.6	Girder B5 with stiffening $s_s = 100$ mm: initial deformation (top left), residual deformation (top right), and increase in deformation (bottom) [mm]. The dashed line represents the longitudinal stiffener. 127
Figure. C.7	Girder B15 without stiffening $s_s = 100$ mm: initial deformation (top left), residual deformation (top right), and increase in deformation (bottom) [mm]. The dashed line represents the longitudinal stiffener. 127
Figure. C.8	Girder B7 with stiffening $s_s = 150$ mm: initial deformation (top left), residual deformation (top right), and increase in deformation (bottom) [mm]. The dashed line represents the longitudinal stiffener. 128
Figure. C.9	Girder B17 with stiffening $s_s = 150$ mm: initial deformation (top left), residual deformation (top right), and increase in deformation (bottom) [mm]. The dashed lines represent the longitudinal stiffener. 128
Figure. C.10	Girder B2 without stiffening $s_s = 150$ mm: initial deformation (top left), residual deformation (top right), and increase in deformation (bottom) [mm]. 128
Figure. C.11	Girder B4 with stiffening $s_s = 200$ mm: initial deformation (top left), residual deformation (top right), and increase in deformation (bottom) [mm]. The dashed line represents the longitudinal stiffener. 129
Figure. C.12	Girder B12 without stiffening $s_s = 200$ mm: initial deformation (top left), residual deformation (top right), and increase in deformation (bottom) [mm]. 129
Figure. C.13	Girder B6 with stiffening $s_s = 250$ mm: initial deformation (top left), residual deformation (top right), and increase in deformation (bottom) [mm]. The dashed line represents the longitudinal stiffener. 129
Figure. C.14	Girder B11 without stiffening $s_s = 250$ mm: initial deformation (top left), residual deformation (top right), and increase in deformation (bottom) [mm]. 130

List of Tables

2.1	Experimental tests of longitudinally stiffened I-shaped steel plate girders reinforced by a single longitudinal stiffener subjected exclusively to patch loading. . .	10
3.1	Geometrical and material characteristics of all the test plate girders of Series B.	18
3.2	Maximum amplitude of initial geometric web panel imperfections for the girders tested once.	20
3.3	Experimentally obtained ultimate strengths for all the tested girders of Series B.	24
4.1	Geometric characteristics of the experimentally tested girders of Series A.	42
4.2	Comparison between the experimentally and numerically obtained ultimate strengths for all the girders of A series. Units are in kN.	51
4.3	Comparison between the experimentally and numerically obtained ultimate strengths for all the girders of Series B. Units are in kN.	52
5.1	Parameters varied in the parametric study.	58
5.2	Parameters kept unaltered in the parametric study for both series A and B.	58
5.3	Patch loading resistance of longitudinally unstiffened steel plate girders ($F_{FEA,unstiff}$) for various geometric imperfections for girders of Series A. Units are in kN.	64
5.4	Normalized patch loading resistance of longitudinally stiffened steel plate girders ($F_{FEA,stiff}/F_{FEA,unstiff}$) for various geometric imperfections for girders of Series A.	65
5.5	Patch loading resistance of longitudinally unstiffened steel plate girders ($F_{FEA,unstiff}$) for various geometric imperfections for girders of Series B. Units are in kN.	66
5.6	Normalized patch loading resistance of longitudinally stiffened steel plate girders ($F_{FEA,stiff}/F_{FEA,unstiff}$) for various geometric imperfections for girders of Series B. Relative stiffness $\gamma_s = 21.67$	67
5.7	Normalized patch loading resistance of longitudinally stiffened steel plate girders ($F_{FEA,stiff}/F_{FEA,unstiff}$) for various geometric imperfections for girders of Series B. Relative stiffness $\gamma_s = 103.46$	68
5.8	Ratio between the ultimate strength of steel plate girders for web panel aspect ratios $\alpha = 1$ and $\alpha = 2$	83
5.9	Numerically obtained ultimate strengths using three different web panel yield stresses for the $\alpha = 2$ case. Units are in kN.	86
A.1	Web panel material properties of all the test steel plate girders of Series B.	114

A.2 Flange material properties of all the test steel plate girders of Series B. 114

Nomenclature

Abbreviations

CAD	Computer-Aided Design
DOF	Degree of Freedom
FEA	Finite Element Analysis
NURBS	Non-Uniform Rational B-Spline

Greek lower case letters

α	web panel aspect ratio ($\alpha = a/h_w$)
β	strengthening effect ($\beta = F_{stiff}/F_{unstiff}$)
χ_F	reduction factor due to local buckling
ϵ_{eng}	engineering strain
ϵ_{ln}	true strain
γ^*	limit value of relative stiffness of the longitudinal stiffener
γ_s	relative stiffness of the longitudinal stiffener
γ_{M1}	partial safety factor
σ_{eng}	engineering stress
σ_{true}	true stress
σ_{vm}	von Mises stress

Roman lower case letters

a	web panel width
b_1	longitudinal stiffener position from the loaded flange
b_f	flange width

b_{st}	longitudinal stiffener width
f_t	flange thickness
f_{uf}	flange ultimate tensile stress
f_{uw}	web panel ultimate tensile stress
f_{yf}	flange yield stress
f_{yw}	web panel yield stress
h_w	web panel depth
k_F	buckling coefficient
l_y	effective loaded length
s_s	patch load length (bearing length)
t_{st}	longitudinal stiffener thickness
t_w	web panel thickness
w_0	imperfection amplitude

Roman upper case letters

E	Young's modulus
F	localized compressive edge load (patch loading)
F_{cr}	critical buckling load
$F_{exp,stiff}$	experimentally obtained ultimate strength of longitudinally stiffened steel plate girders
$F_{exp,unstiff}$	experimentally obtained ultimate strength of longitudinally unstiffened steel plate girders
$F_{FEA,stiff}$	numerically obtained ultimate strength of longitudinally stiffened steel plate girders
$F_{FEA,unstiff}$	numerically obtained ultimate strength of longitudinally unstiffened steel plate girders
S	deviatoric stress tensor

Other symbols used are explained as they appear in the text.

Chapter 1

Introduction

1.1 Motivation

A plate girder is a beam built up of steel plates and shapes connected by welding, bolting, or riveting to form a deep flexural member that a rolling steel mill or factory cannot produce. As such, it is capable of supporting greater loads on longer spans that standard rolled beams or trusses cannot economically carry. Besides a myriad of advantages (e.g., economical, aesthetical, fast to fabricate and erect, et cetera), one of the most important demerits of the plate girders is susceptibility to buckling since they consist of deep web plates. In order to prevent web buckling, plate girders are reinforced with stiffening members, which is usually a more economical approach than using a stockier web. Longitudinal stiffeners are primarily used to increase the bending strength of plate girders, while transverse stiffeners are commonly used to increase shear strength. However, a stability control check for concentrated transverse forces (patch loading) should also be performed, as it could be a decisive design criterion.

Patch loading or partially distributed load is a special load case in which plate and box girders are subjected to localized compressive edge loads in the plane of the web. This load case is present in many applications, including beam-beam and beam-column connections as well as deep crane runway beams loaded by crane wheels. The most realistic load case is during the incremental launching of multi-span steel and composite bridges over temporary or permanent supports. In this case, the patch load appears by means of high reaction forces of a roller acting on the bottom flange. As the load changes continuously in those situations, transversal stiffeners cannot be efficiently used. In all these applications, the girders are frequently supported at cross-sections where no vertical web stiffener exists, and the load is transferred into the web panel through the loaded flange in the plane of a web or eccentrically. It has been observed that the ultimate carrying patch load capacity is achieved after local web buckling and deformation of the loaded flange in the vicinity of load introduction (see Fig. 1.1), while the behavior of the girder is characterized by geometrical and material nonlinearities. By using longitudinal stiffeners for flexural and shear strength, the patch loading resistance can be increased as well. Therefore, knowing the influence of longitudinal stiffeners on the ultimate strength and behavior

of plate girders can result in more elegant and economical designs.

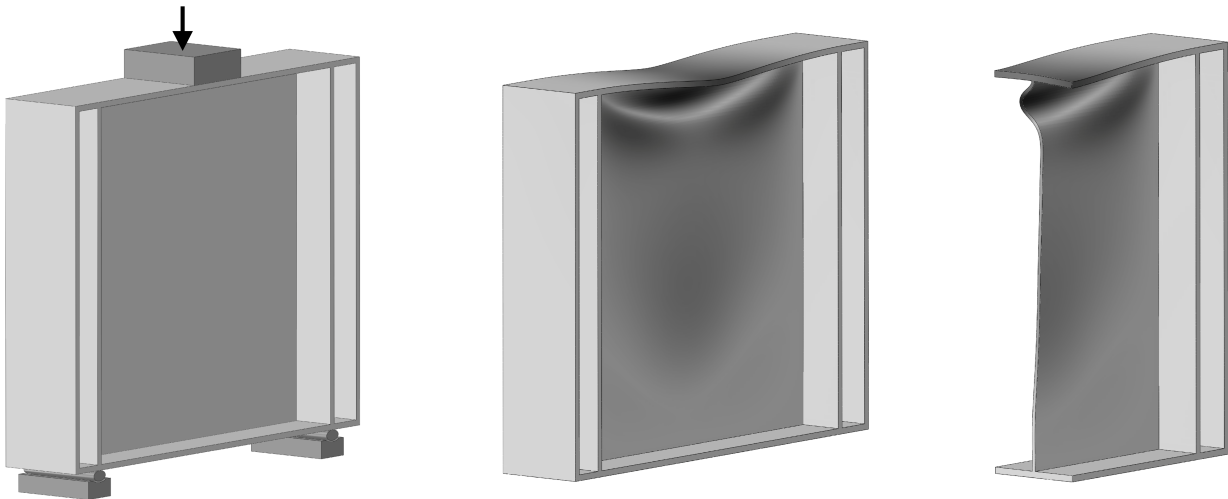


Figure 1.1: Thin-walled plate girder subjected to localized compressive edge load and typical failure mode.

Due to its complexity, the patch loading phenomenon has been extensively researched experimentally and numerically in recent decades. Many geometric and physical parameters that influence the patch loading resistance have been considered: (i) thickness of the web panel, (ii) position, relative stiffness, and number of longitudinal stiffeners, (iii) stiffness of the loaded flange, (iv) yield strength of the loaded flange and web panel, (v) web panel aspect ratio, (vi) applied patch load length, (vii) coexistence of bending moment, et cetera. However, the patch load length has been examined in a limited number of experimental and numerical investigations considering steel plate girders with longitudinal stiffening. Hence, it is not well understood how patch load lengths influence the ultimate capacity of longitudinally stiffened girders. A detailed literature review regarding the utilization of patch load length in combination with longitudinally stiffened steel plate girders is given in the next Chapter. The review shows that studies with a systematic analysis of the influence of patch load length are not present in the literature.

Additionally, the current European design standard EN 1993-1-5 provides a design procedure for determining the patch loading resistance of longitudinally unstiffened and stiffened steel plate girders. However, it has been shown that experimentally and numerically obtained ultimate strengths are not well captured by the design procedure, and certain improvements have been proposed. Most of these improvements are related to the critical load calculation of longitudinally stiffened webs or the effect of the flange yield strength on the patch loading resistance of longitudinally unstiffened plate girders with high slenderness ratios and largely spaced transverse stiffeners. In addition to this resistance model, the current design standard also allows the use of finite element analysis for the ultimate limit state. The essential data for an adequate ultimate limit state design comprises information on unavoidable geometric and structural imperfections. However, the design standard lacks information on these imperfections.

Therefore, there is a need to better understand the influence of various patch load lengths on the patch loading resistance. Moreover, further improvement of the current design standard, design recommendations, and information on imperfections for patch loading are highly indispensable. The current research is primarily devoted to the assessment of the influence of patch load length on the ultimate strength of longitudinally stiffened steel plate girders. The present experimental study was planned as a dual-purpose investigation with the goals (i) to recognize the influence of patch load length on the ultimate strength of longitudinally stiffened plate girders and (ii) to serve for calibration and verification of the numerical model employed in subsequent numerical analyses. The experimental campaign contained a limited number of tests with several different patch load lengths. The range of patch load length was then broadened up in the numerical analysis. The numerical model was further exploited to examine the influence of various geometric imperfections, along with patch load length, on the ultimate strength of longitudinally unstiffened and stiffened steel plate girders. This analysis on geometric imperfections complements the EN 1993-1-5 rules for numerical modeling. Unfavorable geometric imperfections from the patch loading point of view are determined, and geometric imperfection shapes for numerical analysis are recommended.

1.2 Goals

The driving force for this research was the fact that the influence of patch load length on the ultimate strength and behavior of longitudinally stiffened steel plate girders subjected exclusively to patch loading has not been systematically studied in the literature. The focal point is on longitudinally stiffened girders, while unstiffened ones serve to provide an ultimate reference load and for strengthening effect determination. One of the goals of this dissertation is to give a contribution to the patch load phenomenon and provide new experimental results in this field. In addition to the experimental investigation, this dissertation also includes finite element analysis for the ultimate limit state allowed by the current European design standard EN 1993-1-5. The numerical part aims to incorporate initial geometric imperfections into numerical models, their influence on the ultimate strength and behavior of longitudinally unstiffened and stiffened plate girders, and determination of unfavorable geometric imperfection (from the patch loading point of view) in combination with the patch load length.

1.3 Objectives

The main objective of this work is to scrutinize the influence of patch load length on the ultimate strength and behavior of longitudinally unstiffened and stiffened thin-walled I-section steel plate girders reinforced by a single longitudinal stiffener. The problem is examined by performing experimental and numerical studies. The objective of the experimental investigation

is to disclose the influence of patch load length on patch loading resistance and to set up a background for numerical modeling.

The numerical study has several objectives. The main objective of the numerical part is to consider the influence of a wide range of patch load lengths in combination with various geometric imperfections on the ultimate strength and behavior of longitudinally unstiffened and stiffened steel plate girders. Imperfection sensitivity analysis is designed with the objective to resolve shortcomings of current EN 1993-1-5 regarding the use of geometric imperfections in FEA. Moreover, the determination of unfavorable geometric imperfections is also one of the targets in this research.

1.4 Methodology

Analytical, experimental, and numerical methods are executed throughout this dissertation for:

- Analysis of previous experimental investigations conducted on longitudinally stiffened I-shaped steel plate girders reinforced by a single longitudinal stiffener subjected exclusively to patch loading.
- Conducting own experimental testing for determining the ultimate strength and behavior of longitudinally unstiffened and stiffened steel plate girders. In addition, experimental testing for the material characteristics of the web panel and flanges of each girder is performed using multiple standard tensile coupon tests.
- Developing 3D finite element models of plate girders subjected to patch loading that include geometric and material properties, loading, and supporting conditions based on the experimental investigation.
- Calibration and verification of the finite element model for further numerical analyses.
- Performing a parametric study in which a variety of geometric imperfections are considered.
- Determining the influence of patch load length and geometric imperfections on the patch loading resistance, providing design recommendations, and information on unfavorable geometric imperfections

1.5 Thesis layout

The remainder of the dissertation is organized as follows.

Chapter 2 introduces a comprehensive literature overview of experimental and numerical researches conducted on longitudinally stiffened steel plate girders. Based on this review, one can observe that the influence of patch load length was not sufficiently explored in previous experimental and numerical studies. In addition, the influence of various geometric imperfections and the definition of unfavorable geometric imperfections (from the patch loading point of view) are not present in the literature. This Chapter also briefly presents the current EN 1993-1-5 patch loading resistance model used later in the text.

Chapter 3 presents the own experimental campaign performed on thin-walled I-section steel plate girders subjected to patch loading. The study considered longitudinally unstiffened and stiffened girders reinforced by a single flat longitudinal stiffener. The experimental investigation included a total of eight tests. The ultimate capacity and behavior of the girders are presented and discussed thoroughly.

Chapter 4 describes the finite element model used in the numerical part of this research. The employed girder geometry, finite element mesh, boundary and loading conditions, material properties, and initial imperfections are defined. The reliability and accuracy of the numerical model were attested by comparison with experimental data, including a total of twenty-eight tests. The experimentally and numerically obtained patch loading resistances are juxtaposed, followed by comparison of elastoplastic behavior between the experimental and numerical approaches.

Chapter 5 gives a finite element parametric study, in which geometric imperfections, patch load lengths, web panel aspect ratio, and relative stiffnesses of the longitudinal stiffener were varied, while the other geometric parameters were unaltered. Experimentally measured, buckling mode-affine, and hand-defined sinusoidal geometric imperfections were varied in the parametric study along with a variety of patch load lengths. A numerical database of nine hundred simulations was created. The obtained results for each geometric imperfection are presented and thoroughly discussed. Additionally, the influence of the web panel aspect ratio and relative stiffness of the longitudinal stiffener is also given in this Chapter.

Chapter 6 brings analysis and discussion on unfavorable geometric imperfections in steel plate girders subjected to patch loading. Both longitudinally unstiffened and stiffened steel plate girders were considered. Unfavorable geometric imperfections were defined considering geometric imperfections used in Chapter 5 and various relative stiffnesses of the longitudinal stiffener.

Chapter 7 summarizes this work and the main conclusions, along with design recommendations and proposals for further research, are presented.

Additional supplement materials are provided in Appendices. **Appendix A** shows the steel materials properties of the test girders determined by using multiple standard tensile coupon tests. **Appendix B** and **Appendix C** show experimentally measured web panel deformations for two series of girders. These deformations are represented as contour plots of

initial and residual web panel deformations, including an increase in deformation (the difference between the residual and initial deformation).

1.6 Selected publications

The present research is sequentially published in the following papers along with several international conference proceedings

- S. Kovacevic, N. Markovic, D. Sumarac, R. Salatic, Unfavorable geometric imperfections in steel plate girders subjected to localized loads, *Thin-Walled Struct.* 161 (2021) 107412. <https://doi.org/10.1016/j.tws.2020.107412>
- S. Kovacevic, N. Markovic, Experimental study on the influence of patch load length on steel plate girders, *Thin-Walled Struct.* 151 (2020) 106733. <https://doi.org/10.1016/j.tws.2020.106733>
- S. Kovacevic, N. Markovic, D. Sumarac, R. Salatic, Influence of patch load length on plate girders. Part II: Numerical research, *J. Constr. Steel Res.* 158 (2019) 213-229. <https://doi.org/10.1016/j.jcsr.2019.03.025>
- N. Markovic, S. Kovacevic, Influence of patch load length on plate girders. Part I: Experimental research, *J. Constr. Steel Res.* 157 (2019) 207-228. <https://doi.org/10.1016/j.jcsr.2019.02.035>

Chapter 2

Literature review

The patch loading phenomenon started extensively to be investigated in the late 1960s and early 1970s. The first studies were experimental investigations concerning elastic critical buckling and ultimate capacity of longitudinally unstiffened plate girders. Shortly thereafter, the problem included stiffened plate girders. With software development and computational power in the late 1990s and early 2000s, numerical techniques suppressed experimental studies. In this period, the patch loading problem was more analyzed numerically than experimentally. Due to its complexity, the validation of numerical models is performed by comparing their outputs with experimental data. This shows the importance of experimental investigations for this problem. Numerical models are usually verified by several experimental tests. However, in this dissertation, the numerical model is validated by comparison with own and a previous experimental study consisting of twenty-eight tests in total.

Previous experimental and numerical studies considering longitudinally stiffened I-shaped steel plate girders reinforced by a single longitudinal stiffener subjected exclusively to patch loading are presented in this Chapter. In addition, the resistance model defined by the current European design standard EN 1993-1-5 is also briefly presented in this Chapter for readability. It is used throughout the dissertation for comparison with experimental and numerical results.

2.1 Experimental study

This Chapter aims to highlight in a concise way previous experimental studies conducted so far and available in the literature to show that for longitudinally stiffened steel plate girders, the influence of patch load length was not systematically analyzed. Only thin-walled I-section longitudinally stiffened steel plate girders locally loaded in the plane of the web were considered. After carefully updating the available literature, a database that includes sixteen experimental studies (including the current experimental investigation – Chapter 3) with a total of one hundred and seventy-four individual tests is formed. In all these tests, the case of patch

loading applied individually was considered – that is, tests including combine action between patch loading and/or bending and/or shear were not included. Table 2.1 recaps this Chapter and shows applied patch load lengths along with a number of tests analyzed by different authors. The focal point is on patch load length while other details about the experiments are not given and the interested reader is referred to the original references. The patch load length, s_s , is expressed as an absolute value and with respect to the web panel width a or the web panel depth h_w ; usual approach to present this parameter.

Previous experimental investigations considering longitudinally stiffened thin-walled I-section steel plate girders subjected exclusively to patch loading (locally loaded in the plane of the web panel), arranged chronologically, can be found in Refs. [1–25]. In all these studies, different parameters that influence the behavior and ultimate load of longitudinally stiffened steel plate girders are considered – that is, thickness of the web panel, position and stiffness of longitudinal stiffeners, stiffness of the loaded flange, and web panel aspect ratio. Apart from the previous experimental study [21] (summarized in Refs. [24–25]; see the description in Table 2.1), the patch load length, s_s , in the previous experimental studies [1–20,22–23] was mostly constant, and its effect on the ultimate strength has not been systematically investigated. The relevant data (expressed as s_s/a and s_s/h_w) regarding all these experimental investigations [1–25] are given in Table 2.1, while more information can be found in the original references. Apart from the patch loading case, other similar stability problems and load cases are given in these references.

The first experimental works on thin-walled I-section girders with and without longitudinal stiffening were performed by Rockey and Bergfelt [1–3]. From fifty-nine tests, nineteen tests were conducted on longitudinally stiffened steel plate girders using a flat stiffener. The primary purpose of this experimental study was to obtain information about the influence of horizontal stiffeners on the level of the limit load. In these studies, the length of applied patch load was $s_s = 40$ and 120 mm.

A comprehensive study was governed by Roberts and Markovic with fourteen tests on short steel plate girders including both longitudinally unstiffened and stiffened girders with different patch load lengths $s_s = 0, 50, \text{ and } 100$ mm. The results are originally presented in Ref. [4] and later used in Ref. [5]. This research aimed to gain a better insight into the ultimate bearing capacity and shape of failure with a relatively thick web and the behavior of girders with a thin and horizontally stiffened web with a flat stiffener. Only two tests considering longitudinally stiffened steel plate girders with a constant patch load length of 50 mm were investigated.

Oxford [6] performed an experimental campaign considering centrally and eccentrically loaded plate girders. The campaign included both longitudinally stiffened and unstiffened girders while the patch load length was kept constant $s_s = 100$ mm for all the tests. Reportedly, only one case included longitudinally stiffened steel plate girders loaded centrally. Shimizu et al. in Refs. [7–8] were investigated the influence of greater length of patch load on very long

girders (girder span 6 m and 9 m) with transverse stiffeners placed equally at a distance of 0.6 and 1.0 m. The aim of the study was to simulate installation conditions in a construction assembly stage. The length of applied patch load was varied using very high values compared to other researches $s_s = 180, 300, \text{ and } 500$ mm. A total of ten tests was reported. Only one experimental girder was longitudinally stiffened by a flat stiffener (single-sided flat-bar) loaded by a patch load length of 300 mm. In the same year, Galea et al. [9] examined two experimental tests of longitudinally stiffened steel plate girders with a flat stiffener with a constant patch load length of 690 mm.

Skaloud et al. [10–15] conducted the most extensive experimental research with one hundred and fifty-two tests including stiffened and unstiffened steel plate girders. Those results were sequentially published in different reports [10–14], while all results were gathered in Ref. [15]. The investigation was planned to obtain more information about the influence of the position and stiffness of longitudinal stiffeners, type of longitudinal stiffening (stiffener on one or both sides of the web panel), web panel aspect ratio, and stiffness of loaded flange on the ultimate carrying capacity. In this research, there were one hundred and one tests considering longitudinally stiffened steel plate girders with various patch load lengths $s_s = 50, 62, \text{ and } 100$ mm.

A test program of seventy-two tests considering unstiffened and stiffened steel girders was performed by Dubas and Tschamper [16] to better examine the impact of patch load length and the influence of different types of stiffeners on the ultimate capacity. Sixteen tests were conducted on stiffened web plates, and the length of applied patch load was amounted to $s_s = 40$ and 240 mm. Eight girders were longitudinally stiffened with a small torsional rigidity stiffener (single-sided flat-bar) and eight girders had a high torsional rigidity stiffener (closed-section). A series of two tests is performed by Dogaki et al. [17], and the same number of tests is conducted by Salkar [18]. In these two researches [17–18], the patch load length was constant $s_s = 90$ and 127 mm, respectively. In addition, Carretero and Lebet [19] performed an experimental investigation where six longitudinally stiffened steel plate girders using closed-section stiffeners were considered from a total of fourteen tests. In all tests, the patch load length was amounted to 200 and 300 mm. Walbridge and Lebet [20] performed five experimental tests on longitudinally stiffened steel plate girders using closed-section and flat stiffeners. In this analysis, except for the type of longitudinal stiffeners, the main research was dedicated to the position of longitudinal stiffeners while the patch load length was set to $s_s = 200$ mm.

An experimental investigation conducted by Markovic [21] represents an analysis in which the patch load length was varied the most. The study included longitudinally stiffened and unstiffened steel plate girders. A total of twenty tests was performed. Eight steel plate girders with $\alpha = 1$ and four girders with $\alpha = 2$ were longitudinally stiffened with a flat stiffener. The patch load length was varied from $s_s = 0$ mm to $s_s = 150$ mm. The most recent experimental results were obtained by Kuhlmann and Seitz [22–23]. The investigation included longitudinally unstiffened and stiffened plate girders using one or two rigid stiffeners. The study

aimed to investigate the influence of number and position of longitudinal stiffeners and interaction with bending and shear. From a total of seven tests reported, two tests were performed considering pure patch loading case and longitudinally stiffened steel plate girders. The patch load length was constant and assembled by four equally spaced lengths of 100 mm with a total length of 700 mm.

It should be highlighted that some of those experimental tests are also collected in Refs. [22,26–35], but the present literature review is the most detailed one.

Based on this literature review of the existing experimental results, it is clear that the influence of patch load length on longitudinally stiffened steel plate girders was not systematically studied. Analyses considering greater rates of change of this parameter were not presented. That was the driving force for the present experimental investigation to contribute to the patch loading phenomenon.

Table 2.1: Experimental tests of longitudinally stiffened I-shaped steel plate girders reinforced by a single longitudinal stiffener subjected exclusively to patch loading.

Reference	Year	Number of tests	s_s/a	s_s/h_w	s_s [mm]
Rockey et al. [1]	1978	4	0.05	0.05	40
Bergfelt [2–3]	1979&1983	15	0.01-0.11	0.05-0.16	40 (13), 120 (2)
Roberts & Markovic [4–5]	1981	2	0.1	0.1	50
Oxford [6]	1983	1	0.05	0.08	100
Shimizu et al. [7–8]	1987	1	0.5	0.3	300
Galea et al. [9]	1987	2	0.39	0.54	690
Janus et al. [10–15]	1988	101	0.1	0.1-0.2	50 (71), 62 (18), 100 (12)
Dubas & Tschamper [16]	1990	16	0.02-0.14	0.04-0.24	40 (8), 240 (8)
Dogaki et al. [17]	1991	2	0.1	0.1	90
Salkar [18]	1992	2	0.2	0.2	127
Carretero & Lebet [19]	1998	6	0.19-0.25	0.38-0.5	200 (2), 300 (4)
Walbridge & Lebet [20]	2001	5	0.2	0.29	200
Markovic [21] ¹	2003	8	0-0.3	0-0.3	0, 25, 50, 75, 100, 125, 150 (2)
Markovic [21] ²	2003	4	0.05-0.15	0.1-0.3	50, 100, 150 (2)
Kuhlmann & Seitz [22-23]	2004	2	0.58	0.30	700
Kovacevic & Markovic [24] ³	2020	3	0-0.25	0-0.5	0, 200, 250

(.) denotes the number of tests for a given patch load length

¹ Originally published in Ref. [21] and summarized in Ref. [25] (steel plate girders with $\alpha = 1$)

² Originally given in Ref. [21] and summarized in Ref. [24] (steel plate girders with $\alpha = 2$, labeled B3, B5, B7, B17)

³ Experimental tests given in this dissertation (Chapter 3) and published in Ref. [24] (steel plate girders with $\alpha = 2$, labeled B4, B6, B13)

2.2 Numerical study

Scarce work has been found in the literature for the influence of patch load length on the ultimate capacity of longitudinally stiffened steel plate girders examined numerically. In addition, the focus is only on longitudinally stiffened steel plate girders loaded centrally without web openings (cut-outs). For more general reviews, including plate girders subjected to different types of loading, Refs. [36–37] are recommended.

There exists an appreciable amount of literature on the influence of initial geometric imperfections on the patch loading resistance of longitudinally stiffened steel plate girders, but the patch load length and ratios s_s/a and s_s/h_w were mostly constant or not changed in a wide range. For instance, extensive parametric studies carried out on longitudinally stiffened steel plate girders examining the influence of the position of a longitudinal stiffener using different initial geometric imperfection shapes were performed by Graciano et al. [32,38–43]. In all these analyses, the patch load length was kept constant.

Chacon et al. in Refs. [44–45] managed another comprehensive numerical research conducted on longitudinally stiffened steel plate girders, varying the web thickness, flange yield strength, thickness, and position of the longitudinal stiffener. Again, the patch load length was held constant in these studies. Similarly, Kuhlmann and Seitz [22] performed an imperfection sensitivity study considering different shapes of initial geometric imperfections and their influence on the collapse load of longitudinally stiffened steel plate girders under a constant patch load length.

On the other hand, Graciano et al. in Refs. [46–47] applied different patch load lengths in order to get more information about elastic buckling coefficients varying the relative position of the longitudinal stiffener, its flexural rigidity, flange-to-web thickness ratio, and web panel aspect ratio α . A similar linear buckling and post-buckling analysis considering multiple longitudinally stiffened webs have been materialized by Loaiza et al. in Ref. [48] and Ref. [49], respectively. Moreover, elastic buckling analysis performed on longitudinally stiffened and unstiffened web panels under opposite patch loading considering three different patch load lengths was conducted by Mezghanni et al. [50]. A parametric study performed by Kuhlmann and Seitz primarily investigating the influence of stiffener position on the magnification factor under three different patch load lengths is present in Ref. [23,51]. In addition, Maiorana et al. [52] used different values of patch loading length considering primary unstiffened webs with and without perforations. Three different patch load lengths were applied to stiffened webs without perforations. The main goal of the study was to juxtapose ultimate loads with critical ones of a single panel in a multi-panel beam with the whole beam.

Additionally, an extensive finite element study including three hundred and sixty-six numerical simulations focusing on longitudinally stiffened webs has been accomplished by Davaine [26,53–55]. The study was mainly based on deep webs (e.g., from 2 to 5 m). Patch load length was varied according to the web panel depth $s_s/h_w = 0.2 \div 1$ in combination with

different positions of the longitudinal stiffener. A parametric study including nine hundred models and varying different parameters – that is, geometry of the web panel (a, h_w, t_w), flange size (b_f, t_f), patch loading length s_s , location and number of longitudinal stiffeners and their size, has been conducted by Kövesdi [56]. The patch load length was varied from $s_s/a = 0.2$ to $s_s/a = 0.8$ with a total of six patch load lengths. Just recently, four different patch load lengths were incorporated into a numerical analysis performed by Loaiza et al. [34]. The main parameters that were varied are the web panel aspect ratio α and web panel thickness t_w .

All references mentioned above are based on the finite element method, which is the most popular computational tool due to its wide acceptance and versatility. It has been successfully applied in many papers regarding the ultimate strength of plate girders under different loading conditions. On the other hand, a few papers assess the ultimate capacity of plate girders under patch loading or combined action of patch loading and bending using a different numerical technique, for instance, in Refs. [57–58] and Ref. [59], the finite difference method has been used to determine the ultimate and critical loads, respectively, in Refs. [60–61] the dynamic relaxation method is adopted as a numerical analysis method. Additionally, in Ref. [62], the finite strip method has been employed as a computational tool to obtain critical loads of longitudinally stiffened webs under patch loading. In all these references [57–62], the patch load length was constant or varied in a small range.

2.3 European design standard EN 1993-1-5

The design procedure for determining the patch loading resistance of steel plate girders according to the design standard EN 1993-1-5 is briefly given below. The design procedure for longitudinally unstiffened webs was originally proposed in Ref. [63], while the effect of longitudinal stiffening is included according to the work of [64]. According to this model, the patch loading resistance can be determined as [65]

$$F_{Rd} = \chi_F \frac{l_y \cdot f_{yw} \cdot t_w}{\gamma_{M1}}, \quad (2.1)$$

where χ_F is the reduction factor due to local buckling, γ_{M1} is the partial safety factor, and l_y is the effective loaded length defined as

$$l_y = s_s + 2 \cdot t_f \cdot (1 + \sqrt{m_1 + m_2}). \quad (2.2)$$

See Fig. 3.1 for general girder notation. The reduction factor χ_F should be obtained using the following expressions

$$\chi_F = \frac{0.5}{\bar{\lambda}_F} \leq 1.0 \quad \bar{\lambda}_F = \sqrt{l_y \cdot t_w \cdot f_{yw} / F_{cr}}. \quad (2.3)$$

In Eq. (2.2), the dimensionless parameter m_1 is equal to $m_1 = f_{yf} b_f / f_{yw} t_w$, while $m_2 = 0.02 \cdot (h_w / t_f)^2$ if $\bar{\lambda}_F > 0.5$ or $m_2 = 0$ if $\bar{\lambda}_F \leq 0.5$. In Eq. (2.3), F_{cr} represents the critical

buckling load calculated as

$$F_{cr} = 0.9 \cdot k_F \cdot E \cdot t_w^3 / h_w. \quad (2.4)$$

The buckling coefficient k_F for longitudinally unstiffened plate girders can be obtained as

$$k_F = 6 + 2 \cdot (h_w/a)^2, \quad (2.5)$$

while for longitudinally stiffened plate girders, the following expression can be applied

$$k_F = 6 + 2 \cdot (h_w/a)^2 + (5.44 \cdot b_1/a - 0.21) \cdot \sqrt{\gamma_s}, \quad (2.6)$$

where γ_s denotes the relative flexural stiffness of the longitudinal stiffener, defined as

$$\gamma_s = 10.9 \cdot \frac{I_{sl}}{h_w \cdot t_w^3} \leq \gamma^* \quad \gamma^* = 13 \cdot (a/h_w)^3 + 210 \cdot (0.3 - b_1/a). \quad (2.7)$$

In the above equation I_{sl} is the second moment of area of the longitudinal stiffener plus a width of web plate equal to $15 \cdot \epsilon \cdot t_w$ on each side of the stiffener (see clause 9.1(2) in [65] for more details, $\epsilon = \sqrt{235/f_{yw}[N/mm^2]}$); refer to Fig. 3.1 for general notation. Eq. (2.7) was originally developed performing linear buckling analysis, considering the variation of the buckling coefficient k_F in terms of the stiffener relative flexural rigidity γ_s . This equation can serve to classify longitudinal stiffeners as *weak* or *strong*. If the relative stiffness of the longitudinal stiffener γ_s is smaller than the limit value γ^* , the stiffener is classified as *weak*.

Remark: The contribution of patch load length to the ultimate strength is included linearly through the effective loaded length Eq. (2.2). The buckling coefficient of longitudinally unstiffened Eq. (2.5) and stiffened steel plate girder Eq. (2.6) is independent of patch load length (and stiffness of the loaded flange). Hence, the patch loading resistance varies linearly with patch load length, independently of applied load length, for both longitudinally unstiffened and stiffened steel plate girders. This dependence of ultimate strength on the patch load length is further tested in the current research.

Remark: Using the above equations for the patch loading resistance and with standard manipulations, one can show that the web panel yield stress, f_{yw} , influences the ultimate strength with a power of 0.5 – that is, $f_{yw}^{0.5}$. As given later in this dissertation, a higher value of 0.60–0.78 was obtained. More importantly, it was shown that this value is dependent on patch load length.

2.4 Summary

Detailed literature reviews of experimental and numerical investigations focusing on the influence of patch load length on the patch loading resistance of longitudinally stiffened steel plate girders are given in this Chapter. They show that studies primarily dedicated to the influence of patch load length are insufficiently present in the literature. Other parameters that influence

the ultimate capacity have been experimentally and numerically studied in the literature, while the patch load length was mostly constant or varied in a small range. That was the driving force for the present experimental investigation to contribute to the patch loading phenomenon. In addition, the current EN 1993-1-5 patch loading resistance model, with some observed remarks regarding the patch load length, is also presented in this Chapter.

Chapter 3

Experimental work

The author's experimental investigation was planned to continue and extend the extensive experimental study [21]. This experimental study consisted of two series of testing. The first series included steel plate girders with a web panel aspect ratio $\alpha = 1$ (hereafter Series A) and $\alpha = 2$ (hereafter Series B); refer to Chapter 2 and Table 2.1 for more details. Markovic [21] tested all the girders of Series A and girders B1, B3, B5, B2, B7, and B17 of Series B. Girders labeled B16, B13, B14, B15, B12, B4, B11, and B6 represent the author's work. Hence, the current experimental investigation given in this Chapter complements this series of testing. The whole experimental campaign (Series A and Series B) included twenty-eight tests conducted on fourteen steel plate girders (each girder was tested twice). For discussion and comparison with the previous experimental analysis [21], current European design standard EN 1993-1-5 [65], and available experimental results in the literature given in Section 3.2, all the steel plate girders of Series B are included. All measured data for girders B1, B3, B5, B2, B7, and B17 used in Section 3.2 were collected by Markovic [21].

For this testing investigation (all the girders of Series B), the web panel aspect ratio α was increased (more specifically, the distance between the vertical stiffeners at the supports: web panel width) compared to the girders of Series A [21] while the other geometric properties were unchanged. The patch load length was varied from $s_s = 0$ mm to $s_s = 250$ mm ($s_s/h_w = 0 \div 0.5$, $s_s/a = 0 \div 0.25$). Since the patch load length was insufficiently varied in the literature, the present experimental investigation was planned to eliminate this drawback and to elucidate the influence of patch load length on the ultimate strength and behavior of longitudinally stiffened steel plate girders. Apart from longitudinally stiffened steel plate girders, a few girders without longitudinal stiffening were included in this investigation. They served to provide an ultimate reference load for the stiffened ones. Details about the experiment, ultimate strength, and behavior of the experimentally tested girders are given in the next section, including all the girders of Series B. The experimentally obtained ultimate strengths, web panel deformations, and elastoplastic behavior of the tested girders are given in Section 3.2.

3.1 Experimental testing

The experimental research was performed on thin-walled I-section steel plate girders subjected to patch loading. The primary goal of this experimental study was to systematically investigate the ultimate strength and behavior of I-shaped steel plate girders subjected to various patch load lengths. The study considered longitudinally unstiffened and stiffened steel plate girders reinforced by a single flat longitudinal stiffener placed at one-fifth of the girder depth ($b_1 = 0.2h_w$), the optimum location for the flexural and shear resistance [66–68]. The main objective was to investigate the ultimate strength and behavior of longitudinally stiffened steel plate girders while unstiffened ones were used to determine the influence of longitudinal stiffening (strengthening effect β). The longitudinal stiffener and girders (except for the girder width) in this study were the same as in Refs. [15,21]; thus, a direct comparison could be made between these studies.

The whole experimental program (Series B) included fourteen tests (six tests conducted by Markovic in Ref. [21]) performed on seven welded I-shaped steel plate girders. The girders were assembled at the construction company “Mostogradnja” in Belgrade. They were designed as symmetrical and simply supported with transverse stiffeners at both ends. The experiments were carried out at the Laboratory for Testing Construction and Materials at the Faculty of Civil Engineering Podgorica, University of Montenegro. Using reliable modern equipment, experienced laboratory experts, excellent cooperation, professionalism, and experience from other experimental investigations [21,69–74], this experimental testing was accomplished and reliability of the results was guaranteed.

3.1.1 Test specimens

The longitudinally unstiffened steel plate girders were labeled B16, B14, B1, B15, B2, B12, and B11; the longitudinally stiffened ones were labeled B13, B3, B5, B7, B17, B4, and B6. The general notation of a girder is graphically displayed in Fig. 3.1, while all the test configurations are schematically given in Fig. 3.2. The girders with labels from B1 to B7 were initially tested in a previously unloaded state and then turned upside-down and retested (girders B11 to B17). This method is a common procedure for this type of testing since the deformation of the web panel is highly localized near the loaded flange. Consequently, this method has been frequently used in many other similar experimental investigations [1–2,5,21,75–77]. Moreover, it has been shown in Ref. [21] that the web panel deformation propagated only in the upper half of the web panel (for different levels of the ultimate load and residual deformation), and vertical stresses (direction of the applied patch load) in the lower half of the web panel were significantly below the yield stress. Therefore, there was no expected drop in the ultimate strength when girders were retested in the upside-down configuration. In addition, the longitudinal stiffening placed near the unloaded flange did not influence the patch load resistance – that is, when a stiffened

girder was turned upside-down and retested. In order to further eliminate the effects from the first configuration in the upside-down configuration (when girders are retested), testing was performed in such a way that longer patch load lengths were not applied in both configurations.

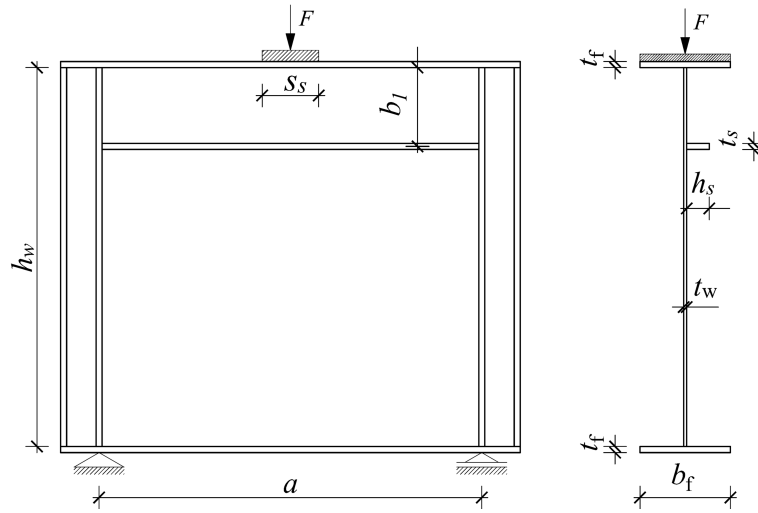


Figure 3.1: Longitudinally stiffened plate girder under transverse concentrated loading, general notation.

The material characteristics, represented as average values for the yield and ultimate tensile stresses of the web panel (f_{yw} , f_{uw}) and flange (f_{yf} , f_{uf}) of each girder, are given in Table 3.1; refer to Appendix A for more details. They were determined by standard tensile coupon tests. The coupons were taken from undeformed areas on the web panel or flanges after testing all the girders. All girders in the present and previous study [21] (seven girders with a web panel aspect ratio $\alpha = 1$ and seven girders with $\alpha = 2$) were ordered from the same manufacture shop. It was requested that the web panels and flanges should be from a specific steel grade, but no additional requirement regarding the yield strength was specified. The girders were randomly assembled and tested. After testing all the girders and using standard tensile coupon tests, it was noticed that some girders had different material characteristics (even though they were included in the requested steel grade). All the girders of Series A in Ref. [21] and most of the girders of Series B had the same material characteristics for flanges and web panels, while girders B1, B2, and B6 had different material characteristics for web panels, as listed in Table 3.1 and Appendix A.

3.1.2 Testing setup and disposition

The girders were tested in a specially prepared steel closed frame, which was fixed into a concrete slab in order to prevent lateral movement of the girders and rotations of the flanges (Fig. 3.3). The load was introduced by a hydraulic pump connected to a load cell and press with a capacity of 800 kN (see positions 5 and 6 in Fig. 3.3). The intensity of force was recorded by a load cell TML CLP-1MNB with a capacity of 1MN and an accuracy step of 0.3 kN. The girders were centrally loaded in the middle of the web panel plane using rigid steel

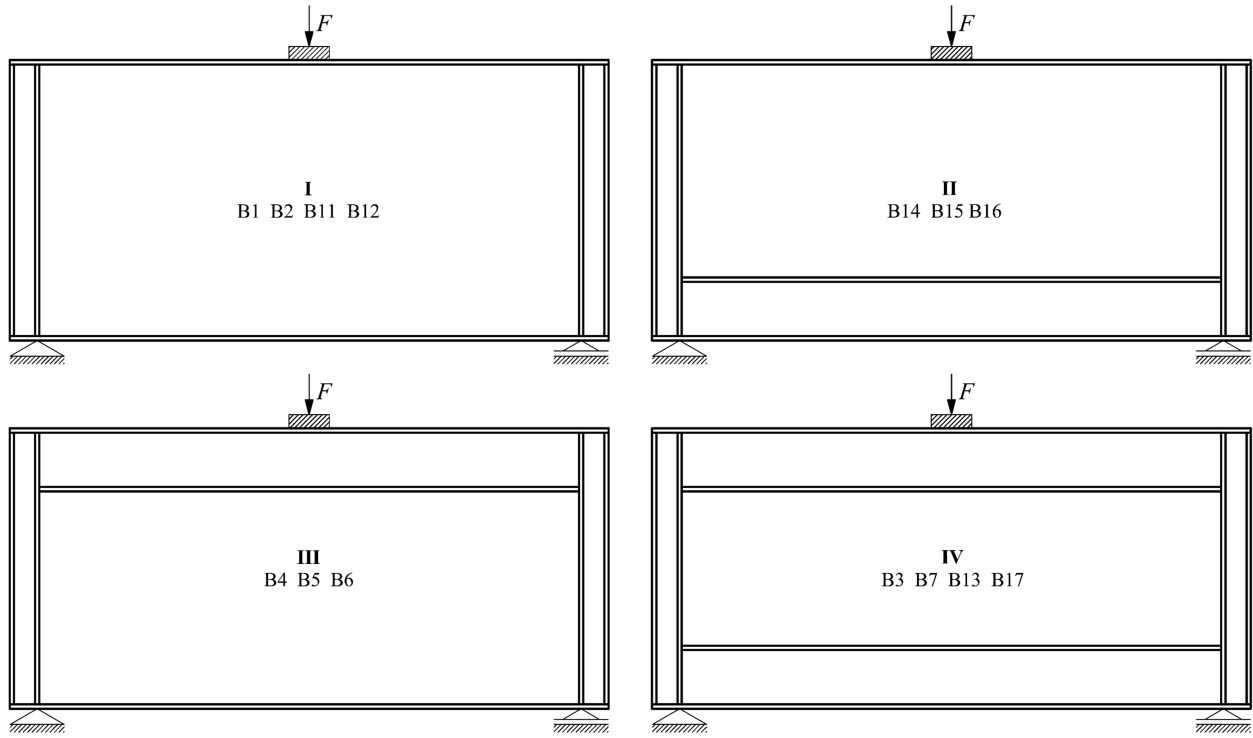


Figure 3.2: Test configurations for all the test plate girders. Longitudinally unstiffened (top row) and longitudinally stiffened steel plate girders (bottom row).

Table 3.1: Geometrical and material characteristics of all the test plate girders of Series B.

No.	Girder	a	h_w	t_w	b_f	t_f	b_1	s_s	h_s	t_s	f_{yw}	f_{yf}	f_{uw}	f_{uf}
	Label	[mm]	[mm]	[mm]	[mm]	[mm]	[mm]	[mm]	[mm]	[mm]	[MPa]	[MPa]	[MPa]	[MPa]
1	B16 ²	1000	500	4	120	8	-	0	-	-	261.7 ⁴	314.0 ⁵	348.0 ⁴	466.0 ⁵
2	B13	1000	500	4	120	8	100	0	30	8	314.5 ⁴	312.5 ⁵	433.5 ⁴	463.0 ⁵
3	B14	1000	500	4	120	8	-	25	-	-	317.7 ⁴	323.0 ⁵	434.2 ⁴	469.5 ⁵
4	B1 ^{1,2}	1000	500	4	120	8	-	50	-	-	257.3 ³	315.5 ⁵	348.0 ³	462.0 ⁵
5	B3 ¹	1000	500	4	120	8	100	50	30	8	314.5 ⁴	312.5 ⁵	433.5 ⁴	463.0 ⁵
6	B15 ²	1000	500	4	120	8	-	100	-	-	318.2 ⁴	311.5 ⁵	435.5 ⁴	459.5 ⁵
7	B5 ^{1,2}	1000	500	4	120	8	100	100	30	8	318.2 ⁴	311.5 ⁵	435.5 ⁴	459.5 ⁵
8	B2 ^{1,2}	1000	500	4	120	8	-	150	-	-	225.5 ⁴	312.5 ⁵	336.7 ⁴	463.5 ⁵
9	B7 ¹	1000	500	4	120	8	100	150	30	8	327.0 ⁵	339.0 ⁶	438.5 ⁵	486.0 ⁶
10	B17 ¹	1000	500	4	120	8	100	150	30	8	327.0 ⁵	339.0 ⁶	438.5 ⁵	486.0 ⁶
11	B12 ²	1000	500	4	120	8	-	200	-	-	225.5 ⁴	312.5 ⁵	336.7 ⁴	463.5 ⁵
12	B4	1000	500	4	120	8	100	200	30	8	317.7 ⁴	323.0 ⁵	434.2 ⁴	469.5 ⁵
13	B11 ²	1000	500	4	120	8	-	250	-	-	257.3 ³	315.5 ⁵	348.0 ³	462.0 ⁵
14	B6	1000	500	4	120	8	100	250	30	8	261.7 ⁴	314.0 ⁵	348.0 ⁴	466.0 ⁵

¹ Originally published in Ref. [21] and summarized in Ref. [24]

² Girders equipped with strain gauges at the web and loaded flange

³ Values obtained from three standard tensile coupon tests

⁴ Values obtained from four standard tensile coupon tests

⁵ Values obtained from two standard tensile coupon tests

⁶ Values obtained from one standard tensile coupon test

blocks for load introduction. The length of an applied patch load s_s was varied from $s_s = 0$

mm (concentrated force introduced by a half-round bar) to $s_s = 250$ mm running the full width of the flange (Fig. 3.4). The thickness of these load blocks was approximately 50 mm. The half-round bar can be introduced as a load from a crane wheel, while the biggest load length can be interpreted as a load applied through a very stiff launching shoe. Neither the load steel blocks nor the two supports at the bottom flange were fastened to the loaded flange (Fig. 3.3). The disposition and working space of the used laboratory are schematically displayed in Fig. 3.3.

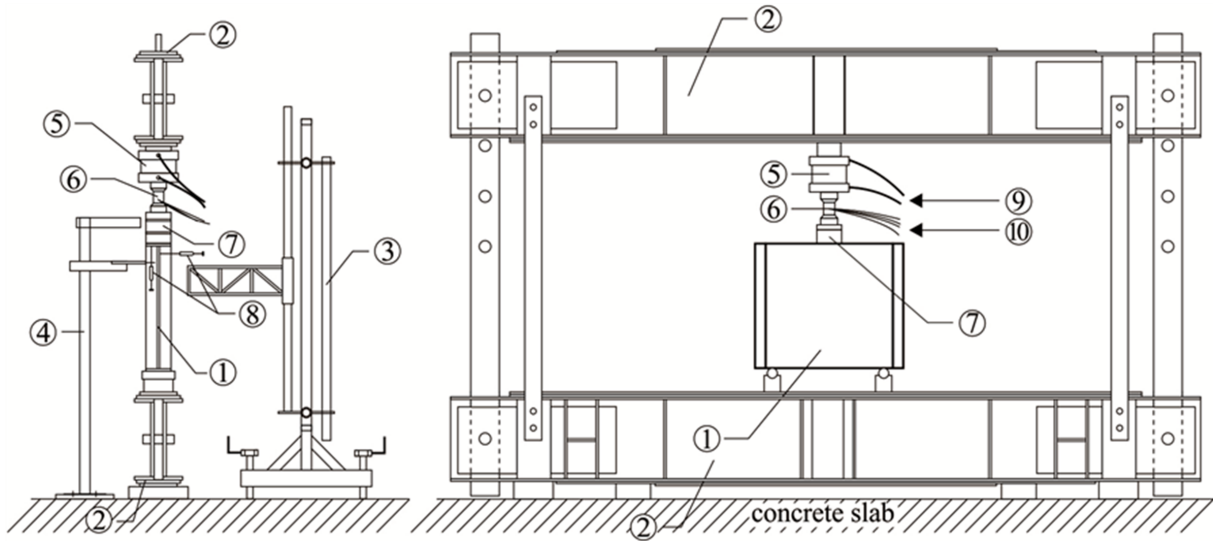


Figure 3.3: Schematic drawing of the laboratory and equipment: 1) test girder, 2) steel closed frame, 3) frame slider for guiding a transducer for web deformations, 4) frame slider for holding a transducer for the upper flange deformation, 5) press, 6) load cell, 7) rigid steel block for load introduction, 8) electrical transducers, 9) pipes for oil supply for hydraulic pump, 10) electrical cables for connecting the load cell and measuring devices.

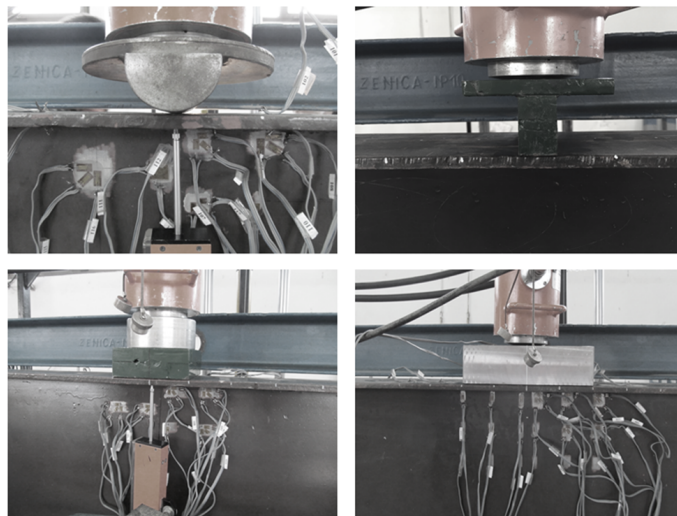


Figure 3.4: Different load blocks (clockwise from top left): $s_s = 0, 25, 250,$ and 100 mm.

3.1.3 Initial geometric imperfections

After test preparation and setup, an initial force increment of 5 kN was applied and initial geometric imperfections of the web panel were recorded using a rectangular grid size of 21x11 points, centrically placed with respect to the web panel (see Fig. 3.5). This measurement was performed using a frame slider (see position 3 in Fig. 3.3) and a displacement transducer (see position 8 in Fig. 3.3). The obtained geometrical scatter data was then used to reproduce each web panel's initial shape to compare it with residual deformations. This information was used later in the text (see Section 3.2 and Appendix C) in order to show the difference in the behavior of longitudinally unstiffened and stiffened steel plate girders. Moreover, the same scatter data can be used for numerical modeling in order to include initial geometric web panel imperfections into numerical models. More details about incorporating experimentally measured geometric imperfections into finite element models are given in Chapter 4. The measured maximum amplitudes of initial geometric web panel imperfections for the girders tested once (B1 to B7) are listed in Table 3.2.

Table 3.2: Maximum amplitude of initial geometric web panel imperfections for the girders tested once.

Girder	B1 ¹	B2 ¹	B3 ¹	B4	B5 ¹	B6	B7 ¹
Maximum amplitude	$h_w/48$	$h_w/100$	$h_w/87$	$h_w/40$	$h_w/140$	$h_w/65$	$h_w/52$

¹ Originally published in Ref. [21]

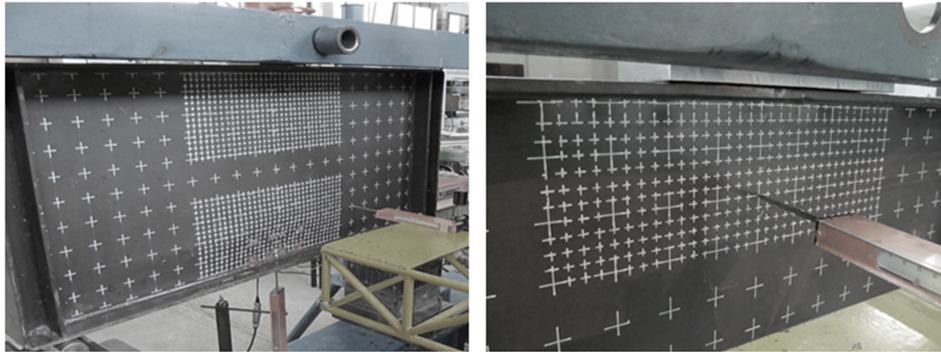


Figure 3.5: Measuring initial geometric web panel imperfections using a rectangular grid size of 21x11 points.

3.1.4 Testing process

After initial geometric imperfections were recorded for the whole web panel, the load was incrementally increased. In the beginning, the first few load increments were approximately 20 kN, and after that, the increment was decreased. Under each load increments, the following data were recorded with a data logger using a text file: (i) web panel out-of-plane deflection at a characteristic point near the loaded flange (Fig. 3.6), (ii) deflection of the loaded (upper)

flange (Fig. 3.6), (iii) deflection of the bottom flange at the center of the girders (centrically below the load), and (iv) for some girders, the strains in many points of the web and some points of the loaded flange (Fig. 3.7). All these displacement measurements were performed by three electrical displacement transducers TML SDP-100C with a step size of 100 mm and an accuracy step of 0.01 mm. For capturing the web panel out-of-plane deflection and deflection of the loaded flange, movable steel frame-sliders (see positions 3 and 4 in Fig. 3.3) were used, while the transducer for deflection of the bottom flange was immovable. This enables monitoring of deformation during the tests. Strains were measured in a number of chosen points by HBM (Hottinger Baldwin Messtechnik GmbH) strain gauges [78]. The strain gauges were mainly individual LY 11-3/120, several LY 11-6/120, and several rosettes RY 11-10/120. The strain gauges were symmetrically glued in pairs to both sides of the web and loaded flange in the vicinity of the point of loading (symmetrically on both sides of the web and mostly symmetrically with respect to the central line of the web), Fig. 3.7. This arrangement enables more information about membrane and bending strains and also provides information regarding the symmetrical response of a whole girder. Positions of the strain gauges were chosen to facilitate comparison for cases with different loading lengths. The presence of the longitudinal stiffeners also influenced the location of the strain gauges.

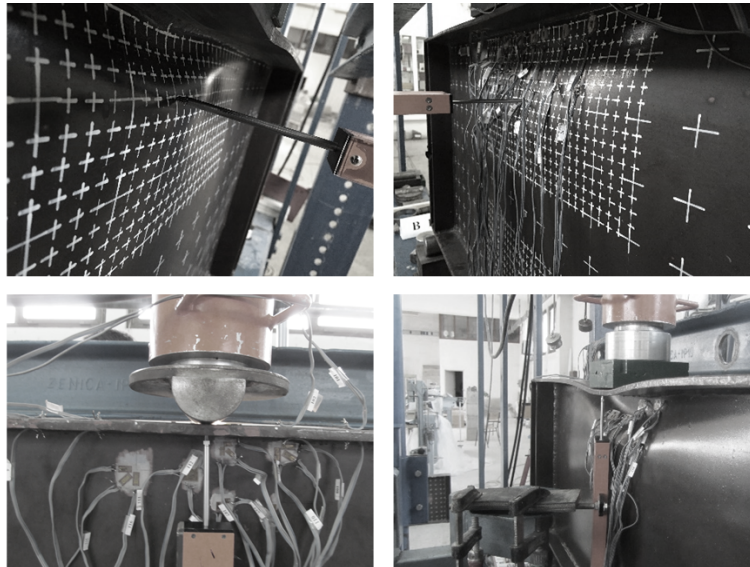


Figure 3.6: Measuring out-of-plane deflection at a characteristic point near the loaded flange (top row) and deflection of the loaded flange (bottom row) during the testing process.

The appearance and development of the lateral deformations of the webs were noticed by measuring out-of-plane deflections at a characteristic point near the loaded flange and with a visual inspection of the girders when the load was increased. In order to follow the behavior of the tested girders during the testing process, some load increments were held for a certain time. The whole web panel centerline out-of-plane deflection was measured using the same steel frame slider and electrical displacement transducer (positions 3 and 8 in Fig. 3.3) used to measure initial geometric web panel imperfections. In addition to the primary mesh grid size (11 points along the web depth), a finer grid size was used in the vicinity where local buckling

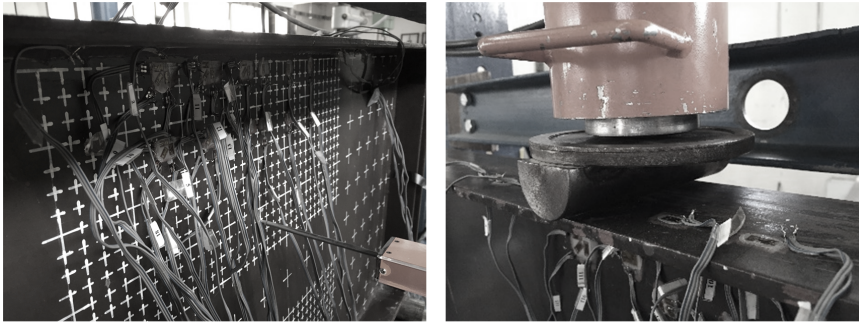


Figure 3.7: Arrangement of strain gauges for the web panel and the loaded flange.

was expected, cf. Fig. 3.6. A total of 14 points were used for capturing the centerline web profile under this load increment. This mesh is used later for an accurate representation of a deformed vertical cross-section of the webs. These centerline web profiles are given in the next section (from Fig. 3.10 to Fig. 3.13) for each girder under specific load increments. Similarly, the deflection of the loaded flange was measured by the steel frame slider (position 4 in Fig. 3.3) and electrical transducer at 17 points under the same load increment. After that, the testing process was continued, and the load increment was increased.

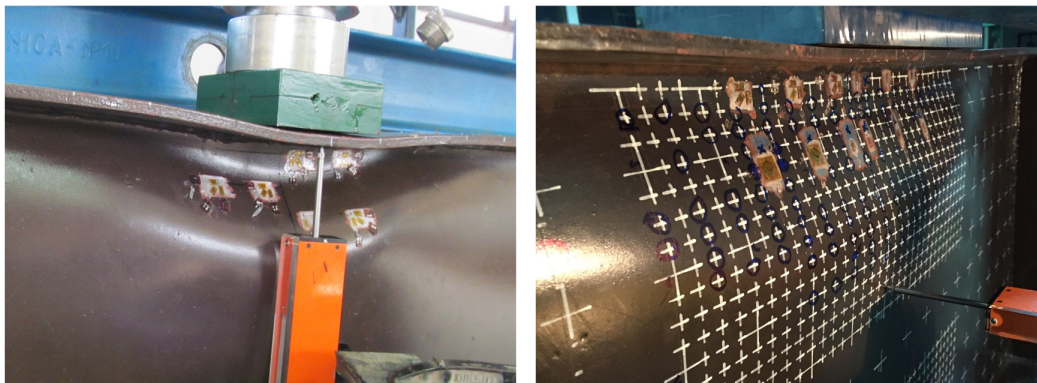


Figure 3.8: Failure modes.

Local buckling of the web panel and local deformation of the loaded flange were developed and visually noticed by increasing the applied load. The force is increased until the ultimate capacity was exhausted, which manifested through rapidly increasing deformations of the web panel and loaded flange in the vicinity of the point of loading without an increase in load. This presents local loss and local buckling zone is noticed under an applied force. When the ultimate strength was reached, the girders were unloaded, residual deformations of the web panel (at the primary mesh grid point and in additional points in the zone where deformation was pronounced, cf. Fig. 3.6) and the loaded flange were measured. This concludes the whole testing process. For some girders, the failure shapes are shown in Fig. 3.8.

3.2 Test results and discussion

In this section, all the steel plate girders of Series B are included. Results and observations regarding the ultimate strength and behavior of the tested girders are presented. Numerous diagrams are generated using experimental data collected during the testing process. The experimentally obtained patch loading resistances are compared with the previous experimental analysis [21], current European design standard EN 1993-1-5 [65], and available experimental results in the literature; followed by web panel and loaded flange deformations. Finally, the elastoplastic behavior of some tested girders is discussed.

3.2.1 Ultimate strength

The experimentally obtained ultimate strengths for all the tested girders are given in Table 3.3 and graphically presented in Fig. 3.9. According to these results, one can conclude that the ultimate load increased with increasing the patch load length for all the tested girders (with and without stiffening). A similar conclusion was found in Ref. [21] for the girders of Series A (web panel aspect ratio $\alpha = 1$). These findings are also in agreement with the experimental study by Ref. [3]. As evident in Fig. 3.9, the results show regularity apart from the results for $s_s = 25$ mm and $s_s = 100$ mm for longitudinally unstiffened steel plate girders, and $s_s = 250$ mm for longitudinally stiffened girders. These girders had different material characteristics for the web panel than the other girders (as explained in Section 3.1.1 and in Table 3.1), which is expanded upon in more detail later in this section.

Additionally, as shown in Ref. [21], an increase in patch load length from $s_s = 0$ mm to $s_s = 150$ mm gives higher ultimate strengths $> 50\%$ for both longitudinally unstiffened and stiffened steel plate girders. However, increasing the web panel aspect ratio to $\alpha = 2$, this finding is only valid for longitudinally stiffened steel plate girders. In the current experimental analysis and for the same increase in patch load length (from $s_s = 0$ mm to 150 mm), the ultimate carrying capacity of longitudinally unstiffened steel plate girders was increased by 34%.

Apart from the present analysis and [21], the influence of patch load length on the ultimate strength of longitudinally stiffened steel plate girders was investigated only in [3,15–16,19], as reported in Table 2.1. However, in Refs. [15,19], different patch load lengths were applied to different geometries (web panel aspect ratio) and, therefore, the influence of patch load length cannot be determined. According to the experimental study by Ref. [3], the patch load resistance of longitudinally stiffened steel plate girders can be increased by 4–9%, increasing the patch load length from 40 mm ($s_s/a = 0.04$, $s_s/h_w = 0.05$) to 120 mm ($s_s/a = 0.11$, $s_s/h_w = 0.16$). In this analysis [3], steel plate girders with a single-sided flat stiffener and web panel aspect ratio of 1.5 were used. Using results from Ref. [21] for the girders of Series A and similar ratios of s_s/a and s_s/h_w – that is, increasing the patch load length from 25 mm ($s_s/a = s_s/h_w$

$= 0.05$) to 75 mm ($s_s/a = s_s/h_w = 0.15$) – the patch load resistance of longitudinally stiffened steel plate girders was increased by 8%, which is in agreement with [11]. However, a much bigger increase in ultimate strength of longitudinally stiffened steel plate girders is reported in Ref. [16]. By increasing the patch load length from 40 mm ($s_s/a = 0.02$, $s_s/h_w = 0.04$) to 240 mm ($s_s/a = 0.14$, $s_s/h_w = 0.24$), an increase in bearing capacity of 35–55% for flat and 50–74% for closed-section stiffeners was obtained. A direct comparison between Refs. [16,21] is not possible since the ratios of s_s/a and s_s/h_w cannot be matched. However, a similar increase (44%) in the bearing capacity of longitudinally stiffened steel plate girders was obtained in Ref. [21] when the patch load length was increased from 25 mm ($s_s/a = s_s/h_w = 0.05$) to 125 mm ($s_s/a = s_s/h_w = 0.25$). Similarly, using the results for $s_s = 50$ mm ($s_s/a = 0.05$, $s_s/h_w = 0.10$) and $s_s = 150$ mm ($s_s/a = 0.15$, $s_s/h_w = 0.30$) for longitudinally stiffened steel plate girders in the present study (see Table 3.3), the ultimate strength was increased by 46%.

Table 3.3: Experimentally obtained ultimate strengths for all the tested girders of Series B.

s_s [mm]	0	25	50	100	150	200	250
Unstiffened girders	B16	B14	B1 ¹	B15	B2 ¹	B12	B11
$F_{exp,unstiff}$ [kN]	129.9	147.9	140.3	176.9	174.6	190.9	199.9
Stiffened girders	B13		B3 ¹	B5 ¹	B7 ¹	B4	B6
$F_{exp,stiff}$ [kN]	148.6		164.9	200.3	240.3 233.9	275.3	290.3
β^2 [kN]				1.13			1.45

¹ Originally published in Ref. [21] and summarized in Ref. [24]

² Strengthening effect β was computed only for the girders with the same material characteristics (see Section 3.1.1 and Table 3.1)

To gain more insight into the influence of web panel aspect ratio on the ultimate strength for different patch load lengths, the experimentally obtained values from Ref. [21] and the present study were analyzed in more detail; similar comparison is provided in Chapter 5 for various geometric imperfections and patch load lengths (Table 5.8). Comparing these two studies, one could conclude that the web panel aspect ratio influences the ultimate strength of both longitudinally unstiffened and stiffened steel plate girders. Using a half-round bar ($s_s = 0$ mm), the ultimate capacity of the longitudinally stiffened steel plate girders dropped by 12%, increasing the web panel aspect ratio (changing the girder width) from $\alpha = 1$ to $\alpha = 2$. Moreover, by increasing the patch load length (e.g., $s_s = 150$ mm), the obtained drop in the ultimate load of longitudinally stiffened steel plate girders decreased to 2–9%. Making a similar comparison for the longitudinally unstiffened steel plate girders was not realistic since the girders in the present analysis ($s_s = 0$ mm and $s_s = 150$ mm) had different materials characteristics than those in Ref. [21]. A decrease in the bearing capacity of longitudinally unstiffened and stiffened steel plate girders accompanying an increase in the web panel aspect ratio was also reported in Ref. [2].

The experimentally obtained values in Table 3.3 are also graphically juxtaposed with the ultimate strengths determined by the current European design standard EN 1993-1-5 [65], Fig. 3.9. The patch load resistances were calculated using Eq. (2.1) – (2.7) in Chapter 2. For this purpose, the yield stresses from Table 3.1 of each girder were used and Young’s modulus $E = 205$ GPa was employed. According to Fig. 3.9, the biggest difference between the experimentally obtained ultimate loads and EN 1993-1-5 for longitudinally unstiffened and stiffened steel plate girders is in relation to greater patch load lengths.

Using this graphical comparison (Fig. 3.9), the following conclusion could be made. Firstly, one could observe that the experimentally obtained ultimate strengths of the longitudinally unstiffened steel plate girders increased linearly, as shown by the thin, dashed black line in Fig. 3.9. The same result was obtained in Refs. [21]. A small variation in the results exists, specifically for $s_s = 25$ mm and $s_s = 100$ mm, for which higher ultimate loads were obtained. Comparing the material characteristics of these two unstiffened steel plate girders ($s_s = 25$ mm and $s_s = 100$ mm) with the rest of the unstiffened girders (see Table 3.1), one can observe that the web panel yield stresses for $s_s = 25$ mm and $s_s = 100$ mm (girders B14 and B15) were approximately 320 MPa, whereas, for the other unstiffened steel plate girders, the web panel yield stresses were between 225 MPa and 260 MPa. This variation in the web panel yield stresses produced a small deviation in the ultimate loads for the unstiffened steel plate girders. Secondly, the ultimate strengths of longitudinally unstiffened steel plate girders determined by EN 1993-1-5 are smaller than the experimental ones. Still, they follow the observed trend in the experimental results (variation in the results for different web panel yield stresses). This finding indicates that the web panel yield stress sensitivity was well captured by the design standard, as shown by the thick, dashed black line in Fig. 3.9.

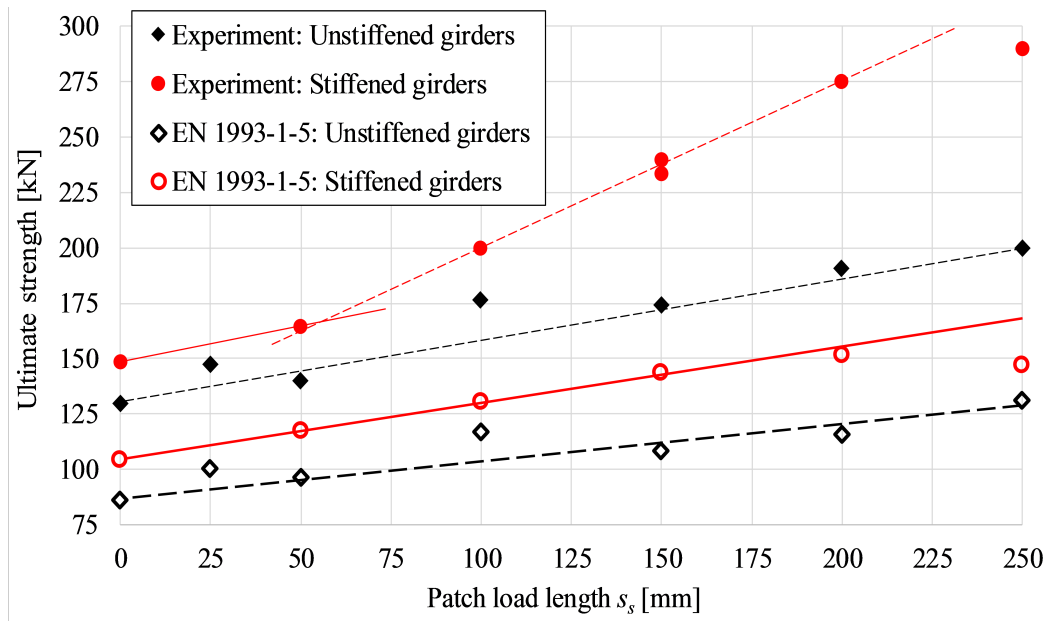


Figure 3.9: Experimentally obtained ultimate strength for all the tested girders and corresponding values according to EN 1993-1-5.

Furthermore, the experimentally obtained ultimate strengths of the longitudinally stiff-

ened steel plate girders for small patch load lengths (approximately between $s_s = 50$ mm and $s_s = 100$ mm) followed the ultimate strength of the unstiffened ones, as shown by the thin, solid red line in Fig. 3.9. After this specific patch load length, the patch loading resistance of the longitudinally stiffened steel plate girders increased much faster with an increase in patch load length, as presented by the dashed red line in Fig. 3.9. Lastly, adding the ultimate capacities of longitudinally stiffened steel plate girders calculated by EN 1993-1-5 [65] to Fig. 3.9, one can notice that these values increased linearly (see the thick, solid red line in Fig. 3.9 where the result for $s_s = 250$ mm is excluded since the girder had different material characteristics. See Table 3.1). The results were significantly below the corresponding experimental results, especially for $s_s > 50 \div 100$ mm. Indeed, looking at the resistance model defined in EN 1993-1-5 (see Section 2.3), one can observe that the ultimate strength of both longitudinally unstiffened and stiffened steel plate girders increases linearly with an increase in patch load length, and it is independent of the value of patch load length.

All the aforementioned findings regarding the comparison between the experimental results and design standard [65] show that further improvements of EN 1993-1-5 are required.

Strengthening effect: The strengthening effect (ratio between the ultimate strength of the longitudinally stiffened and unstiffened steel plate girders) for the girders with the same material characteristics is listed in Table 3.3. In the current analysis, the strengthening effect was between 13% and 45%, as computed based on the two values given in Table 3.3 for $s_s = 100$ mm and $s_s = 250$ mm. However, using linear interpolation through the values for $s_s = 25$ mm and $s_s = 100$ mm for the unstiffened steel plate girders (see Fig. 3.9) and then using extrapolation to get new values for the other unstiffened girders (meaning that the stiffened and unstiffened girders had the same material characteristics), an average strengthening effect of 21% was obtained. A similar strengthening effect of 36%, 36–38%, and 22–36% is reported in Refs. [7,9,20], respectively, in relation to steel plate girders with a single flat stiffener and web panel aspect ratios from 1 to 1.43. In addition, using a high torsional rigidity stiffener (closed section), a strengthening effect of 17–59%, 20–64%, and 44–56% was obtained in Refs. [19–20,22], respectively. However, in Ref. [21] (girders of Series A), a smaller stiffening effect (from 6% to 19%) using a web panel aspect ratio of 1 was found. This finding agrees with other experimental studies [1,4–6,15–16] in which a strengthening effect from 4% to 19% was reported. It is noteworthy that, in all these studies [1,4–6,15–16], the patch load length was constant and the web panel aspect ratio was mostly 1, while the other geometrical characteristics were very different. A direct comparison between the present analysis and [21] clearly shows that the strengthening effect increases with an increase in the web panel width (distance between the vertical stiffeners), which is in agreement with findings in Ref. [2]. It is interesting to note that the influence of patch load length on the strengthening effect is not clear from the above-mentioned references [1,4–7,9,15–16,20,22] since the patch load was constant. The present analysis and [21] show that an appreciable strengthening effect can be obtained when a specific patch load length is reached.

3.2.2 Web deformation

Initial geometric web deformation was recorded before testing, while the residual web and the loaded flange deformations were recorded after the testing process. Moreover, the vertical centerline web profiles were captured for different ultimate load levels (see Fig. 3.10, Fig. 3.11, Fig. 3.12, and Fig. 3.13). They were obtained using measured values at fourteen points along the web depth, as reported in Section 3.1.4. These measurements revealed how web deformation develops under various patch load lengths and how it spreads for plate girders with and without longitudinal stiffening under the same patch load length. One should bear in mind that the given plots for the residual deformation do not represent an actual deformation at the ultimate load. This deformation was measured after the ultimate strength was reached and when the unloading process was finished. Initial, residual, and increase in deformation (obtained as the difference between the residual and initial deformations) of the web panel are represented as contour plots for each girder (see Fig. C.1 to Fig. C.14 in Appendix C). These plots also give valuable information about the formation of the collapse mechanism, and they can be used for its indication. Moreover, these figures (from Fig. C.1 to Fig. C.14) show that random shapes of initial geometric web panel imperfections in the longitudinal and vertical directions as well as different amplitudes, were obtained. The influence of experimentally measured initial geometric imperfections of both series of testing A and B, along with a variety of patch load lengths, is numerically analyzed in Chapter 5 by means of finite element analysis.

Behavior and deformation of the vertical centerline web profile under different levels of the ultimate load of each steel plate girder are given in Fig. 3.10, Fig. 3.11, Fig. 3.12, and Fig. 3.13. These plots clearly show certain indications about the behavior of the girders. Local instability and noticeable web panel deformations were evident after global buckling for both longitudinally unstiffened and stiffened steel plate girders. There was no obvious indication and appearance of the local buckling zone, except near the ultimate load; its registration occurred suddenly for applied forces $> 95\%$ of the ultimate load. This can be seen looking at the vertical web profile at the central cross-section for different levels of an applied force, for the last measured out-of-plane deflection (before the ultimate load was achieved) and for the residual deformation. However, there were differences in the behavior between these two groups of girders before and after the ultimate load was reached.

A significant increase in web deformation of the longitudinally unstiffened steel plate girders was observed below the point of loading, and greater buckling areas were engaged. In this case, the dominating buckle of the initial deformation of the web increased as the applied load increased – that is, it followed the initial deformation, and its vertex moved slightly toward the loaded flange. The final buckling occurred as the load was increased – either in the direction of the buckle, where it bent out in one buckle over the total web depth (see Fig. 3.10b, Fig. 3.11, Fig. 3.12, and Fig. 3.13) or after snap-through buckling, where the web suddenly showed a large lateral deflection opposite to that of the initial buckle (see Fig. 3.10a). The latter occurred only for a very small patch load length ($s_s = 0$ mm). It is also interesting to notice

that the final position of the buckle vertex (considering the residual profile) changed with an increase in the patch load length – that is, increasing patch load length was associated with an increase in the distance between the buckle vertex and the loaded flange.

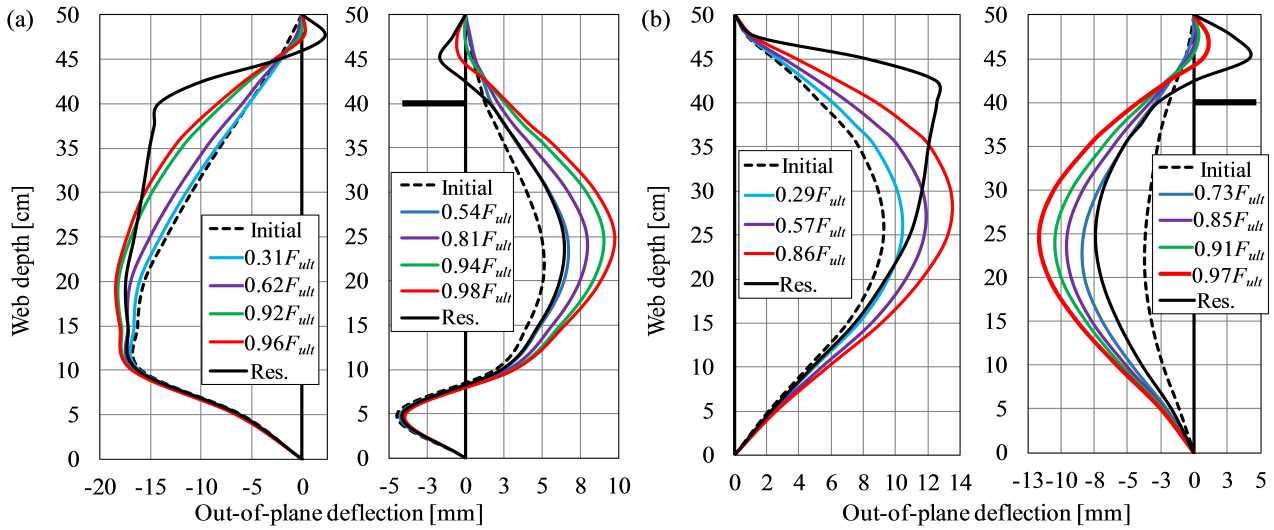


Figure 3.10: Vertical web profiles for different levels of the ultimate load for unstiffened and stiffened steel plate girder: (a) $s_s = 0$ mm: B16 vs. B13. (b) $s_s = 50$ mm: B1 vs. B3.

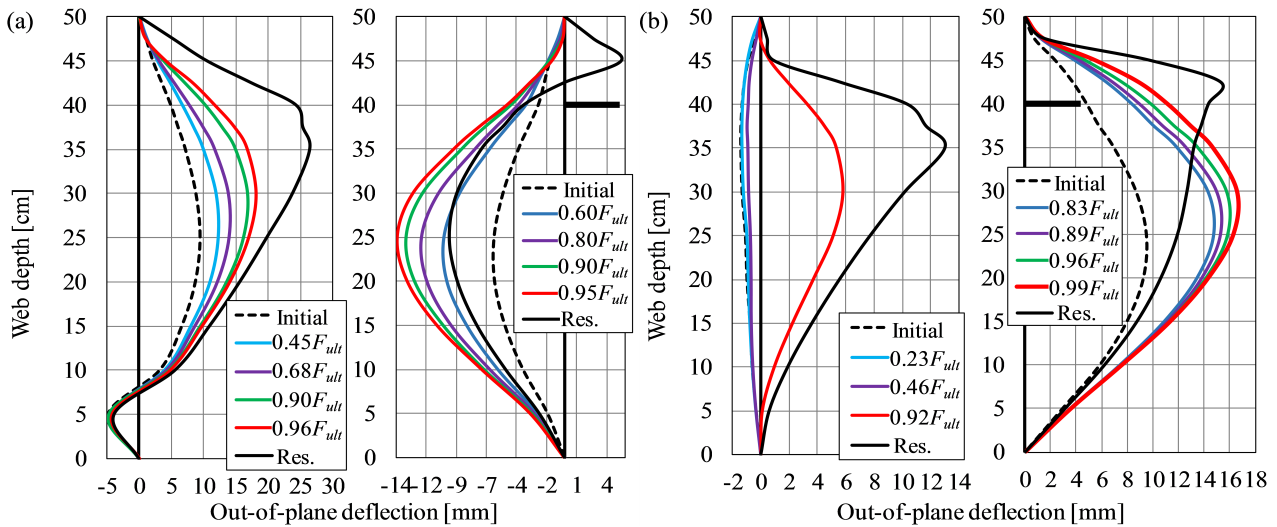


Figure 3.11: Vertical web profiles for different levels of the ultimate load for unstiffened and stiffened steel plate girder: (a) $s_s = 100$ mm: B15 vs. B5. (b) $s_s = 150$ mm: B2 vs. B7.

On the other hand, two different failure modes were observed for the longitudinally stiffened steel plate girders. A very local buckle (both vertically and horizontally) was dominant between the loaded flange and the longitudinal stiffener only for smaller patch load lengths $s_s < 150$ mm (see Fig. 3.10 and Fig. 3.11a). The final buckling occurred after snap-through buckling (opposite to the initial buckle). The web panel snap-through buckling phenomenon was also reported in Refs. [2–3,21]. Therefore, in this case, the failure mode is classified as local buckling of the loaded web sub-panel. The longitudinal stiffener proved to be strong enough (even though it is classified as *weak*, see Eq. (2.7) in Chapter 2) to limit the web deformation in the upper web sub-panel. The longitudinal stiffener remained in the plane of the web – that is,

no longitudinal stiffener buckling was noticed. Moreover, the residual profiles in Fig. 3.10 and Fig. 3.11a clearly show that the deformation below the stiffener (bottom web sub-panel) was smaller than deformations before the ultimate load was reached, which is in contrast with the unstiffened steel plate girders. Thus, in this case ($s_s < 150$ mm), it is more difficult for an initial deformation buckle to propagate from the unstiffened part of the web through the stiffener and move toward the loaded flange, which would be the case if the web was not stiffened.

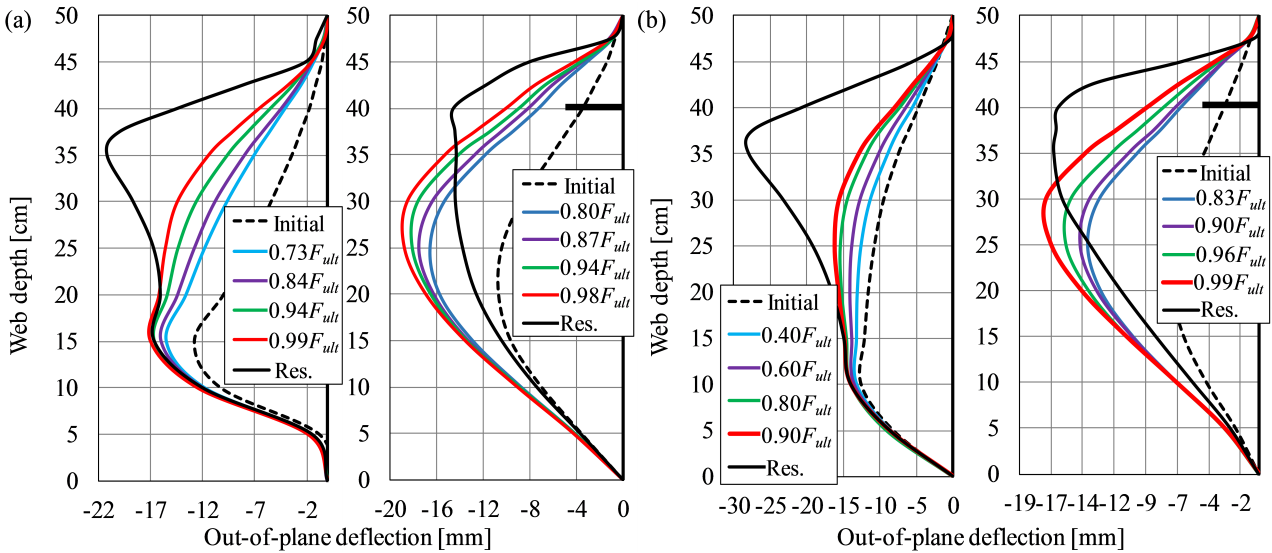


Figure 3.12: Vertical web profiles for different levels of the ultimate load for unstiffened and stiffened steel plate girder: (a) $s_s = 200$ mm: B12 vs. B4. (b) $s_s = 250$ mm: B11 vs. B6.

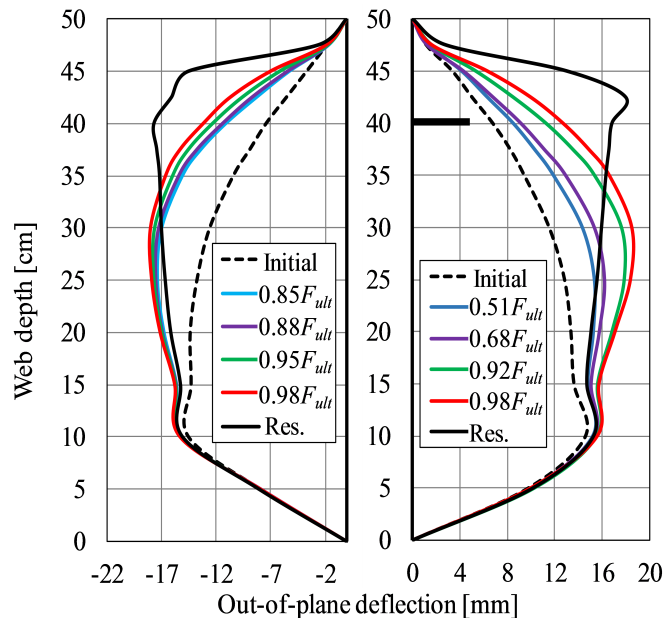


Figure 3.13: Vertical web profiles for different levels of the ultimate load for unstiffened steel plate girder B14 $s_s = 25$ mm (left) and stiffened steel plate girder B17 $s_s = 150$ mm (right).

However, increasing the patch load length changed the buckling pattern (failure mode). More specifically, for $s_s \geq 150$ mm (Fig. 3.11b, Fig. 3.12, and Fig. 3.13), the web bent out in one buckle like the unstiffened girders; the influence of the longitudinal stiffener was still present

but it was much less pronounced. In this case ($s_s \geq 150$ mm), the failure mode is characterized as global buckling (or interaction of global and local buckling) and noticeable longitudinal stiffener buckling was observed; contrary to the case $s_s < 150$ mm where the longitudinal stiffener remained in its initial position in the plane of the web panel. The longitudinal stiffener reduced the out-of-plane web deformation at the stiffener position but proved to be rather weak for this girder span and patch load lengths $s_s \geq 150$ mm. Nevertheless, this study shows that even longitudinal stiffeners classified as *weak* – that is, with relatively small stiffness from the patch loading point of view, can prevent global buckling of the web panel under localized edge loads. The same conclusion was also reported in the experimental study [79] conducted on multiple stiffened web panels ($h_w = 500$ mm, $a = 1000$ mm, $t_w = 4$ mm) with relatively weak longitudinal stiffeners. The authors in Ref. [79] showed that two equally placed longitudinal stiffeners along the girder depth with dimensions $h_s = 40$ mm and $t_s = 4$ mm ($\gamma_s = 27.27$, see Eq. (2.7) in Chapter 2) were sufficient to eliminate the global buckling failure mode for patch load lengths $s_s = 100$ mm and $s_s = 200$ mm.

To highlight the comparison between the behavior of the longitudinally unstiffened versus stiffened steel plate girders even more, and to show the spreading of the buckling zone along the web panel width, the contour plots in Appendix C (see from Fig. C.1 to Fig. C.14) can be considered. In this section, for the sake of brevity, only the increase in deformation (obtained as the difference between residual and initial deformations) for specific patch load lengths (Fig. 3.14) is presented. It is evident from this figure that increasing the patch load length engaged greater buckling zones (in both the longitudinal and vertical direction) in the web panel for both the longitudinally unstiffened and stiffened steel plate girders. The increase in deformation for the longitudinally stiffened girders and for smaller patch load lengths ($s_s < 150$ mm) was highly pronounced between the stiffener and the loaded flange (local buckling failure mode). The longitudinal stiffener was not sufficiently rigid for longer patch load lengths, and the spreading buckling zone in both directions was very similar to the longitudinally unstiffened girders (global buckling failure mode or interaction of local and global buckling).

In addition, Fig. 3.10b, Fig. 3.11, and Fig. 3.12 show that all girders tested once (B1 to B7) had a C-shaped initial deformation (one global buckle along the girder depth), which was either maintained for all levels of the ultimate load and the residual profile, or the shape changed to an S-shape (one local buckle in the upper web sub-panel and opposite buckle in the lower web sub-panel) only for longitudinally stiffened steel plate girders and relatively small patch load lengths ($s_s < 150$ mm) (Fig. 3.10b and Fig. 3.11a). However, these vertical profiles do not give a complete picture of the influence of initial geometric imperfections. Looking at Fig. C.4, Fig. C.5, Fig. C.6, Fig. C.8, Fig. C.10, Fig. C.11, and Fig. C.13 from Appendix C for the girders tested once, it is evident that different shapes were also obtained in the horizontal direction. The influence of the shape of initial geometric imperfections was such that an initial geometric imperfection which had the same shape as the future shape at the ultimate load (collapse-affine geometric imperfections) decreased the carrying capacity more than another shape. On the other hand, an initial geometric imperfection that counteracted the buckling

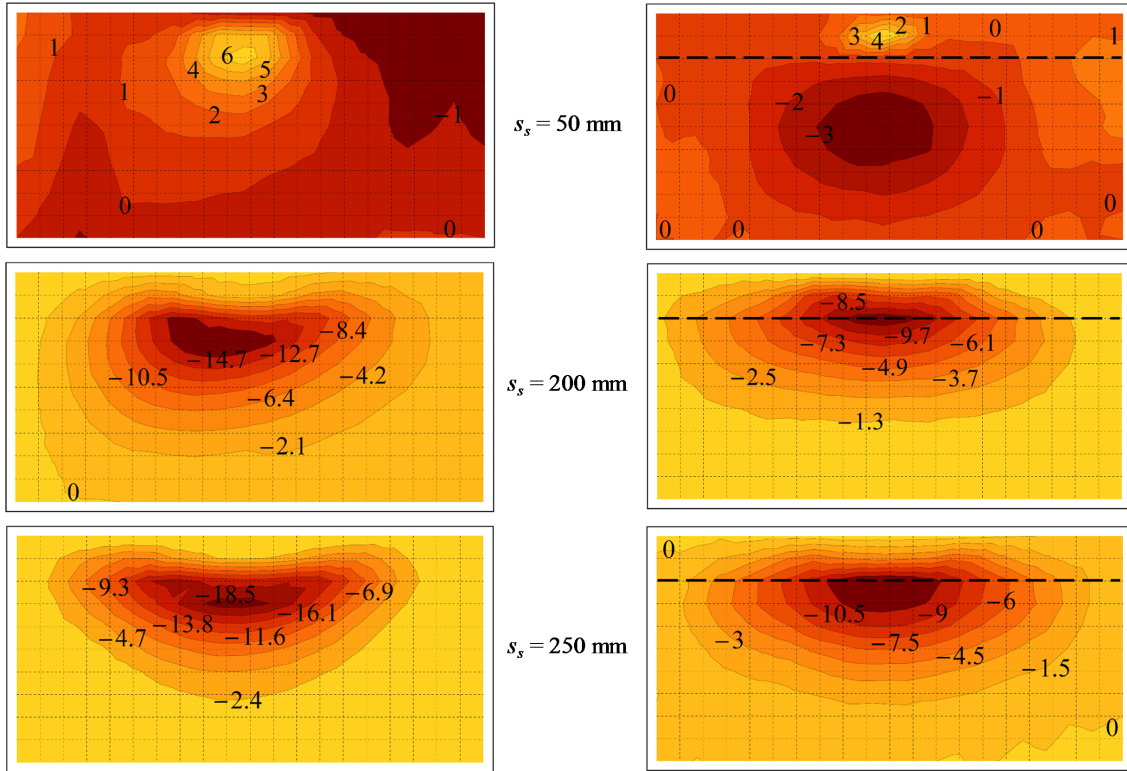


Figure 3.14: Increase in deformation (obtained as the difference between the residual and initial deformation) for unstiffened (left column) and stiffened (right column) steel plate girders (in mm). The dashed line represents the longitudinal stiffener.

pattern increased the ultimate load. The influence of initial geometric imperfections on the patch loading resistance and unfavorable geometric imperfections from the patch loading point of view are studied in more detail in Chapter 5 and Chapter 6.

3.2.3 Flange deformation

Deformations of the loaded flange were very small and highly localized below the point of loading for both the longitudinally unstiffened and stiffened girders. The deformations undoubtedly showed a trend of an increase in the engaged length of the loaded flange accompanying an increase in the patch load length, while their deformations followed the deformation of the web panel. For the sake of brevity, the web panel and loaded flange deformations for applied forces very near the ultimate strength for some girders are given in Fig. 3.15.

3.2.4 Elastoplastic behavior

The elastoplastic behavior of longitudinally unstiffened and stiffened girders is addressed in this section. For this purpose, the elastoplastic behavior of girder B15 (unstiffened) and B5 (stiffened) under a patch load length of $s_s = 100$ mm are compared. The appearance of the first plastic strains in both girders is determined by the limit elastic strains (computed using a



Figure 3.15: Web and flange deformation for applied forces near the ultimate strength for girders (clockwise from top left) B16, B14, B11, and B15.

web panel yield stress of 318.2 MPa (see Table 3.1) and Young's modulus of 205 GPa). For the sake of brevity, only diagrams related to vertical strains (direction of the applied patch load) in the web plate and in the loaded flange that are representative of the behavior for the girders considered are shown. The given vertical strains of both girders were measured at the front and rear surfaces of the web panel. As such, they neither represent the membrane strains (constant across the thickness of the web) nor give information regarding when web panel cross-sections are fully plastic. Yet, this analysis (albeit crude) can be used to show when the first plastic strains (at the web surface) were reached.

Vertical strains for both sides of the web panel of girder B15, located at different positions with respect to the loaded flange and the vertical central line (see Fig. 3.16a), are presented in Fig. 3.17, Fig. 3.18, and Fig. 3.19. It is immediately apparent that a different response was obtained for the rear and front web surface at the same point. This response was directly influenced by web panel initial geometric imperfections, which correspond to the development of bending of the web panel at that point, and thus, different values of strains were obtained at the front and rear surfaces of the web. One can also notice that for points very close to the loaded flange (Fig. 3.17 and Fig. 3.18), the yield started long before the ultimate resistance was reached for applied forces $< 50\%$ of the ultimate load, while for points far away from the loaded flange, the yield started for much higher applied forces (Fig. 3.19). However, comparing these results with the web panel deformation plots (cf. Fig. 3.11a), one can see that this plastification did not necessarily mean the attainment of the ultimate load, and it did not produce noticeable and significant web panel deformations. Moreover, comparing these three figures for vertical strains, it can also be observed that the plastification first occurred for points directly under the applied load (Fig. 3.17a, Fig. 3.18a, and Fig. 3.19a) and then for points displaced further away from the vertical central line (Fig. 3.17b, Fig. 3.18b and Fig. 3.19b).

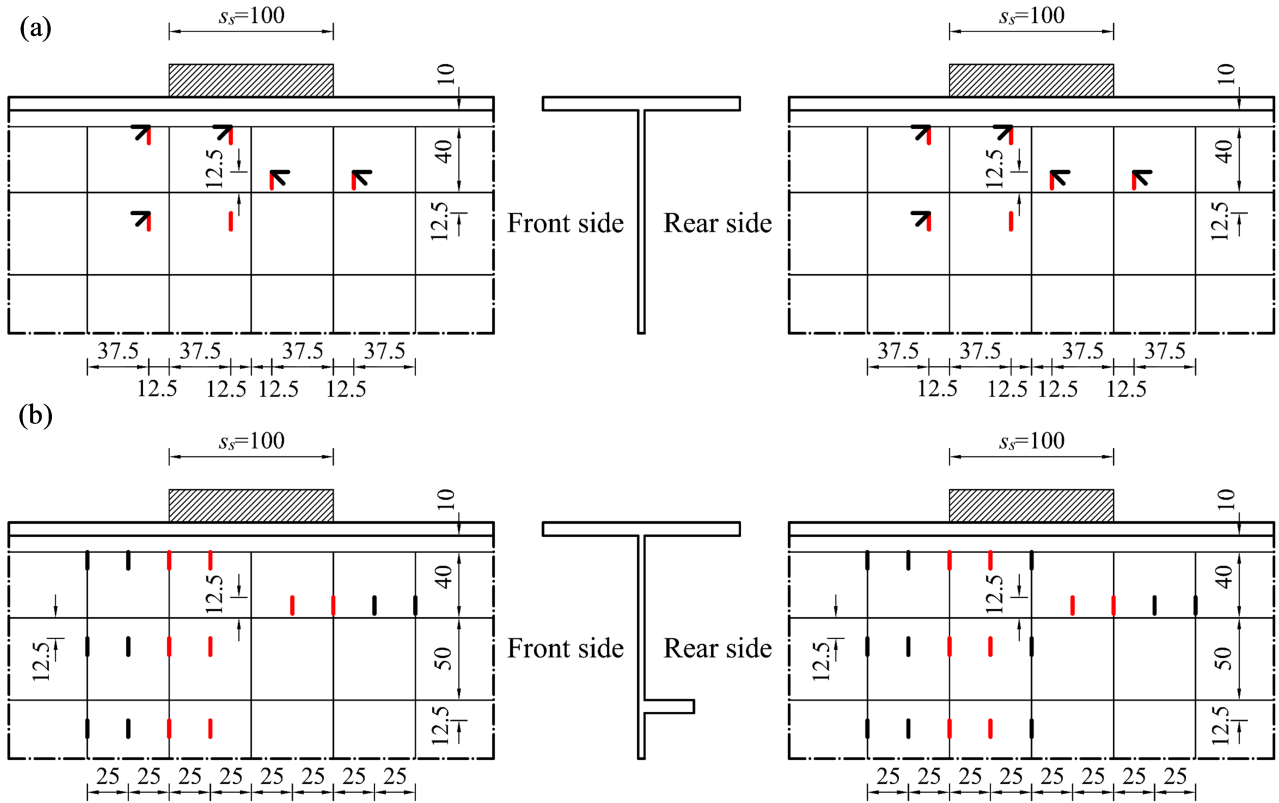


Figure 3.16: Position of strain gauges (in mm) for girders: (a) B15 (unstiffened); (b) B5 (stiffened). Positions of vertical strains given in this section are marked in red.

Strains in the loaded flange for this girder B15 were measured at points shifted 100 mm and 125 mm with respect to the central line of the web panel. In this case, the yield did not take place, and the obtained strains were notably below the yield point.

Vertical strains for both sides of the web panel (cf. Fig. 3.16b) of longitudinally stiffened girder B5 are given in Fig. 3.20, Fig. 3.21, Fig. 3.22, and Fig. 3.23. In this case, for points directly under the applied load (Fig. 3.20), the yield started for forces $< 50\%$ of the ultimate load, which is in agreement with the previous unstiffened case (cf. Fig. 3.17). However, for the points placed 37.50 mm and 62.50 mm from the loaded flange (Fig. 3.21 and Fig. 3.22), the yield started for applied forces between 60% and 70% of the ultimate load, while, for the unstiffened case (cf. Fig. 3.18 and Fig. 3.19), the yield started for smaller applied forces. Moreover, for points below the longitudinal stiffener (Fig. 3.23), the yield did not occur, and all the measured strains were significantly below the elastic ones. Similar to the previous case, this plastification was not enough to produce noticeable and significant deformations in the web panel (cf. Fig. 3.11a), and it does not mean that the ultimate resistance was reached. In addition, strains in the loaded flange for this girder B5 were measured at points shifted 50 mm and 100 mm with respect to the central line of the web, and likewise to the previous unstiffened girder B15, the plastification did not take place before the ultimate load was reached.

From the above elastoplastic analysis for the longitudinally unstiffened (B15) and stiffened (B5) girders, one can conclude that the first plastification can appear at some points in

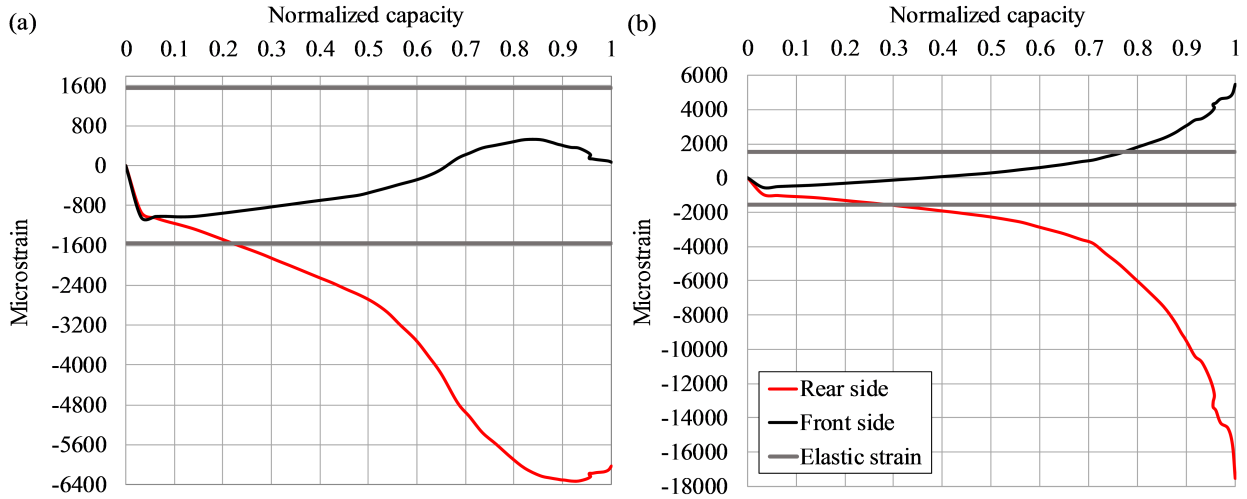


Figure 3.17: Vertical strain in the web plate on both sides (front-rear) for unstiffened girder B15 ($s_s = 100$ mm) at points placed 10 mm from the loaded flange and horizontally displaced from the vertical symmetry line for: (a) 12.5 mm; (b) 62.50 mm.

the vicinity of load introduction in the web panel significantly before the ultimate resistance is reached. The first plastification zones did not indicate noticeable and significant deformations in the web panel. The buckling of the web panel appeared only near the attainment of the ultimate load (cf. Fig. 3.11a) and, therefore, it was visible for much higher patch loads than those at which the yield occurred. In addition, for the points below the longitudinal stiffener and for the case considered ($s_s = 100$ mm), the yield did not occur. Despite the fact that in this experimental analysis the used longitudinal stiffener can be classified as a *weak* stiffener (see Eq. (2.7) in Section 2.3), its rigidity for this case ($s_s = 100$ mm) was enough to restrict the web panel out-of-plane deflection (cf. Fig. 3.11a) and plastification zones between the longitudinal stiffener and the loaded flange. These conclusions follow the general trend noticed in the previous experimental analysis [21] (girders of Series A) for a different web panel aspect ratio.

3.3 Summary

The present experimental study was primarily conducted with the aim of studying the behavior and patch loading resistance of longitudinally unstiffened and stiffened I-shaped steel plate girders, considering the influence of patch load length and web panel aspect ratio. Details about the experiment, results, and observed behavior of the tested girders are presented. The main findings regarding the ultimate strength can be summarized as follows:

- The carrying capacity of longitudinally unstiffened and stiffened steel plate girders increased with increasing patch load length. The ultimate strength of longitudinally unstiffened girders increased linearly with respect to the patch load length, whereas the ultimate load of longitudinally stiffened girders followed this same trend only for small

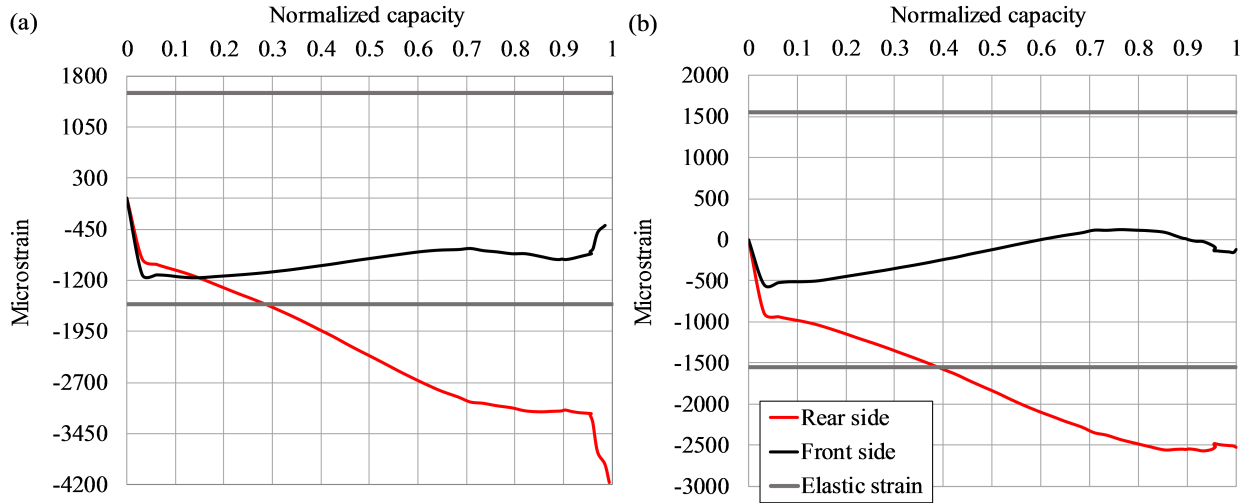


Figure 3.18: Vertical strain in the web plate on both sides (front-rear) for unstiffened girder B15 ($s_s = 100$ mm) at points placed 37.50 mm from the loaded flange and horizontally displaced from the vertical symmetry line for: (a) 12.5 mm; (b) 62.50 mm.

patch load lengths ($50 \text{ mm} < s_s < 100 \text{ mm}$). After a specific patch load length (threshold), the patch loading resistance increased much faster with increasing patch load length and appreciable strengthening effects were obtained.

- The patch loading resistance of longitudinally unstiffened and stiffened steel plate girders can be significantly increased by using larger patch load lengths. By increasing the patch load length from 0 mm to 250 mm, the patch loading resistance was increased $> 50\%$ and 90% for longitudinally unstiffened and stiffened girders, respectively.
- An appreciable increase in ultimate strength can be achieved using longitudinal stiffening. This analysis showed that the ultimate load could be increased $> 40\%$ by using longitudinal stiffening and longer patch load lengths compared to unstiffened girders.
- Increasing the web panel aspect ratio (more specifically, the web panel width) decreased the ultimate strength of longitudinally unstiffened and stiffened girders. The effect of this ratio was more pronounced for longitudinally unstiffened girders; this finding is not airtight since it was obtained considering a limited number of experimental tests and is further studied in Chapter 5.
- The current European design standard EN 1993-1-5 predicts lower ultimate strengths for longitudinally unstiffened and stiffened steel plate girders than the experimentally obtained results in this study. The maximum difference between these two analyses is 64% and 97% for longitudinally unstiffened ($s_s = 200$ mm) and stiffened steel plate girders ($s_s = 250$ mm), respectively. Based on the resistance model in EN 1993-1-5, the patch loading resistance increases linearly with an increase in patch load length (independently of the value of patch load length) for both longitudinally unstiffened and stiffened steel plate girders. This experimental investigation showed that after a specific patch load length (e.g., $s_s \geq 100$ mm), the ultimate strength of longitudinally stiffened steel plate

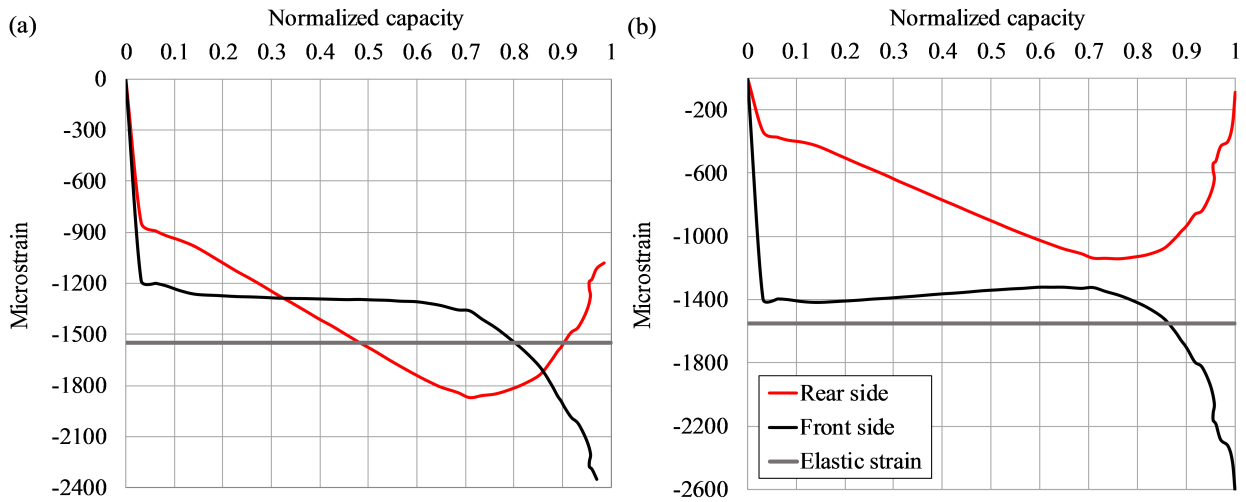


Figure 3.19: Vertical strain in the web plate on both sides (front-rear) for unstiffened girder B15 ($s_s = 100$ mm) at points placed 62.50 mm from the loaded flange and horizontally displaced from the vertical symmetry line for: (a) 12.5 mm; (b) 62.50 mm.

girders increases much faster with increasing patch load length. Thus, the design standard does not well capture those ultimate strengths.

Strain gauge measurements confirmed that the behavior of steel plate girders subjected to patch loading presents a complex elastoplastic behavior with early development of plastification. Local instability and buckling of the web panel of longitudinally unstiffened and stiffened steel plate girders appeared suddenly with no obvious indication and for applied forces $> 95\%$ of the ultimate load, whereas the first plastification appeared in the web panel at some points in the vicinity of the point of loading and for applied forces $> 50\%$ of the ultimate load.

A significant increase in the web deformation of the longitudinally unstiffened girders was observed below the point of loading, and larger buckling areas were engaged. In this case, the dominating buckle of the initial deformation of the web increased as the applied load increased – that is, it followed the initial deformation. The final buckling occurred in the direction of the buckle (it bent out in one buckle over the total web depth) with an increase in the load.

Two different failure modes were observed for longitudinally stiffened steel plate girders. A very local buckle (both vertically and horizontally) was dominant between the loaded flange and the longitudinal stiffener only for smaller patch load lengths ($s_s < 150$ mm). The final buckling occurred after snap-through buckling (opposite to the initial buckle) and local buckling failure mode of the loaded web sub-panel was observed. The longitudinal stiffener proved to be strong enough to limit the web deformation in the upper web sup-panel (the stiffener remained in the plane of the web). Increasing the patch load length ($s_s \geq 150$ mm) changed the failure mode – that is, the web bent out in one buckle similar to the unstiffened girders. In this case, the failure mode is characterized as global buckling (or interaction of global and local buckling) and noticeable longitudinal stiffener buckling was observed. The longitudinal stiffener reduced

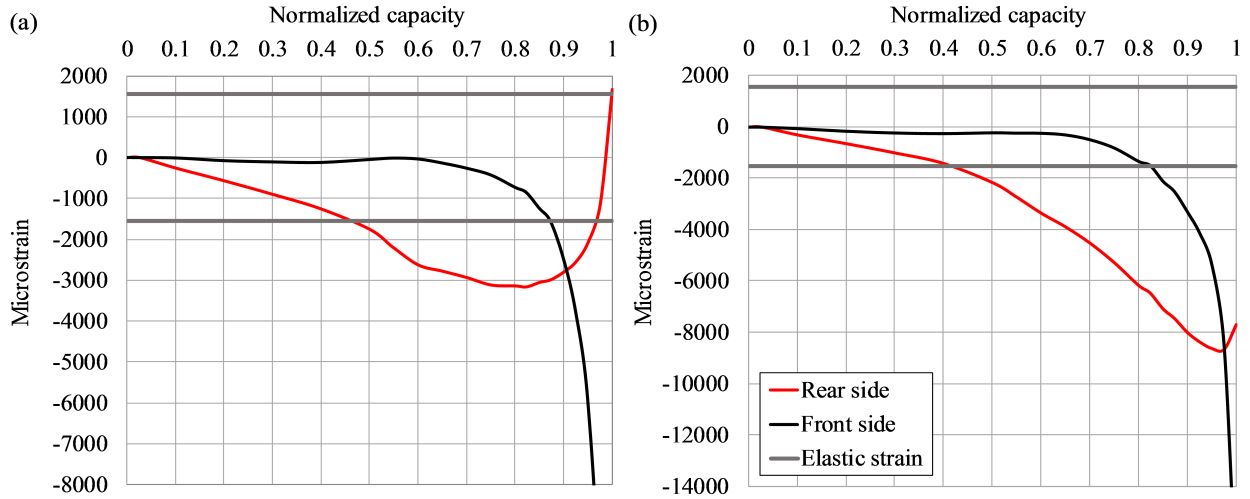


Figure 3.20: Vertical strain in the web plate on both sides (front-rear) for stiffened girder B5 ($s_s = 100$ mm) at points placed 10 mm from the loaded flange and horizontally displaced from the vertical symmetry line for: (a) 25 mm; (b) 50 mm.

the out-of-plane web deformation at the stiffener position but proved to be rather weak for this girder span and patch load lengths $s_s \geq 150$ mm. Thus, the longitudinal stiffener changed the buckling pattern (failure mode) and either restricted the web deformation between the loaded flange and stiffener (for smaller patch load lengths) or reduced the web deformation at the stiffener position (for longer patch load lengths). In both cases, it is more difficult for an initial deformation buckle to propagate from the unstiffened part of the web through the stiffener and move toward the loaded flange. This change in the buckling behavior increased the patch loading resistance, especially for longer patch load lengths. Moreover, based on the elastoplastic analysis, the longitudinal stiffener also decreased stresses in the bottom web sub-panel so that the yield did not occur.

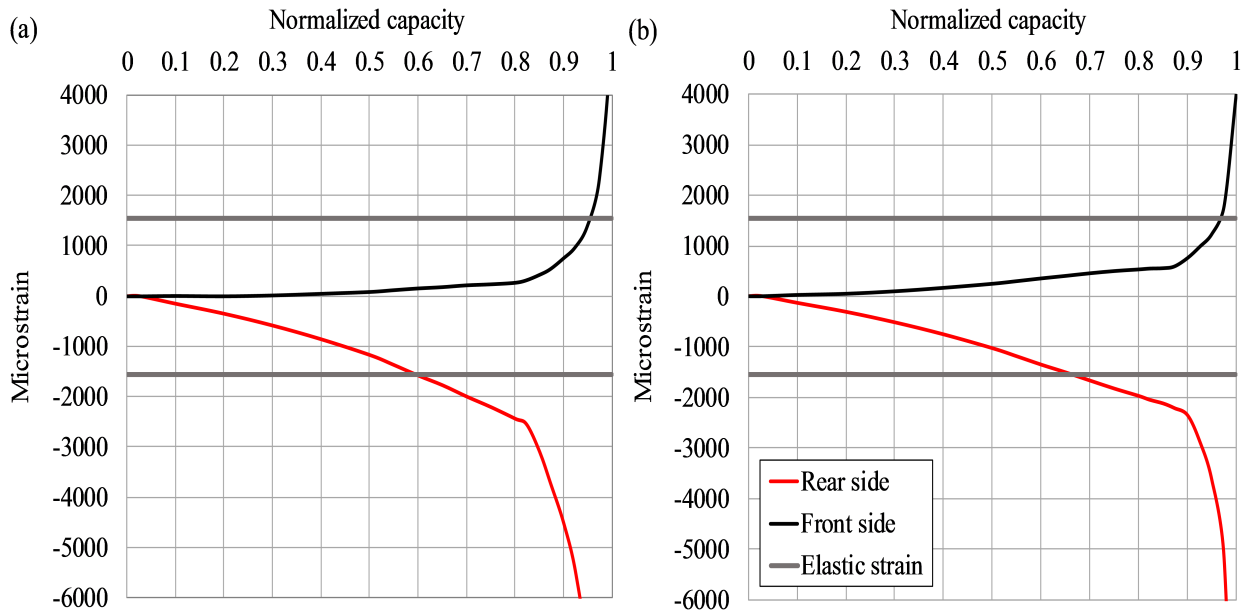


Figure 3.21: Vertical strain in the web plate on both sides (front-rear) for stiffened girder B5 ($s_s = 100$ mm) at points placed 37.50 mm from the loaded flange and horizontally displaced from the vertical symmetry line for: (a) 25 mm; (b) 50 mm.

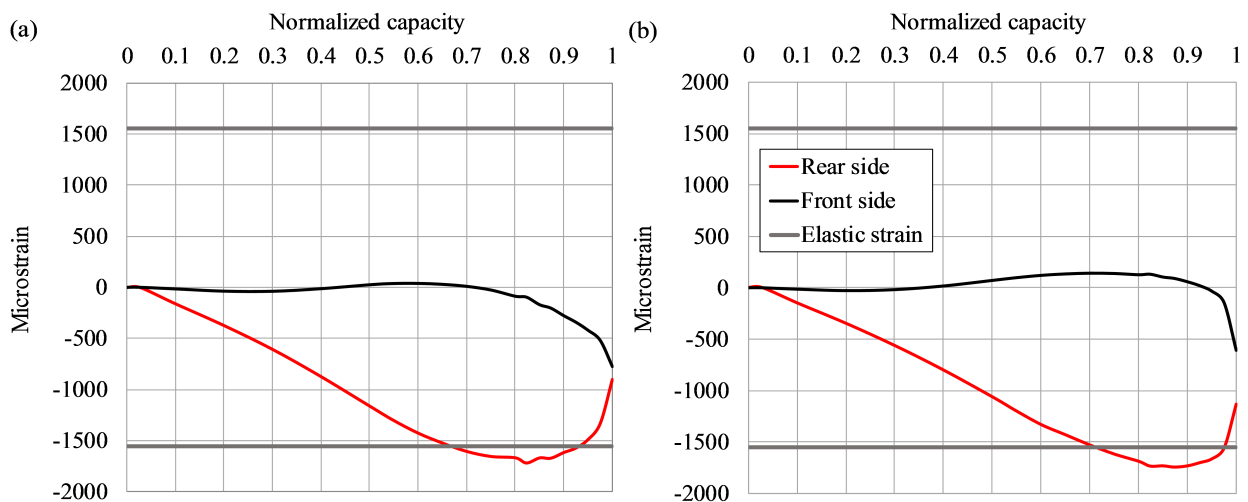


Figure 3.22: Vertical strain in the web plate on both sides (front-rear) for stiffened girder B5 ($s_s = 100$ mm) at points placed 62.50 mm from the loaded flange and horizontally displaced from the vertical symmetry line for: (a) 25 mm; (b) 50 mm.

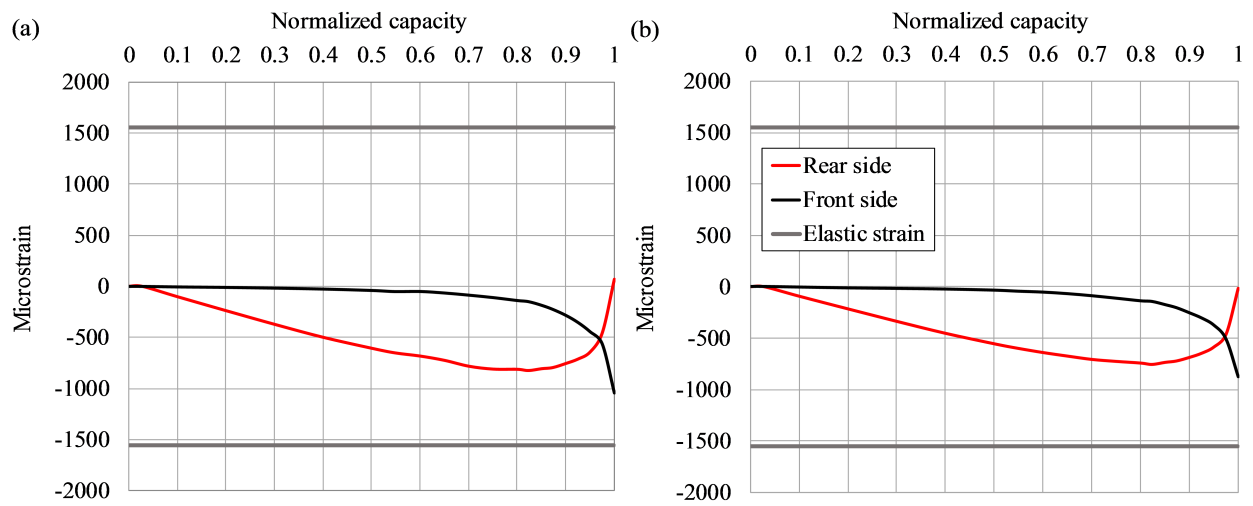


Figure 3.23: Vertical strain in the web plate on both sides (front-rear) for stiffened girder B5 ($s_s = 100$ mm) at points placed 112.50 mm from the loaded flange and horizontally displaced from the vertical symmetry line for: (a) 25 mm; (b) 50 mm.

Chapter 4

Numerical Model

4.1 Introduction

This Chapter presents a nonlinear numerical model used in this research. Nowadays, numerical analysis techniques are widely used in research and design involving steel structures and elements. Numerical modeling techniques are often employed to expand effectively limited experimental tests and scrutinize relevant parameters connected with analyzed problems. The main criterion for a trustworthy and accurate numerical analysis is the concurrence between numerical and experimental results. Thus, adequate and safe modeling of engineering problems presents an essential step in research and design. Moreover, the current European design standard EN 1993-1-5 [65] allows the usage of numerical analyses for the design of plate steel structures. Thus, it is obvious that the numerical approach and modeling technique represent a fundamental tool in research and design.

In this research, the computer simulations are performed by the finite element method, which has been proven to be a powerful tool for modeling the post-buckling behavior of plate girders under patch loading. The following section introduces a nonlinear finite element model which was employed in the parametric study (Chapter 5). The commercial multi-purpose finite element software Abaqus [80] was used as a computational and simulation tool. Patch loading resistances were determined using geometrically and materially nonlinear analysis to capture the post-buckling behavior fully. In order to efficiently and adequately trace the complex nonlinear path of the load-displacement response of girders, which generally can exhibit a decrease in load and/or displacement as the solution evolves, the modified Riks method [81] was used in the finite element analysis. This method is an incremental-iterative procedure and it is suitable for predicting unstable, geometrically nonlinear collapse of a structure including nonlinear materials [80].

The finite element model presented was validated by comparison with both series of testing (girders of Series A given in Ref. [21], and girders of Series B presented in Chapter 3 and Ref. [21]) and evoked further directions of the research. Some details of the present numerical

model and accompanying results in Chapter 5 and Chapter 6 are available in Refs. [82–86]. Numerical studies regarding the ultimate capacity of steel plate girders, including various patch load lengths and initial geometric imperfections, are conducted in Chapter 5 and the results are thoroughly discussed. Analysis regarding unfavorable geometric imperfections (from the patch loading point of view) is given in Chapter 6.

4.2 Finite element model

4.2.1 Geometry

The geometry of the girders considered was based on both series of testing given in Ref. [21] and in Chapter 3. The girder dimensions are tabulated in Table 4.1 and Table 3.1 (Chapter 3) for the girders of Series A and Series B, respectively. The only difference between these two experimental studies was the girder width, which was $a = 500$ mm in Ref. [21] and $a = 1000$ mm for the girders in Chapter 3. The thickness of the transverse stiffeners at both ends was 8 mm. A single flat longitudinal stiffener ($h_s = 30$ mm, $t_s = 8$ mm) reinforced the longitudinally stiffened steel plate girders in both experimental studies, and it was placed at one-fifth of the girder depth ($b_1 = 0.2h_w$), the optimum location for the flexural and shear resistance [66–68]. Refer to Fig. 3.1 in Chapter 3 for plate girder notation.

Table 4.1: Geometric characteristics of the experimentally tested girders of Series A.

No.	Girder Label	a [mm]	h_w [mm]	t_w [mm]	b_f [mm]	t_f [mm]	b_1 [mm]	s_s [mm]	h_s [mm]	t_s [mm]
1	A15 ¹	500	500	4	120	8	-	0	-	-
2	A14 ¹	500	500	4	120	8	100	0	30	8
3	A12 ¹	500	500	4	120	8	-	25	-	-
4	A4 ¹	500	500	4	120	8	100	25	30	8
5	A1 ¹	500	500	4	120	8	-	50	-	-
6	A3 ¹	500	500	4	120	8	100	50	30	8
7	A17 ¹	500	500	4	120	8	100	75	30	8
8	A11 ¹	500	500	4	120	8	-	100	-	-
9	A5 ¹	500	500	4	120	8	100	100	30	8
10	A6 ¹	500	500	4	120	8	100	125	30	8
11	A2 ¹	500	500	4	120	8	-	150	-	-
12	A7 ¹	500	500	4	120	8	100	150	30	8
13	A13 ¹	500	500	4	120	8	-	150	-	-
14	A16 ¹	500	500	4	120	8	100	150	30	8

¹ Experimentally tested in Ref. [21] and summarized in Ref. [25]

4.2.2 Geometry

To build the girder geometry and create a numerical model, the commercial multi-purpose finite element software Abaqus was employed [80]. The girders were modeled in real size using fully integrated four-node quadrilateral shell elements (S4) from the Abaqus element library. This first-order shell element has 6 DOFs per node (three displacements and three rotations). It is applicable for most thick and thin shell applications with large strains. They give realistic results, and it is unnecessary to model plate girders using computationally expensive solid continuum elements or more specialized finite element formulations. Reliability and accuracy of numerical results with the accepted element type were previously proved in other similar studies.

For all load blocks except for the half-round bar ($s_s = 0$ mm – crane wheel loading), a four-node 3D bilinear rigid quadrilateral element R3D4 was used. A very finely structured finite element mesh was applied to all the girders and load blocks with quadrilateral elements only. Special attention is paid to modeling the half-round bar $s_s = 0$ mm since there is no finite loading length. According to the experimental measurement, the radius of the half-round bar was 25 mm and it was modeled as such. Only for this loading block, a general-purpose fully integrated linear brick element C3D8 was employed. It was also meshed with hexahedral elements and the sweep meshing technique was adopted. The girders and load blocks were modeled in full size, and the finite element mesh for three representative models is shown in Fig. 4.1.

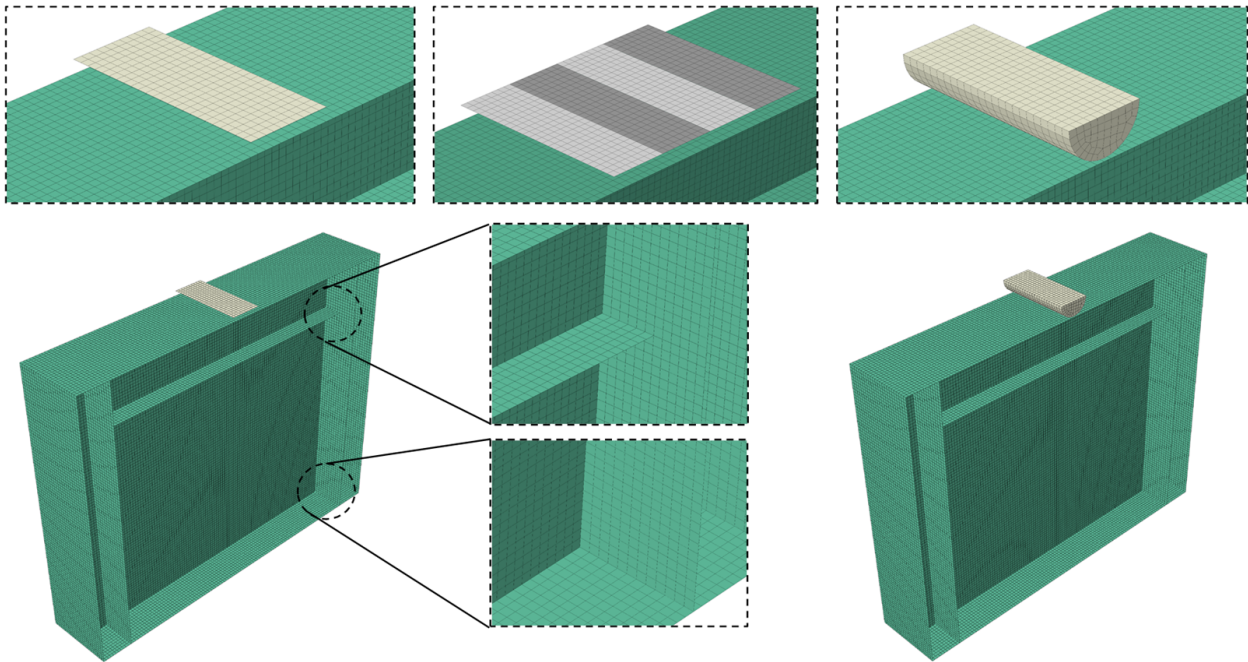


Figure 4.1: Finite element mesh for three representative models. Rigid blocks for $0 < s_s \leq 150$ mm (top-left), 4 independent rigid blocks for $s_s = 150$ mm (top-middle) and half-round bar for $s_s = 0$ mm (top-right). For the setup configuration of these loading blocks in the experiment, see Fig. 4 in Refs. [25] and Fig. 3.4 in Chapter 3.

In addition, an h -refinement (reduction in the element sizes) convergence study was performed for longitudinally stiffened and unstiffened steel plate girders, Fig. 4.2. One can instantaneously see that the last two subsequent mesh refinements (from 5 mm to 1.5 mm) did not change the results substantially – that is, the relative difference for all four girders is around 0.7% but the computational costs were exceedingly increased. Therefore, an element size of 5 mm was accepted for all girders considered in this research. The numerical models contained approximately 175,000 and 180,000 DOFs for longitudinally unstiffened and stiffened steel plate girders of Series A, respectively. The girders of Series B had approximately 260,000 and 266,000 DOFs for longitudinally unstiffened and stiffened steel plate girders, respectively. The load blocks were discretized from 120 to 1200 finite elements depending on the patch load length.

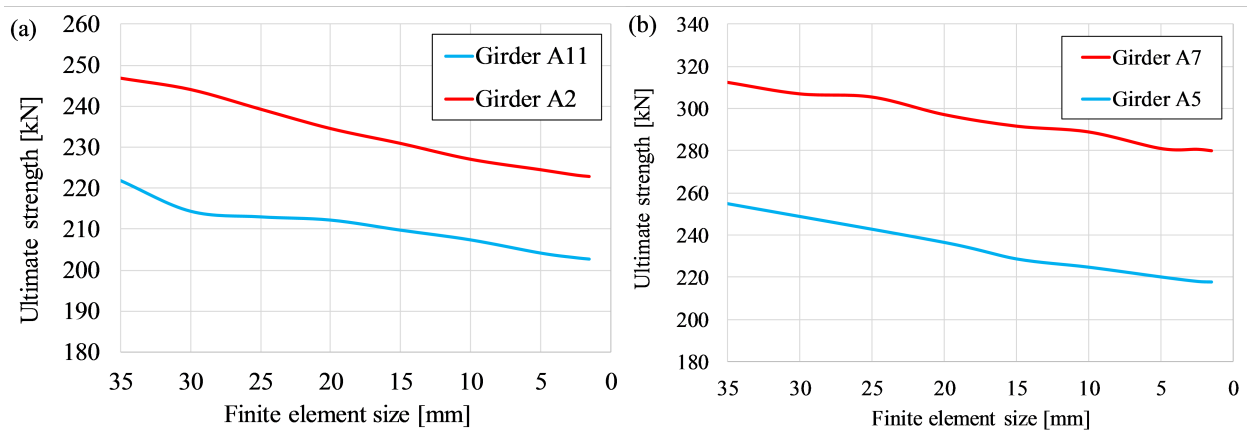


Figure 4.2: Convergence plot for the ultimate strength for longitudinally unstiffened (a) and stiffened (b) steel plate girders.

The structural elements (web plate, flanges, and transverse stiffeners) were merged in order to define a whole girder. A coupling constraint (restricting the motion of the stiffener to the connection line between the web plate and the stiffener) was applied to take into account the influence of the longitudinal stiffener. In this case, all translational and rotational DOFs were constrained. To avoid overlapping at the junction where the flange plates were welded to the web plate, the shell nodes of the flanges were offset so that they were located at the top or bottom surface of the shell instead of the mid-plane. On the other hand, the web plate, transverse, and longitudinal stiffener surface were modeled as the mid-plane.

4.2.3 Boundary and loading conditions

The girders were modeled as simply supported (preventing vertical displacement and displacement perpendicular to the plane of the web panel) at the transverse stiffeners. These boundary conditions correspond to the experimental setup used in Ref. [21] and the testing program in Chapter 3. An additional node at the middle of the lower flange was only constrained in the longitudinal direction of the girder. These boundary conditions were used in both linear buckling, and geometrically and materially nonlinear analyses.

In order to include the same loading conditions as in the experiments [21], the rigid loading blocks (see Fig. 4 in Ref. [25] and Fig. 3.4 in Chapter 3) were modeled as separate structural elements, and applied loads were transferred through these elements onto the upper flange. The width of the load blocks was the same as the upper flange, while the length was varied from 0 to 150 mm. However, for the parametric study (Chapter 5), the patch load length was extended up to 250 mm. The central node of the loading blocks was defined as the master node while the corresponding nodes on the loaded flange were defined as slave nodes. The displacement-controlled approach was applied, accompanied by a small compressive displacement applied to the master node. Then, the analysis is continued by performing an incremental load-deflection analysis using the modified Riks method [81] to trace the complex nonlinear load-displacement response of the girders. To simulate real loading conditions as in the experiments (Ref. [21] and Chapter 3), all DOFs of the master node were restricted except in the vertical direction. The structural interaction between the loading blocks and the loaded flange was defined using an equation-based constraint – that is, the slave nodes followed the master node which enabled an equal displacement for each loaded node on the upper flange. As mentioned above, the half-round bar was modeled differently. In this case, the interaction is defined by a tie-based constraint. The nodes on the bottom side of the half-round bar were tied with the nodes on the upper flange where all DOFs were tied. A surface-to-surface discretization method, along with the finite sliding formulation and contact properties (normal behavior – hard contact, tangential behavior – frictionless), was employed for the contact definition between the loading blocks and the loaded flange.

Remark: The load block for an even distribution of the applied load over the entire load length (special load block for $s_s = 150$ mm, see Fig. 4 in [25]) was idealized with 4 independent rigid blocks, cf. Fig 4.1. This load configuration was only used for comparison with the experimental results (girders A13 and A16). The patch load length $s_s = 150$ mm was modeled as one rigid block in the parametric study (Chapter 5).

Remark: It is worth noting that some authors used rigid boundary conditions (kinematic boundary constraints at both girder ends) instead of vertical stiffeners. However, based on the parametric analysis given in Ref. [87], the authors showed that the application of this approach is only justified for small patch load lengths ($s_s/a \leq 0.25$). Moreover, they pointed out that a better match between experimental and numerical results is obtained including transverse stiffeners. Based on this analysis and since the testing programs in Ref. [21] and in Chapter 3 included patch load lengths from $s_s/a = 0$ to $s_s/a = 0.3$, which is further extended in the parametric analysis (Chapter 5) up to $s_s/a = 0.5$, transverse stiffeners were modeled in all models presented in the current research.

Remark: Another interesting point regarding boundary conditions is the usage of symmetry conditions and modeling one-half of girders. Some authors used the symmetry boundary conditions and modeled one-half of girders, which represents a powerful tool for decreasing computational time and resources. However, in present numerical model, the symmetry boundary

conditions were not included since the experimentally measured geometric imperfections are highly asymmetric and, thus, the whole girder was modeled. In addition, the symmetry boundary conditions incorporated into an eigenvalue buckling analysis entirely generate symmetric buckling modes. On the other hand, modeling the whole girders could also give asymmetric ones. For instance, in current analysis, the third buckling mode for longer patch load lengths is not a symmetric mode; refer to Fig. 5.5 and Fig. 5.9 in Chapter 5. Therefore, care should be taken in order to use this approach in an automated parametric study.

4.2.4 Material properties

The material characteristics of the web panel and flanges of each girder were determined using multiple standard tensile coupon tests. To include material nonlinearity in Abaqus, the engineering stress-strain diagrams (obtained by tensile coupon tests) were transformed into the true stress-true strain relationship

$$\sigma_{true} = \sigma_{eng}(1 + \epsilon_{eng}) \quad (4.1)$$

$$\epsilon_{ln} = \ln(1 + \epsilon_{eng}), \quad (4.2)$$

where σ_{eng} and ϵ_{eng} are engineering stress and strain, respectively. The material was incorporated into the numerical model as isotropic material with the isotropic work hardening assumption using material data obtained from standard tensile tests. The nonlinear stress-strain relationship was idealized by a multi-linear stress-strain curve assuming hardening up to the ultimate strength of the material. After the ultimate stress was reached, an indefinitely ductile plateau was assumed.

The material properties of girders of Series A did not show significant deviations. Hence, one stress-strain curve for the web panels (steel elements with a thickness of 4 mm) and another one for the flange, transverse, and longitudinal stiffeners (steel elements with a thickness of 8 mm) were used in all the simulations presented for girders of Series A, Fig. 4.3. These stress-strain curves represent a mean curve from the behavior of all uniaxial tests for the web panels and flanges. However, the tested girders of Series B could be divided into three groups based on the web panel yield stress f_{yw} – that is, one girder (B2) with f_{yw} approximately 225 MPa, two girders (B1 and B6) with f_{yw} approximately 260 MPa, and four girders (B3, B4, B5, and B7) with f_{yw} approximately 320 MPa. It is worth mentioning that these deviations in the web panel yield stress were not the author’s initial intention, and they were noticed after experimental testing; refer to Appendix A for more details. These values for the yield stresses of each girder group were used for comparison with experimental data and model validation (Section 4.3). The average value of the flange yield stress of all the tested girders of Series B was approximately 318 MPa with no significant fluctuation; refer to Appendix A for more details. The stress-strain curves employed for model validation for the girders of Series B are

given in Fig. 4.4, Fig. 4.5, and Fig. 4.6 for both steel elements with a thickness of 4 and 8 mm. In addition to this, Young's modulus of 205 GPa and Poisson's ratio of 0.3 were employed to define the elastic behavior of the girders in both series A and B.

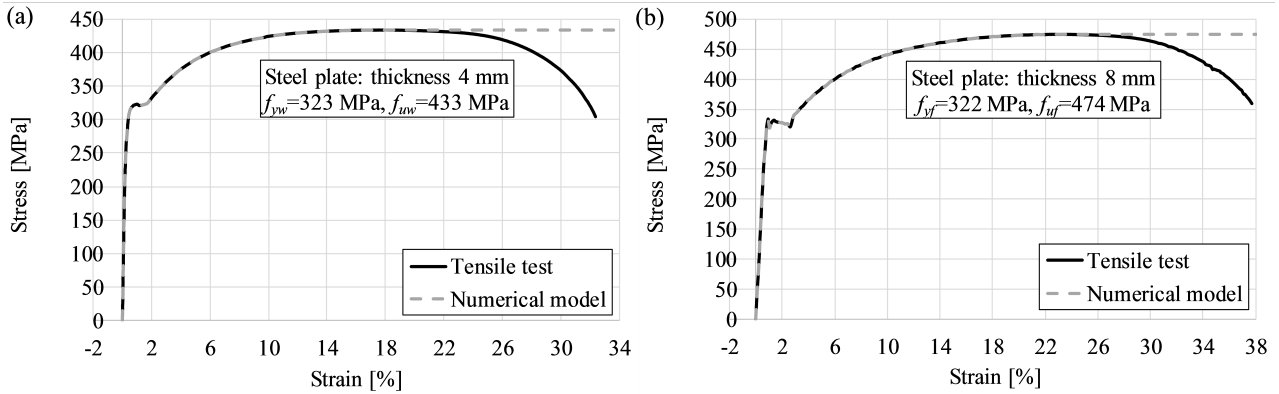


Figure 4.3: Engineering stress-strain curves obtained by tensile test vs. curves used in the simulations for (a) web plate, and (b) flanges, transverse and longitudinal stiffeners for all the girders of Series A.

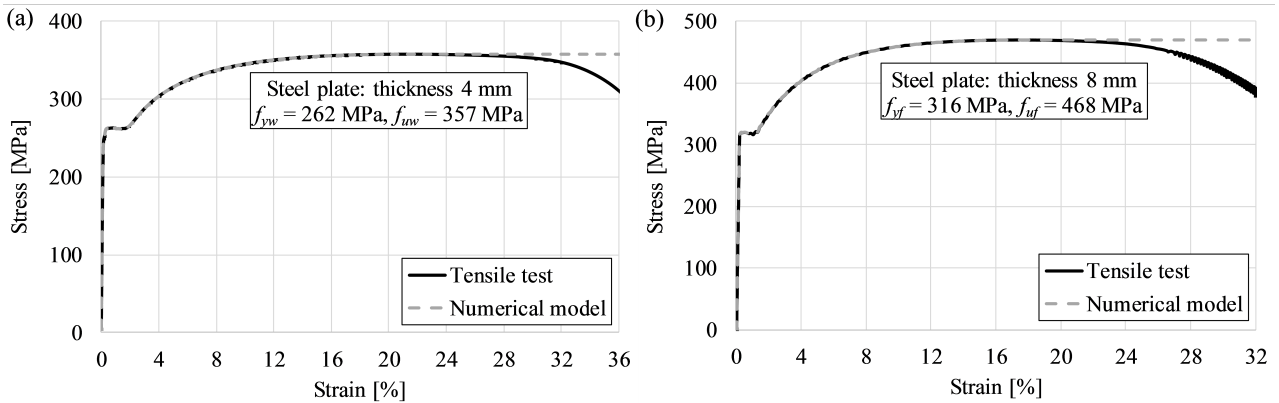


Figure 4.4: Engineering stress-strain curves obtained by tensile test vs. curves used in the simulations for (a) web plate, and (b) flanges, transverse and longitudinal stiffeners for girders B1 and B6.

4.2.5 Initial imperfections

Initial geometric imperfections are defined by initially imperfect plates following a certain shape. They can be introduced into numerical modeling in different ways, e.g., using experimental data (experimentally measured imperfections), buckling mode shapes obtained from an eigenvalue buckling analysis, or considering imperfections as a two-dimensional random field. For a better validation between the numerical model and the experimental results, the experimentally measured initial geometric web panel imperfections (precise shapes of geometric imperfections) were used. Contour plots of web panel geometric imperfections employed in this research can be found in Appendix B and C for the girders of Series A and B, respectively.

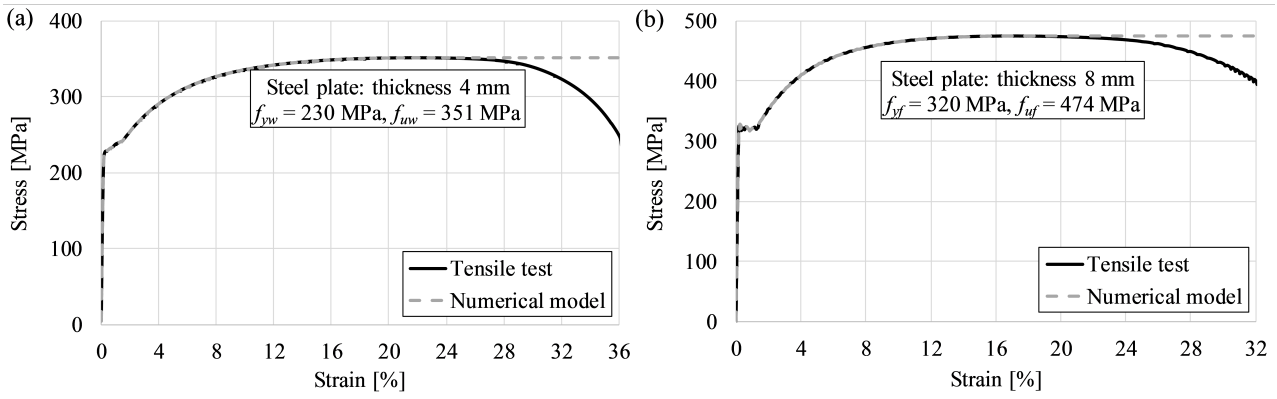


Figure 4.5: Engineering stress-strain curves obtained by tensile test vs. curves used in the simulations for (a) web plate, and (b) flanges, transverse and longitudinal stiffeners for girder B2.

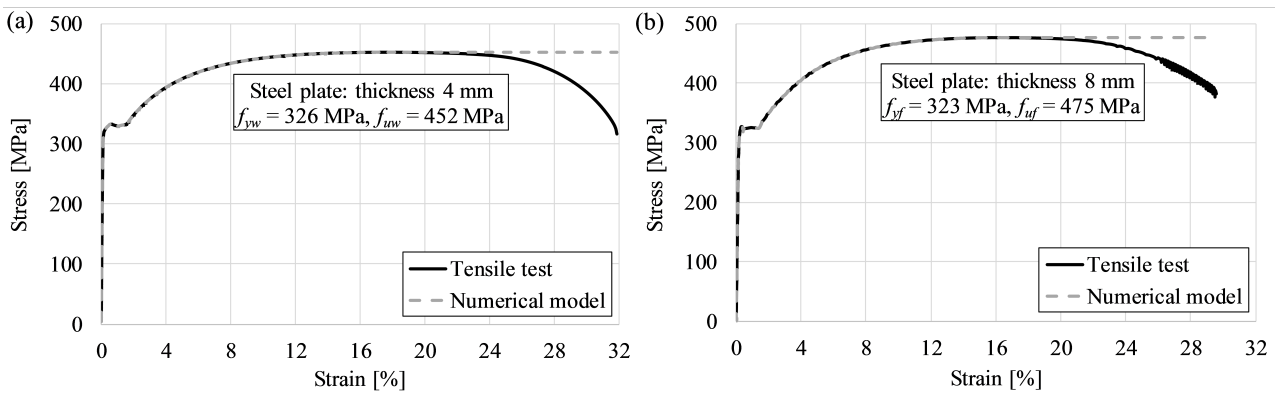


Figure 4.6: Engineering stress-strain curves obtained by tensile test vs. curves used in the simulations for (a) web plate, and (b) flanges, transverse and longitudinal stiffeners for girders B3, B4, B5, and B7.

Special of interest is devoted to studying the influence of initial geometric imperfections in the parametric study presented in Chapter 5. Papers dealing with measured geometric imperfections considering patch loading solely as a load case are scarce. For instance, Refs. [88–89] are dealing with the experimentally measured initial geometric imperfections for longitudinally unstiffened, while Refs. [22,23,52] for stiffened steel plate girders. The modeling technique for the measured initial geometric web panel imperfection is illustrated in Fig. 4.7. Modeling these imperfections represents a challenge and includes the following steps. Firstly, all web panel imperfections were recorded as 3D points (x , y , z coordinates) before each test using a uniform-spaced grid pattern (50x50 mm). Secondly, the point-wise web panel imperfections were then imported into the commercial 3D computer graphics and CAD software Rhinoceros [90] in order to define a NURBS surface. The surface was sketched from the grid of points that lie on the surface using second-order interpolation functions in both directions. After that, the surface developed was exported as an ACIS SAT file and imported into Abaqus.

Contrary to the webs, all other girder elements – the flanges, transverse and longitudinal stiffeners – were modeled as perfectly straight surfaces. The available pre-processor in Abaqus was employed to assemble all the elements to define a whole girder and mesh the model.

Therefore, the meshing step is performed on an imperfect specimen. However, one can introduce the initial geometric imperfections using the opposite way – that is, performing the meshing step on a perfect specimen and changing the coordinates of all nodes according to measured imperfections [91].

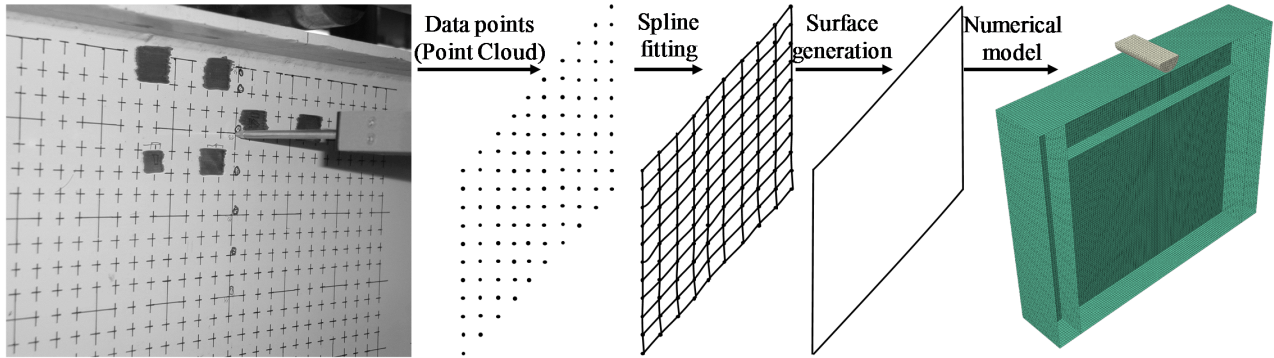


Figure 4.7: Modeling technique for measured initial geometric imperfections.

On the other hand, structural imperfections (characterized by a residual stress pattern and can be differently idealized based on different design codes) were not considered since they do not play a decisive role as reported in Refs. [88,92–93] for longitudinally unstiffened steel plate girders. Also, any flaws concerning unintended rotation of the loaded flange by the load application were not included.

4.3 Model validation

As stated before, one of the objectives of this research is a numerical investigation of the influence of patch load length, in combination with a variety of geometric imperfections, on the ultimate strength and behavior of steel plate girders. To examine the effect of patch load length and geometric imperfections on the ultimate capacity of steel plate girders, a parametric study utilizing finite element analysis is carried out in Chapter 5. To perform parametric research and investigate the problem further, it is necessary to calibrate the numerical model so that the finite element analysis gives a reasonable resemblance to the experiments. The patch loading resistance of all the experimentally tested girders of both series of testing A and B are compared with the above-described numerical model, followed by a comparison of elastoplastic behavior between the experimental and numerical investigations.

The patch loading resistance was determined using geometrically and materially non-linear analysis. The material properties used are described in Section 4.2.4, while initial geometric imperfections were included based on the experimentally measured imperfections and their original amplitudes (Section 4.2.5).

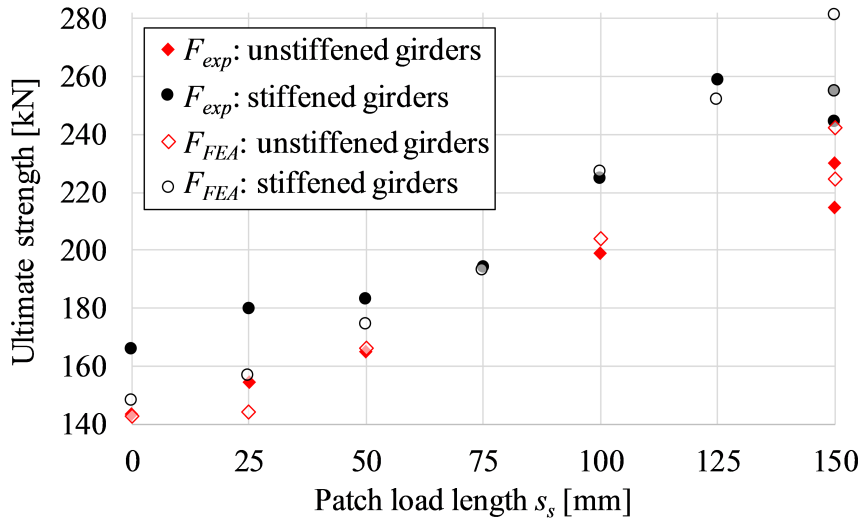


Figure 4.8: Comparison between the experimentally and numerically obtained ultimate strengths for the girders of Series A.

4.3.1 Patch loading resistance

The experimentally and numerically evaluated patch loading resistances were juxtaposed for model validation. Table 4.2 and Table 4.3 show a comparison summary of the numerically and experimentally obtained ultimate strengths for the girders of Series A and B, respectively. A graphical comparison is portrayed in Fig. 4.8 and Fig. 4.9 for both series of testing A and B, respectively. Table 4.2 and Table 4.3 show that the numerically determined ultimate strengths agree remarkably well with the experimental results. The numerical model returned an average error of 0.83% and 2.60% for unstiffened and stiffened girders of Series A, respectively. In addition, the model exhibited an average error of 6.15% and 2.78% for unstiffened and stiffened girders of Series B, respectively. It is noteworthy to observe that the experimentally obtained ultimate loads are slightly larger for smaller patch load lengths than the numerical ones. In view of the preceding analysis, it should be mentioned that all numerical simulations included the same material characteristics for the girders of Series A (cf. Fig. 4.3) and small discrepancies between the results are expected.

4.3.2 Elastoplastic behavior

As a further comparison, the elastoplastic behavior of the experimentally tested girders of Series A and numerical simulations are addressed. As reported in Refs. [21,25], the elastoplastic behavior for girders A1, A2, A3, and A7 is discussed in detail. It is compared here with the present numerical model through von Mises stress contour plots at different ultimate load levels. The von Mises stress is calculated as

$$\sigma_{vm} = \left(\frac{3}{2}\mathbf{S}:\mathbf{S}\right)^{1/2}, \quad (4.3)$$

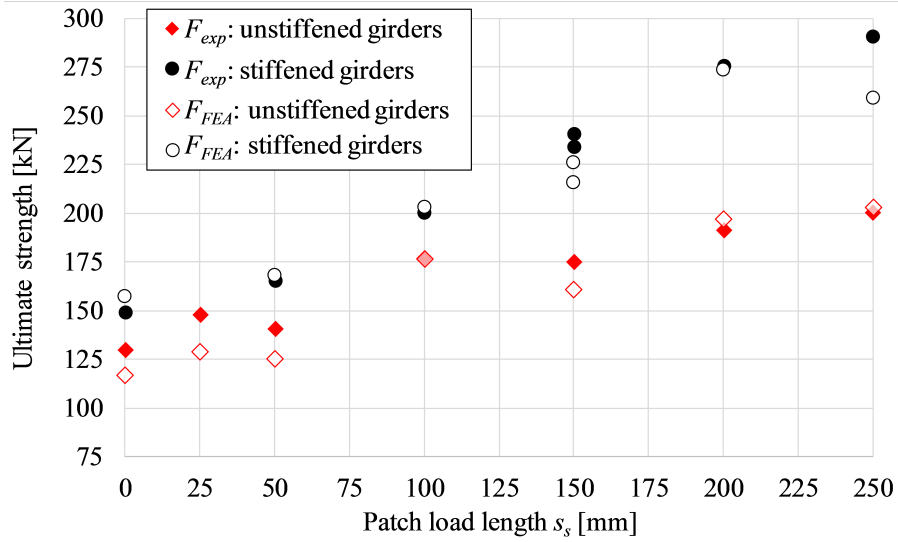


Figure 4.9: Comparison between the experimentally and numerically obtained ultimate strengths for the girders of Series B.

Table 4.2: Comparison between the experimentally and numerically obtained ultimate strengths for all the girders of A series. Units are in kN.

Unstiffened girders	A15 $s_s = 0$ mm	A12 $s_s = 25$ mm	A1 $s_s = 50$ mm	A11 $s_s = 100$ mm	A2 $s_s = 150$ mm	A13 $s_s = 150$ mm (even.distr.)		
$F_{exp,unstiff}$	143.30	154.60	165.00	199.00	215.00	230.00		
$F_{FEA,unstiff}$	142.73	144.32	166.02	204.18	224.53	242.35		
F_{exp}/F_{FEA}^1	1.00	1.07	0.99	0.97	0.96	0.95		
Stiffened girders	A14 $s_s = 0$ mm	A4 $s_s = 25$ mm	A3 $s_s = 50$ mm	A17 $s_s = 75$ mm	A5 $s_s = 100$ mm	A6 $s_s = 125$ mm	A7 $s_s = 150$ mm	A16 $s_s = 150$ mm (even.distr.)
$F_{exp,stiff}$	165.90	180.00	183.00	194.30	225.00	259.00	255.00	244.60
$F_{FEA,stiff}$	148.09	156.89	174.58	193.09	227.13	251.78	281.25	254.71
F_{exp}/F_{FEA}^2	1.12	1.15	1.05	1.01	0.99	1.03	0.91	0.96

¹ Mean = 0.99, coefficient of variation = 4.45%

² Mean = 1.03, coefficient of variation = 7.75%

where \mathbf{S} is the deviatoric stress tensor. As can be seen in Fig. 4.10 and Fig. 4.11, the yielding started at about 50% of the maximum load for patch load length $s_s = 50$ mm, while for patch load length $s_s = 150$ mm, the plastification occurred at 85% of the ultimate load (Fig. 4.12 and Fig. 4.13), which is in full compliance with the discussion addressed in Refs. [21,25]. Furthermore, these figures also proved that stresses in the lower web sub-panel were far below the yield stress. This fact justifies the usage of girders in repeated tests – that is, loaded on the opposite flange. One should bear in mind that the values shown in these figures are averaged at nodes since the von Mises stress is not a nodal field output. The values are stored at the Gauss integration points and for visual detection of plastification, they are extrapolated at

Table 4.3: Comparison between the experimentally and numerically obtained ultimate strengths for all the girders of Series B. Units are in kN.

Unstiffened girders	B16 ² $s_s = 0$ mm	B14 ³ $s_s = 25$ mm	B1 ² $s_s = 50$ mm	B15 ³ $s_s = 100$ mm	B2 ¹ $s_s = 150$ mm	B12 ¹ $s_s = 200$ mm	B11 ² $s_s = 250$ mm
$F_{exp,unstiff}$	129.90	147.90	140.30	176.90	174.60	190.90	199.90
$F_{FEA,unstiff}$	116.39	128.56	125.28	176.61	160.68	196.74	202.86
F_{exp}/F_{FEA}^4	1.12	1.15	1.12	1.00	1.09	0.97	0.99
Stiffened girders	B13 ³ $s_s = 0$ mm	n.a.	B3 ³ $s_s = 50$ mm	B5 ³ $s_s = 100$ mm	B7 ³ B17 ³ $s_s = 150$ mm	B4 ³ $s_s = 200$ mm	B6 ² $s_s = 250$ mm
$F_{exp,stiff}$	148.60		164.90	200.30	240.30 233.90	275.30	290.30
$F_{FEA,stiff}$	157.22		168.07	203.06	225.44 215.33	273.13	258.77
F_{exp}/F_{FEA}^5	0.95		0.98	0.99	1.07 1.09	1.01	1.12

¹ Average web panel yield stress $f_{yw} = 225.50$ MPa, average flange yield stress $f_{yf} = 312.50$ MPa

² Average web panel yield stress $f_{yw} = 259.50$ MPa, average flange yield stress $f_{yf} = 314.75$ MPa

³ Average web panel yield stress $f_{yw} = 319.35$ MPa, average flange yield stress $f_{yf} = 321.50$ MPa

⁴ Mean = 1.06, coefficient of variation = 6.95%

⁵ Mean = 1.03, coefficient of variation = 6.26%

n.a. = not available (this data is missing due to the limited number of tests available from 7 steel plate girders)

nodes using a 75% averaging threshold.

Additionally, the vertical displacement of the load cell was not recorded in the experimental campaign but rather an out-of-plane deflection of the web plate (at a specific point on the web plate or the whole middle line web profile) or the vertical displacement of the loaded flange at points eccentrically placed with respect to the web plane. However, the load-displacement response for the vertical displacement and normalized capacity (normalized with respect to the girder's ultimate load), where the vertical displacement represents the displacement of the loading node, can be extracted from the finite element simulations, Fig. 4.14, Fig. 4.15, and Fig. 4.16. These plots also support the findings from the experiments and show a linear behavior up to at least 80% of the ultimate load. In addition, plotting the load-displacement response for longitudinally unstiffened and stiffened steel plate girders on the same scale clearly shows the difference in the behavior of unstiffened and stiffened webs. One can instantaneously see that nonlinearities for the longitudinally stiffened steel plate girders occurred for much higher loads. After the ultimate strength was reached, the behavior can be the same as for unstiffened webs for small patch load lengths. In contrast, for longer patch load lengths, the load decreased considerably faster for the longitudinally stiffened steel plate girders.

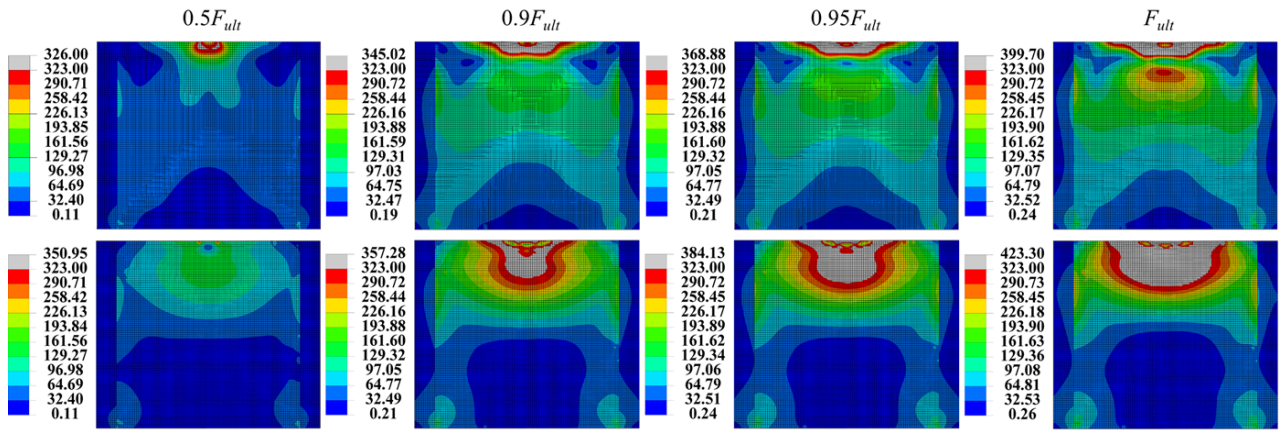


Figure 4.10: von Mises stress contour plots [MPa] for unstiffened steel plate girder A1 ($s_s = 50$ mm) at different levels of the ultimate load. The contour plots at the top represent stresses in the shell surface facing the reader while the bottom plots represent the other surface.

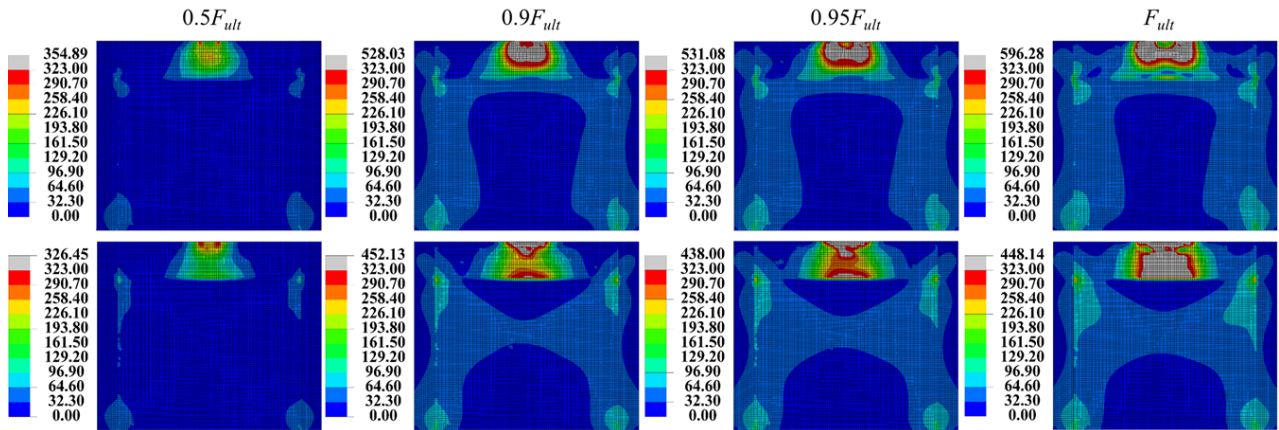


Figure 4.11: von Mises stress contour plots [MPa] for stiffened girder A3 ($s_s = 50$ mm) at different levels of the ultimate load. The contour plots at the top represent stresses in the shell surface facing the reader (longitudinal stiffener's side) while the bottom plots represent the other surface.

4.4 Summary

This Chapter presents the finite element model employed in this research. Details about the girder geometry, finite element mesh, boundary, and loading conditions are discussed. Experimentally measured material properties and geometric imperfections are incorporated into the numerical model for better concurrence with experimental results. Numerically determined ultimate strengths and post-buckling behaviors of longitudinally unstiffened and stiffened steel plate girders are in good agreement with the experiment.

Conclusively, the present numerical model can be further exploited to reach a deeper insight into the behavior and ultimate strength of steel plate girders subjected to patch loading. The finite element modeling technique presented and verification of the model with the experimental results enabled a fruitful basis for parametric analysis. A large number of numerical tests are developed in the next Chapter to investigate imperfection sensitivity analysis of steel

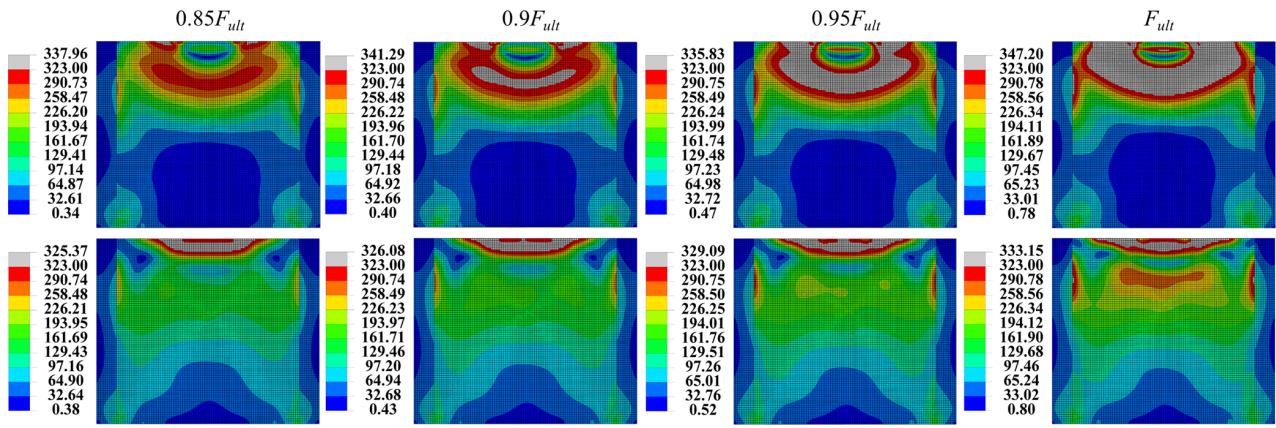


Figure 4.12: von Mises stress contour plots [MPa] for unstiffened girder A2 ($s_s = 150$ mm) at different levels of the ultimate load. The contour plots at the top represent stresses in the shell surface facing the reader while the bottom plots represent the other surface.

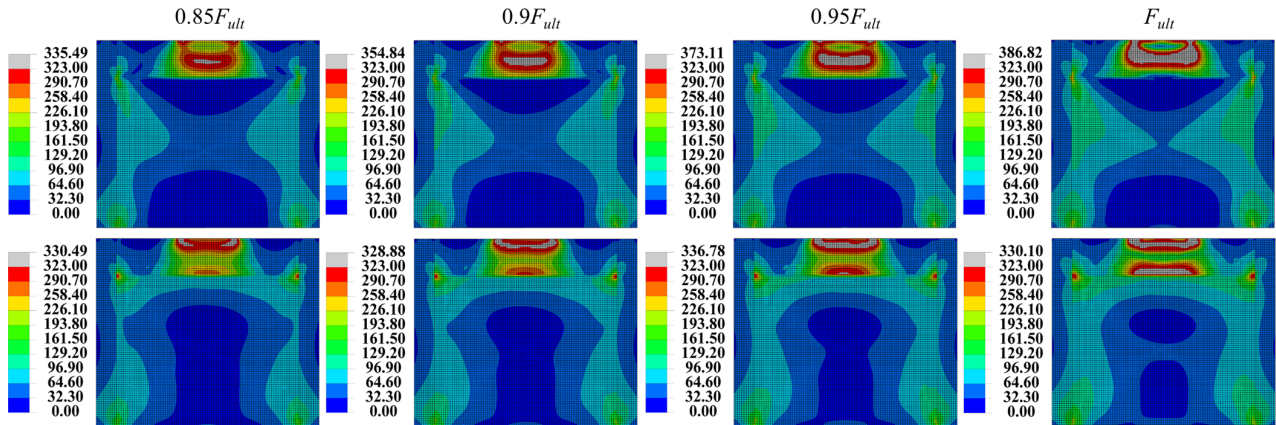


Figure 4.13: von Mises stress contour plots [MPa] for stiffened girder A7 ($s_s = 150$ mm) at different levels of the ultimate load. The contour plots at the top represent stresses in the shell surface facing the reader (longitudinal stiffener's side) while the bottom plots represent the other surface.

plate girders subjected to patch loading.

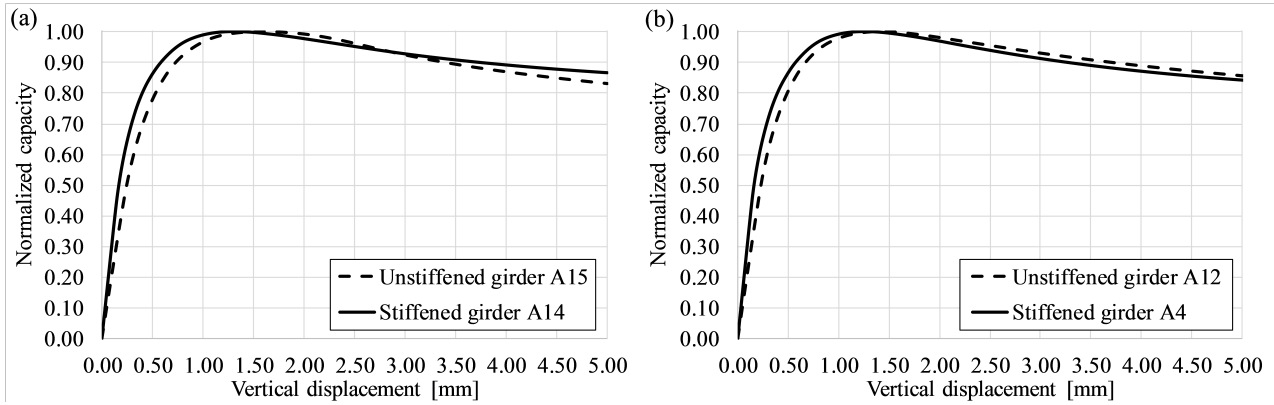


Figure 4.14: Load-displacement response for unstiffened and stiffened steel plate girder under the patch load length of: (a) $s_s = 0$ mm; (b) $s_s = 25$ mm.

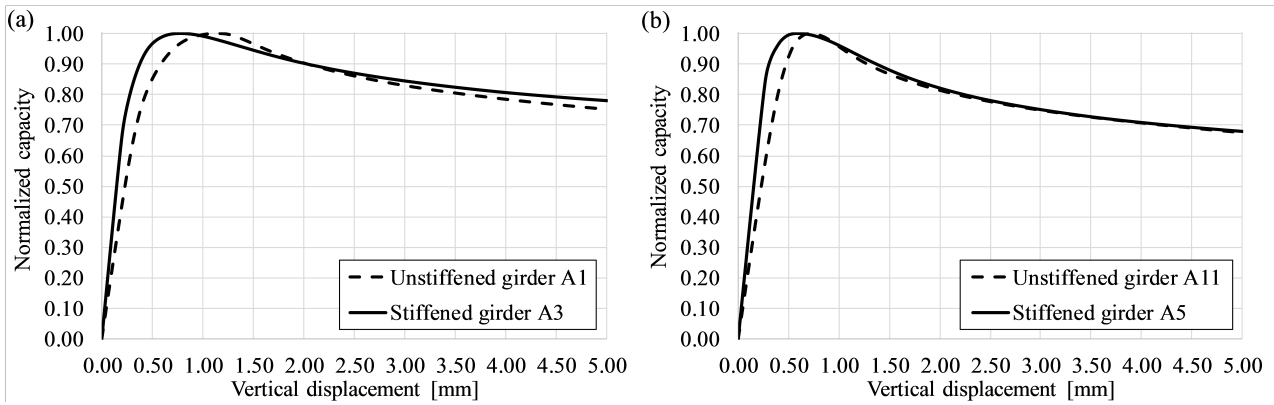


Figure 4.15: Load-displacement response for unstiffened and stiffened steel plate girder under the patch load length of: (a) $s_s = 50$ mm; (b) $s_s = 100$ mm.

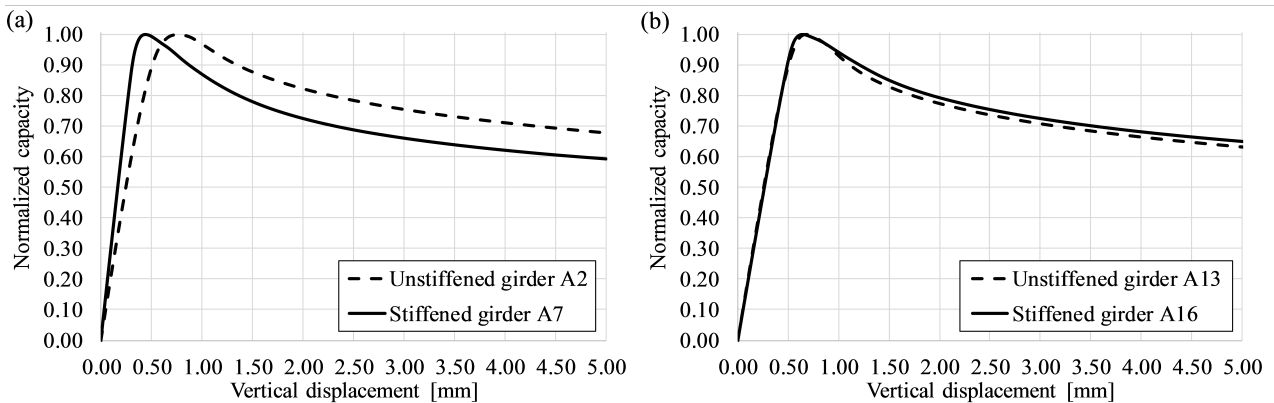


Figure 4.16: Load-displacement response for unstiffened and stiffened steel plate girder under the patch load length of: (a) $s_s = 150$ mm; (b) $s_s = 150$ mm (distribution block).

Chapter 5

Parametric Study

Since the numerical model presented is proved to be valid and accurate for describing the behavior and ultimate strength of the experimental tests (Chapter 4), an additional set of numerical analyses is performed. The present finite element parametric study was designed to determine the effect of a variety of geometric imperfections (in combination with various patch load lengths) on the patch loading resistance of I-shaped steel plate girders.

5.1 Parameters

The patch load length, s_s , was varied from 0 mm ($s_s/h_w = 0$) to 250 mm ($s_s/h_w = 0.50$). Geometric imperfections included the experimentally measured imperfections, buckling mode-affine, and hand-defined sinusoidal imperfections. The geometric imperfections considered were defined similarly to both Series A (girder width $a = 500$ mm, $\alpha = 1$) and Series B (girder width $a = 1000$ mm, $\alpha = 2$); thus, a direct comparison could be made between these analyses. Twenty different geometric imperfections were considered for each series of girders (Series A and Series B). The experimentally measured geometric imperfection shapes for all the girders of Series A and Series B are provided in Appendix B and C, respectively. Representative shapes for one experimentally measured geometric imperfection, buckling mode-affine, and hand-defined sinusoidal imperfections are given further in the text from Fig. 5.1 to Fig. 5.10.

A single flat longitudinal stiffener reinforced stiffened steel plate girders of both Series A and B. One longitudinal stiffener was used for girders of Series A ($h_s = 30$ mm and $t_s = 8$ mm; originally employed in the experimental program [21,25]). Two different flat longitudinal stiffeners were considered for girders of Series B: a relatively *weak* longitudinal stiffener, $\gamma_s = 21.67$ ($h_s = 30$ mm and $t_s = 8$ mm), and a relatively *strong* longitudinal stiffener, $\gamma_s = 103.46$ ($h_s = 55$ mm and $t_s = 8$ mm). The weak longitudinal stiffener proved to be strong enough (e.g., no longitudinal stiffener buckling was noted) for the girder geometry of Series A [21,25] ($\alpha = 1$) and patch load lengths $s_s/h_w < 0.30$ for girders of Series B ($\alpha = 2$). However, for longer patch load lengths for $\alpha = 2$, this longitudinal stiffener proved to be weak (e.g., noticeable

longitudinal stiffener deformation was observed), and thereby a stronger longitudinal stiffener was included in the current study; refer to Chapter 3 for more details. The relative flexural stiffness of the longitudinal stiffener γ_s is defined from Eq. (2.7) in Chapter 2. For the analyzed girder geometries of both series of girders ($\alpha = 1$ and $\alpha = 2$), the limit value of relative stiffness was $\gamma^* = 34$ and $\gamma^* = 146$ for girders of Series A and B, respectively. All parameters varied in the parametric study are summarized in Table 5.1. The current numerical database contains 360 and 540 runs for Series A and Series B, respectively.

Table 5.1: Parameters varied in the parametric study.

Geometric imperfection	Patch load length s_s	Girders	Relative stiffness γ_s^1	Total number of simulations
<ul style="list-style-type: none"> • 14 experimentally measured imperfections • 4 buckling mode-affine imperfections • 2 hand-defined sinusoidal imperfection shapes 	9 different patch load lengths ($s_s/h_w = 0 - 0.50$)	Series A $\alpha = 1$	$\gamma_s = 0$ (unstiffened) $\gamma_s = 21.67^2$	360
		Series B $\alpha = 2$	$\gamma_s = 0$ (unstiffened) $\gamma_s = 21.67^2$ $\gamma_s = 103.46^2$	540

¹ Refer to Eq. (2.7) and [65] for longitudinal stiffener relative stiffness calculation

² Limit value of relative stiffness of the longitudinal stiffener for girders of Series A and B is $\gamma^* = 34$ and $\gamma^* = 146$, respectively

The girder dimensions (Table 3.1 and Table 4.1) and position of the longitudinal stiffener ($b_1 = 0.2h_w$) were kept unaltered. In addition, the material properties of the web panel and flanges were adopted from the experimentally tested girders of Series A [21,25], with the web panel yield stress $f_{yw} = 323$ MPa and flange yield stress $f_{yf} = 322$ MPa accompanying the stress-strain curves given in Fig. 4.3. The maximum geometric imperfection amplitude was set to be $w_0 = h_w/100$, as frequently used in similar studies [40,88,94–95]. All parameters that were kept unchanged in the parametric study are given in Table 5.2.

Table 5.2: Parameters kept unaltered in the parametric study for both series A and B.

Girder dimensions	Material properties	Imperfection amplitude w_0	Position of the longitudinal stiffener b_1
Table 3.1 and Table 4.1	Fig. 4.3	$h_w/100$	$0.2h_w$

5.2 Geometric imperfection shapes

The first geometric imperfections considered were the experimentally measured imperfections for each series of testing. These imperfection shapes for the girders of Series A ($\alpha = 1$) and Series B ($\alpha = 2$) are given in Appendix B and C, respectively. The maximum amplitude of these imperfections was scaled to satisfy an imperfection amplitude of $w_0 = h_w/100$, used in the current research. One representative shape for each series of girders A and B is given in Fig. 5.1.; refer to Chapter 4 and Fig. 4.7 for more details on the implementation of experimentally measured imperfections into the numerical model.

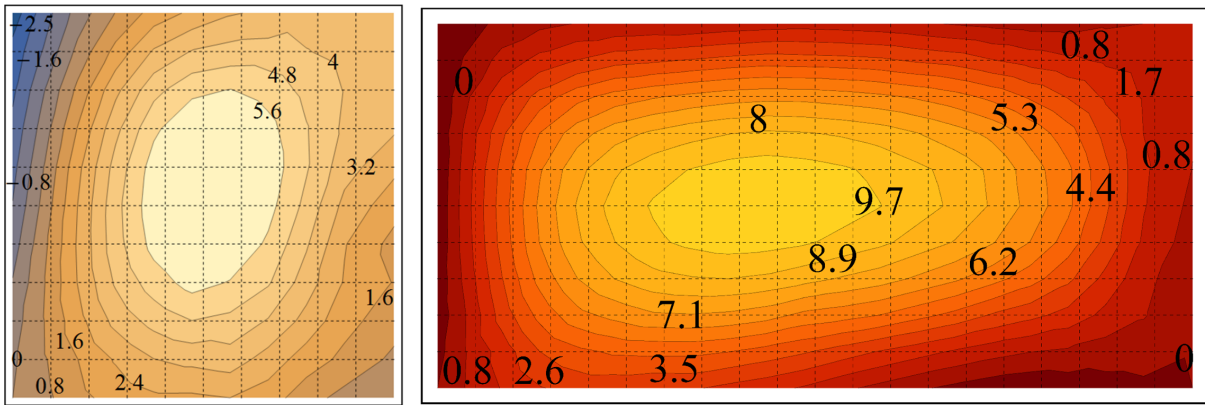


Figure 5.1: Experimentally measured geometric imperfections for girder A1 (left) and girder B1 (right). Refer to Appendix B and Appendix C for the other experimentally measured imperfection shapes for the girders of Series A and B, respectively. Units are in mm.

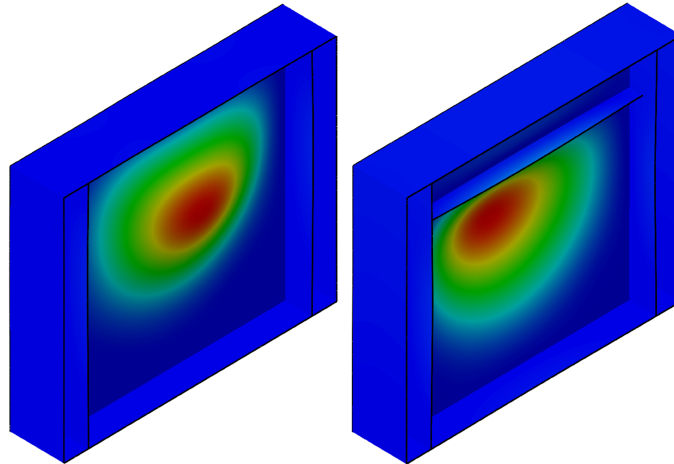


Figure 5.2: First buckling mode of longitudinally unstiffened and stiffened steel plate girders for all patch load lengths considered ($s_s/h_w \leq 0.50$) for girders of Series A.

One of the most popular approaches to introduce geometric imperfections into nonlinear FEA is to use buckling mode shapes (obtained from an eigenvalue analysis) [22,39–40,88,96]. The same method was followed in this study, and the first three buckling mode shapes and their combination were examined in the present numerical analysis. In the linear buckling analysis, no imperfections were included; the web plate was perfectly plain. Similarly to the experimentally measured imperfections, the maximum imperfection amplitude was also set to

be $w_0 = h_w/100$ for the buckling mode shapes and their combination. Representative shapes of the first three buckling modes are shown in Fig. 5.2, Fig. 5.3, Fig. 5.4, Fig. 5.5, and in Fig. 5.6, Fig. 5.7, Fig. 5.8, Fig. 5.9 for girders of Series A and B, respectively. All the buckling mode shapes illustrated in these figures are valid for all the patch load lengths considered ($s_s/h_w \leq 0.50$), except for (i) the third buckling mode shape of girders of Series A for patch load length $s_s/h_w = 0.50$ – an asymmetric buckling mode, Fig. 5.5; (ii) the third buckling mode shape of longitudinally stiffened girders of Series B, which is an asymmetric buckling mode shape for applied patch load lengths $s_s/h_w \geq 0.30$ and $s_s/h_w \geq 0.15$ in the cases of $\gamma_s = 21.67$ and $\gamma_s = 103.46$, respectively (Fig. 5.9).

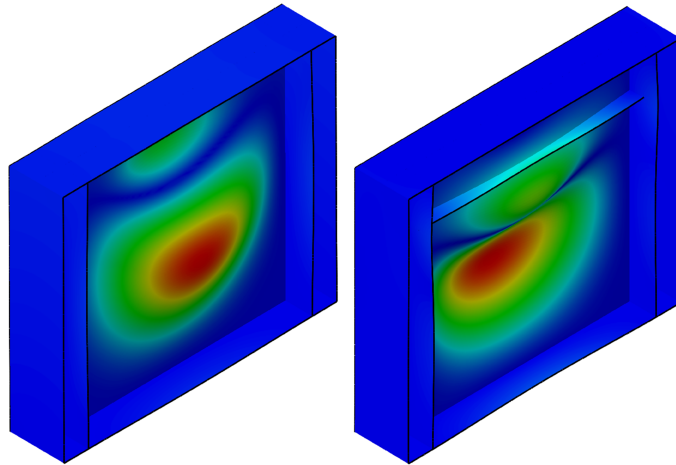


Figure 5.3: Second buckling mode of longitudinally unstiffened and stiffened steel plate girders for all patch load lengths considered ($s_s/h_w \leq 0.50$) for girders of Series A.

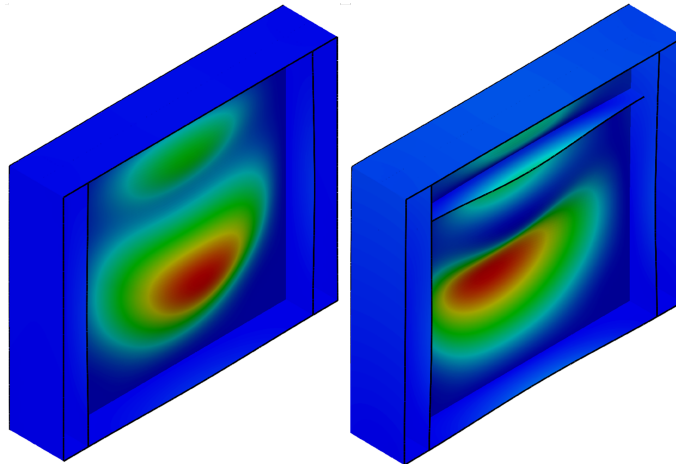


Figure 5.4: Third buckling mode of longitudinally unstiffened and stiffened steel plate girders (valid for $s_s/h_w \leq 0.40$) of Series A.

Additionally, another way to define geometric imperfections is considering a two-dimensional random field. Two hand-defined sinusoidal imperfection shapes were considered, a method of incorporating geometric imperfections employed by [23,26,34–35,40,56,79,88] for I-shaped steel plate girders under patch loading. The hand-defined sinusoidal geometric imperfections considered were represented using sine and cosine functions in both longitudinal and

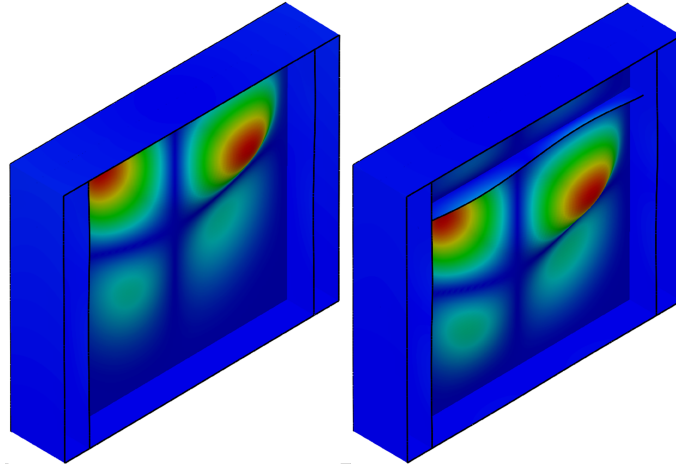


Figure 5.5: Third buckling mode of longitudinally unstiffened and stiffened steel plate girders (valid for $s_s/h_w = 0.50$) of Series A.

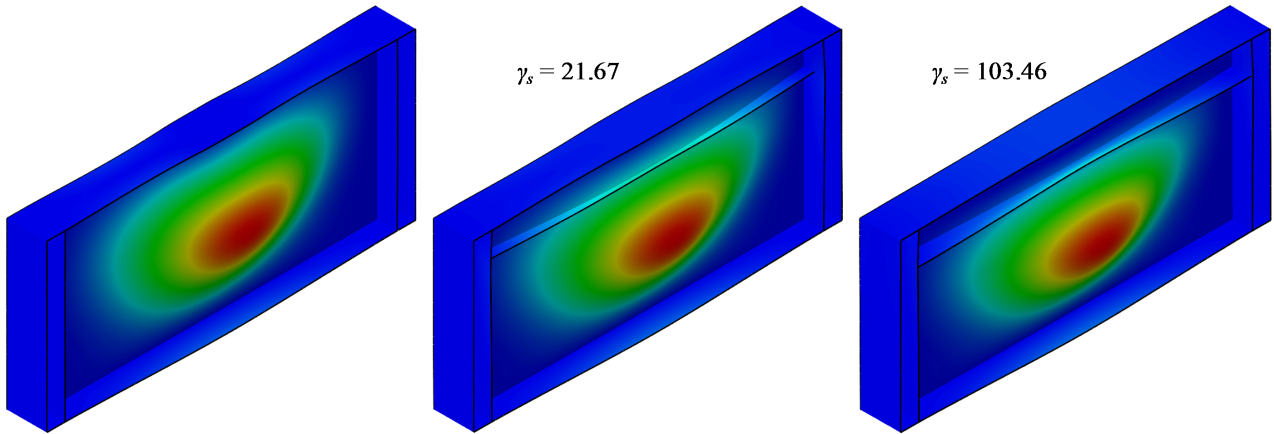


Figure 5.6: First buckling mode of longitudinally unstiffened and stiffened steel plate girders for all patch load lengths considered ($s_s/h_w \leq 0.50$) for girders of Series B.

transverse directions (graphically illustrated in Fig. 5.10), and they can be mathematically described as

$$w(x, y) = w_0 \cdot \sin(\pi x/a) \sin(\pi y/h_w) \quad (5.1)$$

$$w(x, y) = \frac{1}{4} \cdot w_0 \cdot (1 - \cos(2 \cdot \pi x/a))(1 - \cos(2 \cdot \pi y/h_w)), \quad (5.2)$$

where w_0 is a required amplitude.

5.3 Results and discussion

In this section, the obtained results are presented, along with detailed discussions and conclusions. The computationally determined patch loading resistances of longitudinally unstiffened and stiffened steel plate girders for each geometric imperfection considered are listed in Table 5.3 and Table 5.4 for girders of Series A, and in Table 5.5, Table 5.6, Table 5.7 for girders of Series B. The carrying capacity of longitudinally stiffened steel plate girders is normalized

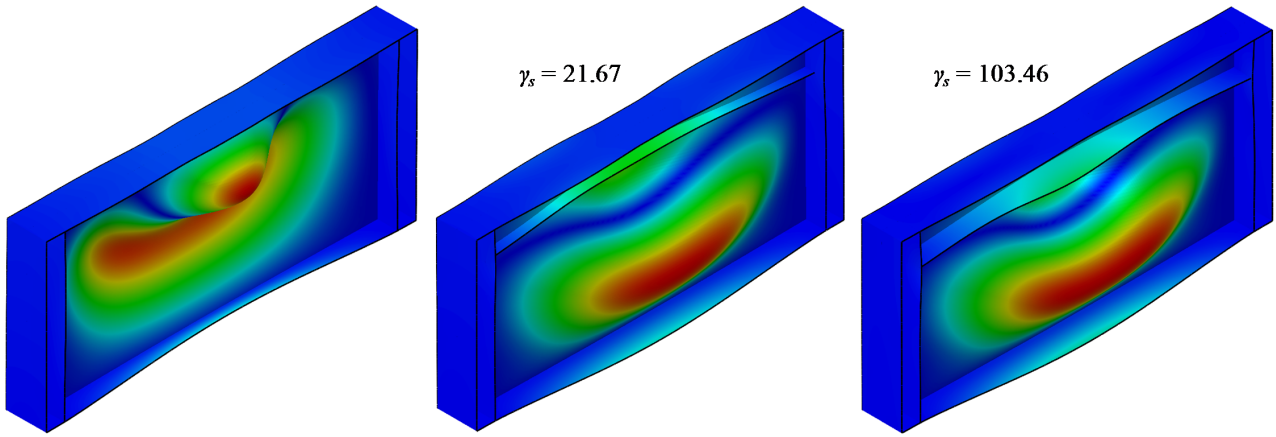


Figure 5.7: Second buckling mode of longitudinally unstiffened and stiffened steel plate girders for all patch load lengths considered ($s_s/h_w \leq 0.50$) for girders of Series B.

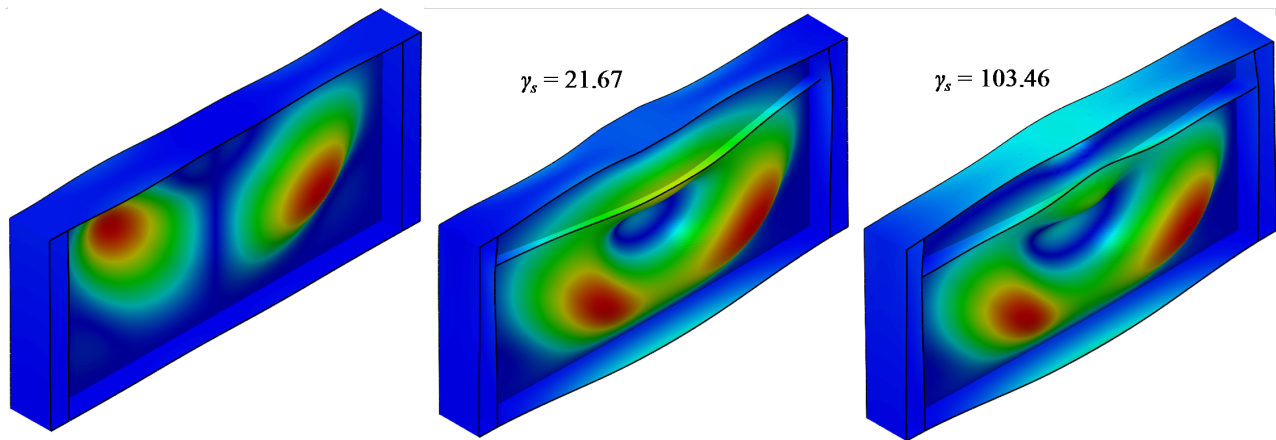


Figure 5.8: Third buckling mode of longitudinally unstiffened (valid for $s_s/h_w \leq 0.50$) and stiffened steel plate girders (valid for $s_s/h_w \leq 0.25$ for $\gamma_s = 21.67$ and for $s_s/h_w \leq 0.10$ for $\gamma_s = 103.46$) of Series B.

with respect to the ultimate strength of longitudinally unstiffened ones in order to show the strengthening effect – that is, the contribution of the longitudinal stiffener. The results are graphically presented as a function of patch load length and ultimate strength for all the geometric imperfections considered and both Series A and B in Fig. 5.11 – Fig. 5.17, Fig. 5.20 – Fig. 5.26, Fig. 5.29, Fig. 5.30, Fig. 5.32, Fig. 5.33, Fig. 5.34, and Fig. 5.35 in the next sections. A more detailed discussion is provided in the following sections as well.

5.3.1 Experimentally measured geometric imperfections

Girders of Series A

Two groups of analysis were established considering the experimentally measured geometric imperfections. The first group included geometric imperfections from steel plate girders that were originally longitudinally unstiffened in the experiment [21,25] (A15, A12, A1, A11, A2, and A13). These results are depicted in Fig 5.11, Fig. 5.12, and 5.13 as a function of patch load

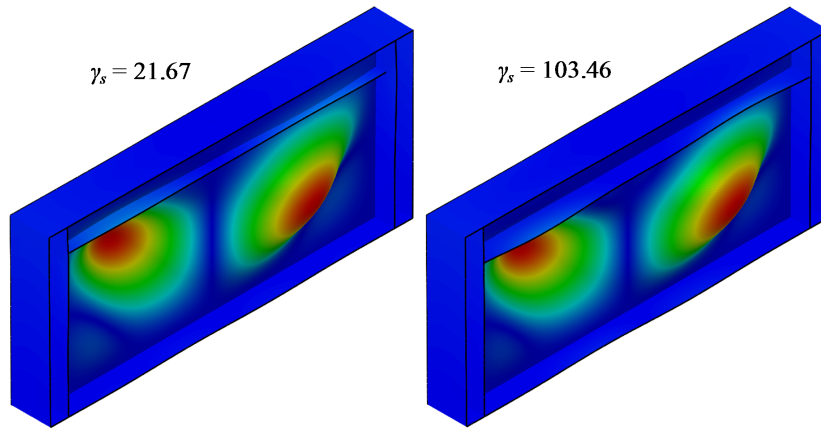


Figure 5.9: Third buckling mode of longitudinally stiffened steel plate girders (valid for $s_s/h_w \geq 0.30$ for $\gamma_s = 21.67$ and $s_s/h_w \geq 0.15$ for $\gamma_s = 103.46$) of Series B.

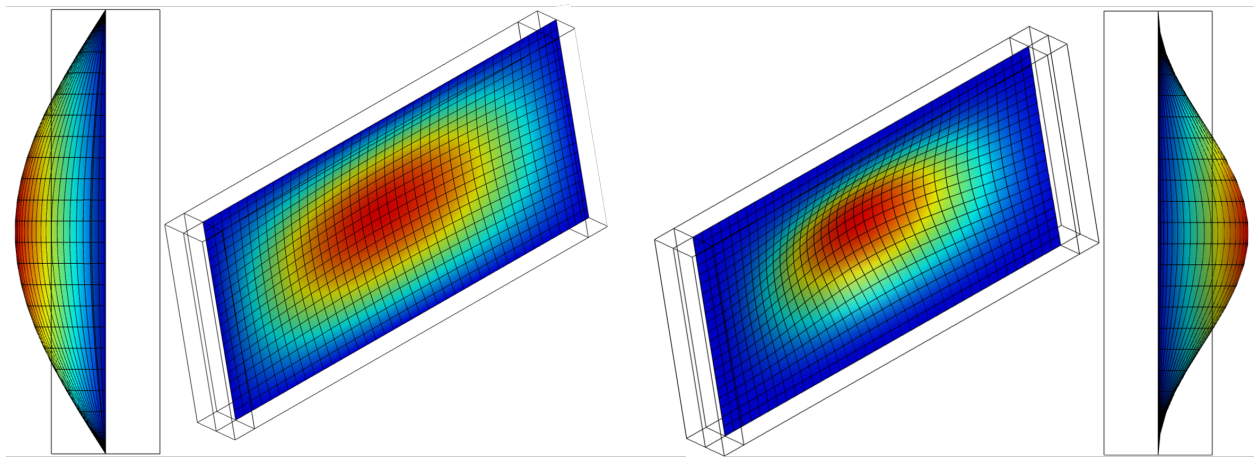


Figure 5.10: Sine (left) and cosine (right) hand-defined geometric imperfections for both series of girders A and B.

length. According to these results, one can instantly notice that the longitudinal stiffener's influence for $s_s/h_w \leq 0.15$ ($s_s = 75$ mm – threshold) was very small since it increased the ultimate capacity of less than 5%. On the other hand, the longitudinal stiffener increased the patch loading resistance significantly for longer patch load lengths, from 30 to 40% for $s_s/h_w = 0.5$ ($s_s = 250$ mm). The second group involved geometric imperfections from steel plate girders that were initially longitudinally stiffened in the experiment [21,25] (A14, A4, A3, A17, A5, A6, A7, A16); refer to Fig. 5.14, Fig. 5.15, Fig. 5.16, and Fig. 5.17 for their graphical representation. A similar conclusion was observed in this case, and the same threshold $s_s/h_w \leq 0.15$ was valid. However, for some geometric imperfections, the threshold shifted even up to $s_s/h_w = 0.30$ ($s_s = 150$ mm). For these geometric imperfections of the second group, the ultimate strength of longitudinally stiffened girders for longer patch load lengths was again increased, but notably less than for the first group of girders, from 15 to 30% for $s_s/h_w = 0.5$ ($s_s = 250$ mm). Only in one case, an appreciable strengthening effect of 40% was achieved for $s_s/h_w = 0.5$. Fig. 5.18 recaps the above conclusions.

Using the numerically obtained results for the experimentally measured imperfections

Table 5.3: Patch loading resistance of longitudinally unstiffened steel plate girders ($F_{FEA,unstiff}$) for various geometric imperfections for girders of Series A. Units are in kN.

Shape of geometric imperfection	s_s/h_w								
	0	0.05	0.10	0.15	0.20	0.25	0.30	0.40	0.50
A1 ¹	142.68	146.20	164.84	179.82	193.07	206.87	220.42	248.12	280.56
A2 ¹	142.82	146.13	165.14	185.47	200.17	214.03	227.86	255.51	285.03
A3 ¹	138.56	141.11	153.76	169.04	184.79	200.78	218.58	258.27	300.94
A4 ¹	146.35	149.72	168.66	189.82	209.02	223.95	239.14	268.11	298.28
A5 ¹	148.78	152.14	170.06	189.67	212.71	234.51	250.64	280.64	311.12
A6 ¹	147.98	151.26	168.80	188.01	210.10	236.13	260.58	291.62	322.04
A7 ¹	150.20	153.75	173.03	193.79	218.06	235.40	253.55	287.54	322.37
A11 ¹	144.68	148.05	166.99	187.97	204.18	218.70	233.23	261.76	292.12
A12 ¹	145.25	148.63	167.69	188.79	204.54	219.60	234.73	264.58	296.66
A13 ¹	146.29	149.82	169.54	191.29	208.57	224.66	240.63	271.73	304.31
A14 ¹	143.04	146.25	164.46	185.00	205.45	219.94	233.65	260.53	289.25
A15 ¹	140.44	143.70	161.28	174.98	187.94	200.93	213.76	239.91	268.02
A16 ¹	144.45	147.43	163.95	182.47	203.88	228.99	253.59	283.58	314.33
A17 ¹	142.25	145.62	165.08	182.13	195.38	208.98	222.29	248.79	276.94
1 st buckling mode	150.24	146.58	163.14	182.19	203.05	223.99	237.50	263.25	291.11
2 nd buckling mode	149.01	146.03	158.65	171.09	183.37	195.32	206.99	230.98	257.71
3 rd buckling mode	149.91	146.76	160.64	174.07	188.19	201.97	215.48	243.50	360.12
1 st + 2 nd + 3 rd mode	159.31	155.39	171.52	188.59	210.22	236.69	262.29	292.35	337.10
Hand-define sine function	153.35	157.05	172.60	185.72	201.24	216.32	230.80	259.49	289.96
Hand-define cosine func- tion	144.62	147.74	163.63	181.12	202.51	227.12	253.78	285.54	316.08

¹ Experimentally measured geometric imperfection shapes are provided in Appendix B

listed in Table 5.3 and Table 5.4 for longitudinally unstiffened and stiffened steel plate girders, respectively, a more detailed quantitative analysis of the influence of geometric imperfections could be handled. Isolating results for the initially unstiffened and stiffened girders, it can be shown that the shape of initial geometric imperfections can play a decisive role for both longitudinally unstiffened and stiffened steel girders. The shape of initial geometric imperfections affected the ultimate load in a range of more than 15%, as portrayed in Fig. 5.19. This was more pronounced for longer patch load lengths, while its impact for $s_s/h_w < 0.10$ ($s_s < 50$ mm) was inappreciable (less than 10%).

Table 5.4: Normalized patch loading resistance of longitudinally stiffened steel plate girders ($F_{FEA, stiff}/F_{FEA, unstiff}$) for various geometric imperfections for girders of Series A.

Shape of geometric imperfection	s_s/h_w								
	0	0.05	0.10	0.15	0.20	0.25	0.30	0.40	0.50
A1 ¹	1.03	1.03	1.04	1.08	1.13	1.18	1.23	1.35	1.39
A2 ¹	1.02	1.02	1.02	1.02	1.07	1.11	1.16	1.28	1.35
A3 ¹	1.06	1.06	1.08	1.09	1.11	1.13	1.14	1.14	1.13
A4 ¹	1.02	1.02	1.02	1.02	1.04	1.07	1.15	1.24	1.30
A5 ¹	1.02	1.02	1.03	1.03	1.03	1.05	1.10	1.20	1.25
A6 ¹	1.02	1.02	1.03	1.04	1.04	1.04	1.05	1.14	1.18
A7 ¹	1.02	1.02	1.03	1.03	1.03	1.07	1.11	1.21	1.26
A11 ¹	1.02	1.02	1.02	1.02	1.06	1.11	1.16	1.27	1.34
A12 ¹	1.02	1.02	1.02	1.02	1.06	1.10	1.15	1.26	1.32
A13 ¹	1.02	1.02	1.02	1.02	1.05	1.09	1.14	1.25	1.30
A14 ¹	1.02	1.02	1.02	1.02	1.03	1.07	1.12	1.22	1.29
A15 ¹	1.03	1.03	1.05	1.09	1.15	1.20	1.26	1.36	1.39
A16 ¹	1.02	1.02	1.03	1.03	1.04	1.03	1.04	1.12	1.17
A17 ¹	1.02	1.02	1.02	1.05	1.10	1.15	1.20	1.31	1.40
1 st buckling mode	1.00	1.04	1.04	1.04	1.05	1.06	1.10	1.17	1.26
2 nd buckling mode	0.95	0.99	1.03	1.07	1.12	1.18	1.23	1.31	1.33
3 rd buckling mode	0.83	0.87	0.89	0.93	0.97	1.00	1.05	1.12	1.20
1 st + 2 nd + 3 rd mode	0.90	0.94	0.95	0.98	0.99	0.99	1.00	1.09	1.20
Hand-define sine function	1.06	1.06	1.09	1.13	1.17	1.23	1.29	1.41	1.45
Hand-define cosine func- tion	1.03	1.03	1.04	1.05	1.05	1.05	1.04	1.12	1.17

¹ Experimentally measured geometric imperfection shapes are provided in Appendix B

Girders of Series B

As can be observed from Table 5.5, Table 5.6, and Table 5.7, the ultimate load of longitudinally stiffened steel plate girders was higher than the carrying capacity of longitudinally unstiffened ones. This proves to be valid for all the patch load lengths considered, $s_s/h_w \leq 0.50$. Using the relatively weak longitudinal stiffener ($\gamma_s = 21.67$) and for all the experimentally measured imperfections, the strengthening effect for smaller patch load lengths – that is, $s_s/h_w \leq 0.15$, was $< 10\%$, while for longer patch load lengths ($s_s/h_w = 0.50$) its value was up to 28%. By contrast, using the relatively strong longitudinal stiffener ($\gamma_s = 103.46$) and including all the experimentally measured imperfections, the strengthening effect did not change for smaller patch load lengths ($s_s/h_w \leq 0.15$), and its contribution was $\leq 10\%$. In this case, $\gamma_s = 103.46$, a significant strengthening effect was prominent for longer patch load lengths ($s_s/h_w = 0.50$),

Table 5.5: Patch loading resistance of longitudinally unstiffened steel plate girders ($F_{FEA,unstiff}$) for various geometric imperfections for girders of Series B. Units are in kN.

Shape of geometric imperfection	s_s/h_w								
	0	0.05	0.10	0.15	0.20	0.25	0.30	0.40	0.50
B1 ¹	122.71	137.00	151.62	166.65	181.61	195.35	204.20	218.72	231.83
B2 ¹	130.06	146.08	161.12	174.48	184.58	192.78	200.16	213.23	225.15
B3 ¹	128.14	143.05	156.07	171.06	186.53	202.17	215.47	233.31	247.91
B4 ¹	128.03	143.23	156.92	172.55	188.61	205.28	220.99	242.77	256.74
B5 ¹	126.86	141.78	156.00	171.62	187.28	203.74	218.00	235.29	248.60
B6 ¹	127.04	142.04	156.32	172.12	188.02	204.85	219.00	236.74	250.83
B7 ¹	124.97	139.74	154.82	170.73	186.47	200.05	209.16	225.14	239.33
B11 ¹	125.14	139.67	153.61	168.89	184.07	199.38	210.47	225.82	239.35
B12 ¹	131.57	147.51	160.55	175.53	191.47	207.42	222.41	242.14	256.01
B13 ¹	128.61	143.80	156.62	171.96	187.65	203.23	218.03	240.21	254.36
B14 ¹	124.44	139.01	153.77	169.29	184.70	199.12	208.32	223.37	236.96
B15 ¹	124.20	138.59	152.72	167.96	183.16	198.33	208.76	223.83	237.06
B16 ¹	127.31	142.21	155.80	171.17	186.72	202.91	216.39	233.45	247.49
B17 ¹	124.78	139.41	154.18	169.69	185.00	198.71	207.51	222.50	236.18
1 st buckling mode	125.54	139.96	153.01	168.00	183.09	197.84	210.14	226.45	239.57
2 nd buckling mode	128.19	144.64	159.19	170.51	180.17	188.77	196.57	210.79	223.93
3 rd buckling mode	142.77	159.34	175.53	189.01	201.39	210.49	217.96	232.11	265.52
1 st + 2 nd + 3 rd mode	130.64	147.14	162.69	177.48	188.85	197.49	205.26	218.75	230.42
Hand-define sine function	134.28	151.12	166.47	180.23	191.18	200.46	208.74	223.26	236.14
Hand-define cosine func- tion	127.79	142.77	155.43	170.48	185.93	201.42	215.48	234.35	247.13

¹ Experimentally measured geometric imperfection shapes are provided in Appendix C

with a maximum value of 48%; the contribution of the longitudinal stiffener is discussed in more detail in Section 5.3.5. The maximum values of the strengthening effect for both cases, $\gamma_s = 21.67$ and $\gamma_s = 103.46$, were computed for experimentally measured geometric imperfection B2. The change in the ultimate strength with respect to the patch load length for all the experimentally measured geometric imperfections is portrayed from Fig. 5.20 to Fig. 5.26.

Additionally, to show the scatter of the ultimate load for different experimentally measured imperfections, these imperfections were divided into two groups. Imperfections labeled as B1, B2, B11, B12, B14, B15, and B16 are related to the girders that were originally unstiffened in the experimental program (see Chapter 3), whereas imperfections marked as B3, B4, B5, B6, B7, B13, and B17 represent the originally stiffened girders. Using imperfections of the experimentally unstiffened steel plate girders, the ultimate load dispersed from 7% ($s_s/h_w =$

Table 5.6: Normalized patch loading resistance of longitudinally stiffened steel plate girders ($F_{FEA, stiff}/F_{FEA, unstiff}$) for various geometric imperfections for girders of Series B. Relative stiffness $\gamma_s = 21.67$.

Shape of geometric imperfection	s_s/h_w								
	0	0.05	0.10	0.15	0.20	0.25	0.30	0.40	0.50
B1 ¹	1.02	1.03	1.04	1.05	1.06	1.08	1.12	1.18	1.20
B2 ¹	1.03	1.04	1.05	1.08	1.13	1.18	1.23	1.26	1.28
B3 ¹	1.04	1.05	1.06	1.07	1.08	1.09	1.11	1.16	1.18
B4 ¹	1.04	1.05	1.06	1.07	1.08	1.09	1.11	1.15	1.18
B5 ¹	1.03	1.04	1.05	1.06	1.07	1.08	1.10	1.16	1.18
B6 ¹	1.03	1.04	1.05	1.06	1.08	1.08	1.10	1.15	1.17
B7 ¹	1.02	1.03	1.04	1.05	1.06	1.08	1.12	1.18	1.20
B11 ¹	1.04	1.04	1.05	1.06	1.08	1.09	1.12	1.17	1.18
B12 ¹	1.04	1.05	1.07	1.08	1.10	1.12	1.14	1.18	1.21
B13 ¹	1.03	1.05	1.06	1.07	1.08	1.10	1.11	1.15	1.18
B14 ¹	1.03	1.04	1.05	1.06	1.07	1.08	1.13	1.17	1.18
B15 ¹	1.03	1.04	1.04	1.05	1.07	1.08	1.11	1.18	1.20
B16 ¹	1.04	1.05	1.06	1.07	1.08	1.09	1.12	1.17	1.19
B17 ¹	1.02	1.03	1.04	1.05	1.06	1.08	1.13	1.19	1.20
1 st buckling mode	1.04	1.06	1.07	1.08	1.09	1.11	1.14	1.20	1.23
2 nd buckling mode	1.04	1.04	1.05	1.09	1.13	1.16	1.16	1.15	1.15
3 rd buckling mode	0.88	0.88	0.90	0.93	0.97	1.01	1.21	1.25	1.18
1 st + 2 nd + 3 rd mode	1.03	1.04	1.04	1.05	1.10	1.15	1.28	1.37	1.42
Hand-define sine function	1.03	1.03	1.04	1.06	1.10	1.16	1.20	1.23	1.25
Hand-define cosine func- tion	1.03	1.05	1.06	1.07	1.09	1.10	1.12	1.18	1.21

¹ Experimentally measured geometric imperfection shapes are provided in Appendix C

0.01) to 14% ($s_s/h_w = 0.50$). Employing the relatively weak longitudinal stiffener ($\gamma_s = 21.67$), the ultimate strength scattered from 4% ($s_s/h_w = 0.01$) to 6% ($s_s/h_w = 0.50$), while for the strong longitudinal stiffener ($\gamma_s = 103.46$) the ultimate load had dispersion of 4% on average for all the included patch load lengths, $s_s/h_w \leq 0.50$. These conclusions are summarized in Fig. 5.27 and Fig. 5.28 for longitudinally unstiffened and stiffened steel plate girders ($\gamma_s = 21.67$ and $\gamma_s = 103.46$), respectively.

Table 5.7: Normalized patch loading resistance of longitudinally stiffened steel plate girders ($F_{FEA, stiff}/F_{FEA, unstiff}$) for various geometric imperfections for girders of Series B. Relative stiffness $\gamma_s = 103.46$.

Shape of geometric imperfection	s_s/h_w								
	0	0.05	0.10	0.15	0.20	0.25	0.30	0.40	0.50
B1 ¹	1.04	1.05	1.06	1.07	1.09	1.11	1.16	1.26	1.33
B2 ¹	1.04	1.05	1.07	1.10	1.16	1.24	1.32	1.45	1.48
B3 ¹	1.06	1.07	1.08	1.09	1.11	1.13	1.16	1.24	1.30
B4 ¹	1.05	1.06	1.08	1.09	1.11	1.12	1.15	1.23	1.30
B5 ¹	1.04	1.05	1.07	1.08	1.10	1.11	1.14	1.23	1.30
B6 ¹	1.05	1.06	1.07	1.08	1.10	1.11	1.15	1.25	1.32
B7 ¹	1.04	1.04	1.05	1.07	1.08	1.11	1.16	1.27	1.35
B11 ¹	1.05	1.06	1.07	1.09	1.10	1.12	1.16	1.26	1.33
B12 ¹	1.05	1.07	1.09	1.10	1.12	1.15	1.19	1.28	1.36
B13 ¹	1.05	1.06	1.08	1.09	1.11	1.13	1.16	1.22	1.28
B14 ¹	1.05	1.06	1.07	1.08	1.10	1.12	1.17	1.28	1.35
B15 ¹	1.04	1.05	1.06	1.08	1.09	1.11	1.15	1.25	1.33
B16 ¹	1.05	1.06	1.08	1.09	1.11	1.13	1.16	1.26	1.33
B17 ¹	1.04	1.05	1.06	1.07	1.09	1.11	1.17	1.27	1.35
1 st buckling mode	1.07	1.09	1.10	1.11	1.14	1.16	1.20	1.29	1.35
2 nd buckling mode	1.04	1.05	1.06	1.10	1.17	1.24	1.32	1.38	1.38
3 rd buckling mode	0.84	0.85	0.87	1.10	1.14	1.22	1.29	1.38	1.30
1 st + 2 nd + 3 rd mode	1.02	1.03	1.04	1.18	1.21	1.30	1.39	1.52	1.57
Hand-define sine function	1.05	1.06	1.07	1.09	1.14	1.20	1.27	1.36	1.41
Hand-define cosine func- tion	1.05	1.06	1.08	1.09	1.11	1.13	1.16	1.24	1.31

¹ Experimentally measured geometric imperfection shapes are provided in Appendix C

5.3.2 Buckling mode-affine geometric imperfections

The present analysis considering geometric imperfections from an eigenvalue study (cf. Fig. 5.2–Fig. 9) confirmed that the first buckling mode does not prove the lowest ultimate strength of longitudinally stiffened steel plate girders [32,39–40,43]. The attained results are graphically shown in Fig. 5.29 and Fig. 5.30 for girders of Series A, and in Fig. 5.32 and Fig. 5.33 for girders of Series B; corresponding numerical values are tabulated in Table 5.3, Table 5.4, Table 5.5, Table 5.6, and Table 5.7.

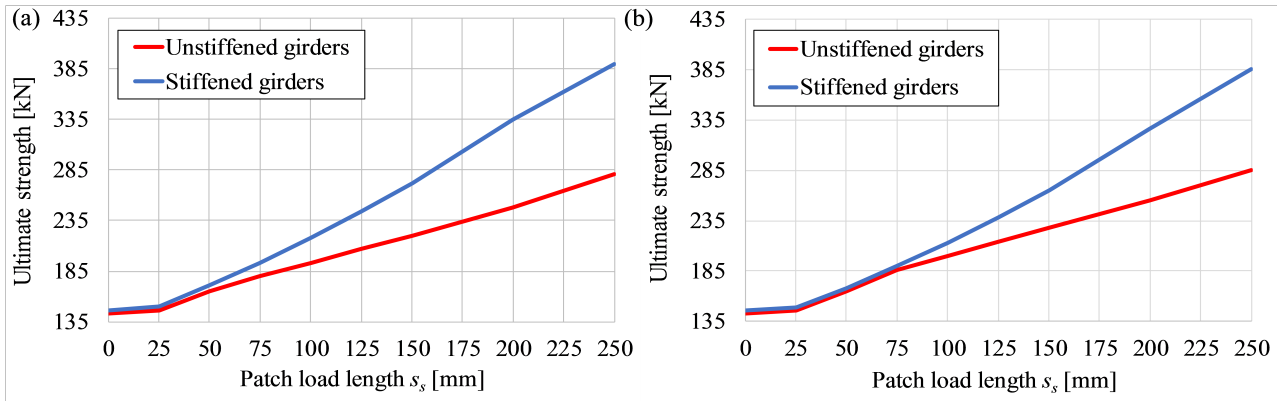


Figure 5.11: Ultimate strength of longitudinally unstiffened and stiffened steel plate girders using experimentally measured geometric imperfections from (a) girder A1 and (b) girder A2.

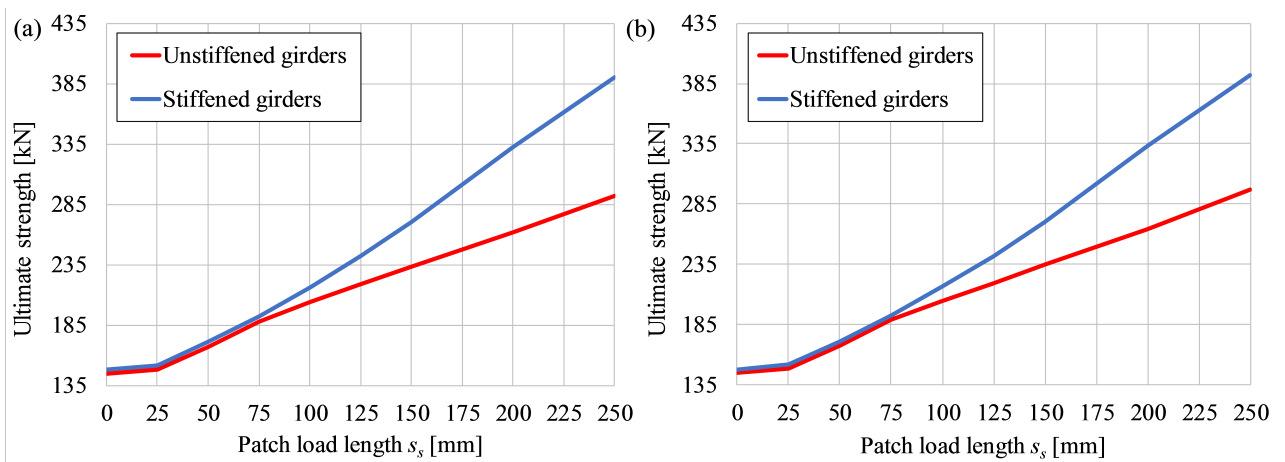


Figure 5.12: Ultimate strength of longitudinally unstiffened and stiffened steel plate girders using experimentally measured geometric imperfections from (a) girder A11 and (b) girder A12.

Girders of Series A

The following conclusion could be made for the first buckling modes. The ultimate strength of longitudinally stiffened steel plate girders was higher than the ultimate strength of unstiffened ones (see Table 5.3 and Table 5.4) for all the patch load lengths under consideration, $s_s/h_w \leq 0.50$. Moreover, the first buckling mode returned the same threshold $s_s/h_w \leq 0.15$ ($s_s = 75$ mm) as in the previous case for the experimentally measured geometric imperfections. The difference between the patch loading resistance of longitudinally unstiffened and stiffened steel plate girders before the threshold was very small (less than 5%).

The lowest ultimate strength for longitudinally stiffened steel plate girders was determined for the third buckling mode. It is lower than the ultimate capacity of longitudinally unstiffened girders for $s_s/h_w \leq 0.20$ ($s_s = 100$ mm). A similar conclusion was found in Refs. [32,39–40,43] for small patch load length ($s_s = 0.04h_w$), longitudinal stiffener positions $b_1/h_w \leq 0.25$, and various imperfection amplitudes ($h_w/1000 - h_w/100$). In addition, the second buckling mode and combination of modes ($1^{st} + 2^{nd} + 3^{rd}$) also returned smaller carrying capacities

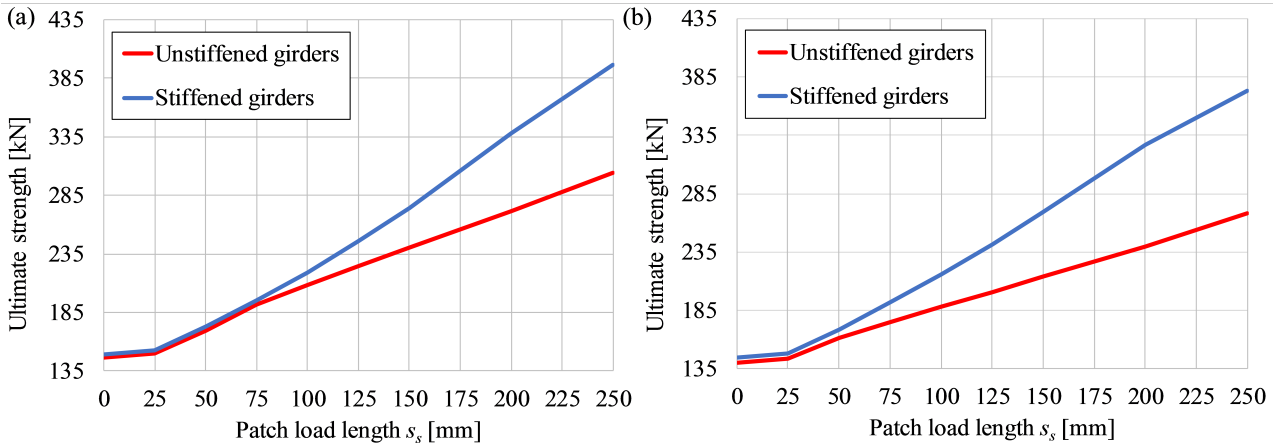


Figure 5.13: Ultimate strength of longitudinally unstiffened and stiffened steel plate girders using experimentally measured geometric imperfections from (a) girder A13 and (b) girder A15.

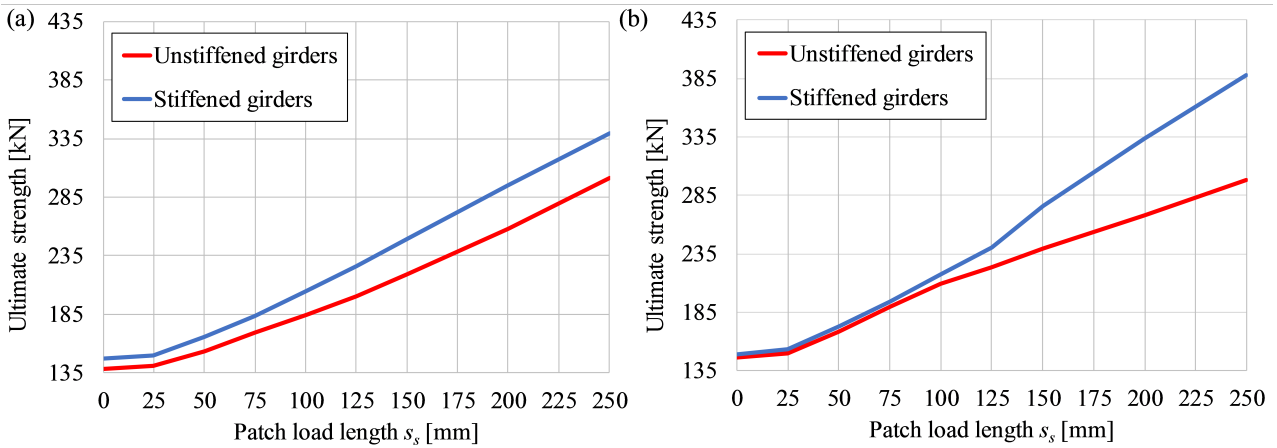


Figure 5.14: Ultimate strength of longitudinally unstiffened and stiffened steel plate girders using experimentally measured geometric imperfections from (a) girder A3 and (b) girder A4.

of longitudinally stiffened girders than ultimate loads of unstiffened ones for $s_s/h_w \leq 0.05$ ($s_s = 25$ mm) and $s_s/h_w \leq 0.25$ ($s_s = 125$ mm), respectively. This finding can be clarified with the shape of the second and third buckling mode for longitudinally stiffened girders. Fig. 5.3 and Fig. 5.4 show that pronounced deformation occurred between the longitudinal stiffener and loaded flange. Its magnitude decreased with increasing the patch load length. As a corollary, this shape of geometric imperfection is much more unfavorable than the second and third buckling mode of longitudinally unstiffened steel plate girders.

Strengthening effect: only the first buckling mode returned strengthening effect for all the patch load lengths considered, $s_s/h_w \leq 0.50$. Its value was 25% for $s_s/h_w = 0.50$ ($s_s = 250$ mm). The third buckling mode and combination of modes gave a similar strengthening effect of 20% for longer patch load length (e.g., $s_s/h_w = 0.50$; $s_s = 250$ mm), while the maximum strengthening effect of approximately 35% was obtained for the second buckling mode. Fig. 5.31 encapsulates these conclusions.

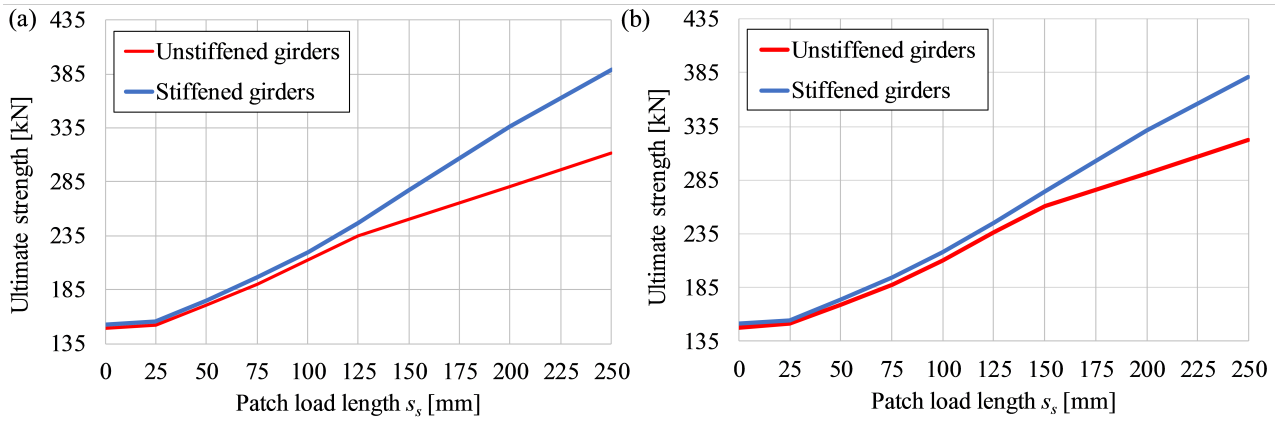


Figure 5.15: Ultimate strength of longitudinally unstiffened and stiffened steel plate girders using experimentally measured geometric imperfections from (a) girder A5 and (b) girder A6.

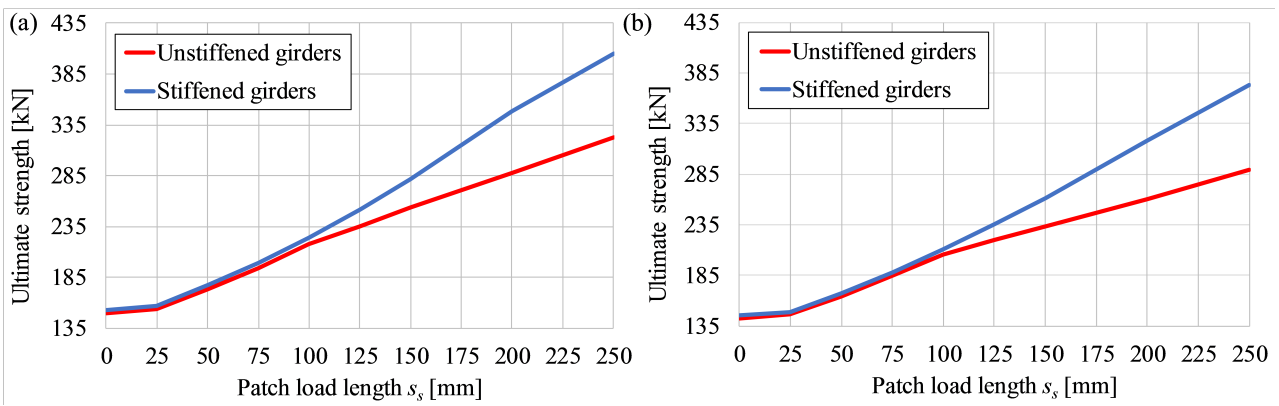


Figure 5.16: Ultimate strength of longitudinally unstiffened and stiffened steel plate girders using experimentally measured geometric imperfections from (a) girder A7 and (b) girder A14.

Girders of Series B

For the first two buckling modes, the following conclusions could be made. The ultimate load of longitudinally stiffened steel plate girders was higher than the ultimate strength of unstiffened ones (see Table 5.5, Table 5.6, Table 5.7) for all the patch load lengths under consideration, $s_s/h_w \leq 0.50$. For the relatively weak longitudinal stiffener ($\gamma_s = 21.67$), the strengthening effect for smaller patch load lengths (e.g., $s_s/h_w \leq 0.15$) was very small, while for longer patch load lengths (e.g., $s_s/h_w = 0.50$), the maximum strengthening effect was up to 23% for the first buckling mode and 15% for the second (see Table 5.6, Fig. 5.32). In the case of the relatively strong longitudinal stiffener, the strengthening effect for $s_s/h_w \leq 0.10$ can be ignored. In this case ($\gamma_s = 103.46$), the maximum strengthening effect of 38% was obtained for the second buckling mode (Table 5.7 and Fig. 5.32).

For the third buckling mode, it is apparent that the patch loading resistance of longitudinally stiffened steel plate girders was lower than the ultimate load of unstiffened ones for patch load lengths $s_s/h_w \leq 0.20$ and $s_s/h_w \leq 0.10$ for $\gamma_s = 21.67$ and $\gamma_s = 103.46$, respectively (Table 5.6, Table 5.7 and Fig. 5.33). A similar conclusion was obtained in the previous section ($\alpha = 1$) for a different patch load length range. The reason lower ultimate strengths of

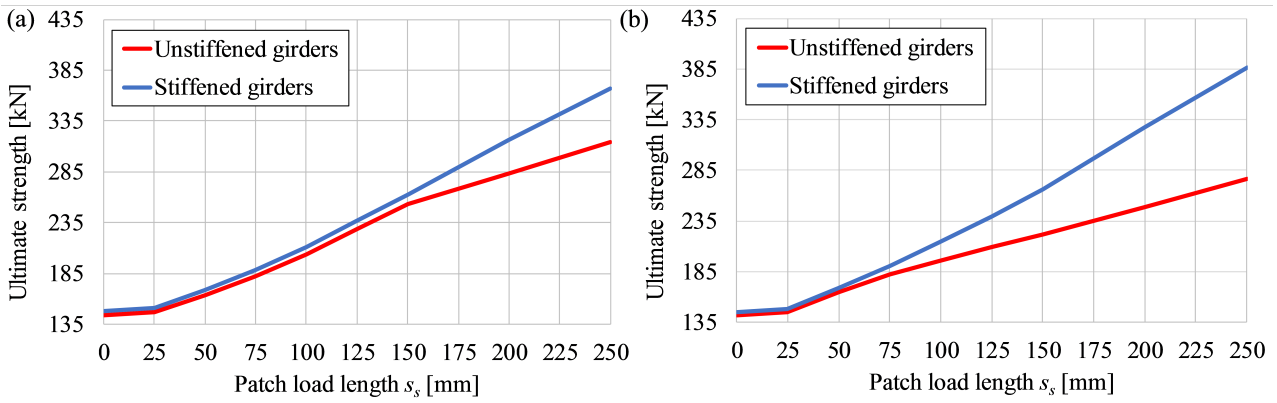


Figure 5.17: Ultimate strength of longitudinally unstiffened and stiffened steel plate girders using experimentally measured geometric imperfections from (a) girder A16 and (b) girder A17.

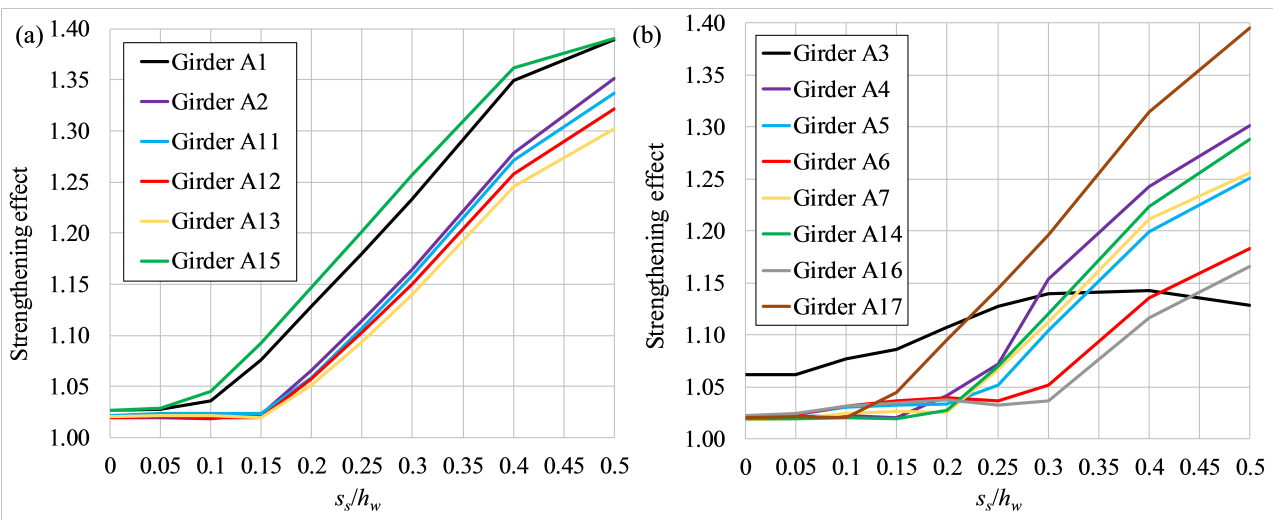


Figure 5.18: Strengthening effect employing the experimentally measured geometric imperfections from initially (a) unstiffened and (b) stiffened steel plate girders.

longitudinally stiffened steel plate girders than those of unstiffened ones were returned in this case is directly influenced by the shape of geometric imperfections. The transition patch load lengths at which the carrying capacity of longitudinally stiffened steel plate girders becomes higher than the ultimate load of unstiffened ones (see the increase in the ultimate strength in Fig. 5.33) are a consequence of the changed buckling pattern (cf. Fig. 5.4, Fig. 5.5, Fig. 5.8, and Fig. 5.9); this is explained in more detail in the next Chapter.

A similar observation was made for the combination of buckling modes ($1^{st} + 2^{nd} + 3^{rd}$) as for the first two buckling modes. The calculated patch loading resistance of longitudinally stiffened steel plate girders was higher than for unstiffened ones (see Table 5.5, Table 5.6, Table 5.7, and Fig. 5.33) for all the patch load lengths considered, $s_s/h_w \leq 0.50$. In the case of $\gamma_s = 21.67$, the strengthening effect was very small for $s_s/h_w \leq 0.15$, while it was significantly pronounced for longer patch load lengths, $s_s/h_w = 0.50$, Table 5.6. On the other hand, for the relative stiffness $\gamma_s = 103.46$, the strengthening effect was very small for $s_s/h_w \leq 0.10$, while a substantial strengthening effect of 57% was obtained for $s_s/h_w = 0.50$, Table 5.7. However,

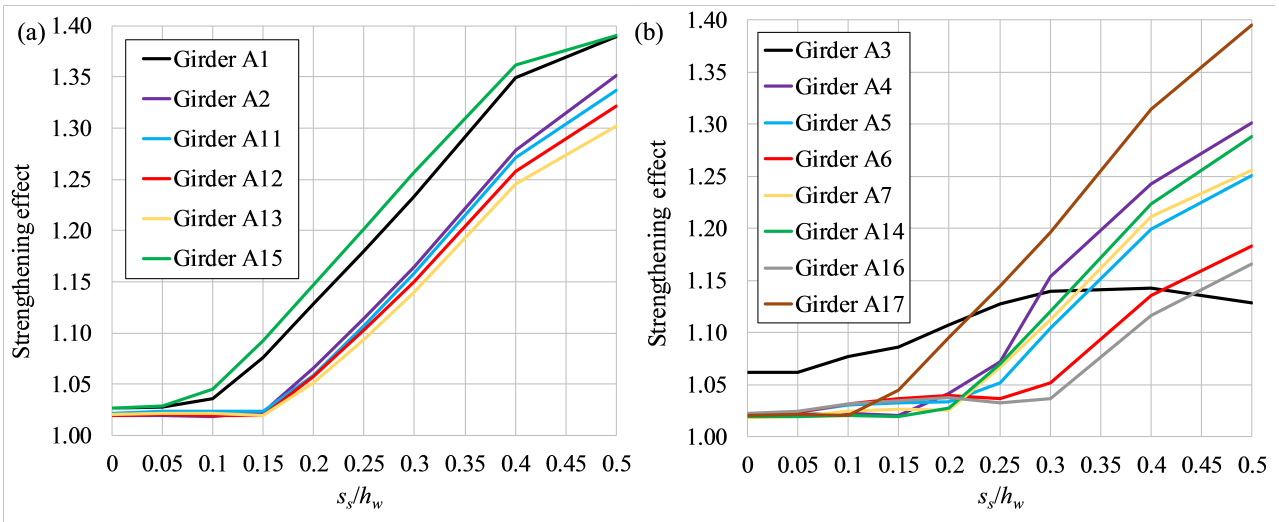


Figure 5.19: Ultimate strength of: (a) longitudinally unstiffened steel plate girders using geometric imperfections from the experimentally unstiffened girders; (b) longitudinally stiffened steel plate girders using geometric imperfections from the experimentally stiffened girders.

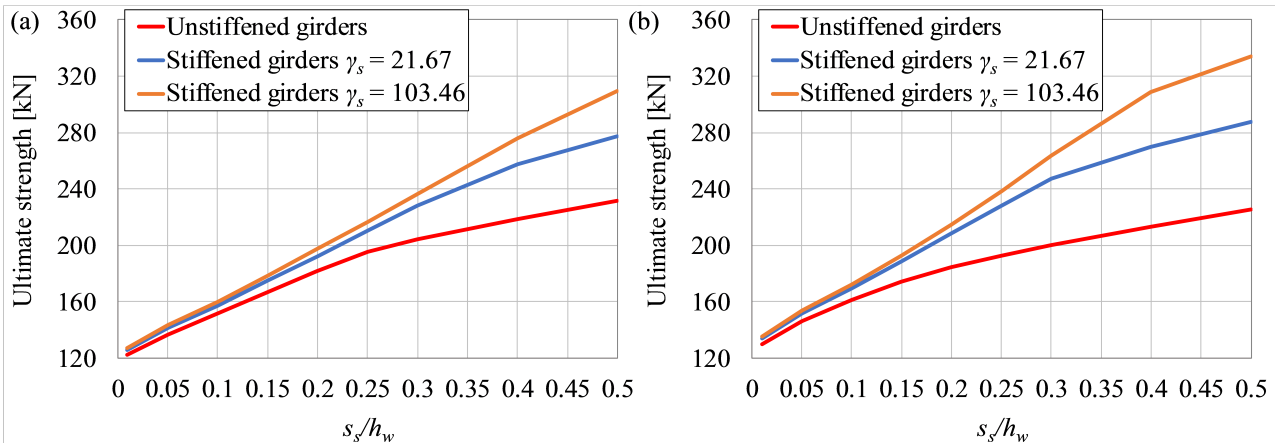


Figure 5.20: Ultimate strength of longitudinally unstiffened and stiffened steel plate girders using experimentally measured geometric imperfections from (a) girder B1 and girder B2.

as shown in the previous section for $\alpha = 1$, this geometric imperfection (the combination of buckling modes) and patch load lengths $s_s/h_w \leq 0.25$, the ultimate strength of longitudinally stiffened steel plate girders was lower than for unstiffened ones. In addition, the second and third buckling modes for the case $\alpha = 1$ also returned smaller patch loading resistance of longitudinally stiffened steel plate girders than for unstiffened ones for $s_s/h_w \leq 0.05$ and $s_s/h_w \leq 0.20$, respectively. These deleterious geometric effects from the second and third buckling modes propagated into the geometric imperfection shape (combination of buckling modes) and decreased the ultimate loads of longitudinally stiffened steel plate girders.

Remark: The strengthening effects presented in this section cannot necessarily be generalized. A strengthening effect is the ratio between the ultimate strength of longitudinally stiffened and unstiffened steel plate girders. As such, it should be evaluated on the same girder geometry and for the same imperfections. Thus, these strengthening effects for the buckling mode-affine geometric imperfections are questionable since they were obtained between longitudinally

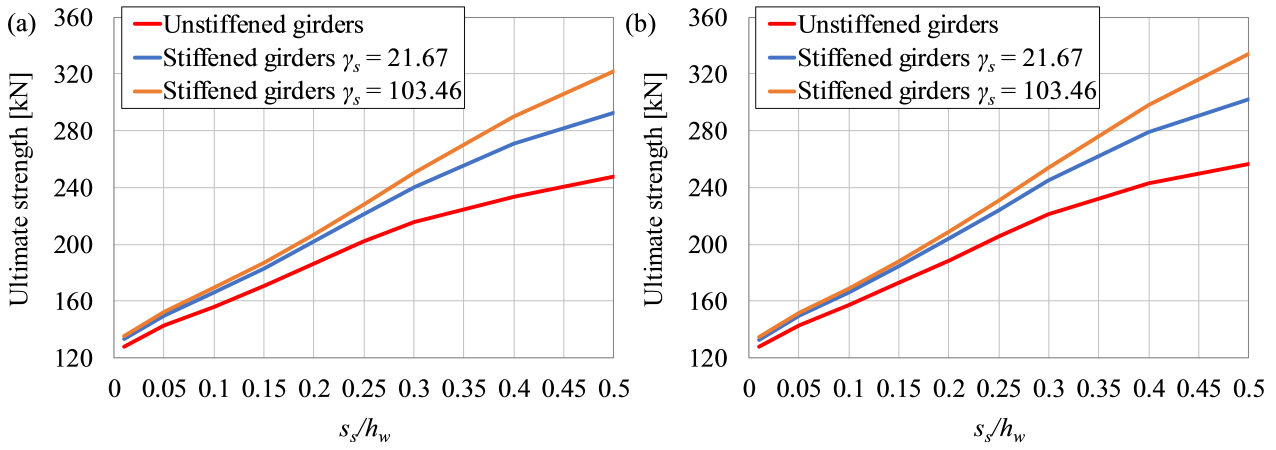


Figure 5.21: Ultimate strength of longitudinally unstiffened and stiffened steel plate girders using experimentally measured geometric imperfections from (a) girder B3 and (b) girder B4.

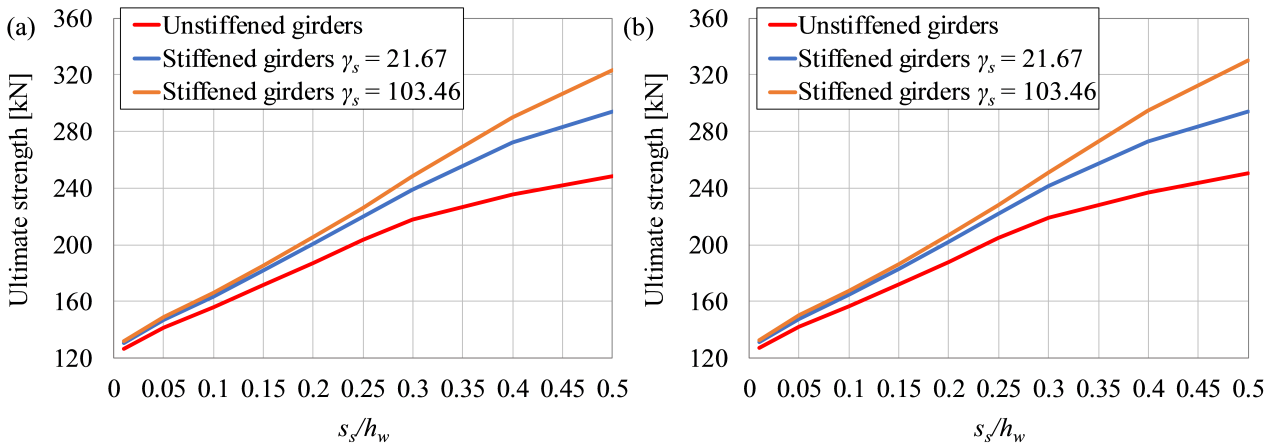


Figure 5.22: Ultimate strength of longitudinally unstiffened and stiffened steel plate girders using experimentally measured geometric imperfections from (a) girder B5 and (b) girder B6.

stiffened and unstiffened steel plate girders, which had different geometric imperfections – that is, buckling mode shapes of longitudinally unstiffened and stiffened steel plate girders did not match. Conversely, the contributions of the longitudinal stiffener to the experimentally measured or hand-defined sinusoidal geometric imperfections were pure strengthening effects.

5.3.3 Hand-defined sinusoidal geometric imperfections

Finally, considering the hand-defined sinusoidal geometric imperfections (cf. Fig. 5.10), a similar trend in the results as for the experimentally measured and buckling mode-affine geometric imperfections was observed. Again, a threshold before which the influence of the longitudinal stiffener had a small impact on the ultimate capacity was returned. For the case $\alpha = 1$ and for small patch load lengths $s_s/h_w \leq 0.05$ ($s_s = 25$ mm), an increase of 5% in the ultimate strength of longitudinally stiffened steel plate girders was noticed, while the maximum increase of 45% was computed for $s_s/h_w \leq 0.50$ ($s_s = 250$ mm), see Fig. 5.36a. Interestingly, the cosine hand-defined geometric imperfection (Eq. (5.2)) had the same threshold $s_s/h_w = 0.30$ ($s_s =$

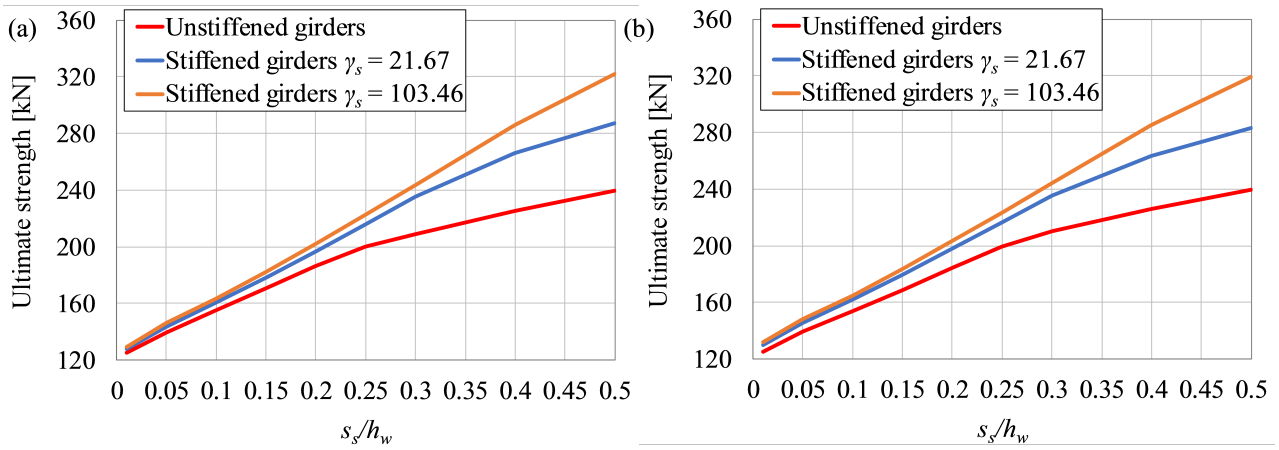


Figure 5.23: Ultimate strength of longitudinally unstiffened and stiffened steel plate girders using experimentally measured geometric imperfections from (a) girder B7 and (b) girder B11.

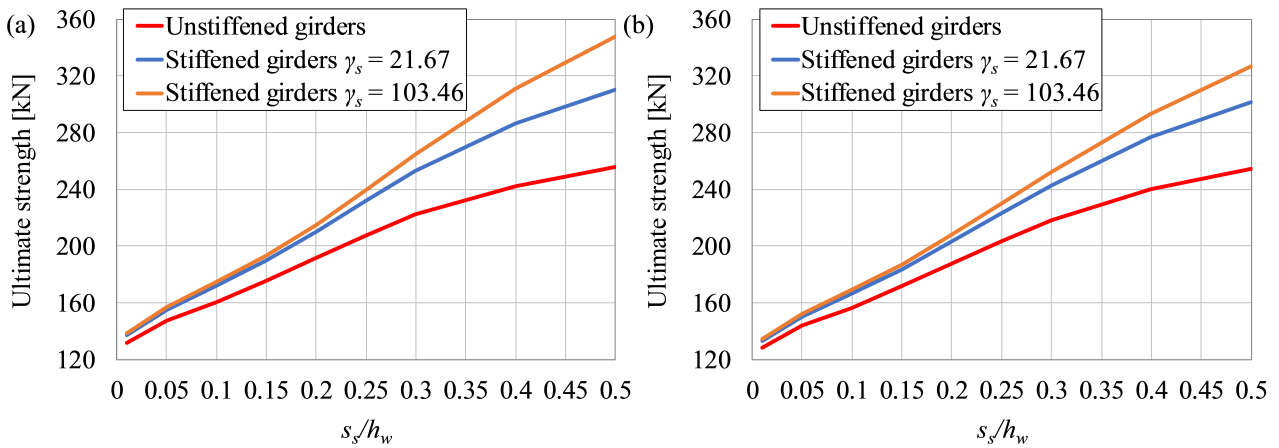


Figure 5.24: Ultimate strength of longitudinally unstiffened and stiffened steel plate girders using experimentally measured geometric imperfections from (a) girder B12 and (b) girder B13.

150 mm) as some experimentally measured geometric imperfections, cf. Fig. 5.18b. More precisely, this geometric imperfection is in correspondence with the one of girder A16. The same strengthening effect of approximately 15% was recorded in both cases, as graphically presented in Fig. 5.36a.

A similar trend in the results as for the first two buckling modes and for the combination of buckling modes ($1^{st} + 2^{nd} + 3^{rd}$) was observed for the case $\alpha = 2$ (girders of Series B). In this case, the carrying capacities of longitudinally stiffened steel plate girders were higher than for unstiffened ones for all the load lengths considered, $s_s/h_w \leq 0.50$, as shown in Fig. 5.35. For both hand-defined geometric imperfections, the strengthening effect was very small for $s_s/h_w \leq 0.15$ (valid for both $\gamma_s = 21.67$ and $\gamma_s = 103.46$), while appreciable strengthening effects of 25% and 21% were returned for $s_s/h_w = 0.50$ for the sine and cosine hand-defined geometric imperfections, respectively (see Table 5.6 and Fig. 5.36b); significantly larger strengthening effects of 41% and 31% were calculated for $s_s/h_w = 0.50$ and for $\gamma_s = 103.46$ (Table 5.7). Further details regarding the strengthening effect are presented in Section 5.3.5.

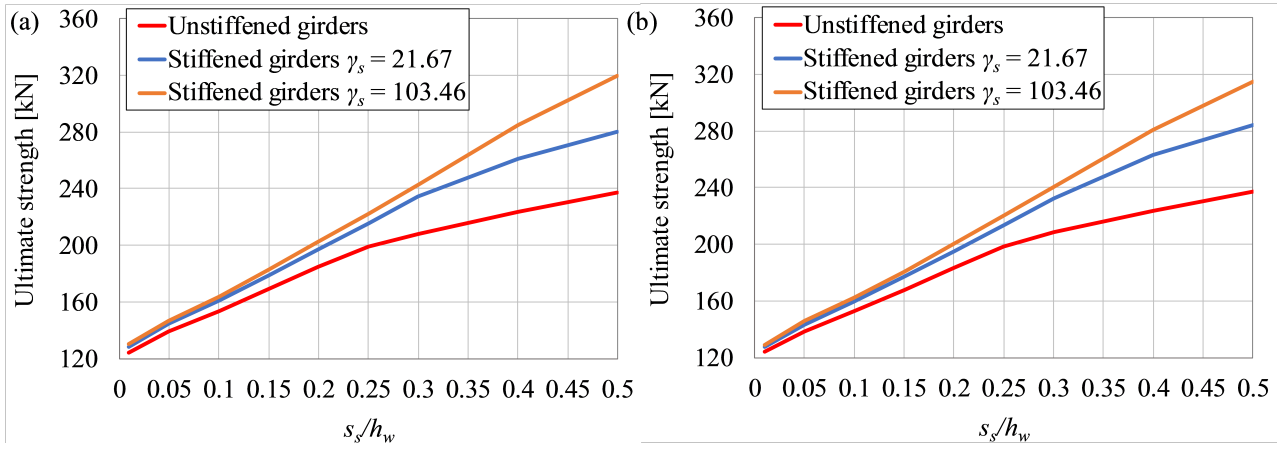


Figure 5.25: Ultimate strength of longitudinally unstiffened and stiffened steel plate girders using experimentally measured geometric imperfections from (a) girder B14 and (b) girder B15.

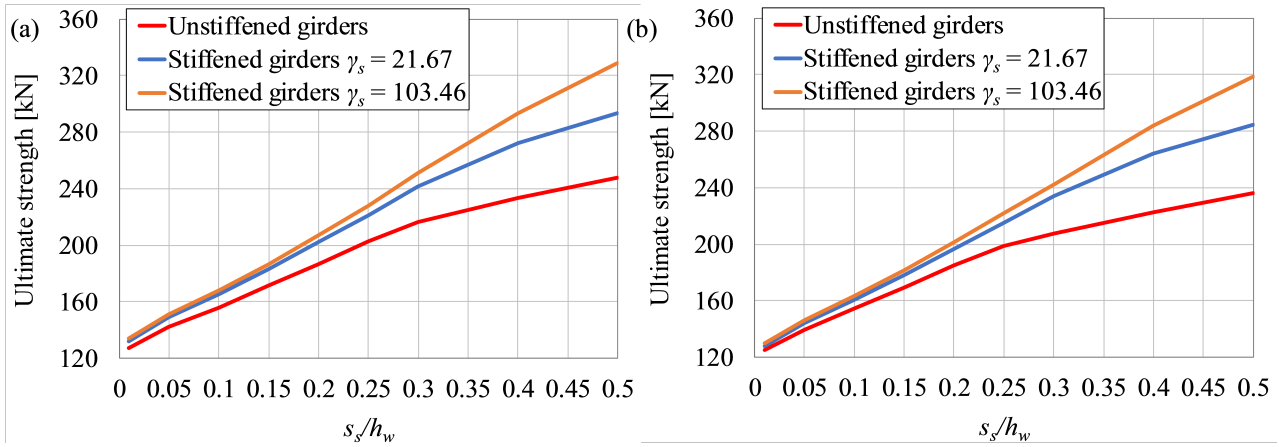


Figure 5.26: Ultimate strength of longitudinally unstiffened and stiffened steel plate girders using experimentally measured geometric imperfections from (a) girder B16 and (b) girder B17.

Moreover, a comparison between these two hand-defined geometric imperfections for the case $\alpha = 2$ showed that lower ultimate strengths were obtained for the cosine hand-defined geometric imperfection for longitudinally unstiffened ($s_s/h_w \leq 0.25$) and stiffened steel plate girders ($s_s/h_w \leq 0.40$ for $\gamma_s = 21.67$ and $s_s/h_w \leq 0.50$ for $\gamma_s = 103.46$). In addition, the average ultimate strength computed over all analyzed geometric imperfections for the $\alpha = 2$ case was captured well by the cosine hand-defined imperfection for both longitudinally unstiffened and stiffened steel plate girders and all the patch load lengths considered, $s_s/h_w \leq 0.50$; furthermore, this justifies the usage of this geometric imperfection in parametric analyses [34–35].

A direct comparison of the obtained results with the available literature is not feasible since different initial geometric imperfections under different patch load lengths were not considered. Moreover, all parameters should match for a complete comparison (e.g., shape of initial geometric imperfection, girder geometry, patch load length, et cetera), since they all affect the ultimate strength. However, the results obtained in this research can be partially juxtaposed with Ref. [34]; even though the girder geometry is different, relevant ratios can be used. Taking

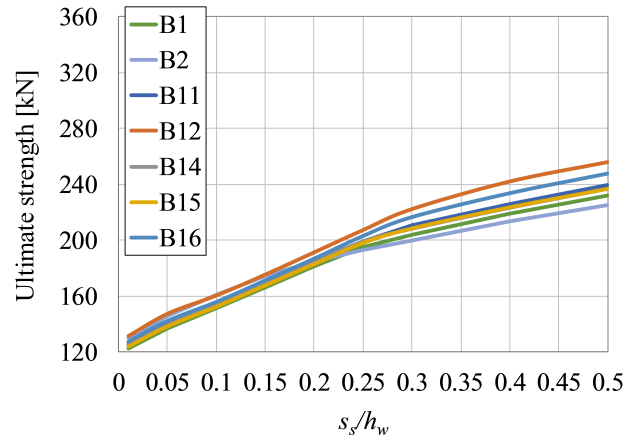


Figure 5.27: Ultimate strength of longitudinally unstiffened steel plate girders using experimentally measured imperfections from the originally unstiffened girders.

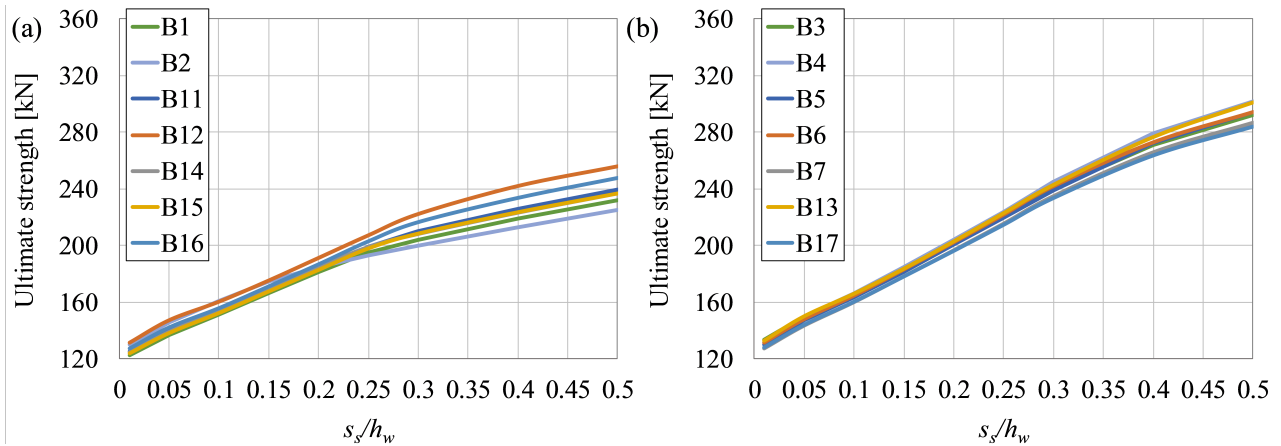


Figure 5.28: Ultimate strength of longitudinally stiffened steel plate girders using experimentally measured imperfections from the originally stiffened girders employing (a) relatively weak ($\gamma_s = 21.67$) and (b) strong longitudinal stiffener ($\gamma_s = 103.46$).

$a = h_w = 3600$ mm ($\alpha = 1$), $t_f = 35$ mm, $t_w = 24$ mm and $b_1 = 720$ mm from Ref. [34], the following ratios $h_w/t_w = 150$, $t_f/t_w = 1.46$, $b_1/h_w = 0.2$ and $b_1/t_w = 30$ (the closest ratios to the current analysis $h_w/t_w = 125$, $t_f/t_w = 2$, $b_1/h_w = 0.2$ and $b_1/t_w = 25$, see Table 4.1) can be used for comparison. The authors in Ref. [34] considered a C-shape initial deformation (idealized with cosine function) which corresponds to the first buckling mode of longitudinally stiffened plate girders. They reported strengthening effects of 1.03, 1.04, 1.09 and 1.19 for patch load lengths $s_s/h_w = 0.10$, 0.20, 0.30 and 0.40, respectively. One can instantaneously see that these results and the results for the first buckling mode in Table 5.4 are in perfect agreement; a small deviation exists only for $s_s/h_w = 0.40$ for the cosine hand-defined geometric imperfection.

Furthermore, an S-shape initial deformation (similar to the second buckling mode in the current study, cf. Fig. 5.3) returned lower ultimate strengths compared to a C-shape initial deformation (described as the cosine hand-defined geometric imperfection) for $a/h_w = 1$, $b_1 \approx 0.2h_w$, and $s_s/h_w = 0.05$ [38,42]. The authors in Refs. [38,42] concluded that the reduction in patch loading resistance of longitudinally stiffened steel plate girders between the S-shape and C-shape geometric imperfections was around 7%. Comparing the current results in Table

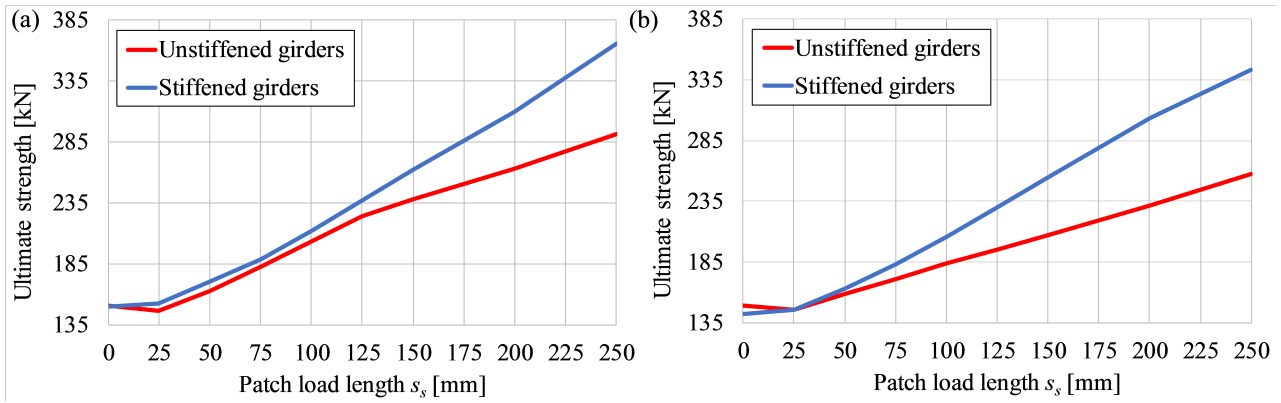


Figure 5.29: Ultimate strength of longitudinally unstiffened and stiffened steel plate girders using geometric imperfections from buckling mode: (a) 1st mode; (b) 2nd mode.

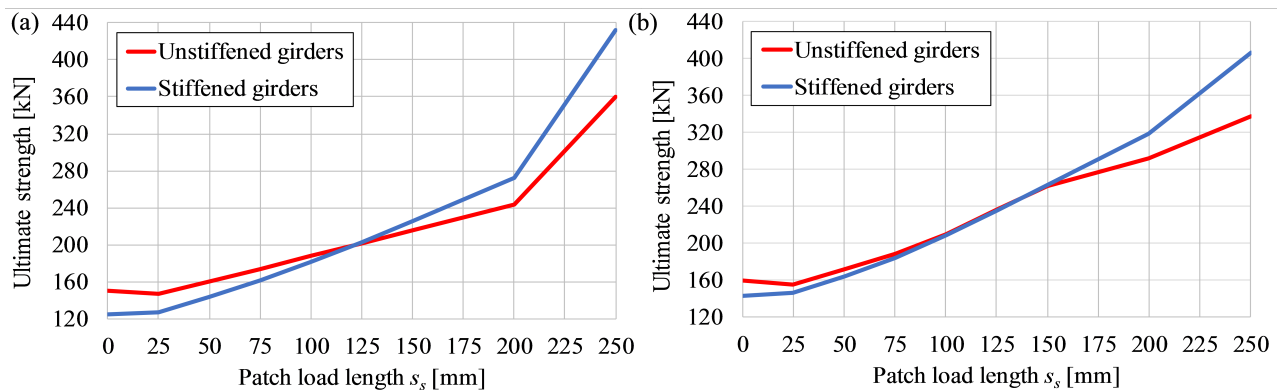


Figure 5.30: Ultimate strength of longitudinally unstiffened and stiffened steel plate girders using geometric imperfections from buckling mode: (a) 3rd mode; (b) combination of modes (1st + 2nd + 3rd).

5.4 for the cosine hand-defined geometric imperfection and the second buckling mode gave a decrease of 5% in the ultimate strength of longitudinally stiffened girders. Thus, both analyses show that an S-shape imperfection is more unfavorable than a C-shape deformation from the patch loading point of view; unfavorable geometric imperfections are discussed in more detail in Chapter 6. A further juxtaposition with the literature is not reasonable since the relevant parameters (a/h_w , h_w/t_w , b_1 , b_1/t_w , et cetera) are different.

To conclude this discussion regarding the imperfection sensitivity of steel plate girders under concentrated transverse loading, additional comparisons, including all the above geometric imperfections, are provided. The ultimate strengths of longitudinally unstiffened and stiffened steel plate girders using buckling mode-affine and hand-defined geometric imperfections are compared with the experimental ones (minimum and maximum values for longitudinally unstiffened and stiffened girders using the experimentally measured imperfections, cf. Fig. 5.19, Fig. 5.27, and Fig. 5.28). It turned out that the ultimate strength of longitudinally unstiffened girders ($\alpha = 1$) considering the experimentally measured imperfections were bounded by the ultimate load using buckling mode-affine geometric imperfections (second buckling mode and combination of modes), Fig. 5.37a. A variation in the ultimate capacity between these two

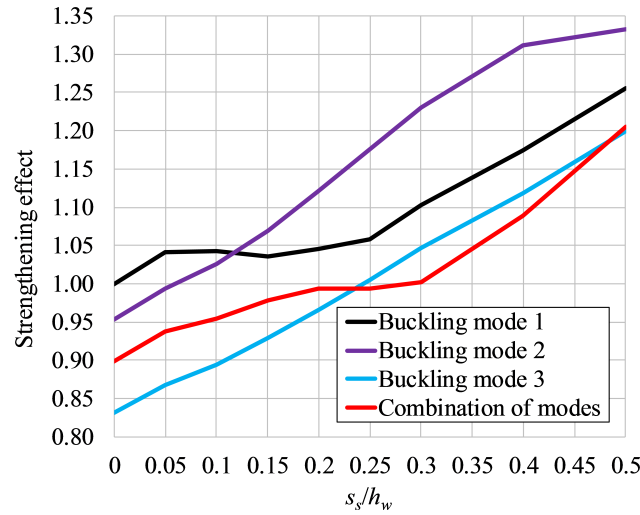


Figure 5.31: Strengthening effect employing the buckling modes as initial geometric imperfections for girders of Series A.

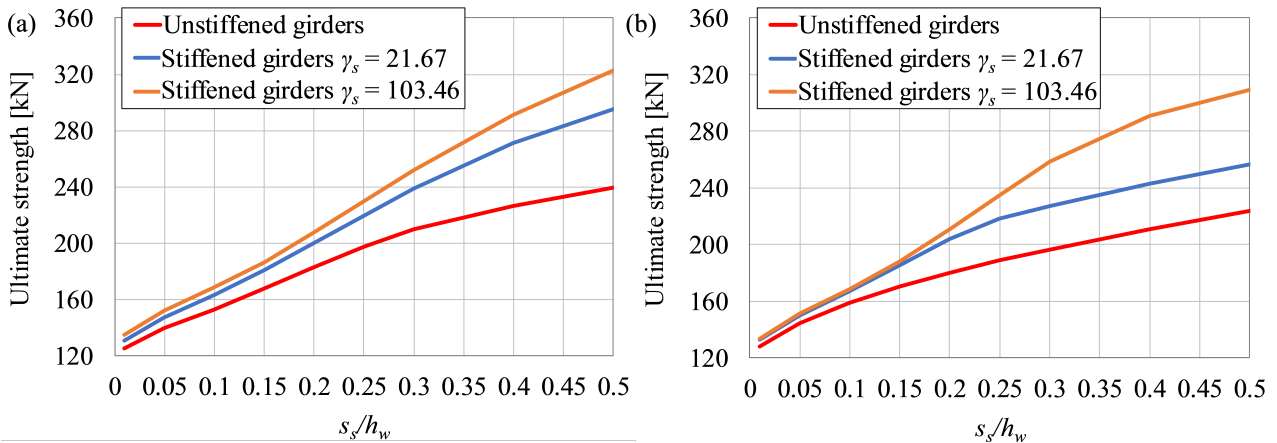


Figure 5.32: Ultimate strength of longitudinally unstiffened and stiffened steel plate girders using the first (a) and second buckling mode shape (b) as initial geometric imperfections.

extreme limits of 13% and 40% was obtained for $s_s/h_w = 0$ and $s_s/h_w = 0.50$, respectively. A similar conclusion was returned for the $\alpha = 2$ case, Fig. 5.38. In this case, the patch loading resistance varied by approximately 15% for both $s_s/h_w = 0$ and $s_s/h_w = 0.50$.

The ultimate strengths of longitudinally stiffened girders ($\alpha = 1$) employing the experimentally measured imperfections were bounded by carrying capacities determined using buckling mode-affine and hand-defined geometric imperfections (third buckling mode and sine hand-defined imperfections), Fig. 5.37b. In this case, the ultimate load varied from 30 ($s_s/h_w = 0$) to 27% ($s_s/h_w = 0.50$). Based on this figure, one can observe that the lower band (third buckling mode) was valid for patch load lengths $s_s/h_w \leq 0.40$. Slightly different findings were observed for the $\alpha = 2$ case. Utilizing a relatively weak longitudinal stiffener ($\gamma_s = 21.67$), the experimentally measured imperfections returned ultimate strengths that were bounded by the third buckling mode and sine hand-defined imperfections for $s_s/h_w \leq 0.25$. In contrast, for longer loading lengths (e.g., $s_s/h_w \geq 0.30$), the ultimate strengths were bounded by the second buckling mode and combination of modes, Fig. 5.39a. Variation in the ultimate capacity

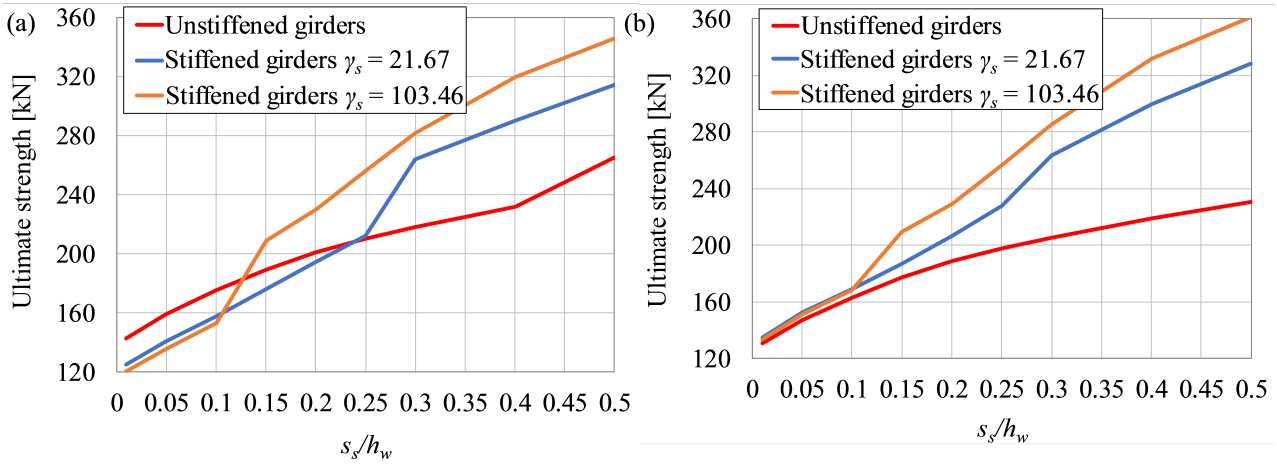


Figure 5.33: Ultimate strength of longitudinally unstiffened and stiffened steel plate girders using the third (a) and combination (b) of buckling mode shapes ($1^{st} + 2^{nd} + 3^{rd}$) as initial geometric imperfections.

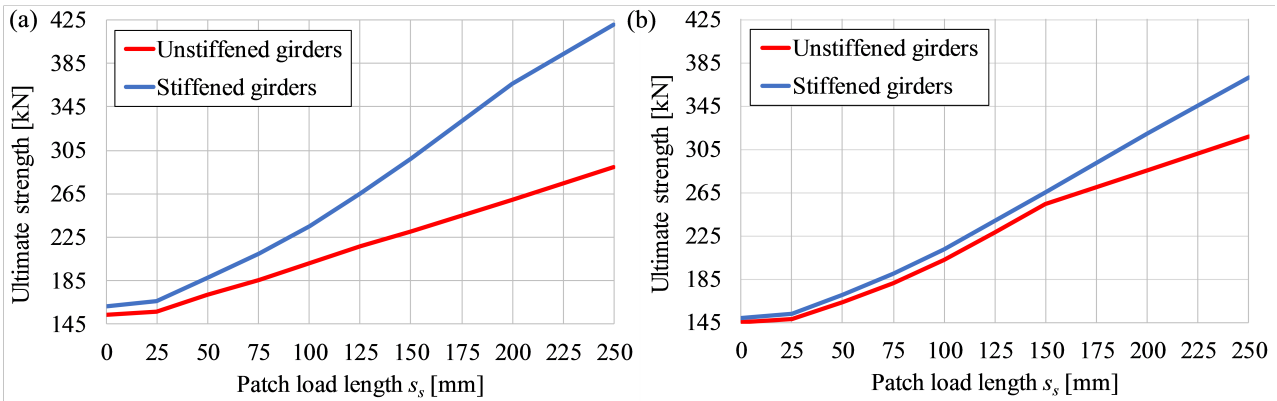


Figure 5.34: Ultimate strength of longitudinally unstiffened and stiffened steel plate girders using sine (a) and cosine (b) hand-defined geometric imperfections. Web panel aspect ratio $\alpha = 1$.

of approximately 10 and 28% were computed for $s_s/h_w = 0$ and $s_s/h_w = 0.50$, respectively. Furthermore, for the $\gamma_s = 103.46$ case, the lowest ultimate strengths were determined by the experimentally measured imperfections for $0.15 \leq s_s/h_w \leq 0.40$, while outside of this range, the lowest ultimate loads were returned employing buckling mode-affine imperfections. Only for small patch load length ($s_s/h_w \leq 0.10$), the experimentally measured imperfections returned ultimate capacities that were bounded by the third buckling mode and sine hand-defined imperfections, Fig. 5.39b.

Discussion in this Section shows that the lowest ultimate strength of longitudinally unstiffened and stiffened steel plate girders is governed by the patch load length, geometric imperfection shape, and the relative stiffness of the longitudinal stiffener. A more detailed analysis of unfavorable geometric imperfections from the patch loading point of view is given in the following Chapter.

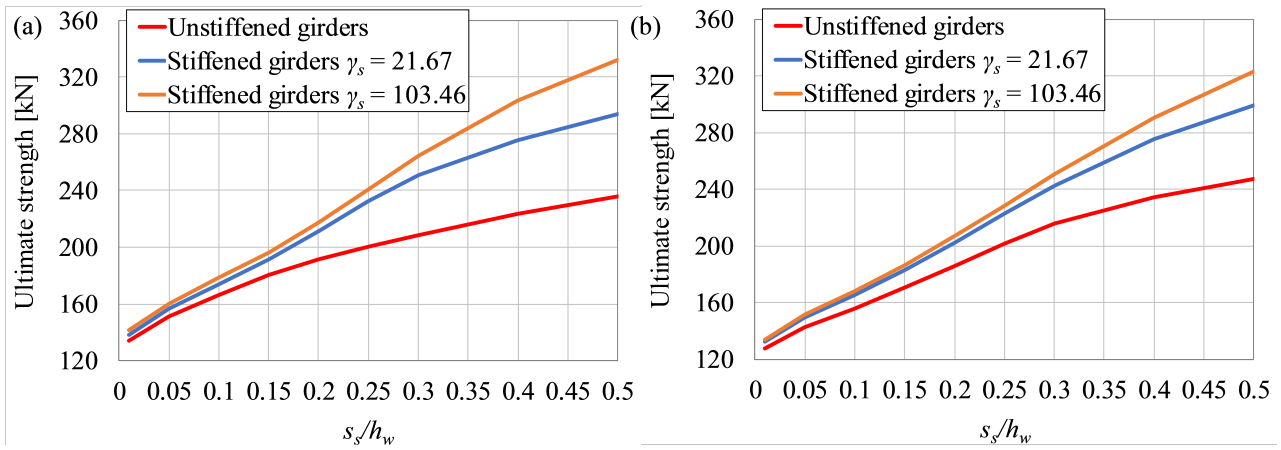


Figure 5.35: Ultimate strength of longitudinally unstiffened and stiffened steel plate girders using sine (a) and cosine (b) hand-defined geometric imperfections. Web panel aspect ratio $\alpha = 2$.

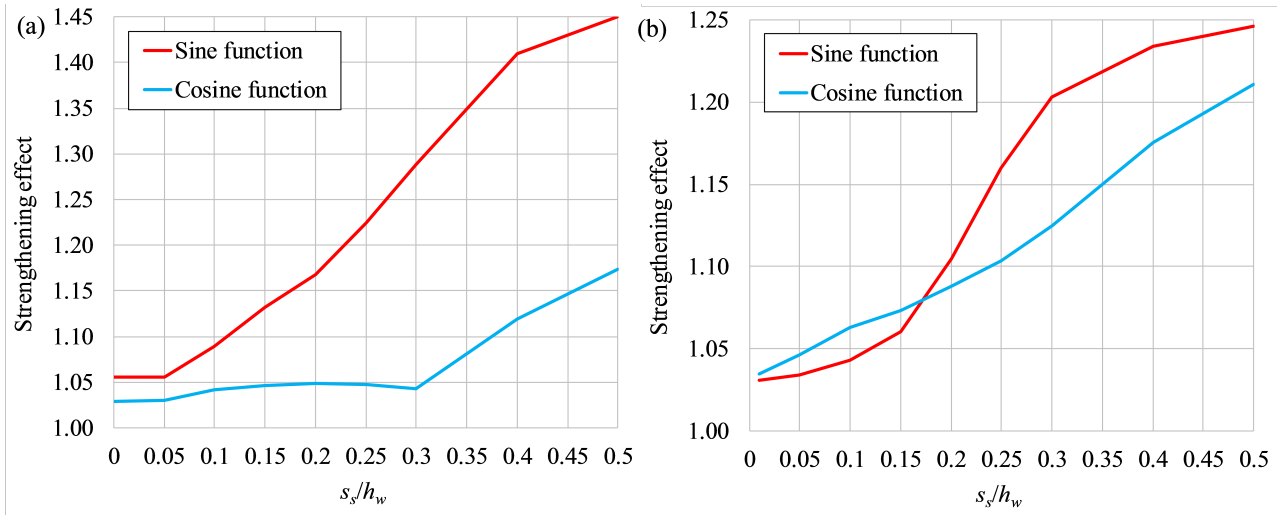


Figure 5.36: Strengthening effect employing initial geometric imperfections by sine and cosine functions for (a) girders of Series A and (b) girders of Series B ($\gamma_s = 21.67$).

5.4 Influence of the web panel aspect ratio

The above discussion is related to the influence of patch load length and various geometric imperfections on the carrying capacity of steel plate girders. Findings regarding the influence of the web panel aspect ratio, α , on the ultimate strength can also be summarized. To illustrate the contribution of the web panel aspect ratio (in combination with a variety of geometric imperfections) to the ultimate strength of steel plate girders, only web panel aspect ratios with the same geometric imperfections should be considered. The experimentally measured imperfections are random shapes in both longitudinal and transverse directions; thus, those imperfections are disregarded in this discussion. Moreover, the first buckling mode shape of longitudinally unstiffened and stiffened steel plate girders for the case $\alpha = 1$ (cf. Fig. 5.2) matches the one for $\alpha = 2$ (cf. Fig. 5.6), while the second and third buckling mode shapes are very different; hence, they are ignored in this discussion as well. The combination of buckling

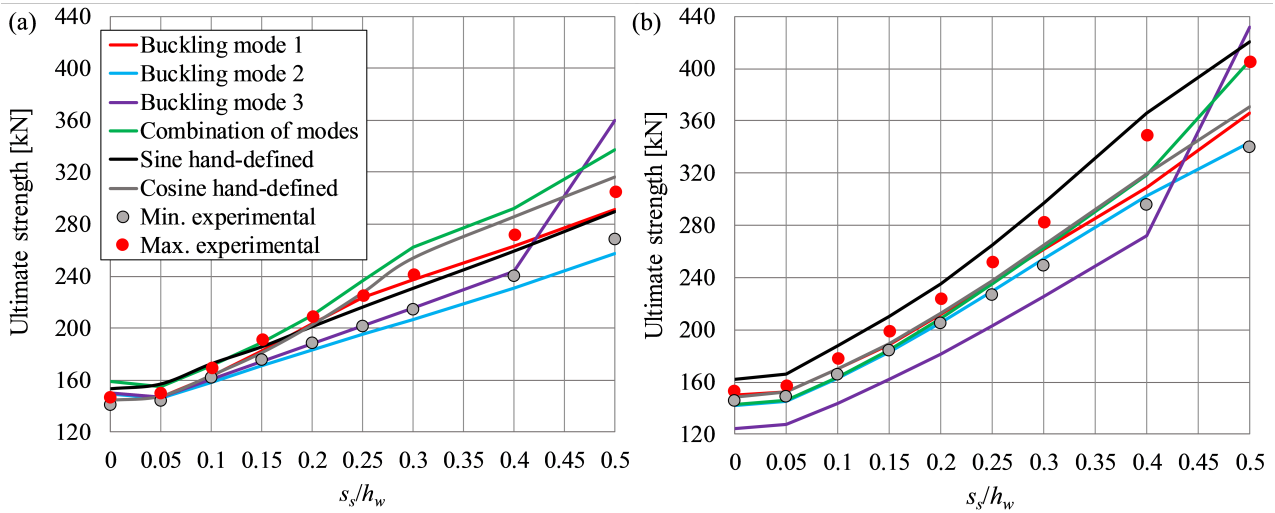


Figure 5.37: Ultimate strength of longitudinally (a) unstiffened and (b) stiffened steel plate girders using various geometric imperfections. Web panel aspect ratio $\alpha = 1$.

modes ($1^{st} + 2^{nd} + 3^{rd}$) is also disregarded in this discussion for the same reason. A direct comparison between these two cases $\alpha = 1$ and $\alpha = 2$ revealed the following:

- An increase in the web panel aspect ratio decreased the patch loading resistance of longitudinally unstiffened steel plate girders for the first buckling mode-affine and hand-defined sinusoidal geometric imperfections for all the patch load lengths considered, $s_s/h_w \leq 0.50$. This decrease was especially pronounced for longer patch load lengths (e.g., $s_s/h_w = 0.50$), whereas for $s_s/h_w \leq 0.15$, the effect of the web panel aspect ratio can be ignored. Ratios between the ultimate strength for web panel aspect ratio $\alpha = 1$ and $\alpha = 2$ are provided in Table 5.8.
- The same conclusion was obtained for longitudinally stiffened steel plate girders considering the first buckling mode-affine and hand-defined sinusoidal geometric imperfections. In this case, the effect of the web panel aspect ratio was minimal for $s_s/h_w \leq 0.15$, while a notable increase in ultimate strength was achieved for $s_s/h_w = 0.50$, Table 5.8. A decrease in the ultimate strength of longitudinally stiffened steel plate girders when the web panel aspect ratio was increased was also observed experimentally [2,21] and computationally [26,34–35].

Succinctly, the impact of the web panel aspect ratio on the carrying capacity of longitudinally unstiffened and stiffened steel plate girders is dependent on the imperfection and patch load length.

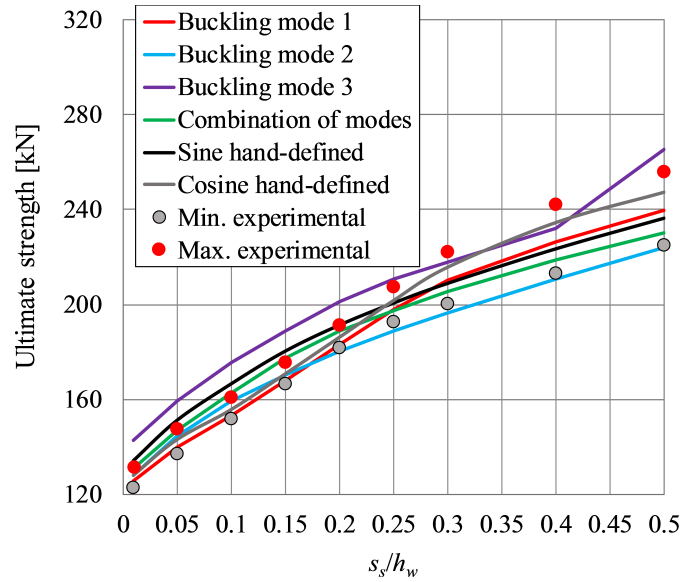


Figure 5.38: Ultimate strength of longitudinally unstiffened steel plate girders using various geometric imperfections. Web panel aspect ratio $\alpha = 2$.

Table 5.8: Ratio between the ultimate strength of steel plate girders for web panel aspect ratios $\alpha = 1$ and $\alpha = 2$.

Girders	Shape of geometric imperfection	s_s/h_w							
		0.05	0.10	0.15	0.20	0.25	0.30	0.40	0.50
Unstiffened	1 st buckling mode	1.05	1.07	1.08	1.11	1.13	1.13	1.16	1.22
	Hand-define sine function	1.04	1.04	1.03	1.05	1.08	1.11	1.16	1.23
	Hand-define cosine function	1.03	1.05	1.06	1.09	1.13	1.18	1.22	1.28
Stiffened	1 st buckling mode	1.03	1.04	1.04	1.06	1.08	1.10	1.14	1.24
	Hand-define sine function	1.06	1.08	1.10	1.11	1.14	1.18	1.33	1.43
	Hand-define cosine function	1.02	1.03	1.04	1.05	1.07	1.09	1.16	1.24

5.5 Influence of relative stiffness γ_s

The contribution of the longitudinal stiffener with relative stiffness $\gamma_s = 21.67$ and $\gamma_s = 103.46$ to the carrying capacity of longitudinally stiffened steel plate girders is represented as strengthening effects in Table 5.6 and Table 5.7 for the $\alpha = 2$ case; only one longitudinal stiffener was considered for the $\alpha = 1$ case. The influence of relative stiffness γ_s on the ultimate strength of longitudinally stiffened steel plate girders for buckling mode-affine geometric imperfections is debatable (as discussed in Section 5.3.2) since the relative stiffness of the longitudinal stiffener changes buckling mode shapes and, thus, initial geometric imperfections. In the current study, the first buckling mode shapes for $\gamma_s = 21.67$ and $\gamma_s = 103.46$ appear to be very similar (cf. Fig. 5.6). However, the second and third buckling mode shapes are very different (cf. Fig. 5.7,

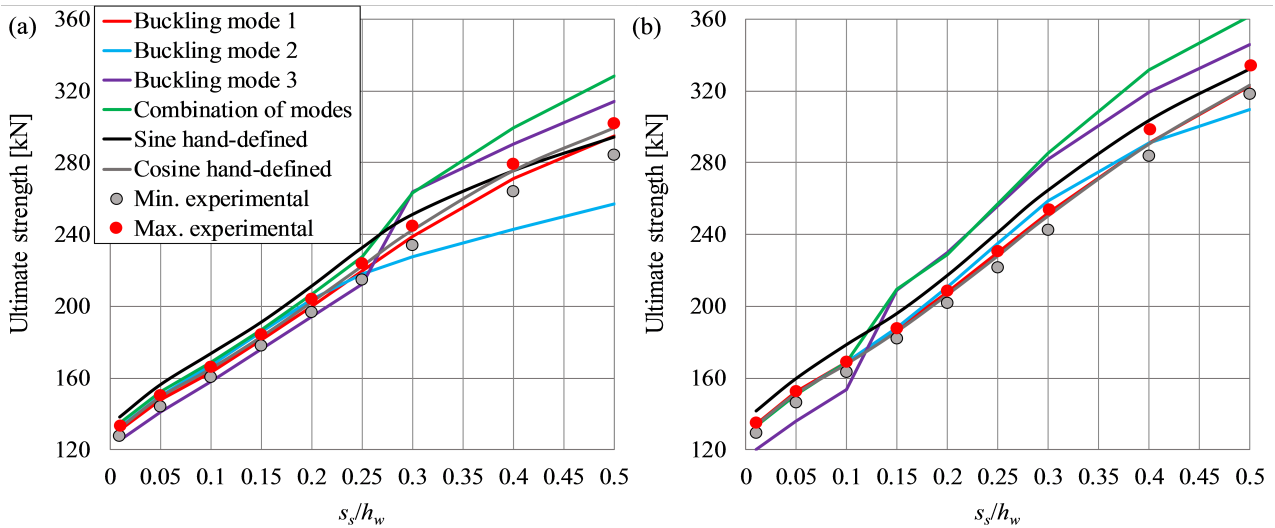


Figure 5.39: Ultimate strength of longitudinally stiffened steel plate girders using various geometric imperfections employing (a) relatively weak ($\gamma_s = 21.67$) and (b) strong longitudinal stiffener ($\gamma_s = 103.46$). Web panel aspect ratio $\alpha = 2$.

Fig. 5.8, and Fig. 5.9); hence, they are disregarded in this discussion. Therefore, using all the experimentally measured, hand-defined, and first buckling mode-affine geometric imperfections, the following conclusions could be drawn:

- An increase in relative stiffness from $\gamma_s = 21.67$ to $\gamma_s = 103.46$ insignificantly increased the ultimate strength of longitudinally stiffened steel plate girders for $s_s/h_w \leq 0.30$. The maximum increase of 7%, with an average value of 2%, was returned for patch load lengths $s_s/h_w \leq 0.30$.
- A noticeable increase in the patch loading resistance of 16%, with an average value of 10%, was obtained for patch load lengths $s_s/h_w \geq 0.40$. These conclusions agree well with the work of [35], in which only one geometric imperfection was considered (cosine hand-defined), and analysis was conducted on steel plate girders with similar geometric ratios as in this work. The above conclusions were derived for the longitudinal stiffener's optimum location for the flexural and shear resistance placed at one-fifth of the girder depth ($b_1 = 0.2h_w$) [66–68].

In summary, an increase in relative stiffness γ_s has a very small effect on the ultimate strength of longitudinally stiffened steel plate girders for patch load lengths $s_s/h_w \leq 0.30$ for the analyzed girder geometry, longitudinal stiffener position, and all the geometric imperfections considered. This analysis demonstrates that increasing the relative stiffness of the longitudinal stiffener (from the patch loading point of view) is justified only for longer patch load lengths.

5.6 Contribution of the web panel yield stress

Although the main focus in this Chapter is on the imperfection sensitivity of steel plate girders under concentrated loading, relevant observations about the web panel yield stress are discussed. Since three different web panel yield stresses – that is, $f_{yw} = 225$ MPa, $f_{yw} = 260$ MPa, and $f_{yw} = 320$ MPa – unexpectedly appeared in the experimental program (Chapter 3) for the $\alpha = 2$ case, their contribution to the ultimate strength was analyzed; very small variations in the flange yield stress can be ignored. For this purpose, the numerical model, which is validated in Chapter 3, was applied and all other parameters were kept unaltered. New numerically evaluated patch loading resistances for all the three web panel yield stresses are tabulated in Table 5.9, whereas the ultimate loads for $f_{yw} = 320$ MPa serve as reference values.

Based on these results, the following conclusions could be made. An increase in the web panel yield stress from 260 MPa to 320 MPa (yield stress ratio 1.23) equally increased the ultimate strength of longitudinally unstiffened and stiffened steel plate girders for the same patch load lengths (small discrepancies exist only for longer patch load lengths). Although the actual yield stress ratio was 1.23, the obtained increase in the ultimate load was well below this ratio. Moreover, this increase in the ultimate strength varied from 1.18 ($s_s/h_w = 0$) to 1.13 ($s_s/h_w \geq 0.40$) for both longitudinally unstiffened and stiffened steel plate girders (Table 5.9). This clearly shows that the web panel yield stress, f_{yw} , influences the ultimate strength with a power of 0.60–0.78 – that is, f_{yw}^λ , where λ is dependent on patch load length and varies from 0.60 to 0.78; smaller values correspond to longer patch load lengths. However, most of the proposed expressions for the patch loading resistance based on failure mechanisms available in the literature as well as in the current design standard EN 1993-1-5 [65] have a fixed value for coefficient λ – that is, $\lambda = 0.50$. For an overview of failure mechanisms refer to [5,29,97].

Similar observations can be noted for the other case – that is, when the web panel yield stress was increased from 225 MPa to 320 MPa (yield stress ratio 1.42). In this case, the bearing capacity was increased by approximately 1.26 for both longitudinally unstiffened and stiffened steel plate girders (except for $s_s/h_w = 0.50$ for longitudinally stiffened steel plate girders). The returned increase in the ultimate strength was again well below 1.42, and it varied from 1.27 to 1.24 for different patch load lengths (Table 5.9). In this case, the web panel yield stress, f_{yw} , contributed to the ultimate load with a power of 0.60–0.67 – that is, f_{yw}^λ , where $\lambda = 0.60$ –0.67. As can be concluded combining these two cases, the coefficient λ is dependent on patch load length, and its value is greater than the most commonly used value, $\lambda = 0.50$.

Additionally, a decrease in these contributions to ultimate load for both examined cases (from 1.18 to 1.13 and from 1.27 to 1.24) accompanying an increase in the patch load length is obvious from the results in Table 5.9 (very small irregularities exist, but they may be influenced by different geometric imperfections). *Material effects* are more dominant for very small patch load lengths ($s_s/h_w = 0$) than *geometric effects*. In this case ($s_s/h_w = 0$), the failure mechanism shape was located in the upper part of the web panel (for longitudinally

unstiffened steel plate girders), and between the longitudinal stiffener and loaded flange for longitudinally stiffened ones. Conversely, *geometric effects* are dominant for longer patch load lengths (a larger buckling area is engaged, failure mechanism shapes are present further away from the loaded flange, and material effects are less dominant); this could explain the observed trend in these results. In any case, further research is needed to verify these conclusions, and they may form the basis for future studies.

The above-presented results and discussions are available in sequentially published papers [82–86].

Table 5.9: Numerically obtained ultimate strengths using three different web panel yield stresses for the $\alpha = 2$ case. Units are in kN.

Unstiffened girders	B16 $s_s = 0$ mm	s_s	B14 $s_s = 25$ mm	s_s	B1 $s_s = 50$ mm	s_s	B15 $s_s = 100$ mm	B2 $s_s = 150$ mm	B12 $s_s = 200$ mm	B11 $s_s = 250$ mm
$F_{FEA,unstiff}$ (320) ¹	137.11		128.56		146.83		176.61	202.83	243.59	232.85
$F_{FEA,unstiff}$ (320)/ $F_{FEA,unstiff}$ (260) ²	1.18		1.17		1.17		1.17	1.15	1.13	1.15
$F_{FEA,unstiff}$ (320)/ $F_{FEA,unstiff}$ (225) ³	1.26		1.24		1.25		1.26	1.26	1.24	1.26
Stiffened girders	B13 $s_s = 0$ mm	s_s	n.a.		B3 $s_s = 50$ mm	s_s	B5 $s_s = 100$ mm	B7 $s_s = 150$ mm	B4 $s_s = 200$ mm	B6 $s_s = 250$ mm
$F_{FEA,stiff}$ (320) ¹	157.22				168.07		203.06	225.44 215.33	273.13	292.72
$F_{FEA,stiff}$ (320)/ $F_{FEA,stiff}$ (260) ²	1.17				1.17		1.18	1.17 1.18	1.16	1.13
$F_{FEA,stiff}$ (320)/ $F_{FEA,stiff}$ (225) ³	1.26				1.26		1.27	1.27 1.27	1.26	1.22

¹ Ultimate strength computed using web panel yield stress $f_{yw} = 320$ MPa and flange yield stress $f_{yf} = 318$ MPa

² Ratio between ultimate strength using $f_{yw} = 320$ MPa and ultimate strength using $f_{yw} = 260$ MPa

³ Ratio between ultimate strength using $f_{yw} = 320$ MPa and ultimate strength using $f_{yw} = 225$ MPa

n.a. = not available (this data is missing due to the limited number of tests available from 7 steel plate girders)

5.7 Summary

The present finite element parametric study was designed to determine the influence of various geometric imperfections (in combination with a variety of patch load lengths) on the patch loading resistance of I-shaped steel plate girders. Experimentally measured, buckling mode-affine, and hand-defined sinusoidal geometric imperfections were varied in the study in combination with varying patch load lengths and relative stiffnesses of the longitudinal stiffener. Several key points were identified regarding the patch load length from the present study:

- The ultimate strength of longitudinally unstiffened and stiffened steel plate girders increases as the patch load length increases. This was shown to be valid for all the geometric imperfections considered.
- For very small patch load lengths (e.g., $s_s/h_w < 0.15$), the ultimate strength of longitudinally stiffened steel plate girders follows the ultimate load of unstiffened ones regardless of the relative stiffness of the longitudinal stiffener and the geometric imperfection; hence, the strengthening effect is very small (less than 10%). On the other hand, for longer patch load lengths (e.g., $s_s/h_w = 0.50$), different substantial strengthening effects can be achieved for different geometric imperfections.
- An increase in the web panel aspect ratio decreased the patch loading resistance of longitudinally unstiffened steel plate girders for all the patch load lengths considered, $s_s/h_w \leq 0.50$. This is especially pronounced for longer patch load lengths (e.g., $s_s/h_w = 0.50$), whereas for $s_s/h_w \leq 0.15$, the effect of the web panel aspect ratio can be ignored. For longitudinally stiffened steel plate girders, the effect of the web panel aspect ratio is minimal for $s_s/h_w \leq 0.15$, while a notable decrease in the ultimate strength was achieved for $s_s/h_w = 0.50$. The level of reduction in the ultimate load of longitudinally unstiffened and stiffened steel plate girders varied depending on imperfection shape and the patch load length. The reduction depended mostly on patch load length.
- An increase in relative stiffness γ_s (from relatively weak to relatively strong longitudinal stiffeners) has a very small effect on the ultimate strength of longitudinally stiffened steel plate girders for patch load lengths $s_s/h_w \leq 0.30$ and all the geometric imperfections considered. In contrast, a noticeable increase in patch loading resistance was obtained for patch load lengths $s_s/h_w \geq 0.40$. Increasing the longitudinal stiffener relative stiffness (from the patch loading point of view) is justified only for longer patch load lengths. This conclusion was derived for the longitudinal stiffener's optimum location for the flexural and shear resistance placed at one-fifth of the girder depth ($b_1 = 0.2h_w$).

Chapter 6

Unfavorable geometric imperfections

6.1 Introduction

As mentioned in the introduction Chapter, the current European design standard EN 1993-1-5 [65] requires a stability control check for concentrated transverse forces. Recent experimental studies [21,79] have shown that the current EN 1993-1-5 patch loading resistance model (refer to Section 2.3 for more details) underestimates the ultimate strength of steel plate girders in certain cases, especially for longitudinally stiffened steel plate girders and longer patch load lengths. In addition to this resistance model, the current design standard also allows the use of finite element analysis for the ultimate limit state. The essential data for an adequate ultimate limit state design comprises information on unavoidable geometric and structural imperfections (residual stresses). The EN 1993-1-5 rules state that a chosen imperfection should yield the lowest resistance. However, the design standard lacks information on these imperfections, and no specific geometric shape or stress pattern is provided. The usual practice for geometric imperfections is to use buckling mode-affine or hand-defined sinusoidal geometric imperfections, approaches frequently used in the literature [23,26,34,40,56,79,88,94–95,98–100]. Following general recommendations on imperfections in Ref. [65], it is not clear from the patch loading point of view which imperfections lead to the lowest ultimate strength.

Structural imperfections do not significantly influence the ultimate strength of steel plate girders under patch loading [74,88,92–93]; thus, they can be excluded from the analysis. However, geometric imperfections have a detrimental effect on the patch loading resistance of steel plate girders. The sensitivity of steel plate girders to geometric imperfections under concentrated transverse loading was studied in Refs. [23,26,40,79,88,98] by studying various geometric imperfections. In these studies, the patch load length was mostly constant or insufficiently varied. Indeed, the patch load length has been mostly constant in experimental investigations and has not been sufficiently studied numerically [23,26,79,56,34–35]; refer to Chapter 2 for literature review.

Determination of the most unfavorable geometric imperfection of structures (often

referred to as the *worst* geometric imperfection) represents a highly nonlinear optimization problem [101–102]. The worst imperfection shape can significantly change with the system geometry or loading conditions. As shown in Ref. [103] for shell structures, it is also highly influenced by the imperfection amplitude. This Chapter sought unfavorable geometric imperfections in steel plate girders under concentrated transverse loading while considering the most often used geometric imperfections for this design case; thus, this research does not refer to the *worst* geometric imperfection. Our goal is to provide broader design guidelines that include a wide range of design situations.

Unfavorable geometric imperfections (from the patch loading point of view) are determined considering the initial geometric imperfections (Fig. 5.6 – Fig. 5.10 and experimentally measured imperfections in Appendix C) and computed numerical results (Table 5.5 – Table 5.7) for girders of Series B ($\alpha = 2$). Findings regarding this analysis are coupled with results for girders of Series A in order to provide more general conclusions.

6.2 Unfavorable geometric imperfections

As Table 5.5 illustrates, the lowest patch loading resistance of longitudinally unstiffened steel plate girders was returned for some experimentally measured and first two buckling mode-affine geometric imperfections. The actual minimum value is a function of patch load length and differs between these imperfections. For example, for patch load lengths $s_s/h_w \leq 0.15$, the lowest carrying capacity is for experimentally measured geometric imperfection B1 (those minimal values are very similar to those of some other experimentally measured imperfections and the first buckling mode-affine imperfections). In contrast, for applied load lengths $s_s/h_w \geq 0.20$, the minimum ultimate load is for the second buckling mode-affine geometric imperfection. The same conclusion that the lowest patch loading resistance was computed for the second buckling mode shape for $s_s/h_w \geq 0.20$ was also found for the $\alpha = 1$ case (Table 5.3) and in Ref. [88] for a constant patch load length ($s_s/h_w = 0.30$) and $\alpha = 1.50$.

On the other hand, the lowest ultimate strength of longitudinally stiffened steel plate girders ($\gamma_s = 21.67$) was obtained for experimentally measured geometric imperfection B1 and third buckling mode-affine imperfections ($s_s/h_w \leq 0.25$), and the second buckling mode-affine imperfections ($s_s/h_w \geq 0.30$). These findings agree with the $\alpha = 1$ case (Table 5.4), in which the transition patch load length that changed the unfavorable geometric imperfection from the third to the second buckling mode-affine imperfection was at $s_s/h_w = 0.40$ (cf. Fig. 5.37b). This transition in the unfavorable geometric imperfection from the third to the second buckling mode-affine imperfection is a direct consequence of the buckling pattern change (as shown in Fig. 5.8 and Fig. 5.9). For the $\gamma_s = 103.46$ case, the lowest ultimate loads were evaluated for the third buckling mode-affine ($s_s/h_w \leq 0.10$) or for experimentally measured geometric imperfection B1 for patch load lengths $s_s/h_w \geq 0.15$ (those minimal values are very close to those of some other experimentally measured imperfections, cosine hand-defined, and first

buckling mode-affine imperfections). Similarly, the authors in Ref. [40] showed that the lowest ultimate strength of longitudinally stiffened steel plate girders under a constant patch load length ($s_s/h_w = 0.04$) was determined for the third buckling mode-affine imperfection with imperfection amplitudes $w_0 \leq h_w/100$ and positions of the longitudinal stiffener $b_1/h_w \leq 0.25$.

The findings above demonstrate that unfavorable geometric imperfections are dependent on patch load length – that is, a specific geometric imperfection can yield the lowest patch loading resistance for a particular patch load length range, which does not need to hold for other patch load lengths. In addition, as explained later in this section, unfavorable geometric imperfections are also dependent on the relative stiffness of the longitudinal stiffener, meaning that different geometric imperfection shapes can lead to the lowest patch loading resistance for different relative stiffnesses. Based on the discussion above, the lowest ultimate strengths given in this study were obtained for the buckling mode-affine or experimentally measured geometric imperfection B1. For further discussion in this section and to provide more general conclusions, two cases are considered. The first case is for a relatively small patch load length, $s_s/h_w = 0.10$, and the second one is for a relatively long load length, $s_s/h_w = 0.30$. For the former, the unfavorable geometric imperfection is experimentally measured geometric imperfection B1 (for unstiffened and stiffened steel plate girders $\gamma_s = 21.67$) and the third buckling mode-affine imperfection (for stiffened steel plate girders $\gamma_s = 103.46$). For the second case ($s_s/h_w = 0.30$), the unfavorable geometric imperfection is the second buckling mode-affine imperfection (for unstiffened and stiffened steel plate girders $\gamma_s = 21.67$) and experimentally measured geometric imperfection B1. The buckling mode affine-imperfections are given in Fig. 5.6–Fig. 5.9, while experimentally measured geometric imperfection B1 is presented in Fig. 6.1.

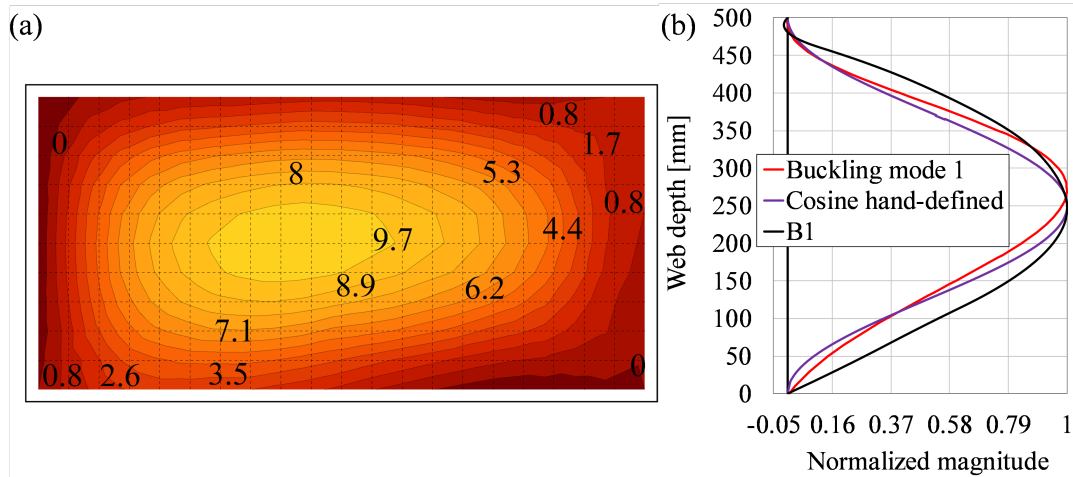


Figure 6.1: (a) Contour plot of experimentally measured geometric imperfection B1. (b) Center line cross-section of the first buckling mode-affine (unstiffened girders), cosine hand-defined, and experimentally measured geometric imperfection B1.

Center line cross-sections of the first three buckling mode-affine imperfections, along with corresponding failure modes at collapse for both cases considered ($s_s/h_w = 0.10$ and $s_s/h_w = 0.30$), are provided in Fig. 6.2 and Fig. 6.3. For the sake of brevity, out-of-plane displacements and failure mechanisms for longitudinally unstiffened and stiffened steel plate

girders at ultimate load level for both cases considered ($s_s/h_w = 0.10$ and $s_s/h_w = 0.30$), obtained only using the first buckling mode-affine geometric imperfections, are given in Fig. 6.4 and Fig. 6.5. As can be observed, the first buckling mode shape of longitudinally unstiffened and stiffened steel plate girders subjected to patch loading resembled a C-shaped initial deformation (one global buckle along the girder depth), as shown in Fig. 6.2 and Fig. 6.3. The shape and position of the maximum amplitude of this buckling mode shape were very similar for both longitudinally unstiffened and stiffened steel plate girders (the maximum amplitude is pronounced in the lower part of the web). An S-shaped deformation (one local buckle in the upper web sub-panel and an opposite buckle in the lower web sub-panel) was returned at collapse (local failure mode) for both longitudinally unstiffened and stiffened steel plate girders for $\gamma_s = 21.67$ and $\gamma_s = 103.46$, as shown in Fig. 6.2 and Fig. 6.4 for loading lengths $s_s/h_w = 0.10$. The failure mechanism was located in the upper part of the web panel (longitudinally unstiffened steel plate girders), and between the loaded flange and longitudinal stiffener for stiffened ones, Fig. 6.4. Similar out-of-plane displacements were computed for all three girders in Fig. 6.4 and with similar values for these displacements in the upper part of the web panel; thus, small load lengths had a low impact on the patch loading resistance regardless of the longitudinal stiffener's relative stiffness. A similar S-shaped deformation at collapse was also obtained for longer patch load lengths ($s_s/h_w = 0.30$) but with less pronounced deformation in the upper web sub-panel, as shown in Fig. 6.3 and Fig. 6.5. In this case ($s_s/h_w = 0.30$), out-of-plane displacements differed for all three girders in Fig. 6.5 and they were significantly lower than in the first case $s_s/h_w = 0.10$ (cf. Fig. 6.4). Hence, using the first buckling mode-affine geometric imperfection returned an S-shaped deformation at collapse regardless of the relative stiffness for both cases ($s_s/h_w = 0.10$ and $s_s/h_w = 0.30$) but with different amount of pronounced deformation in the upper part of the web panel.

The second buckling mode of longitudinally unstiffened and stiffened steel plate girders returned an S-shaped initial deformation, as shown in Fig. 5.7, Fig. 6.2, and Fig 6.3. However, the position and maximum amplitude of this initial deformation differed between longitudinally unstiffened and stiffened steel plate girders. For longitudinally unstiffened steel plate girders, the maximum amplitude was equally pronounced in the upper and lower part of the web panel. By contrast, the position of the maximum amplitude for longitudinally stiffened steel plate girders ($\gamma_s = 21.67$ and $\gamma_s = 103.46$) was dominant in the lower web sub-panel, whereas slight deformation was also present in the upper web sub-panel and at the longitudinal stiffener position. Fig. 6.2 and Fig. 6.3 show similar failure shapes at collapse were returned with pronounced deformations at the longitudinal stiffener position and in the upper web sub-panel.

As can be observed considering the third buckling mode shape of longitudinally unstiffened and stiffened steel plate girders (cf. Fig. 5.8 and Fig. 5.9), the shape and position of the maximum amplitude for this geometric imperfection were very different between longitudinally unstiffened and stiffened plate girders. Asymmetric buckling mode shapes were obtained for longitudinally unstiffened steel plate girders (for all load lengths $s_s/h_w \leq 0.50$) with no deformation directly below the applied load. Therefore, the highest ultimate strengths

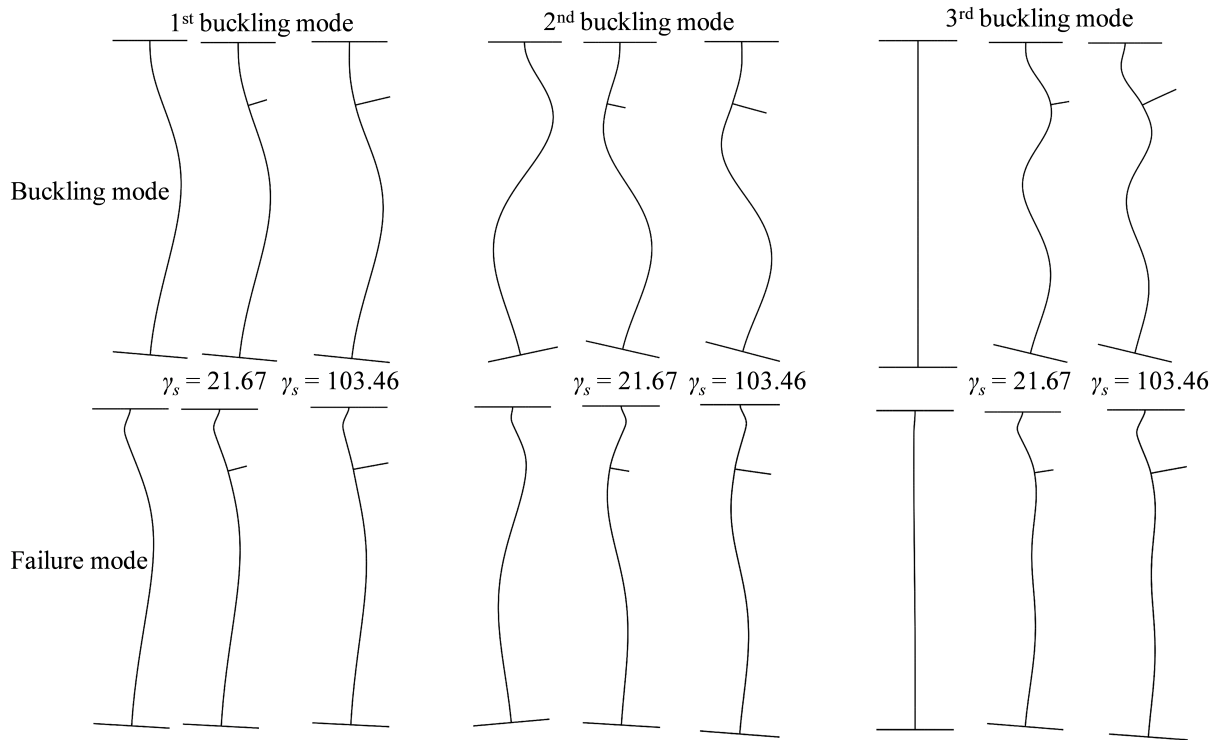


Figure 6.2: Center line cross-section of the first three buckling mode-affine geometric imperfections (magnified 50 times) and corresponding failure modes at collapse (magnified 5 times) for longitudinally unstiffened and stiffened steel plate girders for $s_s/h_w = 0.10$.

of longitudinally unstiffened steel plate girders were determined by juxtaposing all the geometric imperfections considered (except for some extreme values for experimentally measured imperfections for patch load lengths $s_s/h_w = 0.30$ and $s_s/h_w = 0.40$); see Table 5.5. A similar observation was noted in Ref. [88] for a constant patch load length ($s_s/h_w = 0.30$) and for $\alpha = 0.90, 1.50, \text{ and } 5.00$, and thus, the highest patch loading resistances were obtained. For longitudinally stiffened steel plate girders ($\gamma_s = 21.67$ and $\gamma_s = 103.46$) and small patch load lengths $s_s/h_w = 0.10$, a significant, pronounced initial deformation was dominant in the upper web sub-panel and at the stiffener position, as shown in Fig. 5.8 and Fig. 6.2. By contrast, for $s_s/h_w = 0.30$, asymmetric mode shapes were returned with no deformation directly below the applied load (Fig. 5.9 and Fig. 6.3), which in turn, produced noticeably higher ultimate strengths of longitudinally stiffened steel plate girders; see Table 5.6 and Table 5.7.

The following conclusions could be drawn by examining the failure mode shapes at collapse for $s_s/h_w = 0.10$ (cf. Fig. 6.2). All failure mode shapes in Fig. 6.2 showed pronounced deformation directly below the loaded flange in the upper web sub-panel or at the stiffener location (except for the asymmetrical third buckling mode of longitudinally unstiffened steel plate girders), although geometric imperfections were different. The only buckling mode shape that had pronounced deformation directly under the loaded flange was the third buckling mode shape of longitudinally stiffened steel plate girders ($\gamma_s = 103.46$). Indeed, the lowest patch loading resistances were determined for these steel plate girders using the third buckling mode-affine imperfections for the case $s_s/h_w = 0.10$. The buckling mode shapes of longitudinally

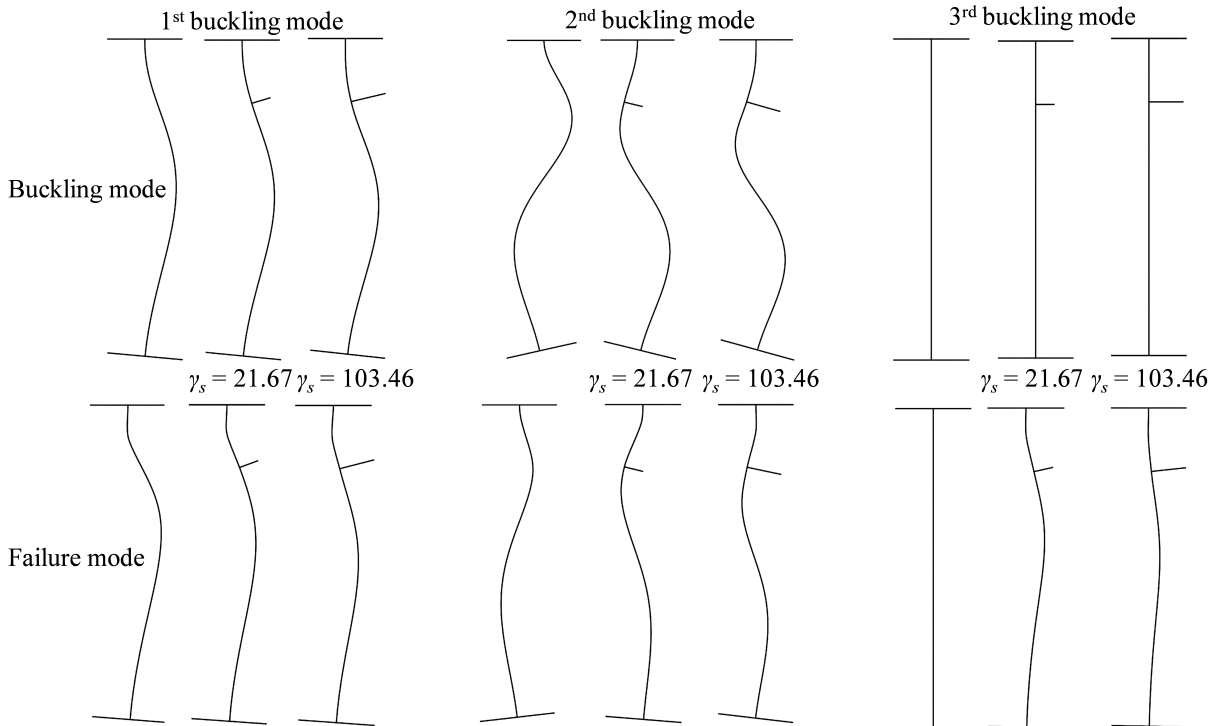


Figure 6.3: Center line cross section of the first three buckling mode-affine geometric imperfections (magnified 50 times) and corresponding failure modes at collapse (magnified 5 times) for longitudinally unstiffened and stiffened steel plate girders for $s_s/h_w = 0.30$.

unstiffened and stiffened steel plate girders ($\gamma_s = 21.67$) did not show pronounced deformation close to the loaded flange. It can be seen in Fig. 6.1(b) that experimentally measured geometric imperfection B1 was very similar to the first buckling mode shape. However, imperfection shape B1 had a small deformation very close to the loaded flange compared to the first buckling mode shape, and thus, the lowest ultimate strengths were obtained for this geometric imperfection for both longitudinally unstiffened and stiffened steel plate girders, $\gamma_s = 21.67$ for $s_s/h_w = 0.10$.

Similar conclusions can be drawn from the failure mode shapes in Fig. 6.3 for longer patch load length $s_s/h_w = 0.30$. Again, very similar failure mode shapes were returned for both longitudinally unstiffened and stiffened steel plate girders (apart from the third buckling mode-affine imperfections – asymmetric buckling mode), although initial geometric imperfections were different. The second buckling mode shape of longitudinally unstiffened steel plate girders resembled the failure mode at collapse, and hence, the lowest ultimate strengths were determined for this geometric imperfection. The same observation was noted for longitudinally stiffened steel plate girders ($\gamma_s = 21.67$) since the longitudinal stiffener was relatively weak. For the much stronger longitudinal stiffener ($\gamma_s = 103.46$), the first three buckling mode shapes did not resemble the failure mode at collapse (the closest one was the first buckling mode shape), as shown in Fig. 6.3. In this case, for $\gamma_s = 103.46$, the failure mode at collapse showed small deformations below the loaded flange and at the stiffener position, while for $\gamma_s = 21.67$, a significantly larger deformation formed at the stiffener position (weak stiffener). The failure mode at collapse is governed by the relative stiffness of the longitudinal stiffener, γ_s , which in turn

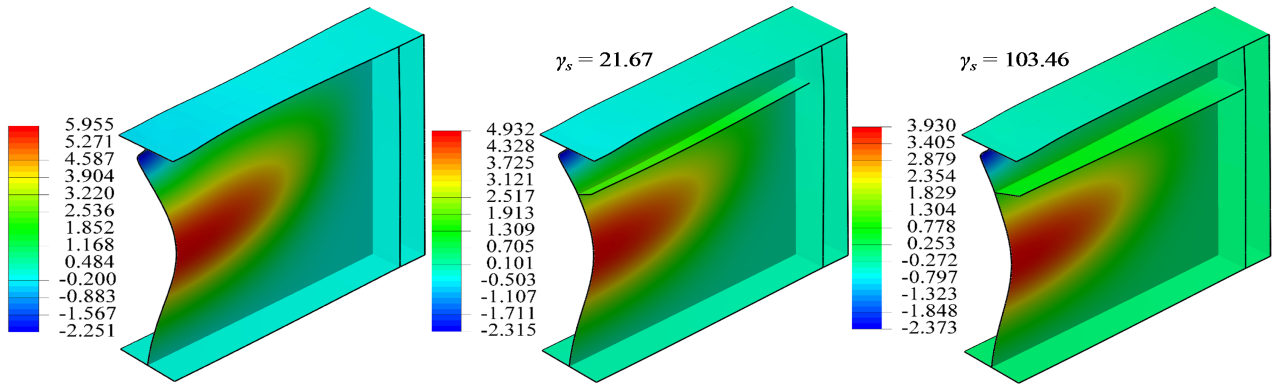


Figure 6.4: Out-of-plane displacement (units are in mm) and failure mechanism for longitudinally unstiffened and stiffened steel plate girders at ultimate load level for $s_s/h_w = 0.10$. The first buckling mode-affine geometric imperfections are employed. Deformation is magnified ten times.

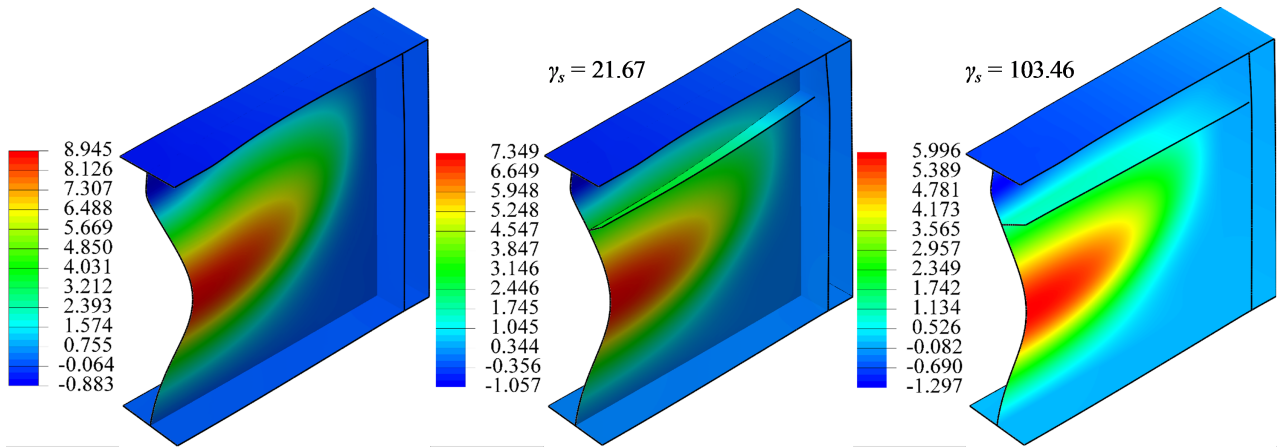


Figure 6.5: Out-of-plane displacement (units are in mm) and failure mechanism for longitudinally unstiffened and stiffened steel plate girders at ultimate load level for $s_s/h_w = 0.30$. The first buckling mode-affine geometric imperfections are employed. Deformation is magnified ten times.

requires a different initial geometric imperfection shape to resemble the failure mode shape. In this case, $\gamma_s = 103.46$, the lowest carrying capacities were computed for experimentally measured geometric imperfection B1, which indeed showed a small deformation close to the loaded flange, as shown in Fig. 6.1(b).

The conclusions above demonstrate that the process of defining unfavorable geometric imperfections in steel plate girders subjected to patch loading is governed by the patch load length and the relative stiffness of the longitudinal stiffener. One can determine different unfavorable geometric imperfections for different values of the patch load length and the longitudinal stiffener's relative stiffness (under a constant imperfection amplitude). The current study shows that the lowest patch loading resistances were returned for geometric imperfections that resembled the deformation at collapse. The concept of collapse-affine geometric imperfections seems impractical for design purposes since a geometrically and materially nonlinear analysis must be conducted before collapse-affine geometric imperfection shapes are determined. However, to be safe, designers can employ this concept of collapse-affine geometric imperfections

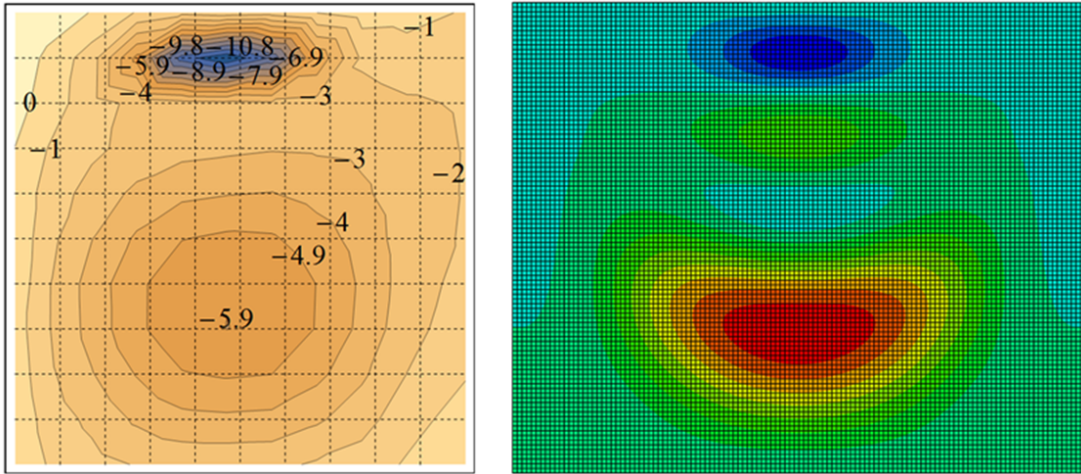


Figure 6.6: Deformed shape at collapse for girder A5 [21] (left) and third buckling mode (right). Units are in mm.

instead of buckling mode-affine geometric imperfections (as recommended in [65]), as these collapse-affine geometric imperfections lead to lower ultimate strengths than those given by buckling modes [99,103]. Indeed, this finding was also observed experimentally in Ref. [21] for longitudinally stiffened girders of Series A ($\alpha = 1$). Fig. 6.6 shows that the deformation at collapse corresponded to the third buckling mode (geometric imperfection shape for which the lowest ultimate strength of longitudinally stiffened girders was computed for $s_s/h_w \leq 0.40$, Fig. 5.37(b)).

The above-presented results and discussions are available in sequentially published papers [82–86].

6.3 Summary

Unfavorable geometric imperfections in steel plate girders subjected to patch loading are governed by the patch load length and the relative stiffness of the longitudinal stiffener. For different values of the patch load length and the relative stiffness of the longitudinal stiffener (under a constant imperfection amplitude), one can identify different unfavorable geometric imperfections. As shown in this Chapter, the lowest patch load resistances were returned for geometric imperfections that resembled the deformation at collapse. The concept of collapse-affine geometric imperfections seems impractical for design purposes since a geometrically and materially nonlinear analysis must be conducted before collapse-affine geometric imperfection shapes are determined. However, for safety, designers can employ this concept of collapse-affine geometric imperfections instead of buckling mode-affine geometric imperfections (as recommended in EN 1993-1-5). In order to simplify the applicability of the collapse-affine imperfection concept, further research should focus on finding an *equivalent shape* that resembles the deformation at failure for different patch load lengths and girder characteristics, such as the relative stiffness of the longitudinal stiffener, web slenderness, et cetera.

Finally, regarding longitudinally unstiffened and stiffened steel plate girders subjected to patch loading, the following conclusions could be drawn for practical and design purposes. Regardless of the longitudinal stiffener relative stiffness and for small patch load lengths, such as $s_s/h_w \leq 0.10$, geometric imperfections that have pronounced deformations directly under the loaded flange lead to lower load resistances. These local geometric imperfections in the upper web sub-panel yield lower ultimate strengths than those defined over the whole web depth (global geometric imperfections). This conclusion was also found to be valid for longitudinally stiffened steel plate girders reinforced by relatively strong longitudinal stiffeners and longer patch load lengths, such as $s_s/h_w = 0.30$. For longitudinally stiffened steel plate girders reinforced by relatively weak longitudinal stiffeners and under longer patch load lengths ($s_s/h_w = 0.30$), geometric imperfections defined in the upper web sub-panel and at the stiffener location (combined geometric imperfections) lead to lower ultimate strengths than global geometric imperfections.

Chapter 7

Conclusions and future work

The present experimental and finite element parametric studies were designed to determine the influence of patch load length, in combination with various geometric imperfections, on the behavior and ultimate capacity of longitudinally unstiffened and stiffened I-shaped steel plate girders. Details about the experiment, results, and observed behavior of the tested girders are presented. Experimentally measured, buckling mode-affine, and hand-defined sinusoidal geometric imperfections were varied in the numerical study in combination with varying patch load lengths and relative stiffnesses of the longitudinal stiffener.

The main findings regarding the ultimate strength from the experimental investigation can be summarized as follows:

- The carrying capacity of longitudinally unstiffened and stiffened steel plate girders increased with increasing patch load length. The ultimate strength of longitudinally unstiffened girders increased linearly with respect to the patch load length, whereas the ultimate load of longitudinally stiffened girders followed this same trend only for small patch load lengths ($50 \text{ mm} < s_s < 100 \text{ mm}$). After a specific patch load length (threshold), the patch loading resistance increased much faster with increasing patch load length and appreciable strengthening effects were obtained.
- The patch loading resistance of longitudinally unstiffened and stiffened steel plate girders can be significantly increased by using longer patch load lengths. By increasing the patch load length from 0 mm to 250 mm, the patch loading resistance was increased $> 50\%$ and 90% for longitudinally unstiffened and stiffened girders, respectively.
- An appreciable increase in ultimate strength can be achieved using longitudinal stiffening. This analysis showed that the ultimate load could be increased $> 40\%$ by using longitudinal stiffening and longer patch load lengths compared to unstiffened girders.
- Increasing the web panel aspect ratio (more specifically, the web panel width) decreased the ultimate strength of longitudinally unstiffened and stiffened girders. The effect of this ratio was more pronounced for longitudinally unstiffened girders; this finding is not

airtight since it was obtained considering a limited number of experimental tests and is further studied in Chapter 5.

- The current European design standard EN 1993-1-5 predicts lower ultimate strengths for longitudinally unstiffened and stiffened steel plate girders than the experimentally obtained results in this study. The maximum difference between these two analyses is 64% and 97% for longitudinally unstiffened ($s_s = 200$ mm) and stiffened steel plate girders ($s_s = 250$ mm), respectively. Based on the resistance model in EN 1993-1-5, the patch loading resistance increases linearly with an increase in patch load length (independently of the value of patch load length) for both longitudinally unstiffened and stiffened steel plate girders. This experimental investigation showed that after a specific patch load length (e.g., $s_s \geq 100$ mm), the ultimate strength of longitudinally stiffened steel plate girders increases much faster with increasing patch load length. Thus, the design standard does not well capture those ultimate strengths for longer patch load lengths.

Several key points were identified regarding the patch load length from imperfection sensitivity analysis:

- The ultimate strength of longitudinally unstiffened and stiffened steel plate girders increases as the patch load length increases. This was shown to be valid for all the geometric imperfections considered.
- For very small patch load lengths (e.g., $s_s/h_w < 0.15$), the ultimate strength of longitudinally stiffened steel plate girders follows the ultimate load of unstiffened ones regardless of the relative stiffness of the longitudinal stiffener and the geometric imperfection; hence, the strengthening effect is very small (less than 10%). On the other hand, for longer patch load lengths (e.g., $s_s/h_w = 0.50$), different substantial strengthening effects can be achieved for different geometric imperfections.
- An increase in the web panel aspect ratio decreased the patch loading resistance of longitudinally unstiffened steel plate girders for all the patch load lengths considered, $s_s/h_w \leq 0.50$. This is especially pronounced for longer patch load lengths (e.g., $s_s/h_w = 0.50$), whereas for $s_s/h_w \leq 0.15$, the effect of the web panel aspect ratio can be ignored. For longitudinally stiffened steel plate girders, the effect of the web panel aspect ratio is minimal for $s_s/h_w \leq 0.15$, while a notable decrease in the ultimate strength was achieved for $s_s/h_w = 0.50$. The level of reduction in the ultimate load of longitudinally unstiffened and stiffened steel plate girders varied depending on imperfection shape and the patch load length. The reduction depended mostly on patch load length.
- An increase in relative stiffness γ_s (from relatively weak to relatively strong longitudinal stiffeners) has a very small effect on the ultimate strength of longitudinally stiffened steel plate girders for patch load lengths $s_s/h_w \leq 0.30$ and all the geometric imperfections considered. In contrast, a noticeable increase in patch loading resistance was obtained

for patch load lengths $s_s/h_w \geq 0.40$. Increasing the longitudinal stiffener relative stiffness (from the patch loading point of view) is justified only for longer patch load lengths. This conclusion was derived for the longitudinal stiffener's optimum location for the flexural and shear resistance placed at one-fifth of the girder depth ($b_1 = 0.2h_w$).

- Unfavorable geometric imperfections in steel plate girders subjected to patch loading are governed by the patch load length and the relative stiffness of the longitudinal stiffener. One can identify different unfavorable geometric imperfections for different values of the patch load length and the relative stiffness of the longitudinal stiffener (under a constant imperfection amplitude). The lowest patch loading resistances were returned for geometric imperfections that resembled the deformation at collapse (collapse-affine geometric imperfections).

Based on the current research, the following design recommendations are given:

- Designers are encouraged to increase the contact surface between the loaded flange and supports (during the incremental launching of multi-span steel and composite bridges over temporary or permanent supports) or other structural elements that transfer loads onto girders. Increasing the applied load length leads to higher ultimate strengths. The patch loading resistance can also be increased using longitudinal stiffening and decreasing the distance between vertical stiffeners (girder width).
- Regardless of the longitudinal stiffener relative stiffness and for small patch load lengths, geometric imperfections that have pronounced deformations directly under the loaded flange lead to lower load resistances. These local geometric imperfections in the upper web sub-panel yield lower ultimate strengths than those defined over the whole web depth (global geometric imperfections), and thus, they should be avoided. For longitudinally stiffened steel plate girders reinforced by relatively weak longitudinal stiffeners and under longer patch load lengths, geometric imperfections defined in the upper web sub-panel and at the stiffener location (combined geometric imperfections) lead to lower ultimate strengths than global geometric imperfections.
- Collapse-affine geometric imperfections are recommended for the use of finite element analysis for the ultimate limit state since they return lower ultimate strengths than buckling mode-affine imperfections.

The main contributions from this dissertation are as follow:

- New experimental results that disclose the influence of patch load length on the patch loading resistance are performed.
- The present experimental investigation confirmed that the ultimate capacity of longitudinally stiffened steel plate girders follows the ultimate load of unstiffened ones for

small patch load lengths, while for longer patch load lengths it increases much faster with increasing patch load length. This conclusion was first reported in the experimental study [21]. For the first time (to the best of the author's knowledge), this conclusion was also confirmed numerically for a broader range of patch load lengths, various geometric imperfections, and relative stiffnesses of the longitudinal stiffener.

- Behavior and patch loading resistance are modeled employing the finite element method. The current numerical model is verified by comparison with twenty-eight experimental tests. The numerical and experimental data is in good agreement. The usual practice in the literature is to validate numerical models with several experimental tests.
- Extensive finite element parametric study that consists of 900 simulations in which experimentally measured, buckling mode-affine, and hand-defined sinusoidal geometric imperfections were varied in combination with varying patch load lengths and relative stiffnesses of the longitudinal stiffener are included.
- Studies with experimentally measured geometric imperfections are scarce. In this dissertation, twenty-eight different experimentally measured imperfections are considered.
- Information on geometric imperfections for numerical modeling and their incorporation into numerical models is presented.
- Design recommendations for patch load length, geometric imperfections, and unfavorable geometric imperfection shapes (from the patch loading point of view) are given.

The following recommendations for future work could be drawn from the current research:

- Additional experimental and numerical investigations, including different geometric parameters and material properties combined with various patch load lengths, are required to understand the patch loading phenomenon further. These studies can determine the threshold – that is, the patch load length after which the ultimate strength of longitudinally stiffened steel plate girders increases much faster with increasing patch load length.
- The web panel yield stress, f_{yw} , influenced the ultimate strength with a power of 0.60–0.78 ($f_{yw}^{(0.60-0.78)}$), and more importantly, this value is dependent on patch load length. The current design standard EN 1993-1-5 uses a power of 0.50 – that is, $f_{yw}^{0.5}$, and it is independent of patch load length. So further studies could be directed in this direction to improve the resistance model in EN 1993-1-5.
- It was observed in the current research that material effects – that is, f_{yw} , are more dominant for very small patch load lengths than geometric effects (imperfection shape and amplitude). In contrast, geometric effects are dominant for longer patch load lengths. The design standard EN 1993-1-5 provides four different models for the material behavior.

However, in this dissertation, only true stress-strain relationships based on experimental testing were used. Hence, parametric studies considering all four material models in combination with various patch load lengths and geometric imperfections could be performed to prove these observations.

- In order to simplify the applicability of the collapse-affine imperfection concept, further research should focus on finding an *equivalent shape* that resembles the deformation at failure for different patch load lengths and girder characteristics, such as the relative stiffness of the longitudinal stiffener, web slenderness, et cetera.

References

- [1] K. Rockey, A. Bergfelt, L. Larsson, Behaviour of Longitudinally Reinforced Plate Girders when Subjected to in Plane Patch Loading, vol 19, Chalmers University of Technology, Division of Steel and Timber Structures, Publication S78, Göteborg, 1978.
- [2] A. Bergfelt, Patch Loading on a Slender Web. Influence of Horizontal and Vertical Web Stiffeners on the Load Carrying Capacity, vol 1, Department of Structural Engineering, Chalmers University of Technology, Publication S79, Göteborg, 1979.
- [3] A. Bergfelt, Girder Web Stiffening for Patch Loading, Department of Structural Engineering, Chalmers University of Technology, Publication S83:1, Göteborg, 1983.
- [4] T. Roberts, Stocky and Stiffened Plate Girders Subjected to Edge Loading, Department of Civil and Structural Engineering, University College Cardiff, Cardiff, 1981.
- [5] N. Markovic, N. Hajdin, A contribution to the analysis of the behaviour of plate girders subjected to patch loading, J. Constr. Steel Res. 21 (1992) 163-173.
- [6] J. Oxfort, Versuche zum Beul- und Krüppelverhalten von unversteiften Trägerstegblechen unter zentrischen und exzentrischen Einzellasten auf dem Obergurt, Stahlbau 52 (1983) 309-312.
- [7] S. Shimizu, S. Yoshida and H. Okuhara, An experimental study on patch-loaded web plates, Proceedings of the ECCS Colloquium on Stability of Plate and Shell Structures, Ghent University, 1987.
- [8] S. Shimizu, H. Yabana, S. Yoshida, A new collapse model for patch-loaded web plates, J. Constr. Steel Res. 13 (1989) 61-73.
- [9] Y. Galea, B. Godart, I. Radouant and J. Raoul, Test of buckling of panels subject to in-plane patch loading, Proceedings of the ECCS Colloquium on Stability of Plate and Shell Structure, Ghent University, 1987.
- [10] I. Karnikova, P. Novak, M. Skaloud, Ultimate load behaviour of longitudinally stiffened steel webs subjected to partial edge loading, Staveb. Čas. VEDA 27 (10) (1979) 752-755.
- [11] I. Karnikova, P. Novak, M. Skaloud, Ultimate load of longitudinally stiffened steel webs subjected to partial edge loading, Staveb. Čas. VEDA 29 č.11/12 (1981) 879-888.
- [12] M. Skaloud, I. Karnikova, Experimental research on the limit state of the plate elements of steel bridges, Rozpravy Československe Akademie VED, RADA Technických VED 95 (1) (1985) 1-141.
- [13] I. Karnikova, M. Skaloud, K. Janus, Effect of longitudinal stiffening on the ultimate strength of thin webs under patch loading, Second Reg. Coll. on Stab. of Steel Struct., Proc. II 1986,

83–89 , Hungary.

- [14] I. Karnikova, M. Skaloud, Experimental research on the ultimate load behaviour of steel plated structures, *Steel Struct., Proc. Intern. Conf., Part I*, 1986, Budva.
- [15] K. Janus, I. Karnikova, M. Skaloud, Experimental investigation into the ultimate load behaviour of longitudinally stiffened steel webs under partial edge loading, *Acta Tech. ČSAV (Czech. Sci. Adv. Views) (2)* (1988) 158-195.
- [16] P. Dubas, H. Tschamper, Stabilité des âmes soumises a une charge concentree et a une flexion globale, *Constr. Metallique 2* (1990) 25-39.
- [17] M. Dogaki, M. Murata, Y. Nishijima, T. Okumura and H. Yonezawa, Ultimate strength of plate girders with longitudinal stiffener under patch loading, *Technology Reports of Kansai University 33* (1991) 121-132.
- [18] R. Salkar, Strength and behavior of webs, with and without stiffeners under local compressive in-plane and eccentric loads (Volumes I and II), Doctoral thesis, University of Maine, USA, 1992.
- [19] A. Carretero, J. Lebet, Introduction des forces concentrees dans les poutres elancees, *Constr. Metallique 1* (1998) 5-18.
- [20] S. Walbridge, J. Lebet, Patch Loading Tests of Bridge Girders with Longitudinal Web Stiffeners, Publication No. 447. Ecole Polytechnique Federale de Lausanne, Lausanne, 2001.
- [21] N. Markovic, Buckling of plate girders under the action of patch loading, Doctoral thesis (in Serbian), University of Belgrade, Serbia, 2003.
- [22] U. Kuhlmann, M. Seitz, Longitudinally stiffened girder webs subjected to patch loading, *Proceedings of Steel Bridge-An International Symposium on Steel Bridge, Millau, France June, 2004* pp. 011/1-011/14.
- [23] M. Seitz, Tragverhalten längsversteifter Blechträger unter quergerichteter Krafteinleitung, Doctoral thesis Institut für Konstruktion und Entwurf der Universität Stuttgart, Stuttgart, 2005.
- [24] S. Kovacevic, N. Markovic, Experimental study on the influence of patch load length on steel plate girders, *Thin-Walled Struct.* 151 (2020) 106733.
- [25] N. Markovic, S. Kovacevic, Influence of patch load length on plate girders. Part I: Experimental research, *J. Constr. Steel Res.* 157 (2019) 207-228.
- [26] L. Davaine, Formulation De La Résistance Au Lancement D'une Âme Métallique De Pont Raidie Longitudinalement, Doctoral thesis (in French) INSA, Rennes, France, 2005.
- [27] R. Chacon, E. Mirambell, E. Real, Transversally stiffened plate girders subjected to patch loading. Part 1. Preliminary study, *J. Constr. Steel Res.* 80 (2013) 483–491.
- [28] C. Graciano, B. Johansson, Resistance of longitudinally stiffened I-girders subjected to concentrated loads, *J. Constr. Steel Res.* 59 (2003) 561–586.
- [29] N. Hajdin, N. Markovic, Failure mechanism for longitudinally stiffened I girders subjected to patch loading, *Arch. Appl. Mech.* 82 (2012) 1377–1391.
- [30] C. Graciano, B. Edlund, Failure mechanism of slender girder webs with a longitudinal stiffener under patch loading, *J. Constr. Steel Res.* 59 (2003) 27–45.

- [31] C. Graciano, Strength of longitudinally stiffened webs subjected to concentrated loading, *J. Struct. Eng. ASCE* 131 (2) (2005) 268–278.
- [32] C. Graciano, Resistance of longitudinally stiffened webs under concentrated loading, XVIII Jornadas Estructurales de la Ingeniería De Colombia y VI Jornadas de Estructuras Metálicas September, 2009, 1–13 , Bogotá, Colombia.
- [33] M. Clarin, Plate buckling resistance. Patch loading of longitudinally stiffened webs and local buckling, Doctoral thesis. 2007:31 Department of Civil and Mining Engineering. Division of Structural Engineering-Steel Structures, Luleå University of Technology, Luleå, Sweden, 2007.
- [34] N. Loaiza, C. Graciano, E. Casanova, Design recommendations for patch loading resistance of longitudinally stiffened I-girders, *Eng. Struct.* 171 (2018) 747–758.
- [35] N. Loaiza, Effect of Longitudinal Stiffening on the Ultimate Resistance of Plate Girders Subjected to Patch Loading, Universidad Nacional de Colombia, Colombia, 2019 (Doctoral thesis).
- [36] Q. Hasan, W.W. Badaruzzaman, A.W. Al-Zand, A.A. Mutalib, The state of the art of steel and steel concrete composite straight plate girder bridges, *Thin-Walled Struct.* 119 (2017) 988–1020.
- [37] C.D. Tetougueni, E. Maiorana, P. Zampieri, C. Pellegrino, Plate girders behaviour under in-plane loading: a review, *Eng. Fail. Anal.* 95 (2019) 332–358.
- [38] C. Graciano, Longitudinally stiffened steel plate girder webs under patch loading, Department of Structural Engineering. Steel and Timber Structures, Chalmers University of Technology, Göteborg, Sweden, 2001.
- [39] J. Martínez, C. Graciano, E. Casanova, Imperfection sensitivity of plate girder webs under patch loading, the third international conference on structural engineering, Mechanics and Computation (SEMC) September, 2007, pp. 958–963 , (Cape Town, South Africa).
- [40] C. Graciano, E. Casanova, J. Martinez, Imperfection sensitivity of plate girder webs subjected to patch loading, *J. Constr. Steel Res.* 67 (2011) 1128–1133.
- [41] C. Graciano, B. Edlund, Longitudinally stiffened girder webs under patch loading, Proceedings of the International Conference on Steel Structures of the 2000’s September 2000, pp. 227–232 , (Istanbul, Turkey).
- [42] C. Graciano, B. Edlund, Nonlinear FE analysis of longitudinally stiffened girder webs under patch loading, *J. Constr. Steel Res.* 58 (2002) 1231–1245.
- [43] J. Martínez, Influencia de imperfecciones geométricas en la capacidad de carga de vigas esbeltas de perfil I, Universidad Simón Bolívar, 2008 (MSc thesis).
- [44] R. Chacon, E. Bock, E. Real, Longitudinally stiffened hybrid steel plate girders subjected to patch loading, *J. Constr. Steel Res.* 67 (2011) 1310–1324.
- [45] R. Chacon, M. Bock, E. Mirambell, E. Real, Hybrid steel plate girders subjected to patch loading, *Steel Constr.* 5 (2012) 3–9.
- [46] C. Graciano, J.Mendes, Elastic buckling of longitudinally stiffened patch loaded plate girders using factorial design, *J. Constr. Steel Res.* 100 (2014) 229–236.
- [47] C. Graciano, N. Loaiza, R. Chacon, Análisis lineal de pandeo de una viga esbelta rigidizada

- longitudinalmente y sometida a carga concentrada, Memorias del Congreso Internacional de Métodos Numéricos en Ingeniería y Ciencias Aplicadas (CIMENICS) July 2016, pp. 209–217, (Caracas, Venezuela).
- [48] N. Loaiza, C. Graciano, R. Chacon, Análisis de autovalores de vigas esbeltas con rigidización múltiple sujetas a cargas concentradas, Memorias del Congreso Internacional de Métodos Numéricos en Ingeniería y Ciencias Aplicadas (CIMENICS) July 2016, pp. 219–227, (Caracas, Venezuela).
- [49] N. Loaiza, C. Graciano, R. Chacon, E. Casanova, Influence of bearing length on the patch loading resistance of multiple longitudinally stiffened webs, 8th European Conference on Steel and Composite Structures (Eurosteel 2017) September 2017, pp. 4199–4204, (Copenhagen, Denmark).
- [50] O. Mezghanni, J. Averseng, A. Bouchaïr, H. Smaoui, Behavior of beam web panel under opposite patch loading, *J. Constr. Steel Res.* 83 (2013) 51–61.
- [51] U. Kuhlmann, M. Seitz, Behavior of longitudinally stiffened girder webs subjected to patch loading, 3rd European Conference on Steel Structures (Eurosteel 2002) September 2002, pp. 581–590, (Coimbra, Portugal).
- [52] E. Maiorana, C. Pellegrino, C. Modena, Imperfections in steel girder webs with and without perforations under patch loading, *J. Constr. Steel Res.* 65 (2009) 1121–1129.
- [53] L. Davaine, J. Raoul, J.M. Aribert, Patch load resistance of longitudinally stiffened bridge girders, Proceedings of Steel Bridge-An International Symposium on Steel Bridge June 2004, pp. 1–16, (Millau, France).
- [54] L. Davaine, J. Aribert, Résistance d’une âme de poutre de pont raidie longitudinalement lors du lancement, *Constr. Métallique* 3 (2005) 3–22.
- [55] L. Davaine, J.M. Aribert, Launching of steel girder bridge. Patch loading resistance of longitudinally stiffened webs, 4th European Conference on Steel and Composite Structures. Research-Eurocodes-Practice. Proceedings Volume A June 2005, pp. 1.4–143/150, (Maastricht, Netherlands).
- [56] B. Kövesdi, Patch loading resistance of slender plate girders with longitudinal stiffeners, *J. Constr. Steel Res.* 140 (2018) 237–246.
- [57] M. Dogaki, Y. Nishijima, H. Yonezawa, Nonlinear behaviour of longitudinally stiffened webs in combined patch loading and bending, *Constructional Steel Design, World Developments. Proceedings of the First World Conference on Constructional Steel Design* December 1992, pp. 141–150, (Acapulco, Mexico).
- [58] M. Dogaki, H. Yonezawa, T. Tanabe, Ultimate strength of plate girders with longitudinal stiffener under patch loading, Proceedings of the 3rd Pacific Structural Steel Conference October 1992, pp. 507–514, (Tokyo, Japan).
- [59] R. White, W. Cottingham, Stability of plates under partial edge loadings, *J. Eng. Mech. Div. Proc. Am. Soc. Civil Eng.* 88 (1962) 67–86.
- [60] S. Shimizu, S. Horii, S. Yoshida, The collapse mechanisms of patch loaded web plates, *J. Constr. Steel Res.* 14 (1989) 321–337.
- [61] S. Shimizu, S. Horii, S. Yoshida, Behaviour of stiffened web plates subjected to the patch

- load, Proceedings of the IUTAM Symposium on Contact Loading and Local Effects in Thin Walled Plated and Shell Structures September 1990, pp. 184–191, (Prague, Czech Republic).
- [62] T.R. Graves Smith, J.T. Gierlinski, Buckling of stiffened webs by local edge loads, *J. Struct. Div. Proc. Am. Soc. Civ. Eng.* 108 (1982) 1357–1367.
- [63] O. Lagerqvist, Patch Loading. Resistance of Steel Girders Subjected to Concentrated Forces, Doctoral Thesis. 1994, 159D, Department of Civil and Mining Engineering, Division of Steel Structures. Luleå University of Technology, Luleå, Sweden, 1995.
- [64] C. Graciano, Patch Loading. Resistance of Longitudinally Stiffened Steel Girder Webs, Doctoral thesis. Department of Civil and Mining Engineering. Division of Steel Structures. Luleå University of Technology, Luleå, Sweden, 2002.
- [65] EN 1993-1-5:2005, Eurocode 3: Design of Steel Structures. Part 1-5, Plated Structural Elements, CEN, 2006.
- [66] C. Dubas, Contribution à l'étude du voilement des tôles raidies, Doctoral thesis (in French), Publications de l'Institut de Statique Appliquée EPFZ, Nr. 1684, ETH Zürich, 1948.
- [67] K. Rockey, D. Leggett, The buckling of a plate girder web under pure bending when reinforced by a single longitudinal stiffener, *Proc. Inst. Civ. Engs.* 21 (1962) 161–188.
- [68] P. Cooper, Bending and shear strength of longitudinally stiffened plate girders, Doctoral thesis, Fritz Laboratory Reports. Paper 1873, 1965.
- [69] D. Lucic, A contribution to the Analysis of Thin-Walled Girders, Doctoral thesis. (in Serbian) University of Belgrade, Faculty of Civil Engineering, Belgrade, 1999.
- [70] D. Lucic, Experimental research on I-girders subjected to eccentric patch loading, *J. Constr. Steel Res.* 59 (9) (2003) 1147–1157.
- [71] B. Scepanovic, I-girders Under Eccentric Local Loading-Experimental-Theoretical Analysis, Master thesis (in Serbian) University of Belgrade, Faculty of Civil Engineering, Belgrade, 2002.
- [72] B. Scepanovic, Analysis of Eccentrically Locally Loaded steel I-Girders, Doctoral thesis (in Serbian) University of Montenegro, Faculty of Civil Engineering, Podgorica, 2010.
- [73] S. Aleksic, Stability of Thin-Walled I-girders Under the Patch Loading in Web Plane, Doctoral thesis (in Serbian) University of Montenegro, Faculty of Civil Engineering, Podgorica, 2010.
- [74] M. Rogac, Theoretical and Experimental Research of Stability Problem Of Thin-Walled I-Girders Subjected to Patch Loading, Doctoral Thesis (in Serbian), University of Montenegro, Faculty of Civil Engineering, Podgorica, 2015.
- [75] T. Roberts, N. Markovic, Stocky plate girders subjected to edge loading, *Proc. Inst. Civ. Eng.* 75 (1983) 539–550. Technical Note 352. Part 2.
- [76] L. Gil-Martin, B. Scepanovic, E. Hernandez-Montes, M. Aschheim, D. Lucic, Eccentrically patch-loaded steel I-girders: the influence of patch load length on the ultimate strength, *J. Constr. Steel Res.* 66 (2010) 716–722.
- [77] S. Aleksic, M. Rogac, D. Lucic, Analysis of locally loaded steel plate girders: model for patch load resistance, *J. Constr. Steel Res.* 89 (2013) 153–164.

- [78] Hottinger Baldwin Messtechnik GmbH, Strain Gauges: First Choice for Strain Measurements, HBM.
- [79] B. Kövesdi, B.J. Mecseri, L. Dunai, Imperfection analysis on the patch loading resistance of girders with open section longitudinal stiffeners, *Thin-Walled Struct.* 123 (2018) 195-205.
- [80] Abaqus Simulia V. 6.14-5, Dassault Systemes, 2016.
- [81] E. Riks, An incremental approach to the solution of snapping and buckling problems, *Int. J. Solid Struct.* 15 (1979) 529–551.
- [82] S. Kovacevic, N. Markovic, D. Sumarac, R. Salatic, Influence of patch load length on plate girders. Part II: numerical research, *J. Constr. Steel Res.* 158 (2019) 213–229.
- [83] S. Kovacevic, N. Markovic, Influence of the length of patch load on the ultimate load of longitudinally stiffened plate girders, in: *Proceedings of the Annual Stability Conference, Structural Stability Research Council (SSRC), St. Louis, MO, USA, 2019.*
- [84] S. Kovacevic, N. Markovic, D. Sumarac, R. Salatic, Unfavorable geometric imperfections in steel plate girders subjected to localized loads, *Thin-Walled Struct.* 161 (2021) 107412.
- [85] S. Kovacevic, N. Markovic, A. Ceranic, M. Bendic, Unfavorable imperfection shapes in steel plate girders for web local crippling, in: *Proceedings of the Annual Stability Conference, Structural Stability Research Council (SSRC), Louisville, Kentucky, USA, 2021.*
- [86] S. Kovacevic, A. Ceranic, N. Markovic, M. Bendic, Patch load resistance of longitudinally stiffened steel plate girders: A parametric study, in: *9th European Conference on Steel and Composite Structures (Eurosteel 2021), Sheffield, UK, 2021.*
- [87] C. Graciano, J. Mendez, D. Zapata-Medina, Influence of the boundary conditions on FE modeling of longitudinally stiffened I-girders subjected to concentrated loads, *Rev. Fac. Ing. Univ. Antioquia* 71 (2014) 221–229.
- [88] R. Chacon, E. Mirambell, E. Real, Influence of designer-assumed initial conditions on the numerical modelling of steel plate girders subjected to patch loading, *Thin-Walled Struct.* 47 (2009) 391–402.
- [89] R. Chacon, Resistance of Transversally Stiffened Hybrid Steel Plate Girders to Concentrated Loads, *Universitat Politecnica de Catalunya Departament d’Enginyeria de la Construcio, Barcelona, 2009* Doctoral thesis.
- [90] Rhinoceros 3D, Robert McNeel & Associates, 2018.
- [91] N.H. Pham, C.H. Pham, K.J.R. Rasmussen, Incorporation of measured geometric imperfections into finite element models for cold-rolled aluminum sections, *Proceedings of the 4th Congrès International de Géotechnique-Ouvrages-Structures (CIGOS) October 2017*, pp. 161–171, (Ho Chi Minh City, Vietnam).
- [92] P. Granath, Behavior of slender plate girders subjected to patch loading, *J. Constr. Steel Res.* 42 (1997) 1–19.
- [93] R. Chacon, M. Serrat, E. Real, The influence of structural imperfections on the resistance of plate girders to patch loading, *Thin-Walled Struct.* 53 (2012) 15–25.
- [94] M.F. Hassanein, Imperfection analysis of austenitic stainless steel plate girders failing by shear, *Eng. Struct.* 32 (2010) 704–713.

- [95] C. Couto, P.V. Real, Numerical investigation on the influence of imperfections in the local buckling of thin-walled I-shaped sections, *Thin-Walled Struct.* 135 (2019) 89–108.
- [96] J. Gozzi, Patch loading resistance of plated girders. Ultimate and serviceability limit state, Department of Civil, Mining and Environmental Engineering. Division of Structural Engineering-Steel Structures, Luleå University of Technology, Sweden, 2007, (Doctoral thesis).
- [97] N. Loaiza, C. Graciano, R. Chacon, Web crippling strength of longitudinally stiffened steel plate girder webs subjected to concentrated loading, *Engineering Journal, American Institute of Steel Construction* 55 (2018) 191–201.
- [98] F.E. Demari, G.P. Mezzomo, Z.M.C. Pravia, Numerical study of slender I-girders with one longitudinal stiffener under patch loading, *J. Constr. Steel Res.* 167 (2020) 105964.
- [99] J.A. Chica, J.T. San Jose, F. Millanes, J.M. Manso, Recommendations on imperfections in the design of plated structural elements of bridges, *J. Constr. Steel Res.* 86 (2013) 183–194.
- [100] L. Gerard, L. Li, M. Kettler, N. Boissonnade, Recommendations on the geometrical imperfections definition for the resistance of I-sections, *J. Constr. Steel Res.* 162 (2019) 105716.
- [101] N. Kristanic, J. Korelc, Optimization method for the determination of the most unfavorable imperfection of structures, *Comput. Mech.* 42 (2008) 859–872.
- [102] E. Lindgaard, E. Lund, K. Rasmussen, Nonlinear buckling optimization of composite structures considering ‘worst’ shape imperfections, *Int. J. Solid Struct.* 47 (2010) 3186–3202.
- [103] W. Schneider, I. Timmel, K. Höhn, The concept of quasi-collapse-affine imperfections: a new approach to unfavorable imperfections of thin-walled shell structures, *Thin-Walled Struct.* 43 (2005) 1202–1224.

Appendix A

Steel material properties

The web panel and flange material properties were determined by using multiple standard tensile coupon tests. The testing process was performed at the Faculty of Technology and Metallurgy, University of Belgrade, Belgrade. Stress and strain data were measured by a Universal Testing Machine “Shimadzu” from the AG-Xplus Series utilizing extensometers with an initial length of 50 mm, Fig. A.1. Typical coupon specimen failure is shown in Fig. A.2.

The web panel material properties are listed in Table A.1, while their graphical representation is given from Fig. A.3 to Fig. A.9. The material properties were obtained from four coupon tests except for girders B1 (B11) and B7 (B17), for which three and two coupon tests were used, respectively.



Figure A.1: Universal Testing Machine Shimadzu AG-Xplus and extensometer with an initial length of 50 mm.



Figure A.2: Typical coupon specimen failure.

Table A.1: Web panel material properties of all the test steel plate girders of Series B.

Girder	f_{yw} [MPa]				f_{uw} [MPa]			
	B1	n.a. ¹	267	256	249	n.a. ¹	356	344
B2	230	228	217	227	338	351	322	336
B3	321	304	310	323	441	435	428	430
B4	331	326	309	305	450	452	418	417
B5	322	315	316	320	441	444	429	428
B6	282	262	248	255	364	357	335	336
B7	324	330			435	442		

¹ Data for this coupon test are not available

Table A.2: Flange material properties of all the test steel plate girders of Series B.

Girder	f_{yw} [MPa]		f_{uw} [MPa]	
	B1	320	311	467
B2	305	320	453	474
B3	310	315	462	464
B4	323	323	463	476
B5	324	299	468	451
B6	316	312	469	463
B7	339		486	

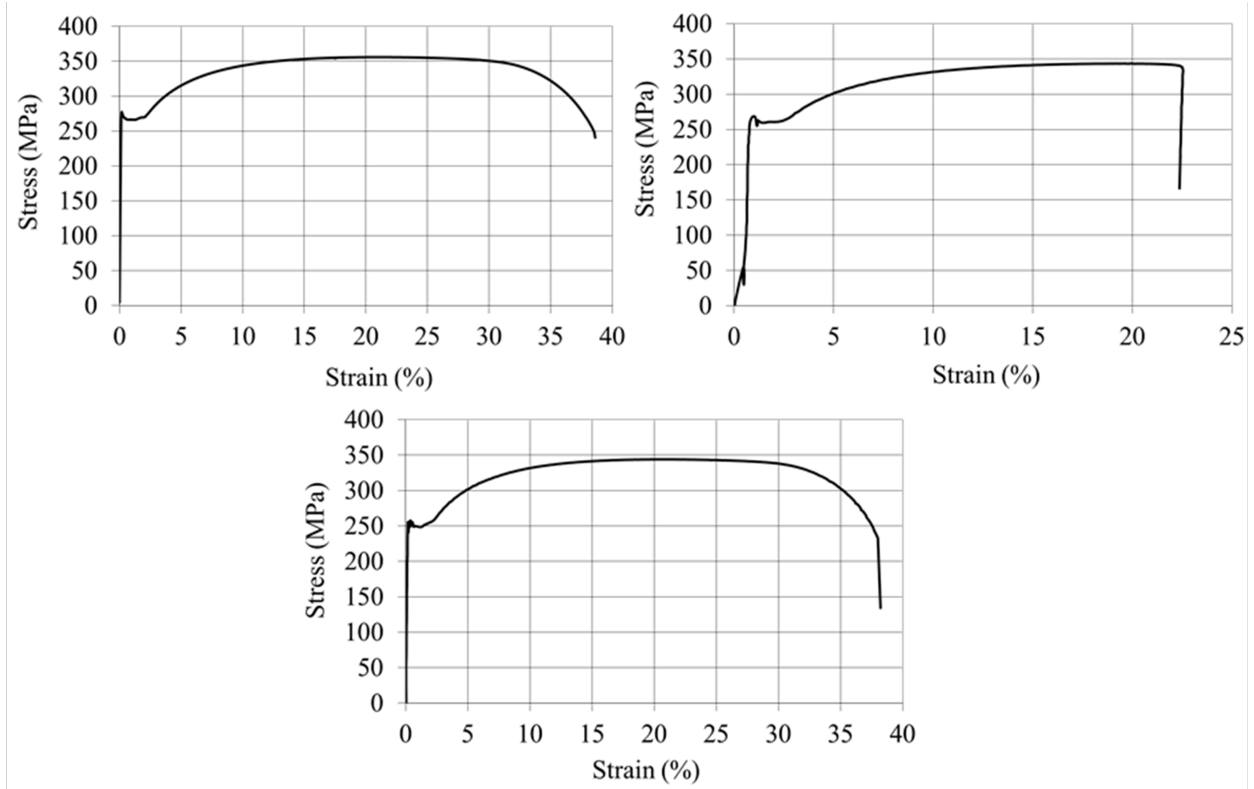


Figure A.3: Engineering stress-strain diagram for different coupon tests for web panel – B1.

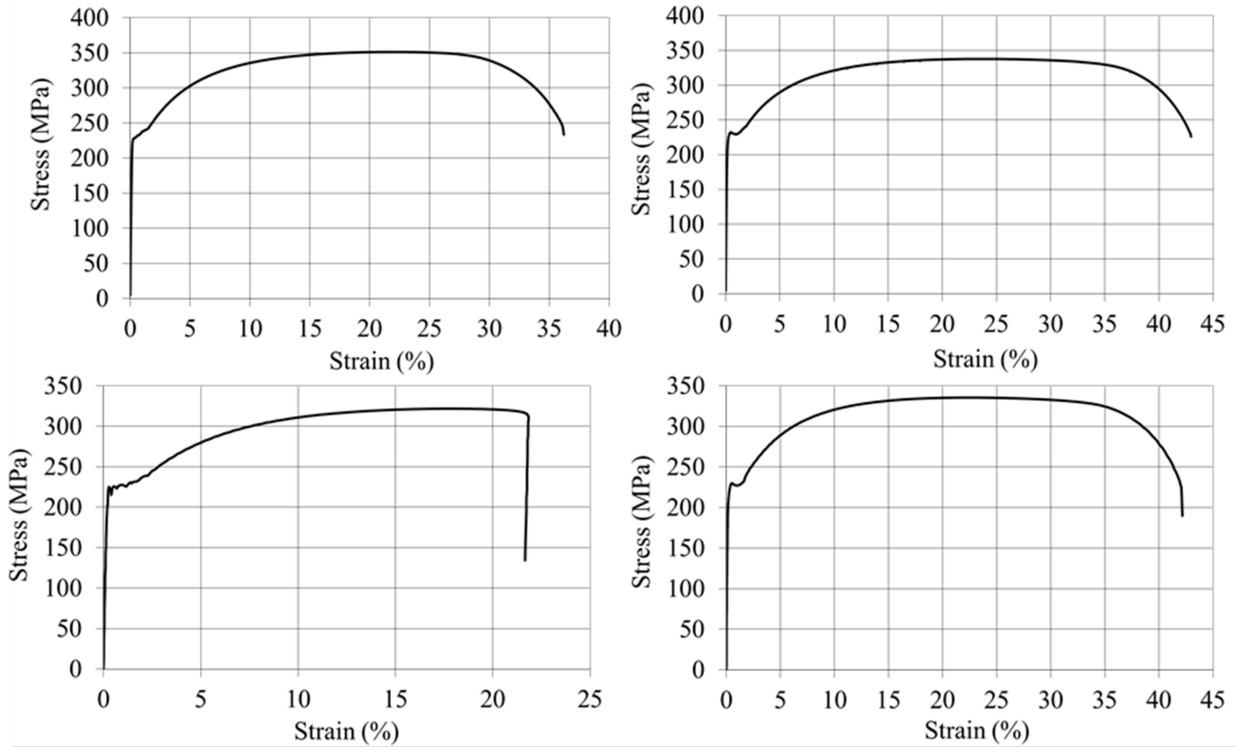


Figure A.4: Engineering stress-strain diagram for different coupon tests for web panel – B2.

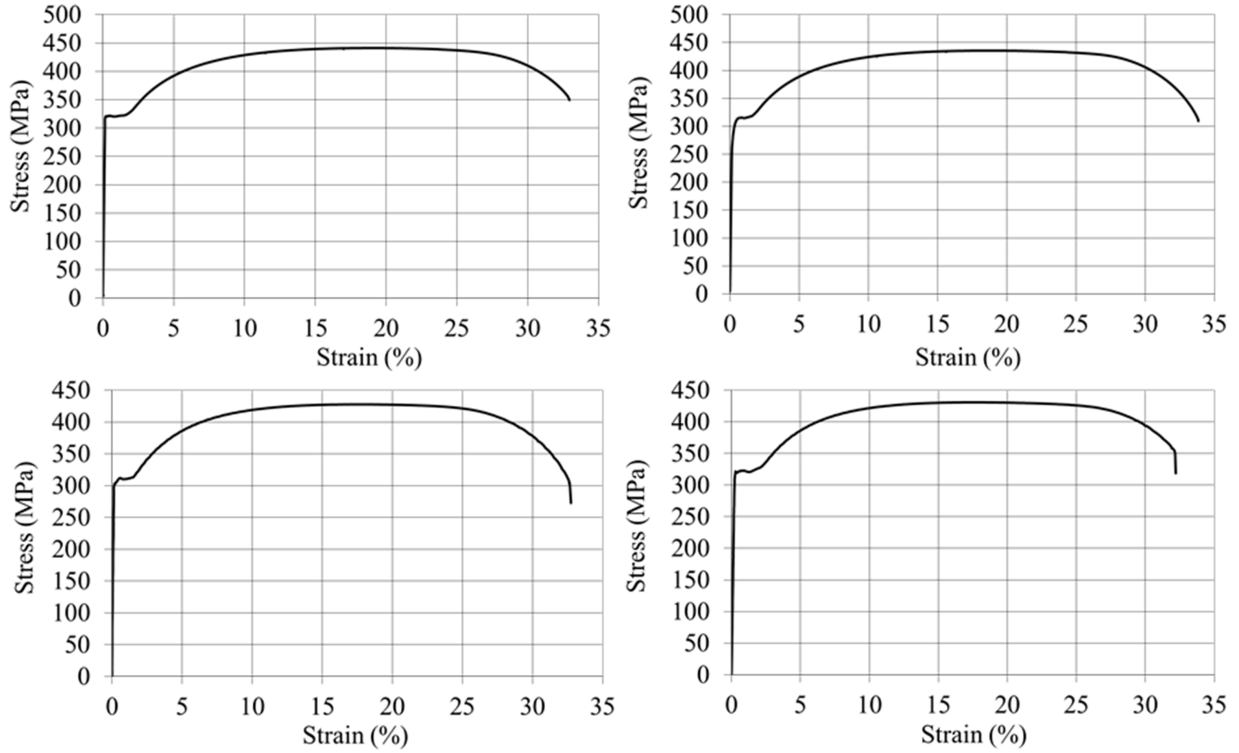


Figure A.5: Engineering stress-strain diagram for different coupon tests for web panel – B3.

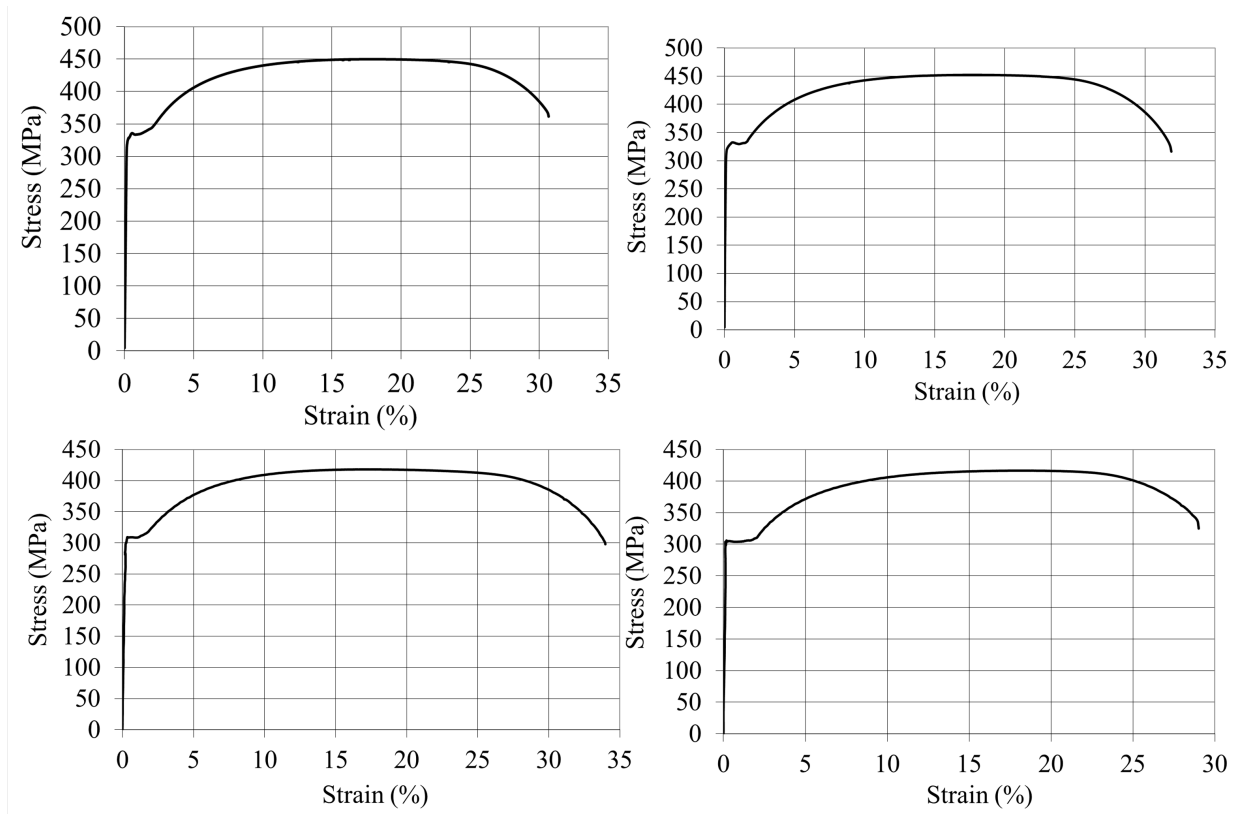


Figure A.6: Engineering stress-strain diagram for different coupon tests for web panel – B4.

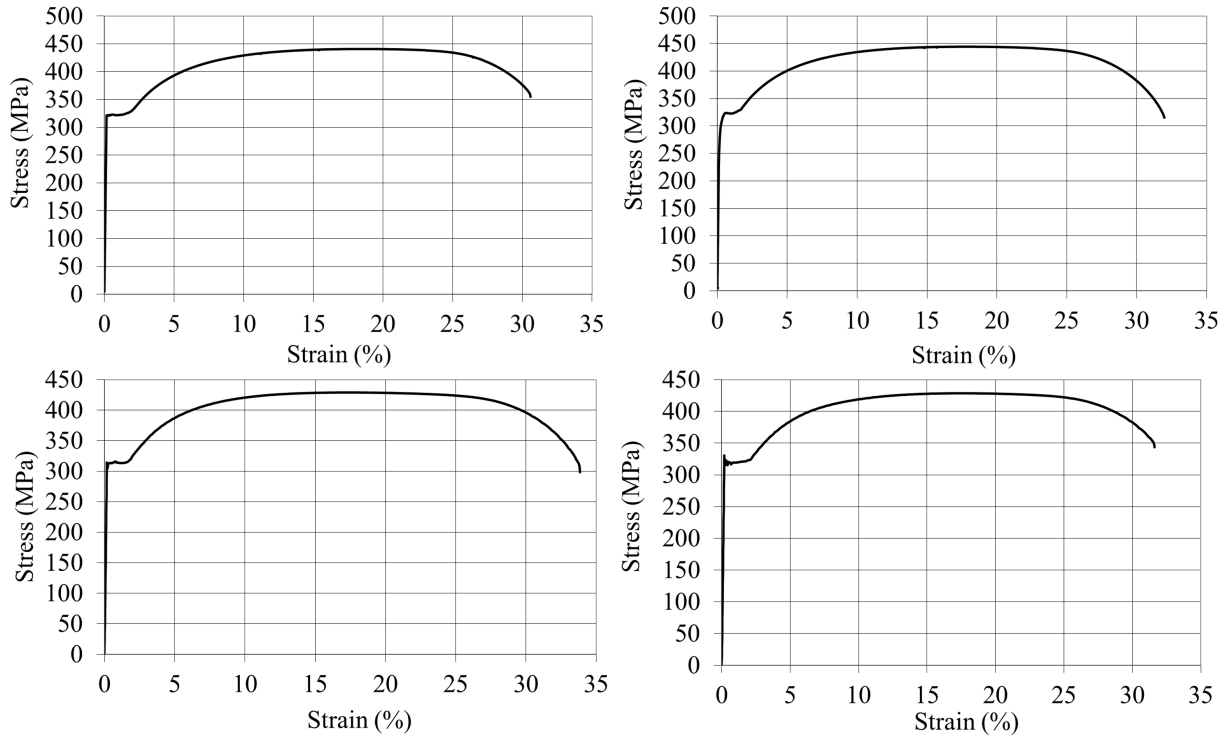


Figure A.7: Engineering stress-strain diagram for different coupon tests for web panel – B5.

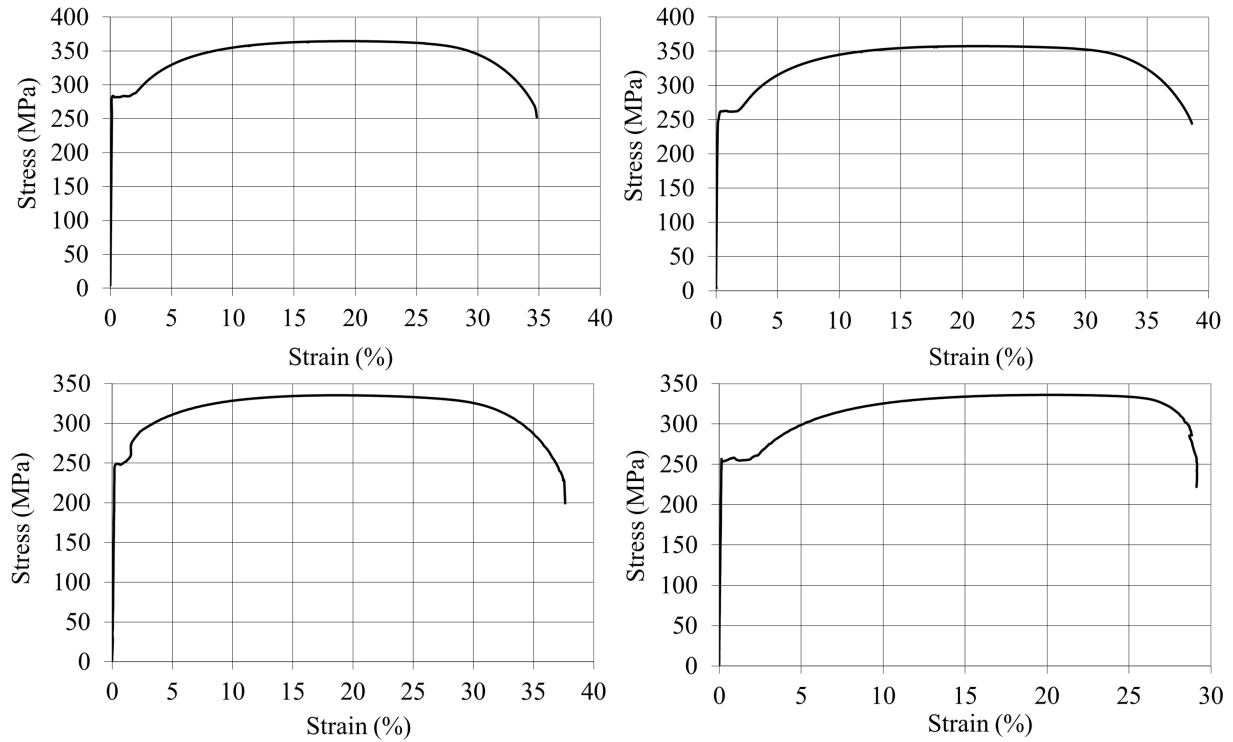


Figure A.8: Engineering stress-strain diagram for different coupon tests for web panel – B6.

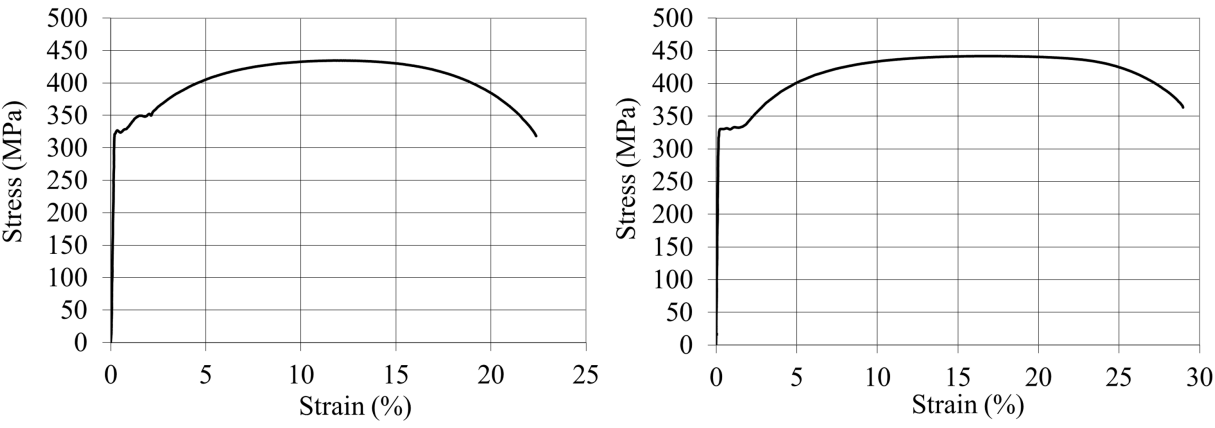


Figure A.9: Engineering stress-strain diagram for different coupon tests for web panel – B7.

Appendix B

Web panel deformation for girders of Series A

Contour plots of initial and residual web panel deformations, including an increase in deformation (the difference between the residual and initial deformation), for all the experimentally tested girders of Series A are given in Fig. B.1 to Fig. B. 14. The plots are sorted according to the patch load length s_s . It should be noted that the extent of the residual deformation depends on how long a girder was kept under loading after the ultimate strength was reached. Thus, the given plots for the residual deformation do not represent an actual deformation at the ultimate load.

Remark: All measured data were collected by Markovic [21]. This Appendix is also published in Ref. [25].

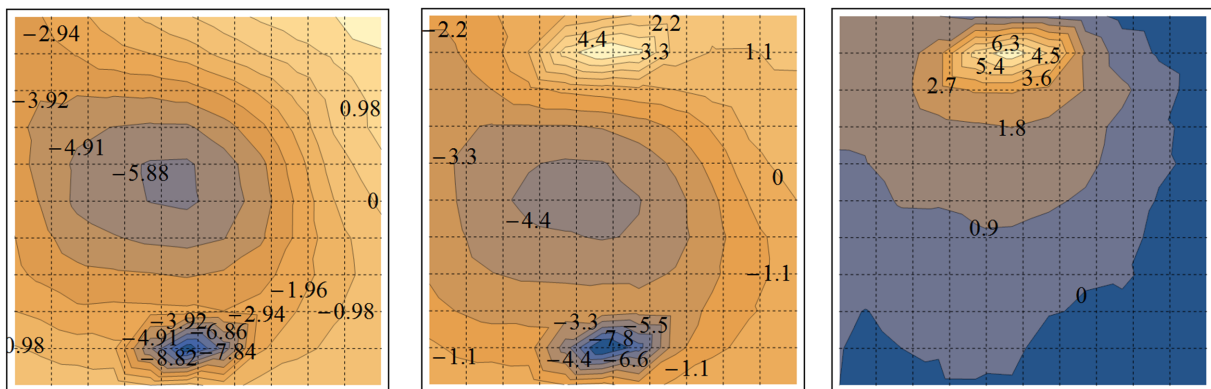


Figure B.1: Girder A14 with stiffening $s_s = 0$ mm: initial deformation (top left), residual deformation (top right), and increase in deformation (bottom) [mm].

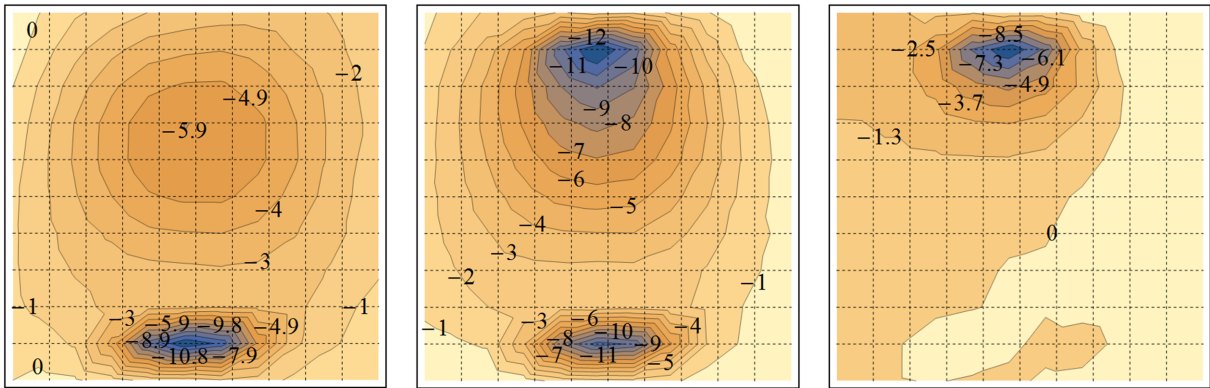


Figure B.2: Girder A15 without stiffening $s_s = 0$ mm: initial deformation (top left), residual deformation (top right), and increase in deformation (bottom) [mm].

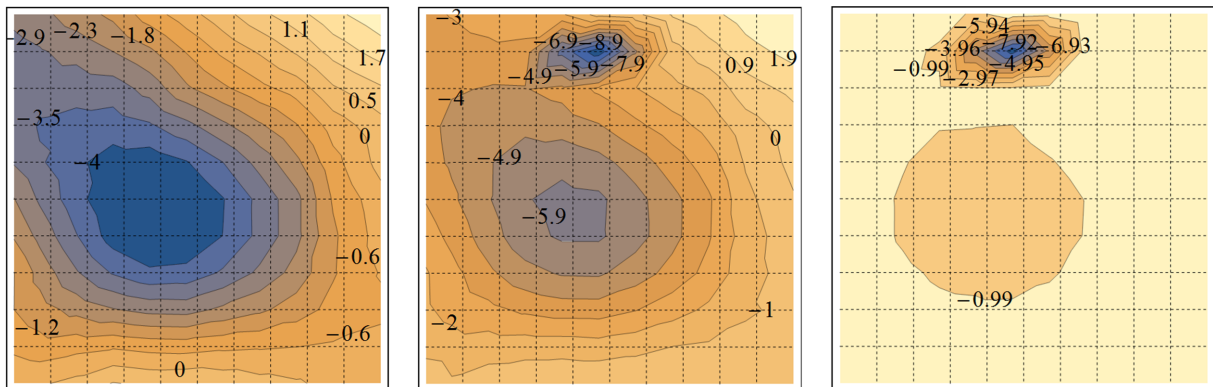


Figure B.3: Girder A4 with stiffening $s_s = 25$ mm: initial deformation (top left), residual deformation (top right), and increase in deformation (bottom) [mm].

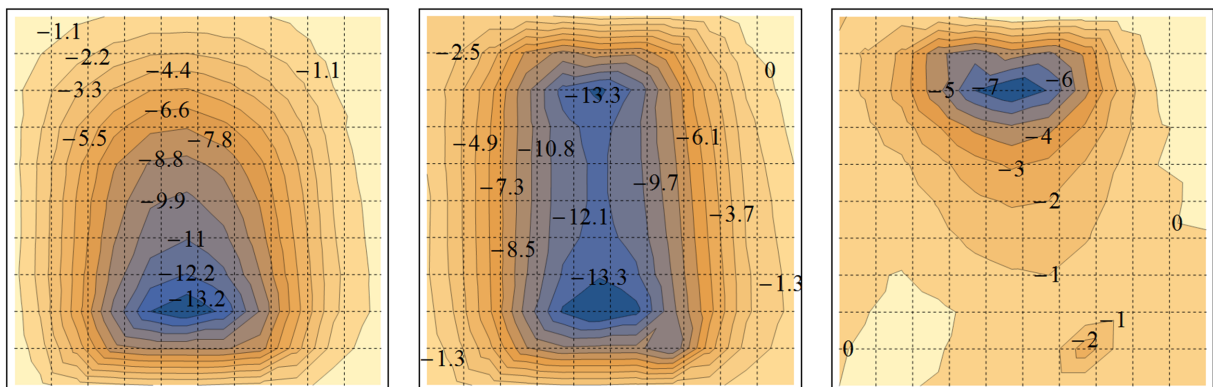


Figure B.4: Girder A12 without stiffening $s_s = 25$ mm: initial deformation (top left), residual deformation (top right), and increase in deformation (bottom) [mm].

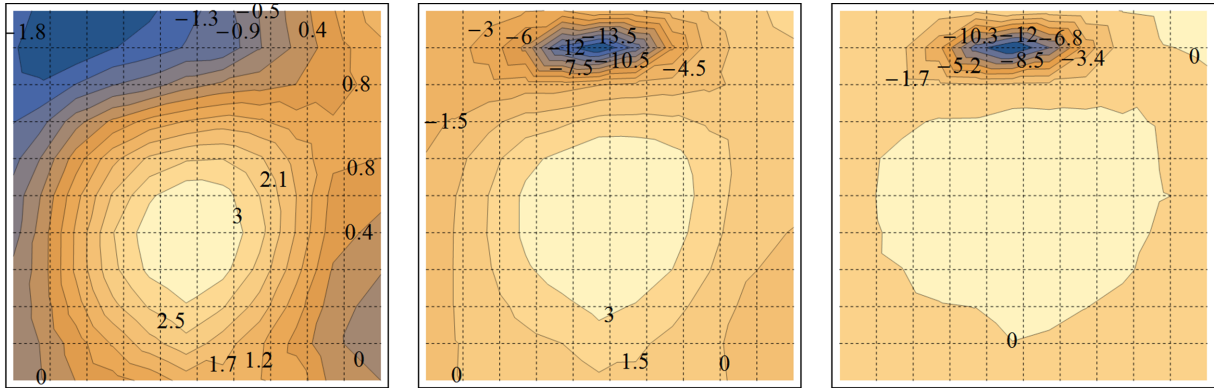


Figure B.5: Girder A3 with stiffening $s_s = 50$ mm: initial deformation (top left), residual deformation (top right), and increase in deformation (bottom) [mm].

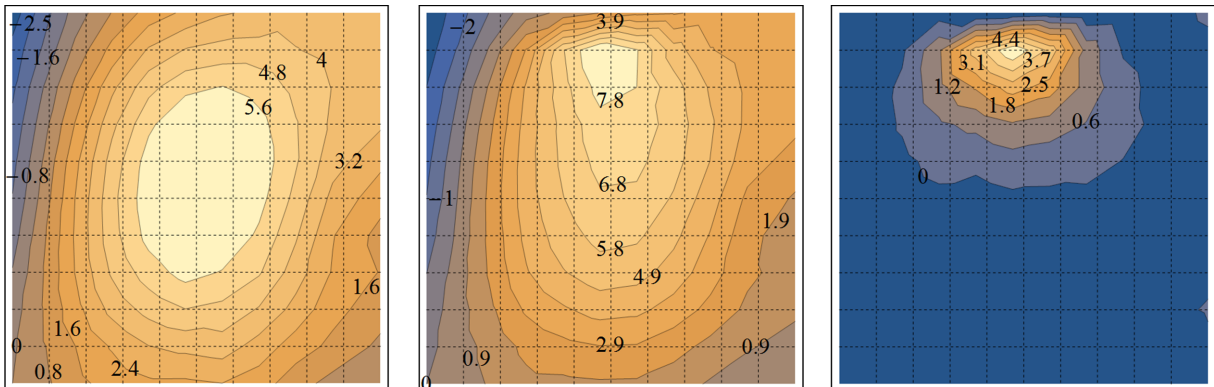


Figure B.6: Girder A1 without stiffening $s_s = 50$ mm: initial deformation (top left), residual deformation (top right), and increase in deformation (bottom) [mm].

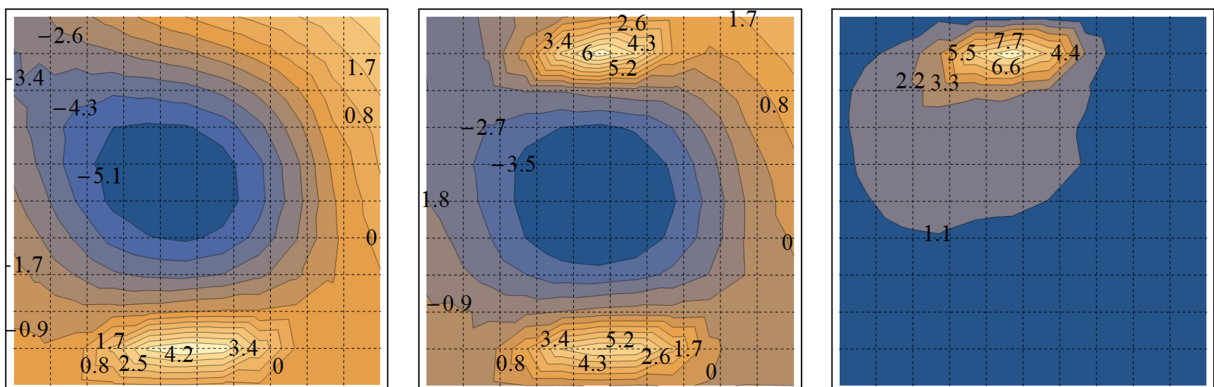


Figure B.7: Girder A17 with stiffening $s_s = 75$ mm: initial deformation (top left), residual deformation (top right), and increase in deformation (bottom) [mm].

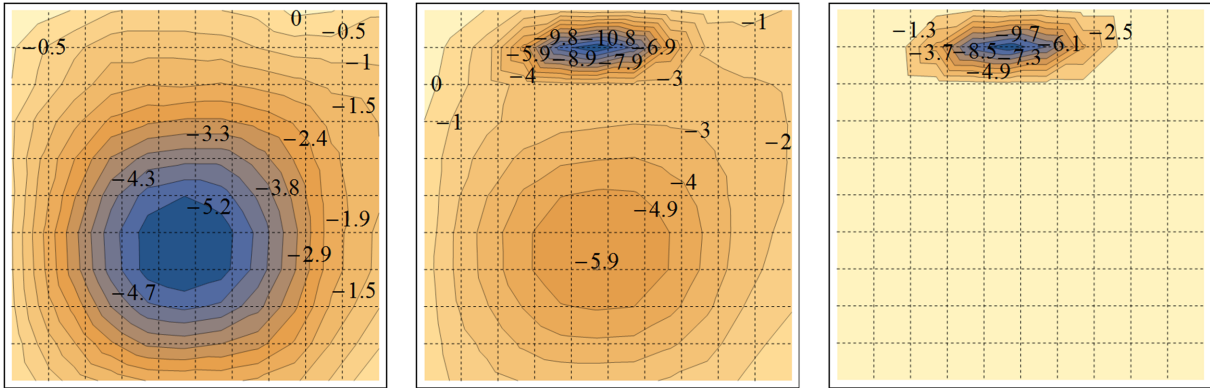


Figure B.8: Girder A5 with stiffening $s_s = 100$ mm: initial deformation (top left), residual deformation (top right), and increase in deformation (bottom) [mm].

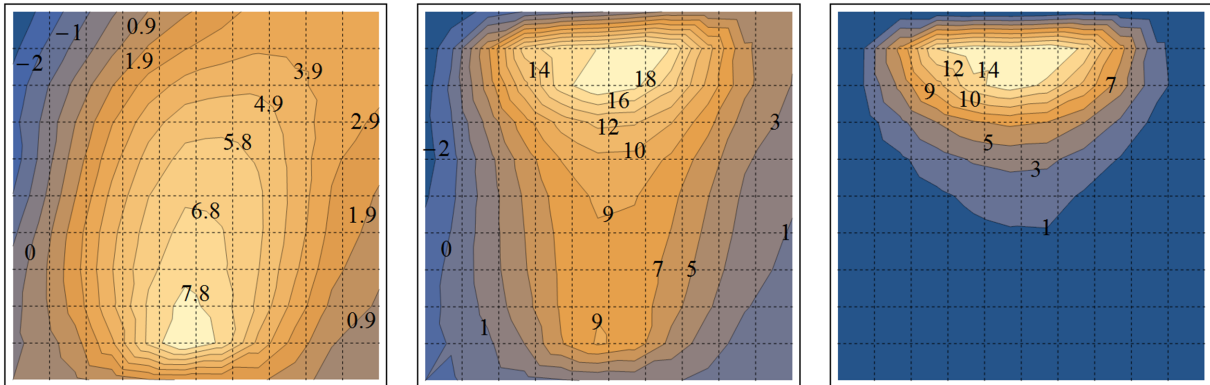


Figure B.9: Girder A11 without stiffening $s_s = 100$ mm: initial deformation (top left), residual deformation (top right), and increase in deformation (bottom) [mm].

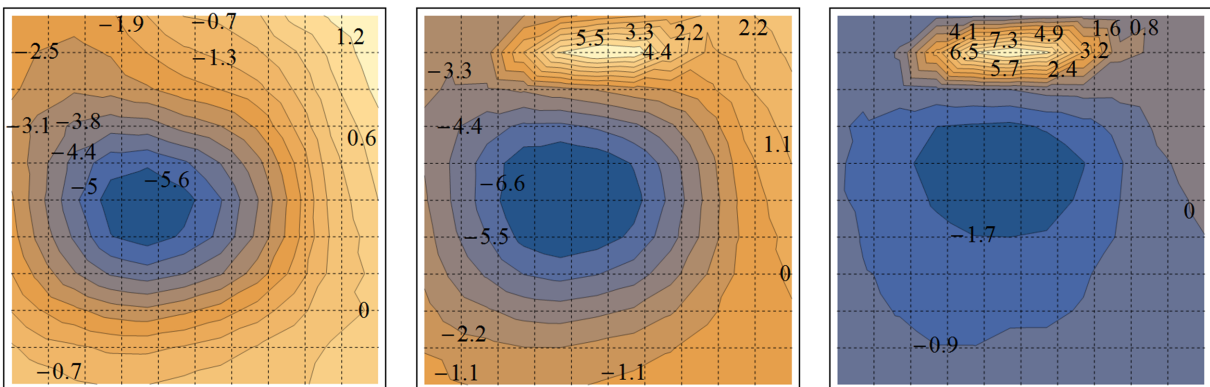


Figure B.10: Girder A6 with stiffening $s_s = 125$ mm: initial deformation (top left), residual deformation (top right), and increase in deformation (bottom) [mm].

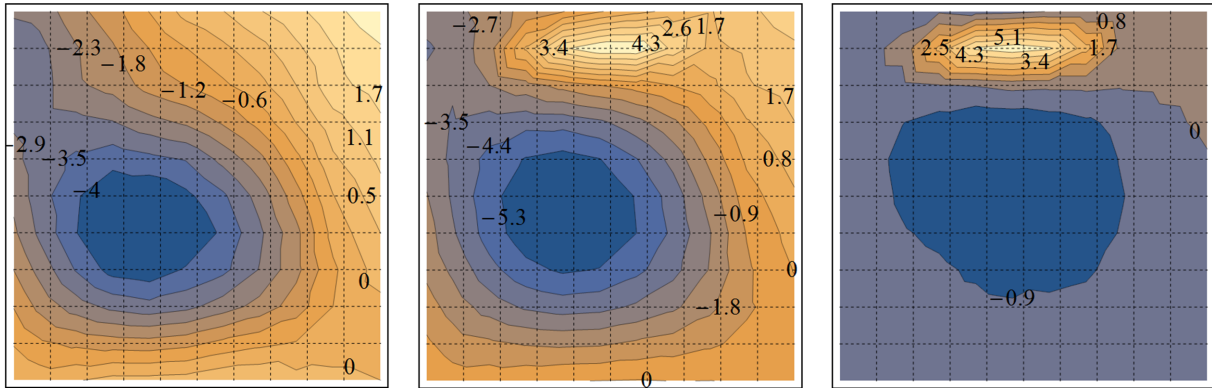


Figure B.11: Girder A7 with stiffening $s_s = 150$ mm: initial deformation (top left), residual deformation (top right), and increase in deformation (bottom) [mm].

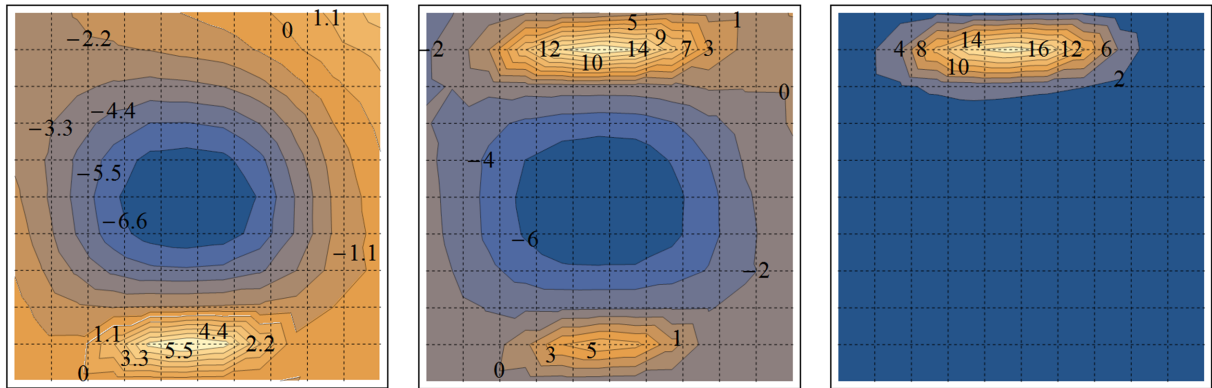


Figure B.12: Girder A16 with stiffening $s_s = 150$ mm: initial deformation (top left), residual deformation (top right), and increase in deformation (bottom) [mm].

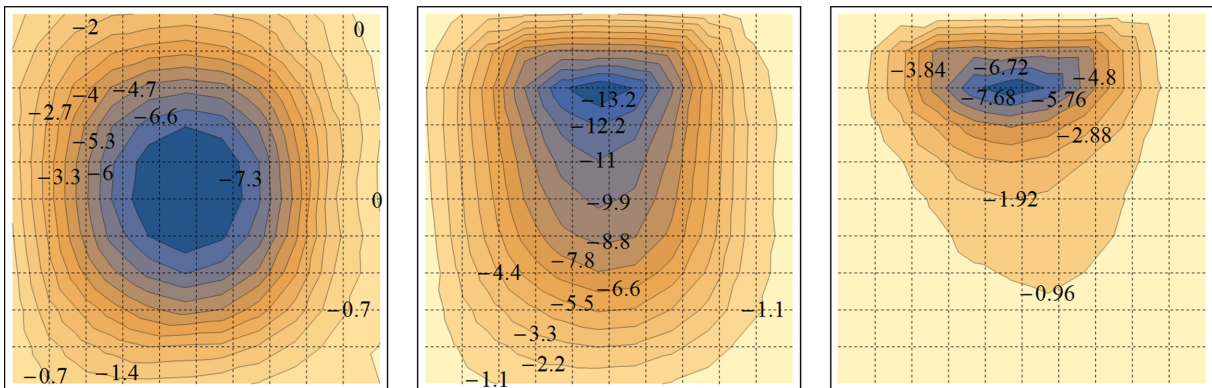


Figure B.13: Girder A2 without stiffening $s_s = 150$ mm: initial deformation (top left), residual deformation (top right), and increase in deformation (bottom) [mm].

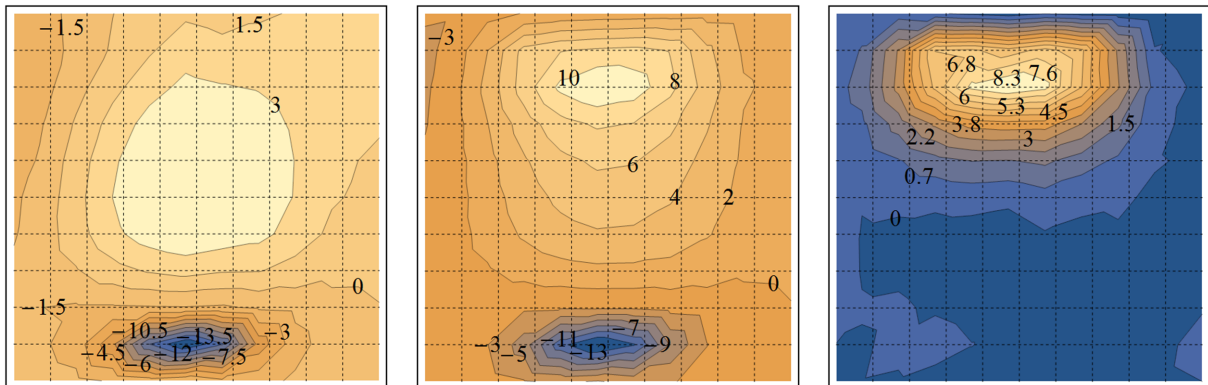


Figure B.14: Girder A13 without stiffening $s_s = 150$ mm: initial deformation (top left), residual deformation (top right), and increase in deformation (bottom) [mm].

Appendix C

Web panel deformation for girders of Series B

Contour plots of initial and residual web panel deformations, including an increase in deformation (the difference between the residual and initial deformation), for all the experimentally tested girders of Series B are given in Fig. C.1 to Fig. C. 14. The plots are sorted according to the patch load length s_s . It should be noted that the extent of the residual deformation depends on how long a girder was kept under loading after the ultimate strength was reached. Thus, the given plots for the residual deformation do not represent an actual deformation at the ultimate load.

Remark: All measured data for girders B1, B3, B5, B2, B7, and B17 were collected by Markovic [21]. This Appendix is also published in Ref. [24].

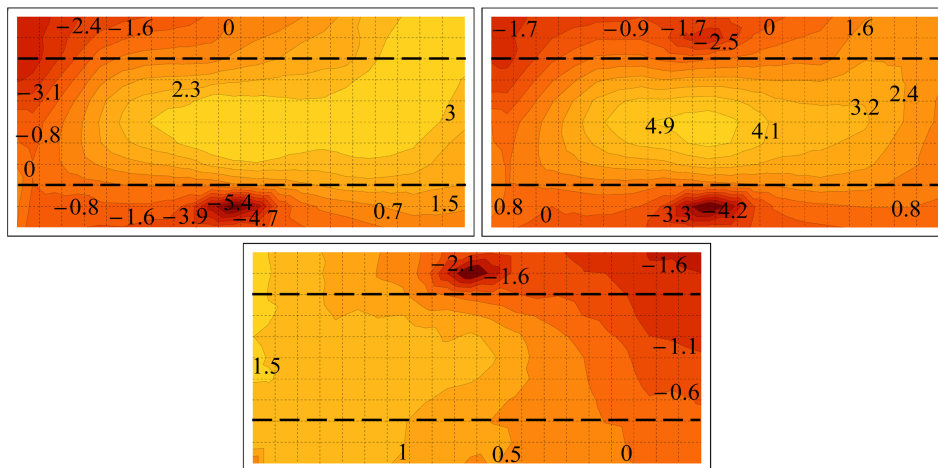


Figure C.1: Girder B13 with stiffening $s_s = 0$ mm: initial deformation (top left), residual deformation (top right), and increase in deformation (bottom) [mm]. The dashed lines represent the longitudinal stiffener.

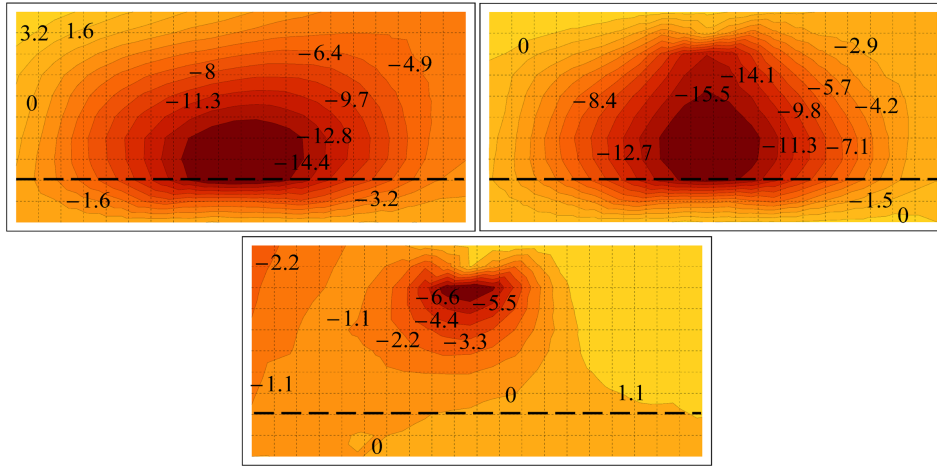


Figure C.2: Girder B16 without stiffening $s_s = 0$ mm: initial deformation (top left), residual deformation (top right), and increase in deformation (bottom) [mm]. The dashed line represents the longitudinal stiffener.

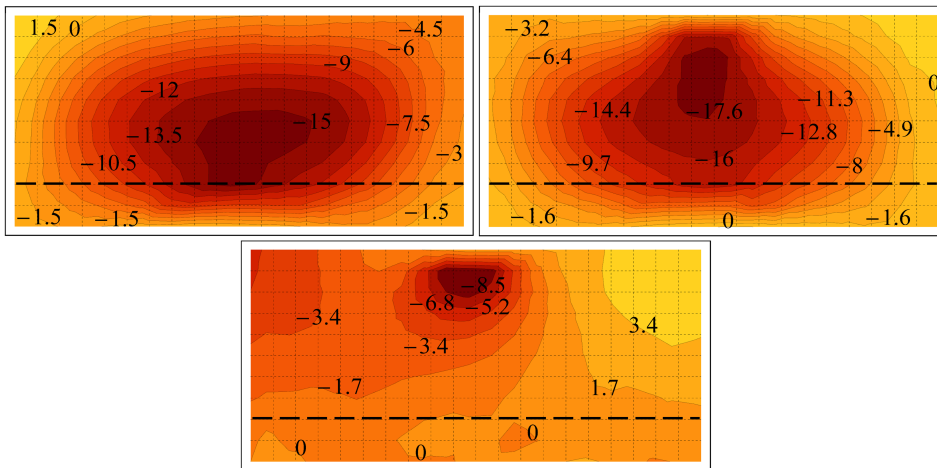


Figure C.3: Girder B14 without stiffening $s_s = 25$ mm: initial deformation (top left), residual deformation (top right), and increase in deformation (bottom) [mm]. The dashed line represents the longitudinal stiffener.

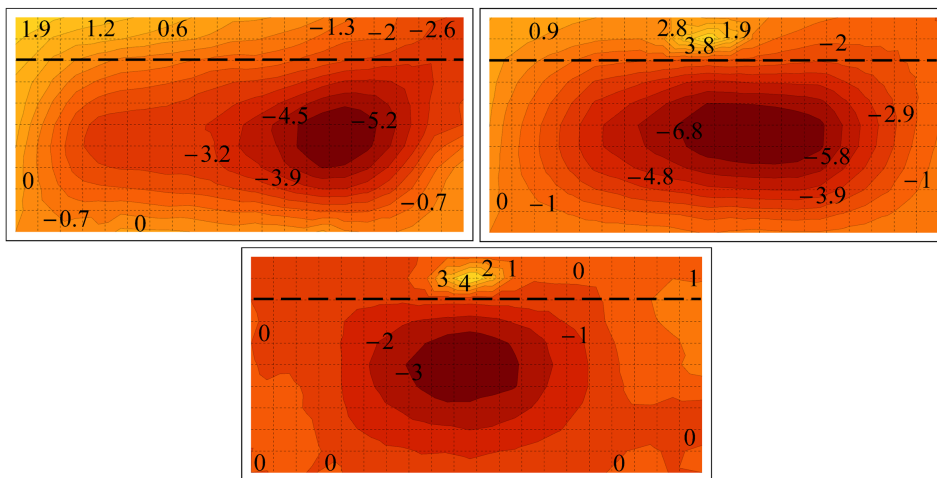


Figure C.4: Girder B3 with stiffening $s_s = 50$ mm: initial deformation (top left), residual deformation (top right), and increase in deformation (bottom) [mm]. The dashed line represents the longitudinal stiffener.

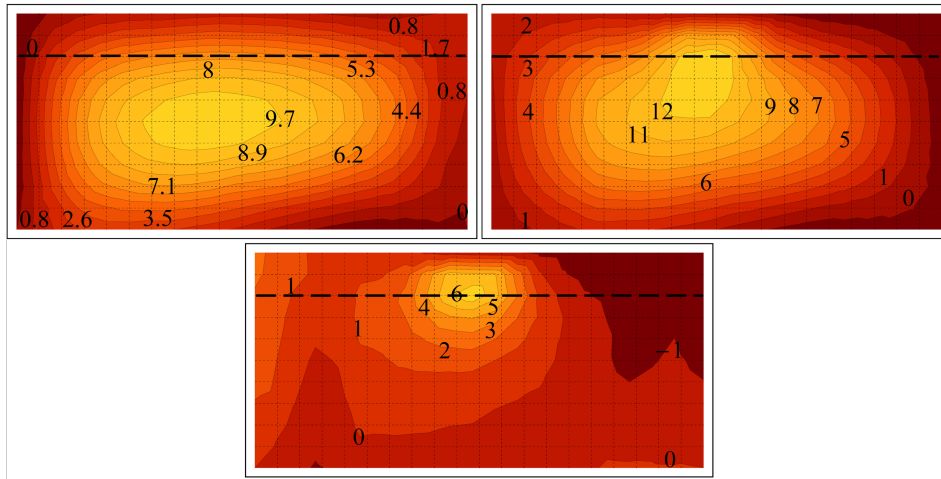


Figure C.5: Girder B1 without stiffening $s_s = 50$ mm: initial deformation (top left), residual deformation (top right), and increase in deformation (bottom) [mm].

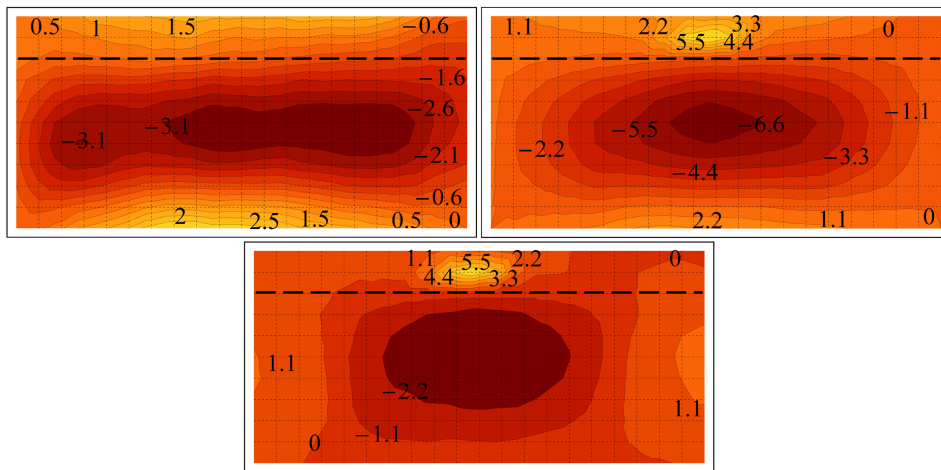


Figure C.6: Girder B5 with stiffening $s_s = 100$ mm: initial deformation (top left), residual deformation (top right), and increase in deformation (bottom) [mm]. The dashed line represents the longitudinal stiffener.

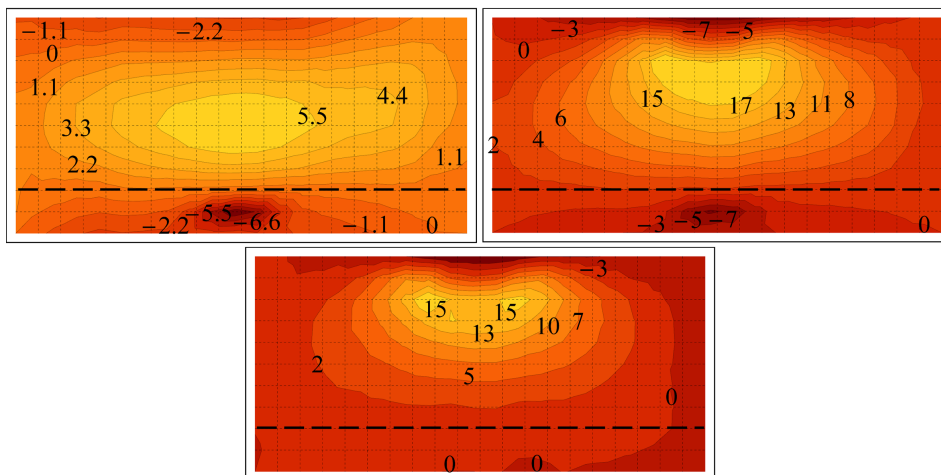


Figure C.7: Girder B15 without stiffening $s_s = 100$ mm: initial deformation (top left), residual deformation (top right), and increase in deformation (bottom) [mm]. The dashed line represents the longitudinal stiffener.

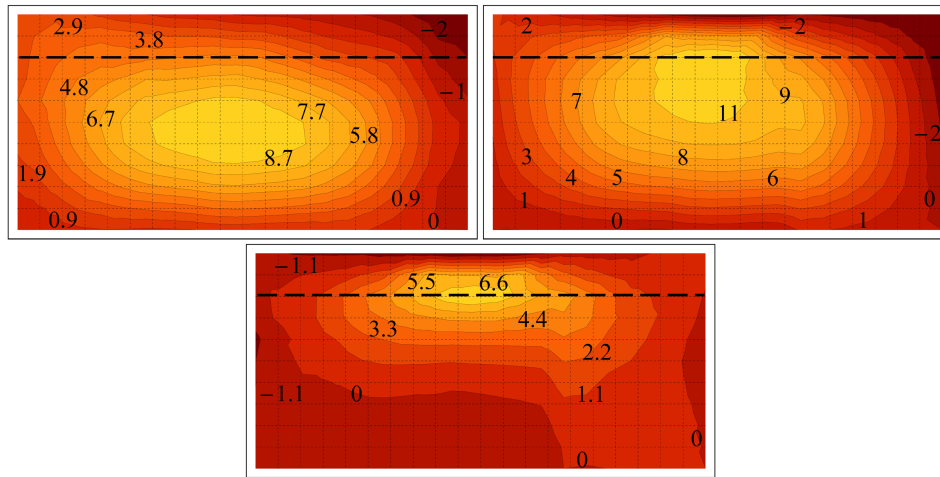


Figure C.8: Girder B7 with stiffening $s_s = 150$ mm: initial deformation (top left), residual deformation (top right), and increase in deformation (bottom) [mm]. The dashed line represents the longitudinal stiffener.

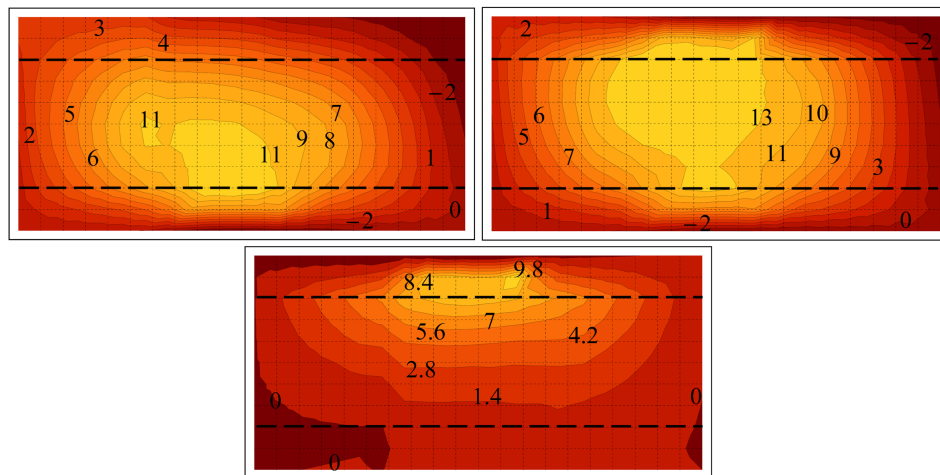


Figure C.9: Girder B17 with stiffening $s_s = 150$ mm: initial deformation (top left), residual deformation (top right), and increase in deformation (bottom) [mm]. The dashed lines represent the longitudinal stiffener.

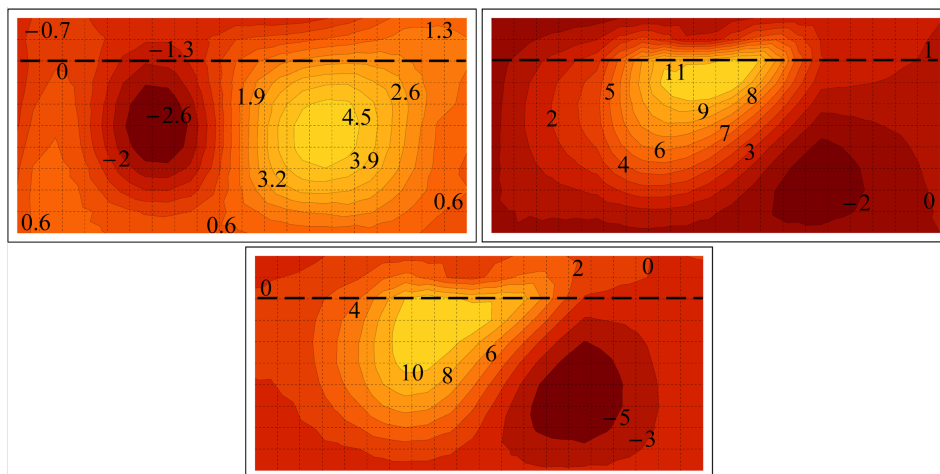


Figure C.10: Girder B2 without stiffening $s_s = 150$ mm: initial deformation (top left), residual deformation (top right), and increase in deformation (bottom) [mm].

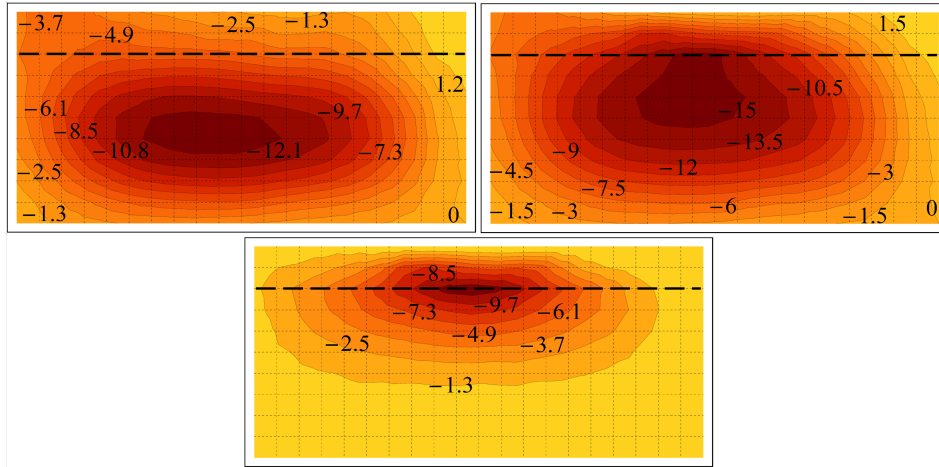


Figure C.11: Girder B4 with stiffening $s_s = 200$ mm: initial deformation (top left), residual deformation (top right), and increase in deformation (bottom) [mm]. The dashed line represents the longitudinal stiffener.

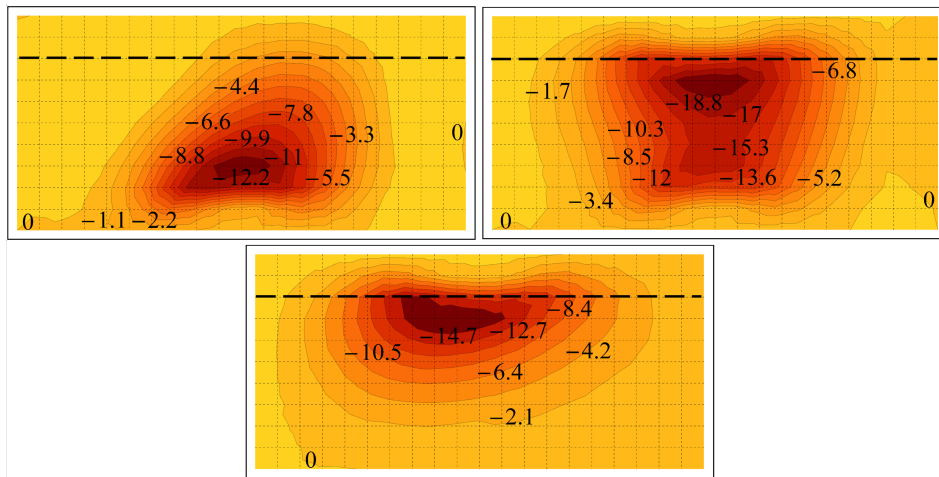


Figure C.12: Girder B12 without stiffening $s_s = 200$ mm: initial deformation (top left), residual deformation (top right), and increase in deformation (bottom) [mm].

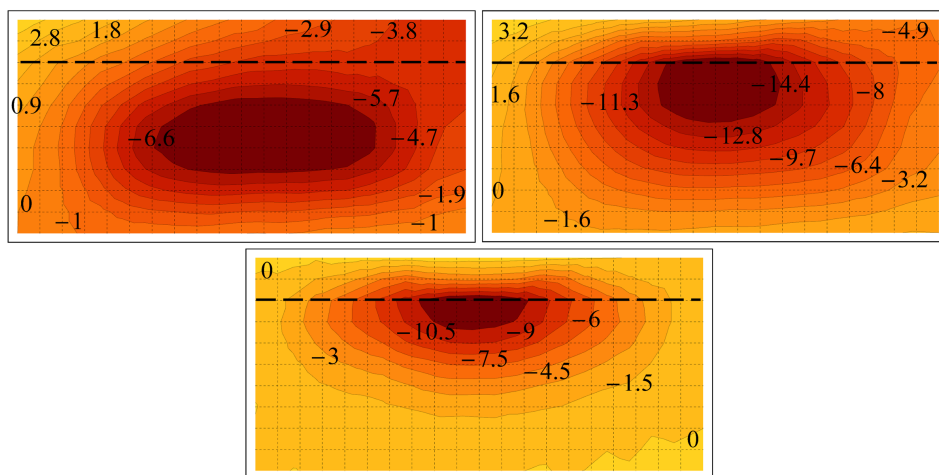


Figure C.13: Girder B6 with stiffening $s_s = 250$ mm: initial deformation (top left), residual deformation (top right), and increase in deformation (bottom) [mm]. The dashed line represents the longitudinal stiffener.

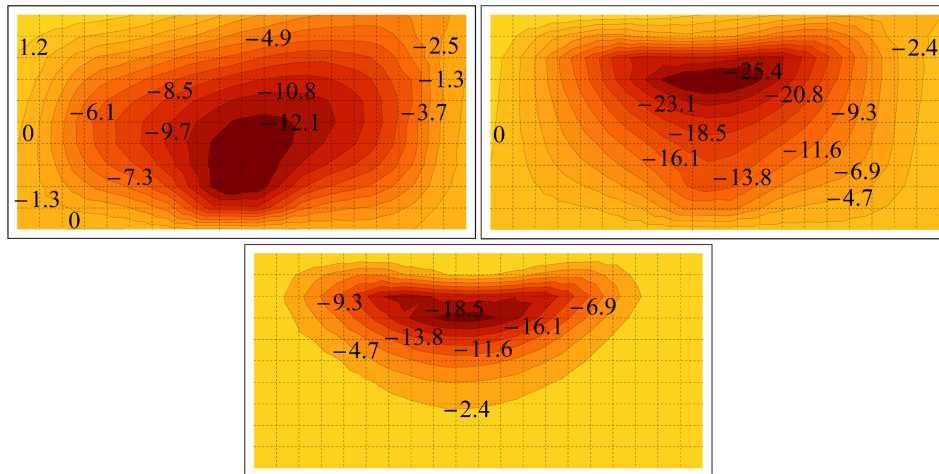


Figure C.14: Girder B11 without stiffening $s_s = 250$ mm: initial deformation (top left), residual deformation (top right), and increase in deformation (bottom) [mm].

Biography

Sasa D. Kovacevic was born on January 4, 1988 in Zagreb, Croatia. He received a B.S. in Civil Engineering from the University of Banja Luka in 2011 and an M.Sc. in Civil Engineering from the University of Belgrade in 2013. After graduation, he has worked as an engineer for the design of Steel Structures in Banja Luka. He moved to Energoprojekt Industry PLC in Belgrade in 2014. Sasa has started his Ph.D. study at the University of Belgrade in 2013 within the Engineering Mechanics and Theory of Structures Department. In 2016 he moved to the USA and started Ph.D. study at Washington State University. He is currently a Research and Teaching Assistant at Washington State University in the School of Mechanical and Materials Engineering.

His multidisciplinary research activities merge the area of Engineering Mechanics, Materials Science, and Applied Mathematics. He is interested in multiscale modeling, from the atomic to micro-, meso-, and large-scales. His research is based on theoretical and computational methods for multiscale and multifield modeling of physical processes and materials with application in processing and service.

During his research work, he has worked on various projects from different scientific fields. He has collaborated with Washington State University, University of Kentucky, Carnegie Mellon University, Idaho National Laboratory, Harbin Institute of Technology in China, and many others.

He currently works on a research project for multiphase field modeling of melting and flow of alloys in space at the International Space Station funded by NASA and projects regarding micromechanics of advanced manufacturing processes.

He has received the Outstanding Teaching Assistant Award from the Mechanical Department at Washington State University, Outstanding Teaching Assistant Award from Voiland College of Engineering and Architecture at Washington State University, and the Graduate & Professional Student Association Dissertation Award at Washington State University.

He has authored and co-authored 12 peer-reviewed papers, over 30 conference proceedings, and holds one patent.

Биографија

Саша Д. Ковачевић је рођен 4. јануара 1988. године у Загребу, Хрватска. Стекао је звање инжењер грађевинарства на Универзитету у Бања Луци 2011. године, а звање мастер инжењер грађевинарства на Универзитету у Београду 2013. године. Након дипломирања радио је као инжењер за пројектовање челичних конструкција у Бања Луци. 2014. године је прешао у Енергопројект Индустрија у Београду. Саша је почео своје докторске студије на Универзитету у Београду у току 2013. године на Катедре за техничку механику и теорију конструкција. 2016. године се сели у САД где започиње докторске студије на државном Универзитету у Савезној Америчкој држави Вашингтон. Тренутно је асистент истраживач и асистент у настави на државном Универзитету у Вашингтону, на Факултету за Машинско инжењерство и материјале.

Његове мултидисциплинарне истраживачке активности су на пољима инжењерске механике, науке о материјалима и примењене математике. Заинтересован је за вишеразмерно моделирање, од атомских, преко микро- и мезо-размера, до великих размера. Његова истраживања се базирају на теоријским и рачунским методама за вишеразмерно и вишефазно моделирање физичких процеса и материјала са применама у обради и употреби.

У току истраживачког рада сарађивао је и радио на различитим пројектима из различитих области. Сарађивао је са државним Универзитетом у Вашингтону, Универзитетом у Кентакију, Карнеги Мелон Универзитетом у Пенсилванији, Националном лабораторијом у Ајдаху, Харбин институтом за технологију из Кине и многим другим.

Тренутно ангажован на пројекту везаном за вишефазно моделирање топљења и течења легура у свемиру на Интернационалној Свемирској Станици, који је подржан од стране NASA-е, као и на пројектима везаним за микромеханику савремених производних процеса.

Добитник је награда за истакнутог асистента у настави од стране Машинског факултета на државном Универзитету у Вашингтону, за истакнутог асистента у настави од стране Воиленд Колеца за Инжењерство и Архитектуру на државном Универзитету у Вашингтону, те признања за дисертацију од стране Удружења дипломаца и постдипломаца на државном Универзитету у Вашингтону.

Аутор и коаутор 12 рецензираних радова објављених у међународним часописима, преко 30 саопштења на интернационалним и домаћим конференцијама, а поседује и један патент.

Прилог 1.

Изјава о ауторству

Потписани-а: Саша Ковачевић

број индекса: 910/13

Изјављујем

да је докторска дисертација под насловом

СТАБИЛНОСТ И ГРАНИЧНА НОСИВОСТ ТАНКОЗИДНИХ ЧЕЛИЧНИХ НОСАЧА
ПОД УТИЦАЈЕМ ДЕЛИМИЧНОГ ОПТЕРЕЋЕЊА

- резултат сопственог истраживачког рада,
- да предложена дисертација у целини ни у деловима није била предложена за добијање било које дипломе према студијским програмима других високошколских установа,
- да су резултати коректно наведени и
- да нисам кршио/ла ауторска права и користио интелектуалну својину других лица.

Потпис докторанда

У Београду, 09.06.2021.



Прилог 2.

Изјава о истоветности штампане и електронске верзије докторског рада

Име и презиме аутора: Саша Ковачевић

Број индекса: 910/13

Студијски програм: Грађевинарство

Наслов рада: СТАБИЛНОСТ И ГРАНИЧНА НОСИВОСТ ТАНКОЗИДНИХ НОСАЧА
ПОД УТИЦАЈЕМ ДЕЛИМИЧНОГ ОПТЕРЕЋЕЊА

Ментор: проф. др Драгослав Шумарац

Потписани/а: Саша Ковачевић

Изјављујем да је штампана верзија мог докторског рада истоветна електронској верзији коју сам предао/ла за објављивање на порталу **Дигиталног репозиторијума Универзитета у Београду**.

Дозвољавам да се објаве моји лични подаци везани за добијање академског звања доктора наука, као што су име и презиме, година и место рођења и датум одбране рада.

Ови лични подаци могу се објавити на мрежним страницама дигиталне библиотеке, у електронском каталогу и у публикацијама Универзитета у Београду.

Потпис докторанда

У Београду, 09.06.2021.



Изјава о коришћењу

Овлашћујем Универзитетску библиотеку „Светозар Марковић“ да у Дигитални репозиторијум Универзитета у Београду унесе моју докторску дисертацију под насловом:

СТАБИЛНОСТ И ГРАНИЧНА НОСИВОСТ ТАНКОЗИДНИХ ЧЕЛИЧНИХ НОСАЧА ПОД УТИЦАЈЕМ ДЕЛИМИЧНОГ ОПТЕРЕЋЕЊА

која је моје ауторско дело.

Дисертацију са свим прилозима предао/ла сам у електронском формату погодном за трајно архивирање.

Моју докторску дисертацију похрањену у Дигиталном репозиторијуму Универзитета у Београду и доступну у отвореном приступу могу да користе сви који поштују одредбе садржане у одабраном типу лиценце Креативне заједнице (Creative Commons) за коју сам се одлучио/ла.

1. Ауторство (CC BY)

2. Ауторство – некомерцијално (CC BY-NC)

3. Ауторство – некомерцијално – без прерада (CC BY-NC-ND)

4. Ауторство – некомерцијално – делити под истим условима (CC BY-NC-SA)

5. Ауторство – без прерада (CC BY-ND)

6. Ауторство – делити под истим условима (CC BY-SA)

(Молимо да заокружите само једну од шест понуђених лиценци, кратак опис лиценци дат је на полеђини листа).

Потпис аутора

У Београду, 09.06.2021.

1. **Ауторство.** Дозвољава се умножавање, дистрибуцију и јавно саопштавање дела, и прераде, ако се наведе име аутора на начин одређен од стране аутора или даваоца лиценце, чак и у комерцијалне сврхе. Ово је најслободнија од свих лиценци.

2. **Ауторство – некомерцијално.** Дозвољава се умножавање, дистрибуцију и јавно саопштавање дела, и прераде, ако се наведе име аутора на начин одређен од стране аутора или даваоца лиценце. Ова лиценца не дозвољава комерцијалну употребу дела.

3. **Ауторство – некомерцијално – без прерада.** Дозвољава се умножавање, дистрибуцију и јавно саопштавање дела, без промена, преобликовања или употребе дела у свом делу, ако се наведе име аутора на начин одређен од стране аутора или даваоца лиценце. Ова лиценца не дозвољава комерцијалну употребу дела. У односу на све остале лиценце, овом лиценцом се ограничава највећи обим права коришћења дела.

4. **Ауторство – некомерцијално – делити под истим условима.** Дозвољава се умножавање, дистрибуцију и јавно саопштавање дела, и прераде, ако се наведе име аутора на начин одређен од стране аутора или даваоца лиценце и ако се прерада дистрибуира под истом или сличном лиценцом. Ова лиценца не дозвољава комерцијалну употребу дела и прерада.

5. **Ауторство – без прерада.** Дозвољава се умножавање, дистрибуцију и јавно саопштавање дела, без промена, преобликовања или употребе дела у свом делу, ако се наведе име аутора на начин одређен од стране аутора или даваоца лиценце. Ова лиценца дозвољава комерцијалну употребу дела.

6. **Ауторство – делити под истим условима.** Дозвољава се умножавање, дистрибуцију и јавно саопштавање дела, и прераде, ако се наведе име аутора на начин одређен од стране аутора или даваоца лиценце и ако се прерада дистрибуира под истом или сличном лиценцом. Ова лиценца дозвољава комерцијалну употребу дела и прерада. Слична је софтверским лиценцама, односно лиценцама отвореног кода.